frontiers | Research Topics

Advanced veterinary topics in elasmobranchs

Edited by
Natalie D. Mylniczenko, Alexa Delaune and Alisa Newton

Published in
Frontiers in Veterinary Science

FRONTIERS EBOOK COPYRIGHT STATEMENT

The copyright in the text of individual articles in this ebook is the property of their respective authors or their respective institutions or funders. The copyright in graphics and images within each article may be subject to copyright of other parties. In both cases this is subject to a license granted to Frontiers.

The compilation of articles constituting this ebook is the property of Frontiers.

Each article within this ebook, and the ebook itself, are published under the most recent version of the Creative Commons CC-BY licence. The version current at the date of publication of this ebook is CC-BY 4.0. If the CC-BY licence is updated, the licence granted by Frontiers is automatically updated to the new version.

When exercising any right under the CC-BY licence, Frontiers must be attributed as the original publisher of the article or ebook, as applicable.

Authors have the responsibility of ensuring that any graphics or other materials which are the property of others may be included in the CC-BY licence, but this should be checked before relying on the CC-BY licence to reproduce those materials. Any copyright notices relating to those materials must be complied with.

Copyright and source acknowledgement notices may not be removed and must be displayed in any copy, derivative work or partial copy which includes the elements in question.

All copyright, and all rights therein, are protected by national and international copyright laws. The above represents a summary only. For further information please read Frontiers' Conditions for Website Use and Copyright Statement, and the applicable CC-BY licence.

ISSN 1664-8714
ISBN 978-2-8325-6302-1
DOI 10.3389/978-2-8325-6302-1

About Frontiers

Frontiers is more than just an open access publisher of scholarly articles: it is a pioneering approach to the world of academia, radically improving the way scholarly research is managed. The grand vision of Frontiers is a world where all people have an equal opportunity to seek, share and generate knowledge. Frontiers provides immediate and permanent online open access to all its publications, but this alone is not enough to realize our grand goals.

Frontiers journal series

The Frontiers journal series is a multi-tier and interdisciplinary set of open-access, online journals, promising a paradigm shift from the current review, selection and dissemination processes in academic publishing. All Frontiers journals are driven by researchers for researchers; therefore, they constitute a service to the scholarly community. At the same time, the *Frontiers journal series* operates on a revolutionary invention, the tiered publishing system, initially addressing specific communities of scholars, and gradually climbing up to broader public understanding, thus serving the interests of the lay society, too.

Dedication to quality

Each Frontiers article is a landmark of the highest quality, thanks to genuinely collaborative interactions between authors and review editors, who include some of the world's best academicians. Research must be certified by peers before entering a stream of knowledge that may eventually reach the public - and shape society; therefore, Frontiers only applies the most rigorous and unbiased reviews. Frontiers revolutionizes research publishing by freely delivering the most outstanding research, evaluated with no bias from both the academic and social point of view. By applying the most advanced information technologies, Frontiers is catapulting scholarly publishing into a new generation.

What are Frontiers Research Topics?

Frontiers Research Topics are very popular trademarks of the *Frontiers journals series*: they are collections of at least ten articles, all centered on a particular subject. With their unique mix of varied contributions from Original Research to Review Articles, Frontiers Research Topics unify the most influential researchers, the latest key findings and historical advances in a hot research area.

Find out more on how to host your own Frontiers Research Topic or contribute to one as an author by contacting the Frontiers editorial office: frontiersin.org/about/contact

Advanced veterinary topics in elasmobranchs

Topic editors

Natalie D. Mylniczenko — Walt Disney World, United States

Alexa Delaune — Mississippi Aquarium, United Kingdom

Alisa Newton — Ocearch, United States

Citation

Mylniczenko, N. D., Delaune, A., Newton, A., eds. (2025). *Advanced veterinary topics in elasmobranchs*. Lausanne: Frontiers Media SA. doi: 10.3389/978-2-8325-6302-1

Table of contents

frontiers | Frontiers in Veterinary Science

TYPE Editorial
PUBLISHED 22 April 2025
DOI 10.3389/fvets.2025.1600135

Check for updates

OPEN ACCESS

EDITED AND REVIEWED BY
Irene Iglesias,
National Institute for Agricultural and Food Research and Technology, Spain

*CORRESPONDENCE
Natalie D. Mylniczenko
✉ natalie.mylniczenko@disney.com

RECEIVED 25 March 2025
ACCEPTED 31 March 2025
PUBLISHED 22 April 2025

CITATION
Mylniczenko ND (2025) Editorial: Advanced veterinary topics in elasmobranchs.
Front. Vet. Sci. 12:1600135.
doi: 10.3389/fvets.2025.1600135

COPYRIGHT
© 2025 Mylniczenko. This is an open-access article distributed under the terms of the Creative Commons Attribution License (CC BY). The use, distribution or reproduction in other forums is permitted, provided the original author(s) and the copyright owner(s) are credited and that the original publication in this journal is cited, in accordance with accepted academic practice. No use, distribution or reproduction is permitted which does not comply with these terms.

Editorial: Advanced veterinary topics in elasmobranchs

Natalie D. Mylniczenko*

Disney's Animals, Science and Environment, Animal Programs, Lake Buena Vista, FL, United States

KEYWORDS

shark, ray, veterinary, medicine, imaging, surgery

Editorial on the Research Topic
Advanced veterinary topics in elasmobranchs

While sharks and rays are extremely popular fishes in aquariums, published elasmobranch veterinary medicine literature remains sparse (1–7). This Research Topic's articles pull together multiple disciplines to examine many important aspects of elasmobranch medicine that deserve greater attention.

Surgical articles detail procedures addressing ereproductive health in two of the most popular collected elasmobranch species. A case study on ovariectomy in the southern ray provides a basis for contraception and potentially resolving common reproductive disease issues. A study on Caesarian section in the cownose ray may help improve reproductive outcomes in other animals.

Two articles synergistically focus on the health and diseases of the inner ear. A vivid pictorial description of chondrocranial anatomy highlights normal inner ear anatomy and contrasts it with three large disease cases. Then a case series from multiple institutions describes diseases, diagnostics, and treatments of the endolymphatic system of the inner ear for the first time (Greene et al.).

Multiple articles present important diagnostics. Butyrate, a known energy molecule in sharks and rays, was reliably evaluated using hand held point of care units (Dannemiller et al.). A traumatic stingray case receives extensive veterinary medical imaging. Ultrasound is used to identify embryo abnormalities in shark eggs (Adams et al.).

Clinical articles provide additional tools for the treatment of elasmobranch disease. A pharmacologic article identifies systemically appropriate doses of voriconazole in undulate rays (Cañizares-Cooz et al.). A large case series of varying levels of ocular parasitic infiltration of corneas in cownose rays presents treatment strategies and outcomes. A sand tiger article diagnoses adomavirus in skin lesions and documents full resolution of clinical signs.

Finally, an important evaluation of thyroid assays found that traditional hormone testing has limited value for goiter, but that iodine testing may be valuable for this in combination with ultrasound and some previously unreported conditions (Wheaton et al.).

Elasmobranch medicine is an under-served topic in aquarium care. This compilation of articles shares the important research of many veterinarians working to improve the health of elasmobranchs in captivity.

Author contributions

NM: Project administration, Writing – original draft, Conceptualization, Writing – review & editing.

Acknowledgments

Thank you to the editors, authors, and reviewers that contributed to this Research Topic, you are truly amazing and at the forefront of our field. Thank you to Kevin Maxson who provides unwavering support of efforts in progressing elasmobranch veterinary medicine.

Conflict of interest

NM is employed by The Walt Disney Company.

Publisher's note

All claims expressed in this article are solely those of the authors and do not necessarily represent those of their affiliated organizations, or those of the publisher, the editors and the reviewers. Any product that may be evaluated in this article, or claim that may be made by its manufacturer, is not guaranteed or endorsed by the publisher.

References

1. Taubenberger JK, Reid AH, Krafft AE, Bijwaard KE, Fanning TG. Initial genetic characterization of the 1918 "Spanish" influenza virus. *Science*. (1997) 275:1793–6. doi: 10.1126/science.275.5307.1793

2. Smith M, Warmolts D, Thoney D, Hueter R. *The Elasmobranch Husbandry Manual: Captive Care of Sharks, Rays and their Relatives.* Columbus, OH: Special Publication of the Ohio Biological Survey (2004). p. 4.

3. Smith M, Warmolts D, Thoney D, Hueter R, Murray M, Ezcurra J. *The Elasmobranch Husbandry Manual II.* Columbus, OH: Special Publication of the Ohio Biological Survey (2017).

4. Carrier JC, Simpfendorfer CA, Heithaus KE, Yopak R. *Biology of Sharks and Their Relatives.* Boca Raton, FL: CRC Press (2022).

5. Clayton KE, Seeley L. Sharks and medicine. In: Miller RE, Lamberski N, Calle PP, editors. *Fowler's Zoo and Wild Animal Medicine Current Therapy.* Miamisburg, OH: Elsevier (2019). p. 338–44.

6. Hadfield C, Clayton L. *Clinical Guide to Fish Medicine*. Hoboken, NJ: Wiley (2021).

7. Mylniczenko ND. Medical management of rays. In: Miller RE, Fowler ME, editors. *Zoo and Wild Animal Medicine Current Therapy.* Philadelphia, PA: Elsevier (2011). p. 170–76.

frontiers | Frontiers in Veterinary Science

TYPE Original Research
PUBLISHED 20 December 2023
DOI 10.3389/fvets.2023.1254340

Check for updates

OPEN ACCESS

EDITED BY
Natalie D. Mylniczenko,
Walt Disney World, United States

REVIEWED BY
Alexandra Schoen,
University of Manitoba, Canada
Lily Parkinson,
Chicago Zoological Society, United States

*CORRESPONDENCE
Nicholas G. Dannemiller
✉ ngdannem@ncsu.edu

RECEIVED 06 July 2023
ACCEPTED 28 November 2023
PUBLISHED 20 December 2023

CITATION
Dannemiller NG, Cray C, Westmoreland LS and Christiansen EF (2023) Diagnostic agreement between three point-of-care glucose and β-hydroxybutyrate meters and reference laboratory methods in stingrays.
Front. Vet. Sci. 10:1254340.
doi: 10.3389/fvets.2023.1254340

COPYRIGHT
© 2023 Dannemiller, Cray, Westmoreland and Christiansen. This is an open-access article distributed under the terms of the Creative Commons Attribution License (CC BY). The use, distribution or reproduction in other forums is permitted, provided the original author(s) and the copyright owner(s) are credited and that the original publication in this journal is cited, in accordance with accepted academic practice. No use, distribution or reproduction is permitted which does not comply with these terms.

Diagnostic agreement between three point-of-care glucose and β-hydroxybutyrate meters and reference laboratory methods in stingrays

Nicholas G. Dannemiller[1,2]*, Carolyn Cray[3], Lori S. Westmoreland[1,2] and Emily F. Christiansen[1,2]

[1]Department of Clinical Sciences, College of Veterinary Medicine, North Carolina State University, Raleigh, NC, United States, [2]North Carolina Aquariums, Raleigh, NC, United States, [3]Division of Comparative Pathology, Department of Pathology and Laboratory Medicine, University of Miami Miller School of Medicine, Miami, FL, United States

Point-of-care (POC) glucose and β-hydroxybutyrate (β-HB) meters can potentially provide rapid insight into an elasmobranch's metabolic state in clinical and field research settings. This study evaluated the diagnostic agreement of three commercial POC meters against reference laboratory methods for glucose and β-HB concentrations in stingrays. Blood was collected during anesthetized exams from 28 stingrays representing four species: cownose rays (*Rhinoptera bonasus*), Atlantic stingrays (*Hypanus sabina*), southern stingrays (*Hypanus americanus*), and yellow stingrays (*Urobatis jamaicensis*). Glucose and β-HB concentrations were measured with each POC meter using whole blood and plasma; in parallel, plasma glucose and β-HB concentrations were measured via reference laboratory methods. Agreement between POC meters and reference laboratory methods was assessed using Bland–Altman methods, Passing-Bablok regression, observed total error, percent relative error, and linear mixed effect models. Plasma glucose and β-HB concentrations determined by reference laboratory methods ranged from <20–63mg/dL to 0.05–5.38mmol/L, respectively. One human POC meter—the Precision Xtra—showed the greatest agreement with reference laboratory methods when measuring glucose with whole blood [mean bias and 95% CI: 0 (−3–4) mg/dL] and β-HB with plasma [mean bias and 95% CI: 0.1 (−0.04–0.2) mmol/L]. Stingray sex, weight, buffy coat, and packed cell volume did not significantly affect the agreement between POC meters and reference laboratory methods. Across all three POC meters, mean bias and imprecision for plasma β-HB concentrations were relatively small (0–0.1mmol/L and 0%, respectively). Utilizing POC meters to measure glucose and β-HB in stingrays may be viable when reference methods are unavailable.

KEYWORDS

batoid, clinical pathology, elasmobranch, ketone, metabolism

1 Introduction

Elasmobranchs (sharks, skates, and rays) are an ancient and diverse group of cartilaginous fish that play essential ecologic roles in aquatic ecosystems globally. Over 200 stingray species are grouped in the order Myliobatiformes, suborder Myliobatoidei (1). Most stingrays are demersal and can be found in tropical to subtropical marine or freshwater habitats. Stingray

species are increasingly listed as vulnerable or endangered on the International Union for Conservation of Nature Red List of Threatened Species, an unfortunate trend shared by all elasmobranchs, with almost 1/3 being threatened with extinction (2). Consequently, stingrays are common in public aquariums due to their ecological importance and increasing need for conservation.

One unique physiologic feature of elasmobranchs is their preferential use of ketone bodies—especially β-hydroxybutyrate (β-HB)—rather than fatty acids for aerobic metabolism under normal conditions, predominately in skeletal and cardiac muscle (3–5). Besides providing buoyancy, elasmobranchs' large, lipid-dense livers serve as ketogenic powerhouses (4). Within the liver, acetyl coenzyme A is formed from long-chain fatty acids by mitochondrial β-oxidation and utilized in numerous metabolic reactions, including generating ketone bodies. Ketone bodies are highly water-soluble, energy-rich fuels exported to extra-hepatic tissues without the need for protein-binding (3). Furthermore, ketone bodies likely play a significant role in supporting metabolism during periods of fasting in elasmobranchs (3–6). While the concentration of ketone bodies in fed elasmobranchs is similar to that observed in fasted (0–3 mmol/L) or ketoacidotic (> 3 mmol/L) mammals, marked ketosis has been found during starvation or prolonged fasting (4).

Glucose is potentially of less metabolic importance in elasmobranchs, although differences between tissues, species, and metabolic states exist (3–5, 7, 8). Plasma glucose concentrations are often low relative to teleosts and terrestrial vertebrates and appear relatively unchanged after feeding or during long-term fasting (3). Some elasmobranch species reportedly tolerate wide ranges of plasma glucose concentrations with no observed clinical effects (3). Nevertheless, a stress-induced increase in catecholamines or corticosteroids (e.g., 1α-hydroxycorticosterone) has been speculated to possibly correlate with increased glucose mobilization, which may reflect increased demand as an oxidative fuel source or supply increased rates of anaerobic glycolysis (3–5, 9, 10). This is best highlighted by the hyperglycemia observed in elasmobranchs as a response to various stressors, including capture, handling, and transport (10–13).

Conventional measurement of glucose and β-HB concentrations in veterinary medicine requires serum or plasma to be submitted to a reference laboratory. As an alternative to laboratory-based assays in human and veterinary medicine, point-of-care (POC) meters typically provide rapid results, require smaller sample volumes, and require no centrifugation or cold chain before testing (14). Within veterinary medicine, the diagnostic accuracy of POC glucose and β-HB meters have been explored in multiple domestic (15–21) and non-domestic species (22–28). Point-of-care glucose and β-HB meters may aid veterinarians, researchers, and wildlife managers working with elasmobranchs, including stingrays, by providing almost instant insight into their physiologic stress or metabolic state.

This study evaluated the diagnostic agreement of three commercial POC glucose and β-HB meters with reference laboratory methods for glucose and β-HB concentrations in stingrays. We hypothesized that the results from the POC meters evaluated would have sufficient agreement with reference laboratory methods and precision for clinical and field research purposes for glucose and β-HB concentrations in stingrays.

2 Materials and methods

2.1 POC meters and reference laboratory

Glucose and β-HB concentrations determined by three commercially available POC meters were compared to results from reference laboratory methods. Each meter measures glucose or β-HB concentrations independently using corresponding test strips. All three meters measure glucose concentration via a glucose-1-dehydrogenase enzymatic reaction in which glucose is converted to gluconolactone using a coenzyme to convert nicotinamide adenine dinucleotide (NAD+) to its reduced form NADH. NADH is re-oxidized to NAD+ by a redox mediator, which is measured via amperometry (i.e., an electrical current) and is directly proportional to glucose concentration (14). Similarly, all three meters measure β-HB concentration via a β-HB-dehydrogenase enzymatic reaction in which β-HB is converted to acetoacetate, leading to a concurrent equimolar reduction of NAD+ to NADH. NADH is re-oxidized to NAD+ by a redox mediator, which is measured via amperometry (i.e., an electrical current) and is directly proportional to β-HB concentration (14). Each meter and its respective test strips were stored and operated following manufacturer instructions; only the correct corresponding test strips provided by the manufacturer were used for each respective meter. Before all data collection, meters were calibrated following manufacturer instructions. None of the meters were operated outside their recommended temperature (10–50°C or 50–122°F) and humidity (10–90%) ranges.

The first POC meter evaluated was the BHBCheck Plus Blood Ketone & Glucose Monitoring System (PortaCheck, Moorestown, NJ, United States), a veterinary-licensed POC meter that requires 0.7 µL of whole blood, measures glucose concentrations within 20–600 mg/dL, and β-HB concentrations within 0.1–8.0 mmol/L. The BHBCheck Plus meter is intended for heparinized or non-heparinized bovine venous whole blood with a 20–40% packed cell volume (PCV).

The second POC meter evaluated was the Precision Xtra Blood Glucose & Ketone Monitoring System (Abbott Laboratories, Chicago, IL, United States), a human-licensed POC meter that requires 1.5 µL of whole blood, measures glucose concentrations within 20–500 mg/dL, and β-HB concentrations within 0–8.0 mmol/L. The Precision Xtra meter is intended for freshly drawn human capillary whole blood with a 30–60% PCV.

The third POC meter evaluated was the Nova Vet™ Ketone/Glucose Meter (Nova Biomedical, Waltham, MA, United States), a veterinary-licensed POC meter that requires 0.4 µL whole blood for glucose and 0.8 µL whole blood for β-HB, measures glucose concentrations within 20–600 mg/dL, and β-HB concentrations within 0.1–8.0 mmol/L. The Nova Vet™ meter is intended for heparinized or non-heparinized bovine whole blood with a 25–60% PCV.

Plasma glucose and β-HB concentrations were measured using a VITROS® 5600 analyzer (Ortho Clinical Diagnostics, Rochester, NY, United States) maintained at the reference laboratory (University of Miami, Miami, FL, United States). The analyzer is maintained per manufacturer instructions and quality assurance best practices. Glucose was determined by a colorimetric glucose oxidase assay based on peroxidase-catalyzed oxidative coupling, producing a red-colored quinoneimine dye with color intensity directly

proportional to glucose concentration (Vitro glucose reagent, Ortho Clinical Diagnostics, Rochester, NY, United States). β-HB was determined via a colorimetric β-HB dehydrogenase assay based on the reduction of the tetrazolium salt INT to a red-colored formazan dye with a color intensity directly proportional to β-HB concentration (Stanbio Chemistry Beta-Hydroxybutyrate LiquiColor® Assay, EKF Diagnostics USA, Boerne, TX, United States). All assays were run per manufacturer instructions.

2.2 Animals and sampling

Twenty-eight stingrays (15 males, 13 females) under managed care at the North Carolina Aquariums at Fort Fisher, Pine Knoll Shores, and Roanoke Island underwent routine annual preventative health exams and phlebotomy between September 2022 and October 2023. Four species were represented in the sample population: cownose rays (*Rhinoptera bonasus*, $n = 6$, min-max weight: 3.85–6.8 kg), Atlantic stingrays (*Hypanus sabina*, $n = 10$, min-max weight: 0.8–1.8 kg), southern stingrays (*Hypanus americanus*, $n = 4$, min-max weight: 5.4–9.2 kg), and yellow stingrays (*Urobatis jamaicensis*, $n = 8$, min-max weight: 0.6–1.65 kg). Stingrays were deemed clinically healthy for study inclusion via absence of abnormalities on physical exam (e.g., skin lesions, color changes, coelomic distension, etc.). All animals were fasted for 12–48 h and efficiently captured via a net from a holding or exhibit system in <5 min. Stingrays were anesthetized using 75–100 mg/L MS-222 buffered 1:1 by weight with sodium bicarbonate or marine buffer. After each stingray reached adequate anesthetic depth (approximately 5–10 min), blood was collected from a pectoral fin or mesopterygial vessel as previously described, using heparinized 22-gauge needles and 3 mL syringes (29). Needles and syringes were pre-heparinized before phlebotomy by aspirating a small volume of 1,000 U/mL sodium heparin and forcefully expelling it. Stingray handling and sampling was performed according to procedures approved by North Carolina State University's Institutional Animal Care and Use Committee (IACUC #21–117).

2.3 Data collection

Immediately following phlebotomy, heparinized whole blood glucose and β-HB concentrations were measured using all three POC meters in a randomized order. Microhematocrit tubes were filled with heparinized whole blood, sealed with clay, and centrifuged for 5 min at 10,000 *g* (PowerSpin™ MH Centrifuge, UNICO, Dayton, NJ, United States). PCV and buffy coat (BC) were read using a hematocrit capillary tube reader (Veterinary Information Network®, Inc., Davis, CA, United States); total solids (TS) were determined via a handheld clinical refractometer (Jorgensen Laboratories, LLC, Loveland, CO, United States). The remainder of the heparinized whole blood sample was kept in a smaller cooler on ice until being centrifuged for 5 min at 3,000 *g* (Mini Centrifuge, Bio-Rad Laboratories, Inc., Hercules, CA, United States) within 1 h of sample collection. Heparinized plasma was separated from packed red blood cells (RBCs) using a disposable pipette, and plasma glucose and β-HB concentrations were measured using all three POC meters. The remaining plasma was placed in a 2-mL cryovial and shipped overnight to the glucose and β-HB reference laboratory (University of Miami, Miami, FL, United States). To measure POC meter precision (i.e., intra-assay variability or repeatability), heparinized whole blood glucose and β-HB concentrations were measured with each POC meter five times in rapid succession immediately following phlebotomy in a subset of two yellow stingrays. Heparinized plasma glucose and β-HB concentrations were measured with each POC meter five times in rapid succession immediately following centrifugation.

2.4 Statistical analyses

For glucose and β-HB concentrations below the lower limit of quantification (LLOQ) of the three POC meters and reference laboratory analyzer, imputation was performed by substituting half of the respective instrument's LLOQ (e.g., if the LLOQ was 20 mg/dL, 10 mg/dL was inputted). To date, there is no widespread consensus on handling data below the LLOQ of an instrument (30). This study used imputation with half the LLOQ because it introduces less bias into the estimates than other single imputation approaches (30, 31). Summary statistics for glucose and β-HB were compiled for the three POC meters and reference laboratory analyzer. Using reference laboratory results, summary statistics of glucose and β-HB concentrations were also compiled by stingray species.

The diagnostic agreement (i.e., accuracy) between the three POC meters and reference laboratory results was assessed by calculating the observed total error (TE_{obs}) and percent relative error, as well as using Bland–Altman methods (32) and Passing-Bablok regression (33, 34) for both glucose and β-HB using whole blood and plasma. The precision (i.e., intra-assay variability or repeatability) of the three POC meters for both glucose and β-HB using whole blood and plasma was assessed by calculating the percent coefficient of variation (CV) using five replicates with Equation 1:

$$CV\,(\%) = \frac{Standard\ Deviation_{POC}}{Mean_{POC}} \times 100 \qquad (1)$$

Percent bias and TE_{obs} of the three POC meters for both glucose and β-HB using whole blood and plasma were calculated with Equations 2 and 3, respectively:

$$Bias\,(\%) = \left| \frac{Mean_{Reference} - Mean_{POC}}{Mean_{Reference}} \right| \times 100 \qquad (2)$$

$$TE_{obs}\,(\%) = 2 \times CV\,(\%) + Bias\,(\%) \qquad (3)$$

The percent relative error between each POC meter result and the reference laboratory result was calculated with Equation 4 for glucose and β-HB:

$$Relative\ Error\,(\%) = \left| \frac{Result_{POC} - Result_{Reference}}{Result_{Reference}} \right| \times 100 \qquad (4)$$

The proportions of results with a percent relative error < 12, 15, and 20% were calculated for each POC meter for both glucose and β-HB using whole blood and plasma and compared to the US Food and Drug Administration relative error guidelines for human glucometers as previously described (26). For Bland–Altman plots and statistics, bias was calculated by subtracting the reference laboratory result from the POC meter result (32). The mean bias and the limits of agreement (LoAs) were then calculated for each POC meter for both glucose and β-HB using whole blood and plasma (32); LoAs were calculated with Equation 5:

$$LoA = Mean_{Difference} \pm \left(1.96 \times Standard\ Deviation_{Difference}\right) \quad (5)$$

Bias was considered statistically significant if the mean bias's 95% confidence interval (95% CI) did not include 0 (32). For Passing-Bablok regression, constant bias was present if the *y*-intercept's 95% CI did not include 0, whereas proportional bias was present if the slope's 95% CI did not include 1 (33, 34).

To explore the effect of multiple variables on the difference between the POC meters and the reference laboratory analyzer, linear mixed-effect models were constructed for each POC meter for both glucose and β-HB. The difference between the POC meter and reference laboratory for either glucose and β-HB was included as the dependent variable; sex (male or female), weight, PCV, BC, and matrix (plasma or whole blood) were included as fixed effects; and stingray species and individual stingrays were included as random effects.

Data were collated in a standard spreadsheet software spreadsheet (Microsoft Excel, Microsoft Corporation, Redmond, WA, United States). All analyses were performed in the free statistical software R (v4.3.1, R Foundation for Statistical Computing, Vienna, Austria). *p* values <0.05 were considered significant. Data organization and summary statistics were performed using the dplyr (v1.1.2) (35) and psych (v2.3.6) (36) packages and their dependents. Bland–Altman plots and statistics were performed using the blandr (v0.5.3) (36) and ggplot2 (v3.4.3) (37) packages and their dependents. Passing-Bablok regression analyses were performed using the mcr package (v1.3.2) (38) and its dependents. Linear mixed-effect models were constructed using the lmerTest (v3.1.3) (39) package.

3 Results

Plasma glucose and β-HB concentrations, as determined by the reference laboratory, ranged from <20–63 mg/dL (median: 35 mg/dL) and 0.05–5.38 mmol/L (median: 0.22 mmol/L, Table 1), respectively. PCV, BC, and TS for all stingrays ranged from 11–32% (median: 24%), 0–4% (median: 0%), and 4.4–8.1 g/dL (median: 7.0 g/dL). Glucose concentration ranges as determined by the reference laboratory were similar across species: < 20–53 mg/dL (median: 26 mg/dL) for Atlantic stingrays, 32–59 mg/dL (median: 48 mg/dL) for cownose rays, 23–39 mg/dL (median: 36 mg/dL) for southern stingrays, and < 20–63 mg/dL (median: 30 mg/dL) for yellow stingrays. Similarly, β-HB concentration ranges as determined by the reference laboratory were similar across species: 0.1–0.4 mmol/L (median: 0.22 mmol/L) for Atlantic stingrays, 0.08–0.69 mmol/L (median: 0.31 mmol/L) for cownose rays, 0.14–0.28 mmol/L (median: 0.23 mmol/L) for southern stingrays, and 0.05–5.38 mmol/L (median: 0.22 mmol/L) for yellow stingrays with the maximum of the yellow stingray range being skewed by one individual (5.38 mmol/L). With the one apparent yellow stingray outlier removed, the β-HB concentration range was 0.05–0.52 mmol/L for conspecifics included in this study.

The CV or imprecision of the three POC meters for glucose was less when using plasma (maximum: 0–4.9%) than whole blood (maximum: 11%); similarly, the CV of the three POC meters for β-HB was less when using plasma (maximum: 0%) than whole blood (maximum: 12.5%). The CV was 0% for all three POC meters when measuring β-HB using plasma (Table 2). All three POC meters had less TE_{obs} for both whole blood and plasma when measuring β-HB than glucose (Table 2). The proportions of results with percent relative error < 12, 15, and 20% were tabulated for each POC meter for glucose and β-HB using whole blood and plasma (Table 2).

Bland–Altman methods found the BHBCheck meter had significant positive bias (i.e., overestimated) for both glucose and β-HB regardless of the matrix (Table 3; Figures 1, 2). The Precision Xtra meter had a significant positive bias for glucose using plasma and β-HB using whole blood (Table 3; Figures 1, 2). The Nova Vet™ had significant negative bias (i.e., underestimated) for glucose regardless of the matrix (Table 3; Figures 1, 2). For glucose, the mean bias ranged from −18 to 48 mg/dL using whole blood and from −14 to 69 mg/dL using plasma across the three POC meters (Table 3). For β-HB, the mean bias ranged from −0.1 to 0.2 mmol/L using whole blood and from 0 to 0.1 mmol/L using plasma across the three POC meters (Table 3).

Passing-Bablok regression analyses found that the BHBCheck meter had a significant constant bias for glucose regardless of matrix and β-HB using plasma and a significant proportional bias for glucose using plasma (Table 3; Figures 3, 4). The Precision Xtra meter had a significant constant bias for glucose using whole blood and β-HB using plasma, as well as a significant proportional bias for both glucose and β-HB regardless of the matrix (Table 3; Figures 3, 4). The Nova Vet™ meter had a significant constant bias for β-HB using plasma and a significant proportional bias for glucose using whole blood and β-HB using plasma (Table 3; Figures 3, 4).

Linear mixed-effect models found sex, weight, PCV, and BC had no significant effect on differences between the individual POC meters and the reference laboratory for glucose or β-HB. Matrix had no significant effect on differences between the BHBCheck or Nova Vet™ meters and the reference laboratory methods for glucose or β-HB. However, matrix did have a significant effect on β-HB, but not glucose, for the Precision Xtra meter: differences in β-HB concentrations were significantly lower using whole blood than plasma (matrix estimate ± standard error: −2.3 ± 0.71 mmol/L, *p* value = 0.002).

4 Discussion

This study evaluated the diagnostic agreement (i.e., accuracy) between three commercial POC glucose and β-HB meters to reference laboratory methods using whole blood and plasma from four stingray species commonly found in managed care environments. Plasma glucose concentrations determined by a reference laboratory method were similar to previous reports in cownose rays and southern stingrays (40–42); likewise, β-HB concentrations determined by a reference laboratory method fell within previously reported ranges in elasmobranchs (4). Of the three POC meters evaluated, the Precision Xtra—a human-licensed glucometer—showed the greatest agreement

TABLE 1 Summary statistics of whole blood (WB) and plasma (P) glucose and β-hydroxybutyrate (β-HB) concentrations in stingrays determined by three commercial point-of-care glucose and β-HB meters and reference laboratory methods.

Analyte	Analyzer	Matrix	*n*	Mean	SD	Median	Min	Max
Glucose (mg/dL)	BHBCheck	WB	22	79	21	79	16	119
		P	22	99	30	99	56	154
	Precision Xtra	WB	28	35	20	39	< 20	71
		P	28	44	22	45	< 20	88
	Nova Vet™	WB	28	16	11	< 20	< 20	46
		P	28	20	15	< 20	< 20	54
	Reference Lab	P	28	34	15	35	< 20	63
β-HB (mmol/L)	BHBCheck	WB	28	0.7	0.8	0.6	0.2	4.4
		P	28	0.6	0.9	0.4	0.1	5.3
	Precision Xtra	WB	28	0.7	0.9	0.6	0.1	5.2
		P	28	0.5	0.8	0.3	0	4.3
	Nova Vet™	WB	28	0.4	0.5	0.3	< 0.1	2.9
		P	28	0.6	0.5	0.5	0.2	3.3
	Reference Lab	P	28	0.44	0.98	0.22	0.05	5.38

SD, Standard deviation; Min, Minimum; and Max, Maximum.

TABLE 2 Percent coefficient of variation (CV), bias, and observed total error (TE_{obs}) for whole blood (WB) and plasma (P) glucose and β-hydroxybutyrate (β-HB) concentrations in stingrays determined by three commercial point-of-care glucose and β-HB meters.

Analyte	Analyzer	Matrix	*n*	CV	Bias	TE_{obs}	< 12% RE	< 15% RE	< 20% RE
Glucose (%)	BHBCheck	WB	22	2.4	3188.2	3,193	0	0	0
		P	22	2.7	3127.4	3132.8	0	0	0
	Precision Xtra	WB	28	11	3316.8	3338.8	46.4	64.3	71.4
		P	28	4.9	3289.1	3298.9	21.4	21.4	35.7
	Nova Vet™	WB	28	0	3371.4	3371.4	17.9	17.9	21.4
		P	28	0	3359.1	3359.1	21.4	25	32.1
β-HB (%)	BHBCheck	WB	28	12.4	103	127.8	3.6	3.6	10.7
		P	28	0	88.4	88.4	10.7	10.7	10.7
	Precision Xtra	WB	28	0	103	103	14.3	14.3	14.3
		P	28	0	65.8	65.8	10.7	10.7	21.4
	Nova Vet™	WB	28	0	37.9	37.9	10.7	10.7	21.4
		P	28	0	80.3	80.3	10.7	14.3	21.4

The American Society for Veterinary Clinical Pathology guidelines advise TE_{obs} be <20% for point-of-care measurements within and above the reference interval. The percentages of measurements with percent relative error (RE) < 12, 15, and 20% are reported for each point-of-care meter, analyte, and matrix. The US Food and Drug Administration requires 95 and 98% of measurements to be within 12 and 15% of reference concentrations for glucometers intended for professional human healthcare use and 96 and 100% of measurements to be within 15 and 20% of reference concentrations for glucometers intended for over-the-counter use in human patients.

with the reference laboratory methods when measuring glucose from whole blood (mean bias: 0 mg/dL) and measuring β-HB from plasma (mean bias: 0.1 mmol/L) in stingrays. Stingray sex, weight, PCV, and BC did not significantly affect differences between the POC meters and the reference laboratory results. All three POC meters had better precision (i.e., intra-assay variability or repeatability) when using plasma than whole blood to measure glucose. Regarding the study's hypothesis, the mean bias and CV for plasma β-HB concentrations was relatively small (min-max: 0–0.1 mmol/L and 0%, respectively) across all three POC meters, suggesting POC β-HB measurement may have sufficient agreement with reference laboratory methods and precision for clinical and field research purposes.

The American Society for Veterinary Clinical Pathology (ASVCP) has developed guidelines for quality assurance and control of POC glucose measurement in light of the rising number of commercially available POC glucometers (43). Point-of-care meter error can be categorized as pre-analytical, analytical, and post-analytical (43). Pre-analytical error was minimized in the present study by adequate observer training and using similar sampling techniques and venipuncture sites. However, species- or individual-specific matrix properties (e.g., blood viscosity, rheology, mean corpuscular volume, etc.) may have contributed to error between the three POC meters and the reference laboratory analyzer, particularly for glucose concentrations. The distribution of glucose between RBCs and plasma

TABLE 3 Bland–Altman statistics and Passing-Bablok regression results for whole blood (WB) and plasma (P) glucose and β-hydroxybutyrate (β-HB) concentrations in stingrays determined by three commercial point-of-care glucose and β-HB meters and reference laboratory methods.

			Bland–Altman statistics			Passing-Bablok regression	
Analyte	Analyzer	Matrix	Bias	Lower LoA	Upper LoA	Intercept	Slope
Glucose (mg/dL)	BHBCheck	WB	48 (41, 56)*	15 (2, 28)	81 (68, 94)	37 (3, 55)*	1.4 (0.9, 2.4)
		P	69 (61, 78)*	31 (17, 46)	107 (92, 121)	29 (8, 46)*	2.3 (1.9, 2.8)*
	Precision Xtra	WB	0 (−3, 4)	−17 (−23, −11)	18 (12, 24)	−6 (−21, −1)*	1.3 (1.1, 1.6)*
		P	10 (6, 14)*	−10 (−17, −3)	29 (23, 36)	−5 (−15, 1)	1.4 (1.3, 1.7)*
	Nova Vet™	WB	−18 (−23, −14)*	−40 (−47, −32)	3 (−4, 10)	10 (−7, 10)	0 (0, 0.6)*
		P	−14 (−18, −10)*	−33 (−39, −27)	5 (−2, 11)	−5 (−20, 10)	0.7 (0, 1.1)
β-HB (mmol/L)	BHBCheck	WB	0.2 (0.1, 0.3)*	−0.3 (−0.5, −0.1)	0.8 (0.6, 1)	0.2 (0, 0.3)	1.3 (0.9, 2.5)
		P	0.1 (0.1, 0.2)*	−0.1 (−0.1, 0)	0.4 (0.3, 0.4)	0.1 (0.1, 0.2)*	1.1 (1, 1.4)
	Precision Xtra	WB	0.2 (0.1, 0.3)*	−0.2 (−0.3, −0.1)	0.6 (0.5, 0.8)	0 (−0.2, 0.1)	2 (1.5, 2.7)*
		P	0 (−0.1, 0.2)	−0.5 (−0.7, −0.3)	0.6 (0.4, 0.8)	−0.1 (−0.2, 0)	1.7 (1.3, 2.2)*
	Nova Vet™	WB	−0.1 (−0.3, 0.1)	−1.1 (−1.4, −0.7)	1 (0.6, 1.3)	0 (−0.2, 0.7)	1.1 (−2.2, 1.8)
		P	0.1 (−0.1, 0.3)	−0.8 (−1.1, −0.5)	1 (0.7, 1.3)	0.5 (0.3, 0.6)*	0 (−0.4, 0.6)*

The mean difference (Bias) and the limits of agreement (LoA)—defined as the mean difference ± 1.96 times the standard deviation of the differences—were calculated for each meter. Bias was considered statistically significant (*) if the mean difference's 95% confidence interval (95% CI) did not include 0. For Passing-Bablok regression, constant bias was present (*) if the 95% CI for the *y*-intercept did not include 0, whereas proportional bias was present (*) if the 95% CI for the slope did not include 1.

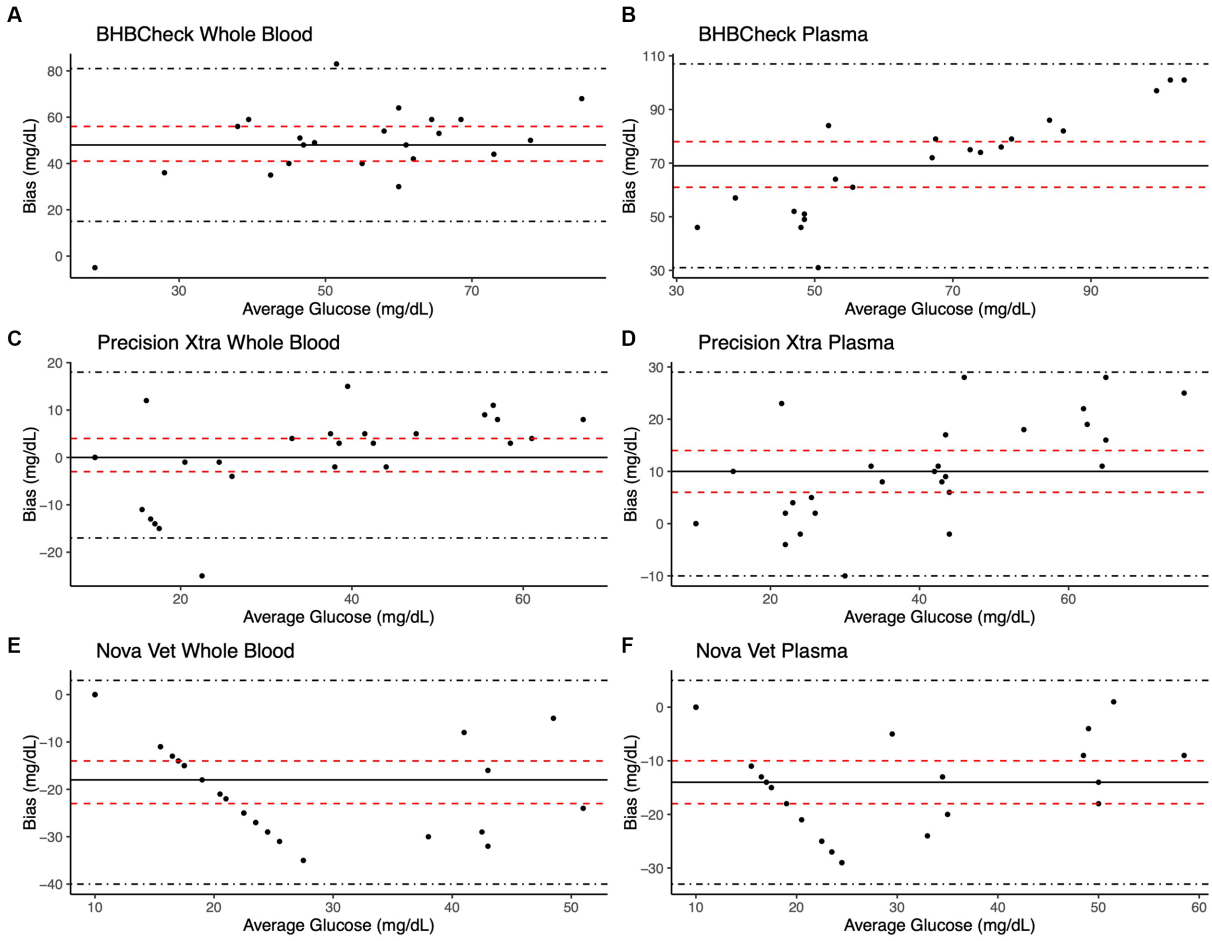

FIGURE 1
Bland–Altman plots of whole blood **(A, C, E)** and plasma **(B, D, F)** glucose concentrations in stingrays determined by three commercial point-of-care meters compared to reference laboratory methods. Black dots represent individual stingrays. The mean difference (Bias, solid black line) and the limits of agreement (LoA, black dot-dashed lines)—defined as the mean difference ± 1.96 times the standard deviation of the differences—were calculated for each meter. Bias was considered statistically significant if the 95% confidence interval (red dashed lines) mean difference did not include 0.

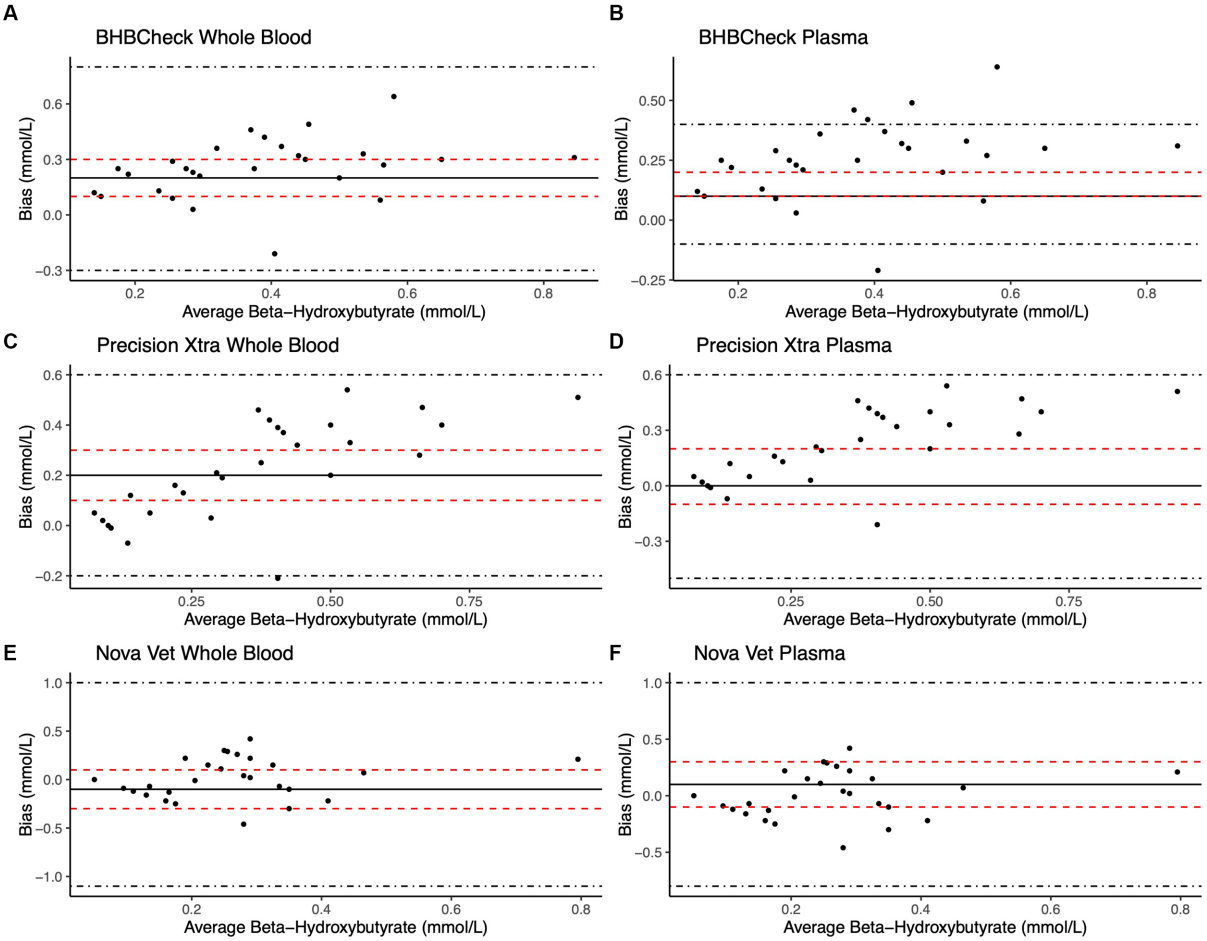

FIGURE 2
Bland–Altman plots of whole blood **(A, C, E)** and plasma **(B, D, F)** β-hydroxybutyrate (β-HB) concentrations in stingrays determined by three commercial point-of-care meters compared to reference laboratory methods. Black dots represent individual stingrays. The mean difference (Bias, solid black line) and the limits of agreement (LoA, black dot-dashed lines)—defined as the mean difference±1.96 times, the standard deviation of the differences—were calculated for each meter. Bias was considered statistically significant if the 95% confidence interval (red dashed lines) of the mean difference did not include 0. To avoid skewing the Bland–Altman plots, a single yellow stingray outlier was removed (β-HB=5.38mmol/L via the reference laboratory method).

is an important matrix-related variable across species (43). Glucose is distributed equally between RBCs and plasma in humans, whereas in canine, feline, rabbit, and avian patients, glucose in circulation is found predominantly in plasma (43). To the authors' knowledge, the distribution of glucose between RBCs and plasma in the four stingray species sampled is unknown and remains a potential avenue of future physiologic research. Analytical error was minimized during data collection by using test strips before they expired, routine calibration using manufacturer-provided control materials, and not operating the POC meters under extreme environmental conditions. Post-analytical error was avoided by using consistent units of measurement (mg/dL for glucose, mmol/L for β-HB) and recording results immediately after being displayed by the POC meters.

In human and veterinary patients, anemia or hemoconcentration can falsely increase or decrease POC meter glucose or β-HB measurements (15, 18, 21, 43, 44). In stingrays, linear mixed-effect models found PCV had no significant effect on differences between the three POC meters and the reference laboratory analyzer, despite a subset of sampled stingrays with PCV values lower than the recommended ranges for the meter. Possible reasons PCV influences POC meter glucose or β-HB measurements include built-in conversion factors or increased diffusion rate in test strips with lower PCV (43). This study did not assess whether analytical interference occurred due to other blood gas or biochemical parameters such as pH, pO_2, cholesterol, bilirubin, or biliverdin (43). All sampled stingrays were anesthetized with MS-222 to ensure safe and efficient handling, which could have resulted in analytical interference secondary to perianesthetic physiologic changes (e.g., acid–base status, body temperature, ventilation, vasoconstriction, etc.). Although veterinary studies are lacking, POC glucometers are less accurate intraoperatively in human patients under anesthesia (45, 46).

The ASVCP guidelines advise TE_{obs} for laboratory instruments, including POC glucose and β-HB meters, to be <10% for values below the reference interval or < 20% for values within and above the reference interval (43, 47). All three POC meters for both glucose and β-HB using whole blood and plasma had TE_{obs} > 20%, indicative of undesirable analytical performance. Furthermore, the US Food and Drug Administration requires 95 and 98% of measurements to be within 12 and 15% of reference concentrations for POC glucometers intended for professional healthcare use and 96 and 100% of measurements to be within 15 and 20% of reference concentrations for POC glucometers intended for over-the-counter use (26). All three

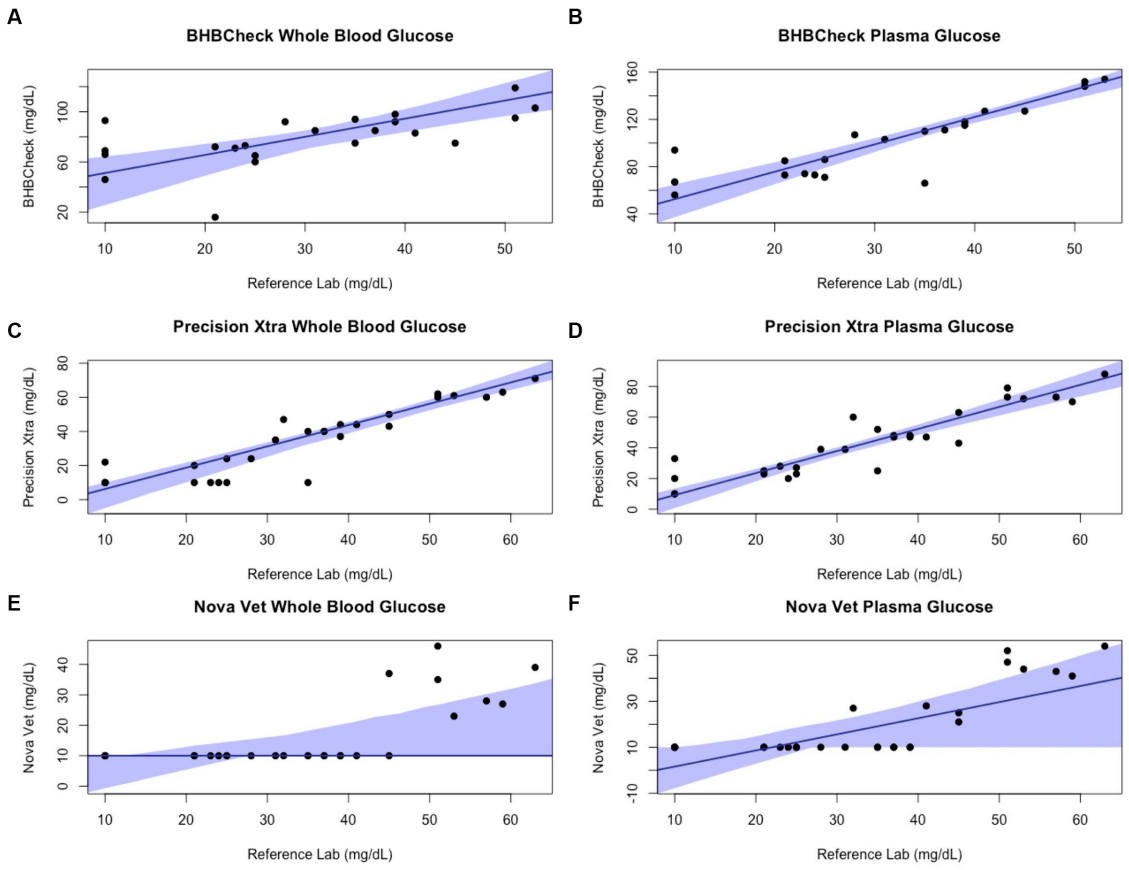

FIGURE 3
Passing-Bablok plots of whole blood and plasma glucose concentrations in stingrays determined by three commercial point-of-care meters compared to reference laboratory methods. Black dots represent individual stingrays. The solid blue line and associated shading represent the estimated regression line and its 95% confidence interval. For Passing-Bablok regression, constant bias was present if the 95% CI for the *y*-intercept did not include 0, whereas proportional bias was present if the 95% CI for the slope did not include 1.

POC meters evaluated did not meet US Food and Drug Administration relative error guidelines for human glucometers when measuring whole blood or plasma glucose concentrations in stingrays (27). To the authors' knowledge, neither the US Food and Drug Administration nor ASVCP has produced guidelines for POC β-HB meters despite their frequent use in monitoring diabetes mellitus in humans and domestic small animals.

Regardless of specific statistical analyses employed to compare new and established diagnostic methods, it is essential to appraise the clinical relevance of their analytic agreement. Clarke or Parkes Error Grid Analysis has historically been used in human and veterinary POC glucometer research to understand better potential clinical outcomes associated with POC meter accuracy (48, 49). This study implemented neither method due to the wide range of glucose and β-HB concentrations observed in elasmobranchs and little consensus on pathophysiologic thresholds for either analyte (e.g., hypoglycemic, ketonemia). However, the BHBCheck meter could potentially lead to highly inaccurate glucose interpretations due to the magnitude of its mean bias using whole blood (48 mg/dL) or plasma (69 mg/dL) and the narrow range of glucose concentrations observed by the reference laboratory (< 20–63 mg/dL). Passing-Bablok regression analyses found that all three POC meters mainly exhibited significant positive proportional bias (i.e., 95% CI > 1) measuring glucose and β-HB, signifying greater error at higher concentrations. Consequently, future research should assess agreement with a reference laboratory under potential pathophysiologic states or physiologic extremes (e.g., hyperglycemia secondary to long-line capture, ketonemia due to prolonged fasting, etc.).

Limitations of the present study include limited sample sizes per species ($n < 10$) and variable fasting durations before sampling, given differences in husbandry routines at the separate facilities. While imputation by substituting values below the LLOQ with a constant was employed in the present study, multiple imputation, maximum likelihood estimation, or kernel density estimation may be better alternative approaches. Although variation in venipuncture sites can influence PCV in sharks (50) and downstream biochemical analyses in other taxa, no statistically significant differences between venipuncture sites were found in southern stingrays (51). Although plasma was separated from RBCs promptly via centrifugation, glucose and β-HB concentrations could have decreased slightly between venipuncture and processing due to metabolism by cellular constituents.

Rapid, reliable detection of hyperglycemia due to physiologic stress could help veterinarians and researchers working with elasmobranchs more objectively monitor their welfare during capture, handling, and transport. Similarly, accurate POC measurement of β-HB could provide almost instant, cost-effective

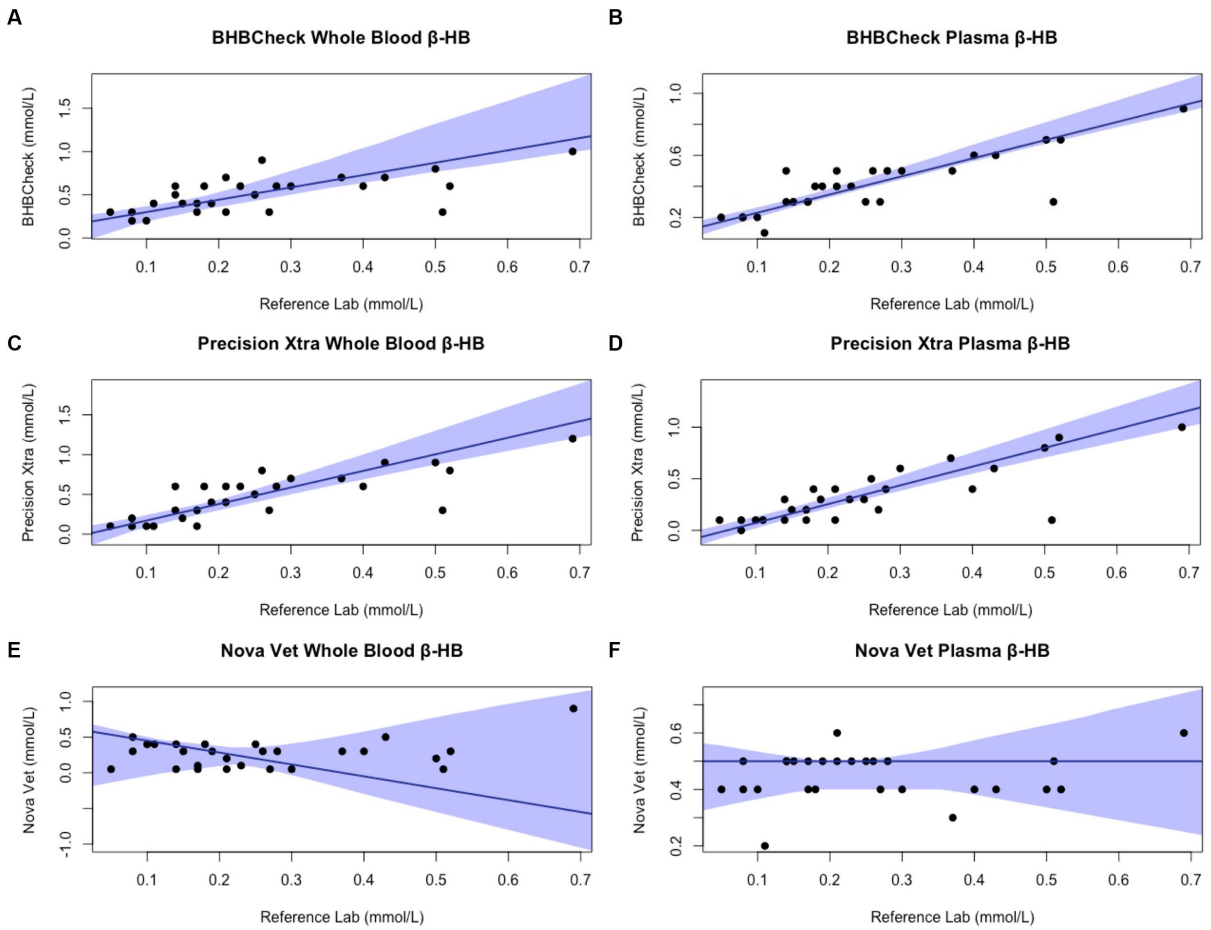

FIGURE 4
Passing-Bablok plots of whole blood and plasma β-hydroxybutyrate (β-HB) concentrations in stingrays determined by three commercial point-of-care meters compared to reference laboratory methods. Black dots represent individual stingrays. The solid blue line and associated shading represent the estimated regression line and its 95% confidence interval. For Passing-Bablok regression, constant bias was present if the 95% CI for the *y*-intercept did not include 0, whereas proportional bias was present if the 95% CI for the slope did not include 1. To avoid skewing the Passing-Bablok plots, a single yellow stingray outlier was removed (β-HB = 5.38 mmol/L via the reference laboratory method).

insight into the metabolic state of the elasmobranch patient vs. the turnaround time and expense of sending a sample to a reference laboratory. Further research should investigate POC meter clinical utility under different metabolic states in elasmobranchs. Using POC meters to measure glucose and β-HB concentrations in stingrays may be possible when reference methods are inaccessible. β-HB measurement using plasma will likely have sufficient accuracy and precision for clinical and field research purposes for the three POC meters evaluated in this study, especially the human-licensed glucometer, Precision Xtra.

Data availability statement

The raw data supporting the conclusions of this article will be made available by the authors, without undue reservation.

Ethics statement

The animal study was approved by North Carolina State University Institutional Animal Care and Use Committee. The study was conducted in accordance with the local legislation and institutional requirements.

Author contributions

ND: Conceptualization, Investigation, Data Curation, Formal analysis, Writing – original draft, Writing – review & editing. CC: Writing – review & editing. LW: Writing – review & editing. EC: Writing – review & editing.

Funding

The NC State College of Veterinary Medicine Support Fund for Aquatic Animal Medicine provided funding for this study.

Acknowledgments

The authors thank Craig Harms, Maria Serrano, Heather Broadhurst, Megan Cabot, Caitlin Hepps Keeney, Ashley Souza, Christian Capobianco, Kaitlynn Hicks, the animal care staff of the North

Carolina Aquariums, and the staff of the University Miami Avian & Wildlife Laboratory for their support and assistance with data collection.

Conflict of interest

The authors declare that the research was conducted in the absence of any commercial or financial relationships that could be construed as a potential conflict of interest.

Publisher's note

All claims expressed in this article are solely those of the authors and do not necessarily represent those of their affiliated organizations, or those of the publisher, the editors and the reviewers. Any product that may be evaluated in this article, or claim that may be made by its manufacturer, is not guaranteed or endorsed by the publisher.

References

1. Aschliman NC, Claeson KM, McEachran JD. Phylogeny of Batoidea In: JC Carrier, JA Musick and MR Heithaus, editors. *Biology of Sharks and Their Relatives*. *2nd* ed. Boca Raton: CRC Press (2012)

2. Dulvy NK, Pacoureau N, Rigby CL, Pollom RA, Jabado RW, Ebert DA, et al. Overfishing drives over one-third of all sharks and rays toward a global extinction crisis. *Curr Biol*. (2021) 31:4773–4787.e8. doi: 10.1016/j.cub.2021.08.062

3. Ballantyne JS. Jaws: the inside story. The metabolism of elasmobranch fishes. *Comp Biochem Physiol B Biochem Mol Biol*. (1997) 118:703–42. doi: 10.1016/S0305-0491(97)00272-1

4. Speers-Roesch B, Treberg JR. The unusual energy metabolism of elasmobranch fishes. *Comp Biochem Physiol A Mol Integr Physiol*. (2010) 155:417–34. doi: 10.1016/j.cbpa.2009.09.031

5. Ballantyne JS. Metabolism of elasmobranchs (Jaws II) In: RE Shadwick, AP Farrell and CJ Brauner, editors. *Fish Physiology*, vol. *34*. Cambridge, MA: Academic Press (2015). 395–456.

6. Wood CM, Walsh PJ, Kajimura M, McClelland GB, Chew SF. The influence of feeding and fasting on plasma metabolites in the dogfish shark (*Squalus Acanthias*). *Comp Biochem Physiol A Mol Integr Physiol*. (2010) 155:435–44. doi: 10.1016/j.cbpa.2009.09.006

7. Walsh PJ, Kajimura M, Mommsen TP, Wood CM. Metabolic organization and effects of feeding on enzyme activities of the dogfish shark (*Squalus Acanthias*) rectal gland. *J Exp Biol*. (2006) 209:2929–38. doi: 10.1242/jeb.02329

8. Deck CA, Anderson WG, Conlon JM, Walsh PJ. The activity of the rectal gland of the North Pacific spiny dogfish *Squalus Suckleyi* is glucose dependent and stimulated by glucagon-like Peptide-1. *J Comp Physiol B*. (2017) 187:1155–61. doi: 10.1007/s00360-017-1102-9

9. Bouyoucos IA, Schoen AN, Wahl RC, Anderson WG. Ancient fishes and the functional evolution of the corticosteroid stress response in vertebrates. *Comp Biochem Physiol A Mol Integr Physiol*. (2021) 260:111024. doi: 10.1016/j.cbpa.2021.111024

10. Harding L, Gallagher A, Jackson A, Bortoluzzi J, Dolton HR, Shea B, et al. Capture heats up sharks. *Conserv Physiol*. (2022) 10:coac065. doi: 10.1093/conphys/coac065

11. Cliff G, Thurman GD. Pathological and physiological effects of stress during capture and transport in the juvenile dusky shark, *Carcharhinus Obscurus*. *Comp Biochem Physiol A Mol Integr Physiol*. (1984) 78:167–73. doi: 10.1016/0300-9629(84)90111-7

12. Hoffmayer ER, Parsons GR. The physiological response to capture and handling stress in the Atlantic sharpnose shark *Rhizoprionodon terraenovae*. *Fish Physiol Biochem*. (2001) 25:277–85. doi: 10.1023/A:1023210620904

13. Prohaska BK, Talwar BS, Grubbs RD. Blood biochemical status of deep-sea sharks following longline capture in the Gulf of Mexico. *Conserv Physiol*. (2021) 9:coaa113. doi: 10.1093/conphys/coaa113

14. Chong SK, Reineke EL. Point-of-care glucose and ketone monitoring. *Top Companion Anim Med*. (2016) 31:18–26. doi: 10.1053/j.tcam.2016.05.005

15. Wess G, Reusch C. Assessment of five portable blood glucose meters for use in cats. *Am J Vet Res*. (2000) 61:1587–92. doi: 10.2460/ajvr.2000.61.1587

16. Tommaso MD, Aste G, Rocconi F, Guglielmini C, Boari A. Evaluation of a portable meter to measure ketonemia and comparison with ketonuria for the diagnosis of canine diabetic ketoacidosis. *J Vet Intern Med*. (2009) 23:466–71. doi: 10.1111/j.1939-1676.2009.0302.x

17. Henderson DW, Schlesinger DP. Use of a point-of-care Beta-Hydroxybutyrate sensor for detection of Ketonemia in dogs. *Can Vet J*. (2010) 51:1000–2.

18. Tennent-Brown BS, Koenig A, Williamson LH, Boston RC. Comparison of three point-of-care blood glucose meters for use in adult and juvenile alpacas. *J Am Vet Med Assoc*. (2011) 239:380–6. doi: 10.2460/javma.239.3.380

19. Weingart C, Lotz F, Kohn B. Validation of a portable hand-held whole-blood ketone meter for use in cats. *Vet Clin Pathol*. (2012) 41:114–8. doi: 10.1111/j.1939-165X.2011.00389.x

20. Zeugswetter FK, Rebuzzi L. Point-of-care B-Hydroxybutyrate measurement for the diagnosis of feline diabetic ketoacidaemia. *J Small Anim Pract*. (2012) 53:328–31. doi: 10.1111/j.1748-5827.2012.01204.x

21. Wess G, Reusch C. Evaluation of five portable blood glucose meters for use in dogs. *J Am Vet Med Assoc*. (2000) 216:203–9. doi: 10.2460/javma.2000.216.203

22. Acierno MJ, Mitchell MA, Schuster PJ, Freeman D, Sanchez-Migallon Guzman D, Jr TNT. Evaluation of the agreement among three handheld blood glucose meters and a laboratory blood analyzer for measurement of blood glucose concentration in Hispaniolan Amazon parrots (*Amazona ventralis*). *Am J Vet Res*. (2009) 70:172–5. doi: 10.2460/ajvr.70.2.172

23. Burdick S, Mitchell MA, Neil J, Heggem B, Whittington J, Acierno MJ. Evaluation of two point-of-care meters and a portable chemistry analyzer for measurement of blood glucose concentrations in juvenile white-tailed deer (*Odocoileus virginianus*). *J Am Vet Med Assoc*. (2012) 240:596–9. doi: 10.2460/javma.240.5.596

24. Petritz OA, Antinoff N, Chen S, Kass PH, Paul-Murphy JR. Evaluation of portable blood glucose meters for measurement of blood glucose concentration in ferrets (*Mustela putorius furo*). *J Am Vet Med Assoc*. (2013) 242:350–4. doi: 10.2460/javma.242.3.350

25. Proulx M-P, Vergneau-Grosset C, Hébert J, Bédard C, Maccolini É. Comparison of a Portage blood glucose meter analyzer with a benchtop point-of-care chemistry analyzer for measurement of blood glucose concentration in client-owned ferrets (*Mustela putorius furo*). *J Exot Pet Med*. (2022) 43:22–8. doi: 10.1053/j.jepm.2022.07.004

26. Meade SM, Di Girolamo N, Cray C, Aquilino N, DiGeronimo PM, Brandão J. Point-of-care ketone meters may be used to estimate serum B-Hydroxybutyrate concentrations in healthy African penguins (*Spheniscus demersus*). *Am J Vet Res*. (2022) 83:ajvr.21.11.0192. doi: 10.2460/ajvr.21.11.0192

27. Hiebert K, Reich S, Allender MC. Evaluation of the agreement between 2 point-of-care glucometers and a laboratory automated analyzer in North American raptors. *J Avian Med Surg*. (2022) 36:278–86. doi: 10.1647/21-00006

28. Lieske CL, Ziccardi MH, Mazet JAK, Newman SH, Gardner IA. Evaluation of 4 handheld blood glucose monitors for use in seabird rehabilitation. *J Avian Med Surg*. (2002) 16:277–85. doi: 10.1647/1082-6742(2002)016[0277:EOHBGM]2.0.CO;2

29. Westmoreland LSH, Archibald KE, Christiansen EF, Broadhurst HJ, Stoskopf MK. The mesopterygial vein: a reliable venipuncture site for intravascular access in Batoids. *J Zoo Wildl Med*. (2019) 50:369–74. doi: 10.1638/2018-0137

30. Giskeødegård GF, Lydersen S. Measurements below the detection limit. *Tidsskr Nor Laegeforen*. (2022) 142. doi: 10.4045/tidsskr.22.0439

31. Beal SL. Ways to fit a Pk model with some data below the quantification limit. *J Pharmacokinet Pharmacodyn*. (2001) 28:481–504. doi: 10.1023/A:1012299115260

32. Bland JM, Altman DG. Statistical methods for assessing agreement between two methods of clinical measurement. *Lancet*. (1986) 327:307–10. doi: 10.1016/S0140-6736(86)90837-8

33. Passing H, Bablok W. A new biometrical procedure for testing the equality of measurements from two different analytical methods. Application of linear regression procedures for method comparison studies in clinical chemistry, part I. *J Clin Chem Clin Biochem*. (1983) 21:709–20. doi: 10.1515/cclm.1983.21.11.709

34. Passing H, Bablok W. Comparison of several regression procedures for method comparison studies and determination of sample sizes. Application of linear regression procedures for method comparison studies in clinical chemistry, part II. *J Clin Chem Clin Biochem*. (1984) 22:431–45. doi: 10.1515/cclm.1984.22.6.431

35. Wickham H, François R, Henry L, Müller K, Vaughan D (2023). Dplyr: A grammar of data manipulation. R package version 1.1.2.

36. Datta D. (2017). Blandr: A Bland-Altman method comparison package for R. R package version 0.5.3.

37. Wickham H. *Ggplot2: Elegant Graphics for Data Analysis*. New York, New York: Springer (2016).

38. Potapov S, Mode LF, Schuetzenmeister A, Manuilova E, Dufey F, Raymaekers J (2023). Mcr: Method comparison regression. R package version 1.3.2.

39. Kuznetsova A, Brockhoff P, Christensen R. Lmertest package: tests in linear mixed effects models. *J Stat Softw*. (2017) 82:1–26. doi: 10.18637/jss.v082.i13

40. Cain DK, Harms CA, Segars A. Plasma biochemistry reference values of wild-caught southern stingrays (*Dasyatis americana*). *J Zoo Wildl Med*. (2004) 35:471–6. doi: 10.1638/03-107

41. Ferreira CM, Field CL, Tuttle AD. Hematological and plasma biochemical parameters of aquarium-maintained cownose rays. *J Aquat Anim Health*. (2010) 22:123–8. doi: 10.1577/H09-048.1

42. Grant K, Campbell T. Hematology and plasma biochemistry value differences between acclimated and recently captive female southern stingrays, *Dasyatis Americana*. *J Zoo Aquar Res*. (2020) 8:59–66. doi: 10.19227/jzar.v8i1.254

43. Gerber KL, Freeman KP. ASVCP guidelines: quality assurance for portable blood glucose meter (glucometer) use in veterinary medicine. *Vet Clin Pathol*. (2016) 45:10–27. doi: 10.1111/vcp.12310

44. Selleri P, Di Girolamo N, Novari G. Performance of two portable meters and a benchtop analyzer for blood glucose concentration measurement in rabbits. *J Am Vet Med Assoc*. (2014) 245:87–98. doi: 10.2460/javma.245.1.87

45. Mraovic B, Schwenk ES, Epstein RH. Intraoperative accuracy of a point-of-care glucose meter compared with simultaneous central laboratory measurements. *J Diabetes Sci Technol*. (2012) 6:541–6. doi: 10.1177/193229681200600308

46. Karon BS, Donato LJ, Larsen CM, Siebenaler LK, Wells AE, Wood-Wentz CM, et al. Accuracy of capillary and arterial whole blood glucose measurements using a glucose meter in patients under general anesthesia in the operating room. *Anesthesiology*. (2017) 127:466–74. doi: 10.1097/ALN.0000000000001708

47. Harr KE, Flatland B, Nabity M, Freeman KP. ASVCP guidelines: allowable total error guidelines for biochemistry. *Vet Clin Pathol*. (2013) 42:424–36. doi: 10.1111/vcp.12101

48. Clarke WL, Cox D, Gonder-Frederick LA, Carter W, Pohl SL. Evaluating clinical accuracy of systems for self-monitoring of blood glucose. *Diabetes Care*. (1987) 10:622–8. doi: 10.2337/diacare.10.5.622

49. Parkes JL, Slatin SL, Pardo S, Ginsberg BH. A new consensus error grid to evaluate the clinical significance of inaccuracies in the measurement of blood glucose. *Diabetes Care*. (2000) 23:1143–8. doi: 10.2337/diacare.23.8.1143

50. Mylniczenko ND, Curtis EW, Wilborn RE, Young FA. Differences in hematocrit of blood samples obtained from two venipuncture sites in sharks. *Am J Vet Res*. (2006) 67:1861–4. doi: 10.2460/ajvr.67.11.1861

51. Phillips BE, Christiansen EF, Stoskopf MK, Broadhurst H, George R, Harms CA. Comparison of hematology, plasma biochemistry, and blood gas variables between 2 venipuncture sites in southern stingrays (*Dasyatis americana*). *Vet Clin Pathol*. (2016) 45:627–33. doi: 10.1111/vcp.12424

frontiers | Frontiers in Veterinary Science

TYPE Original Research
PUBLISHED 06 June 2024
DOI 10.3389/fvets.2024.1376851

Check for updates

OPEN ACCESS

EDITED BY
Alisa Newton,
Ocearch, United States

REVIEWED BY
Claire Vergneau-Grosset,
Université de Montréal, Canada
Panagiotis Azmanis,
Dubai Falcon Hospital, United Arab Emirates

*CORRESPONDENCE
Pablo Morón-Elorza
✉ p-moron@hotmail.com

RECEIVED 26 January 2024
ACCEPTED 27 May 2024
PUBLISHED 06 June 2024

CITATION
Cañizares-Cooz D, Rojo-Solís C, Rubio-Langre S, García-Párraga D, Encinas T and Morón-Elorza P (2024) Updates on antifungal pharmacotherapy in elasmobranchs: pharmacokinetics of 4 mg/kg voriconazole after IM and IV administration in undulate skates (*Raja undulata*) maintained under human care.
Front. Vet. Sci. 11:1376851.
doi: 10.3389/fvets.2024.1376851

COPYRIGHT
© 2024 Cañizares-Cooz, Rojo-Solís, Rubio-Langre, García-Párraga, Encinas and Morón-Elorza. This is an open-access article distributed under the terms of the Creative Commons Attribution License (CC BY). The use, distribution or reproduction in other forums is permitted, provided the original author(s) and the copyright owner(s) are credited and that the original publication in this journal is cited, in accordance with accepted academic practice. No use, distribution or reproduction is permitted which does not comply with these terms.

Updates on antifungal pharmacotherapy in elasmobranchs: pharmacokinetics of 4 mg/kg voriconazole after IM and IV administration in undulate skates (*Raja undulata*) maintained under human care

Daniela Cañizares-Cooz[1], Carlos Rojo-Solís[2], Sonia Rubio-Langre[1], Daniel García-Párraga[2,3], Teresa Encinas[1] and Pablo Morón-Elorza[1,3]*

[1]Department of Pharmacology and Toxicology, Faculty of Veterinary Medicine, Complutense University of Madrid, Madrid, Spain, [2]Veterinary Services, Oceanogràfic, Ciudad de las Artes y las Ciencias. C/ Eduardo Primo Yúfera (Científic) 1B, Valencia, Spain, [3]Research Department, Fundación Oceanogràfic de la Comunitat Valenciana, Oceanogràfic, C/ Eduardo Primo Yúfera (Científic) 1B, Valencia, Spain

Introduction: Fungal diseases are frequently associated with elevated mortality rates in elasmobranchs. Currently, there is a notable absence of scientifically validated therapeutic medications that can ensure both effectiveness and safety when administered to this group of animals. The empirical prescription of azole antifungal agents, particularly voriconazole, has been posited as a potentially efficacious treatment approach for addressing most common mycoses in sharks and rays. However, there are still no published pharmacokinetic studies supporting its use in elasmobranchs and there is a lack of scientific base for its utilization in elasmobranchs.

Methods: For this study, voriconazole was administered intravenously (IV) and intramuscularly (IM), at a single dose of 4 mg/kg to six adult undulate skates (*Raja undulata*). A washout period of 8 weeks was left between each route of administration. Blood samples were collected both before and at ten predetermined intervals after each dosing (0.25, 0.5, 1, 1.5, 2, 4, 8, 12, 24, and 36 h after drug administration). Plasma concentrations were quantified using a validated high-performance liquid chromatography method, and pharmacokinetic (PK) data was analyzed through non-compartmental methods.

Results: The mean extrapolated concentration at 0 h (C_0) after IV administration was 27.19 ± 7.15 μg/mL and the mean peak plasma concentrations (C_{max}) ± SEM after IM administration resulted 2.98 ± 0.28 μg/mL at a mean time to maximum concentration (T_{max}) of 1.33 ± 0.17 h. Terminal half-lives were calculated and resulted 11.18 ± 1.32 h for IV injections and 9.59 ± 1.38 h for IM injections. The area under the curve extrapolated to infinity was determined as 58.14 ± 2.79 h·μg/ml following IV injections and 37.60 ± 6.67 h·μg/ml following IM injections. The IM-administered voriconazole exhibited a mean absolute bioavailability of 64.67 ± 11.47%.

Discussion: These discoveries provide backing for the possible application of voriconazole through the intramuscular route in undulate skates and support using lower dosage regimens compared to those required for oral administration, emphasizing the importance of conducting further pharmacokinetic studies with antifungals in elasmobranchs.

KEYWORDS

antimycotic, shark, ray, chondrichthyans, pharmacology, *Fusarium*, half-life, azoles

Introduction

Fungal diseases have been documented in elasmobranchs under human care in aquariums since the late 1980s. Despite their low incidence in fish, these diseases have proven to be highly lethal in various teleost and elasmobranch species (1). The involvement of several fungi, including *Purpureocilium* spp., *Exophiala* spp., and *Fusarium* spp., is frequently observed (2). Many of these fungal infections, known as invasive mycoses, are considered emerging diseases in elasmobranchs and can result in skin and eye problems or systemic spread in individuals with weakened immune systems, causing severe sickness and can ultimately lead to death (1, 3). *Fusarium solani* or *F. solani* Species Complex is emerging as a serious illness for both humans and animals and affects a wide range of elasmobranch species with Hammerhead sharks (Family *Sphyrnidae*) the most susceptible (4). Unfortunately, a lack of information about the treatment, medical protocols, and environmental management of mycoses in these species has resulted in high mortality rates (5, 6).

The treatment for these diseases in elasmobranchs should combine environmental management as well as pharmacotherapy, which is based in the use of antifungals. Antifungal drugs are commonly prescribed to improve clinical signs or lesions in affected animals, with azole antifungals one of the available therapeutic options for the treatment of systemic fungal infections in elasmobranchs (7). Azoles, a group of antifungal drugs characterized by an imidazole ring, inhibit the 14α-demethylase enzyme in fungi, disrupting ergosterol synthesis and leading to toxic metabolites that hinder fungal growth (8, 9). Therefore, a dual mechanism of action occurs: the absence of ergosterol induces a fungistatic effect and the accumulation of reactive oxygen species (ROS) resulting from the loss of membrane integrity and organelle functionality, along with toxic metabolites, leads to a fungicidal effect (10).

Although different azoles have been used empirically for the treatment of fungal diseases in elasmobranchs and other aquatic animal species, there are no studies that prove their kinetic disposition and efficacy. Among azole antifungals, voriconazole appears to be the treatment of choice, as it has produced one of the lowest minimum-inhibitory concentrations (MIC) against *Fusarium solani* during *in vitro* studies, with a MIC_{90} of 2 µg/mL. Furthermore, voriconazole has also provided very low MIC for other fungi isolated from elasmobranchs such as *Purpureocilium lilacinus* (0.5 µg/mL) (4, 11). However, further evidence regarding the use of this drugs in elasmobranchs is necessary.

The pharmacokinetic behavior of voriconazole is well-documented across a broad range of animal species, in which this drug is employed for its promising pharmacological properties, tolerability and efficacy. Dogs tolerated voriconazole administered orally at 6 mg/kg with a C_{max} of 3.07 µg/mL, while cats tolerated 4 to 6 mg/kg, resulting in a C_{max} of 2.2 µg/mL without showing adverse effects. Dogs showed a shorter $t_{1/2\beta}$ (3.13 h) than cats (40.50 h), but both maintained detectable plasma concentrations 24 h post-administration (12, 13). When dealing with aquatic mammals, belugas (*Delphinapterus leucas*) treated orally with voriconazole at 3 mg/kg twice daily, reached plasma concentrations of 2 µg/mL, which were effective for the treatment of *Fusarium solani* infections in this species (14). In avian species, African penguins (*Spheniscus demersus*) given oral voriconazole at 5 mg/kg, attained a C_{max} of 1.89 µg/mL, with an extended elimination phase lasting 10.92 h (15). There seems to be great interspecific variability in voriconazole tolerance in reptiles. Deaths of cottonmouth snakes (Agkistrodon piscivorous) were reported 12 h after subcutaneous administration of 5 mg/kg. Other reptile species, including green sea turtles (*Chelonia mydas*), western pond turtles (*Actinemys Marmorata*), and red-eared sliders (*Trachemys scripta elegans*), have tolerated voriconazole well at subcutaneous and/or oral doses of 10 mg/kg (16–19). These interspecific variations underscore the limitations of interspecific drug and dosages extrapolation, while showing the importance of performing pharmacokinetic, pharmacodynamic and toxicity studies in the different animal groups and species.

Very limited information is available for azole use in fish, with a miconazole study in cyprinids (*Labeo rohita*) revealing no adverse effects after oral administration of 25.22 mg/kg, reaching a C_{max} of 20.28 µg/mL, with an extended elimination half-life of 77 h (20). When focusing on elasmobranchs, voriconazole is mainly prescribed orally at dosages ranging from 5 to 50 mg/kg every 12 h; recent studies even recommend oral dosages of voriconazole over 50 mg/kg in sharks, with therapeutic drug monitoring (6). In addition, there are empirical reports of satisfactory results after the parenteral administration of voriconazole at 4 mg/kg intramuscularly every 48 h to lesser devil rays (*Mobula hypostoma*) and 4 mg/kg intravenously at a single dose to a Bonnethead shark (*Sphyrna tiburo*) (21). The mentioned medical reports dealing with fungal infections in elasmobranchs emphasize the lack of scientific information in this field and show that the determination of species-specific voriconazole pharmacokinetics in sharks is needed. Considering that the extrapolation of pharmacotherapeutic protocols is very limited in fish, the initial step toward establishing safe and effective dosing regimens in these animals is the conduction of pharmacokinetic studies.

Recent studies have advanced in the field of pharmacokinetic research in elasmobranchs, establishing safe and efficient methodologies applicable to the study of various drugs (7, 22–24). These investigations have revealed significant interindividual

variabilities and low oral absorption of certain drugs in elasmobranchs, prompting consideration of alternative parenteral administration routes such as intramuscular injection (22–25). Oral administration in elasmobranchs has proven challenging and can be voluntary or forced; voluntary administration depends on the animal to voluntarily eat the piece of food loaded with the medication and has the problem that when sharks and rays are sick, they often develop anorexia. The second option for oral administration is forced feeding via delivering whole food items using tongs or via gavage administration, which require the capture and restraint of the animals and often leads to regurgitation of the medication (7). The combination of a short esophagus and a large, expandable stomach enables elasmobranchs to store large prey or quantities of food (26). These anatomical features allow them to easily regurgitate items that they cannot digest, posing a complication when administering drugs orally and producing great interindividual variations in pharmacokinetic studies administering the medication orally (24). Detailed observation of the animal is necessary after administration to prevent voluntary regurgitation, whether associated with handling or not (7). Additionally, the difficulty of a lack of scientific data for these species is increased as previous pharmacokinetic studies have shown great interspecific differences in the pharmacokinetic properties for some drugs in this group of animals (23). This is concerning, as the efficacy of antifungal treatments is strongly related with the maintenance of optimal drug levels in plasma (8, 27). Given the difficulties associated with oral administration, together with the high oral doses required in sharks (30–50 mg/kg), parenteral administration may offer a more efficient option in elasmobranchs, allowing dosage reductions while maintaining elevated plasma concentrations. Despite being in an early stage, the possibilities for research and pharmacokinetic studies of antifungals in sharks and rays are very broad.

Voriconazole is available in oral formulations (tablets and suspension) for human use, as well as solution for intravenous administration; intravenous voriconazole, despite only being available for human use, has been also administered intramuscularly and subcutaneously in different animal species without showing adverse effects (12, 13, 15–17, 28). The application of voriconazole in elasmobranchs for clinical purposes, while currently limited, shows promise as an efficacious treatment for fungal infections. Nevertheless, there is a need for comprehensive investigations into the pharmacokinetics, pharmacodynamics, and toxicity profiles to thoroughly evaluate the viability of azoles in these unique species. This study intended to provide some light in this matter, evaluating the pharmacokinetic profile of voriconazole in elasmobranchs following administration via less frequent routes: the pharmacokinetic study of intravenous and intramuscular administrations.

Materials and methods

This experimental study was designed as an observational, prospective, consecutive study with a washout period of 8 weeks. The processes related to the management of animals and the collection of samples were executed in conformity with and received authorization from the Animal Care and Welfare Committee at the Oceanogràfic of Valencia, as well as the Generalitat Valenciana, with the project identification codes OCE-22-19 and 2024-VSC-PEA-0091.

Animals and experimental conditions

A group of six adult undulate skates (*Raja undulata*) (3 males and 3 females) were included in this study. These skates had been housed and cared for within the Oceanogràfic of Valencia[1] for at least 5 years. The eligibility of these skates for participation was meticulously established through comprehensive health assessments, encompassing clinical histories, physical examinations, hematology evaluations, and plasma biochemistry analyses using analytical records from the aquarium and previously published hematology and plasma chemistry values for the species as a reference (29). These assessments confirmed their overall well-being. Upon the commencement of the study, the weights of all the skates were recorded, exhibiting a weight range spanning from 3.3 to 4.8 kg. The computed mean, accompanied by its standard deviation (± SD), for these weight measurements was documented as 4.13 ± 0.49 kg. Sexual classification was determined based on the presence or absence of claspers, while the categorization of these individuals as adults relied on their size, in accordance with established adult size ranges that had been previously documented (30, 31). Furthermore, all specimens exhibited evidence of reproductive activity, substantiated by frequent observations of male–female mating encounters and the deposition of eggs by female individuals.

During the pharmacokinetic (PK) study, the skates were temporarily relocated to 10,000-liter cylindrical tanks situated within the quarantine facility of the aquarium. The environmental conditions within these tanks were rigorously controlled, featuring: 12 h artificial light cycle followed by a 12 h darkness period; a constant water temperature maintained at 18°C; a salinity of 34 g/L in the water; pH levels maintained within the range of 7.9 to 8.1; negligible ammonia presence and a maximum nitrite and nitrate concentration of 0.05 ppm and 50 ppm, respectively. Furthermore, temporary tanks included access to shaded areas and environmental enrichment opportunities for resting. The feeding regimen consisted of providing the skates with previously thawed portions of teleosts and cephalopods once daily, six days per week, with a minimum fasting period of 24 h prior to the initiation of the study. Throughout the study, vigilant visual monitoring was conducted to promptly identify any potential clinical abnormalities associated with the handling process, blood collection procedures, or drug-related toxicity.

Experimental protocol and sampling

This study used a single dose of 4 mg/kg, rather than the much higher dose prescribed orally (30–50 mg/kg every 12 h) in previous clinical case reports with elasmobranchs because this low dose administered intramuscularly to different ray species had already produced a decrease in the fungal load and an improvement of the clinical signs in previous reports (6, 21). In addition, a pilot study with 4 mg/kg IM voriconazole using two adult undulate skates at Oceanogràfic had already showed plasma concentrations considered clinically effective in elasmobranchs.

Voriconazole was administered at a single dose of 4 mg/kg to all six undulate skate individuals via intravenous (IV) and intramuscular

1 http://www.cac.es/oceanografic

(IM) route, with a washout period of eight-week between studies. For both administration routes parenteral voriconazole (Voriconazole Normon® 200 mg powder for injection, Barcelona 08013, Spain) was diluted to a concentration of 20 mg/mL using sterile water for injection and administered using a 23-gauge (0.6 × 25 mm) needle attached to a 1 mL syringe. Voriconazole dosages ranged from 13.2 mg to 19.2 mg, and injection volumes ranged from 0.66 mL to 0.96 mL. Skates were carefully captured with a rubber net and manually restrained underwater.

In the case of IV administration, animals were placed in dorsal recumbency to induce tonic immobility (TI). Vascular access was achieved through the caudal vasculature using a ventral approach, and administration was slow and constant, ensuring that vascular access was maintained throughout (5).

For IM administration, animals were kept in a dorsoventral position, with the injection site above water. The injection was performed dorsally, into the pectoral fin musculature (see Figure 1), with the needle inserted approximately 20 mm into the muscle. Pressure was applied at the injection site post-administration to minimize drug leakage (5).

Blood extraction utilized a ventral approach to the caudal vasculature employing a 21-gauge (0.8 × 40 mm) needle attached to a 1-ml syringe. Each skate was positioned in dorsal recumbency to induce TI, optimizing blood collection efficiency while minimizing the risk of muscle damage. The tail and posterior half of the animal were raised to the surface, while the head and gills remained submerged. Blood samples of 0.4 mL each were obtained before voriconazole administration and at specified intervals following voriconazole IV or IM administration: 15, 30 min, and 1, 1.5, 2, 4, 8, 12, 24, and 36 h. All collected samples underwent separate processing.

To ensure that dosing regimes are safe, pharmacological studies should ensure safety, both in terms of drug dosage and potential side effects, as well as possible adverse effects caused by the experimental procedure. The evaluation of skate behavior in this study was conducted by veterinarians and the responsible aquarist, who were familiar with the pretreatment behavior of the animals and visually observed the animals during and after sampling.

FIGURE 1
Injection site (pectoral fin musculature) utilized for the intramuscular (IM) administration of voriconazole in undulate skate (*R. undulata*) during this study (red square). Please observe that the animal is manually restrained dorsoventrally during the drug administration process. Quarantine facilities, Oceanogràfic of Valencia, Spain.

Blood processing

Following blood extraction, samples were directly placed into 1 mL lithium heparin tubes (Aquisel® 1 mL 12 × 55mm, AQUISEL S.L., Abrera 08630, Spain). These samples were stored at 4°C, transported to the aquarium's laboratory, and processed within 45 min of collection. In the laboratory, heparin tubes were centrifuged at 590 g for 5 min at room temperature (24°C) using an Ortoalresa® centrifuge (Ortoalresa® RT106 Na 170,007/01, 132 mm rotor radius, 35-degree angle fixed, Ortoalresa-Alvarez Redondo S.A., Daganzo de Arriba 28,814, Spain). The resulting plasma was collected and transferred to 1.5 mL Eppendorf tubes, which were subsequently frozen at −20°C and dispatched to the Pharmacology and Toxicology Department of the Complutense University of Madrid for the measurement of voriconazole concentrations.

Voriconazole quantification

Voriconazole concentration in each plasma sample was determined using a combination of previously described reverse-phase high performance liquid chromatographic methods, validated for its use in elasmobranch plasma at the laboratory of the Department of Pharmacology and Toxicology of the Complutense University of Madrid (32, 33). In this study, a C18 column (Mediterranean Sea C-18 column; Teknokroma Analítica S.A., Barcelona 08173, Spain) was mounted to the chromatography system (Hitachi High-Tech Corporation; equipped with a 5,160-model injection pump with manual purge valve, 5,280-model auto-injector with cooling unit, and a 100 µL syringe, 5,410-model variable ultraviolet detector, 08210, Barbera Del Valles, Barcelona, Spain). A mixture of Milli-Q® filtered H_2O an Acetonitrile (60:40 [vol:vol]) was used as a mobile phase, which was delivered via an isocratic flow at a rate of 0.8 mL/min. The wavelength of the UV detector was 262 nm. Chromatographic peak integration was employed for drug quantification. In drug concentration measurements, 100 µL of shark plasma were combined with 25 µL $HClO_4$ (1 M). It was vortexed for 1 min, mixed with 400 µL Methanol, vortexed again for 30 s and then centrifuged at max G (14,000 rpm) for 5 min. Finally, 200 µL supernatant were collected and injected into the chromatography system. A calibration curve constructed using methanol solutions of known voriconazole concentrations (ranging from 0.05 to 15 µg/mL), exhibited linear absorbance at the studied concentrations ($R^2 > 0.99$). The limit of quantification was 9 ng/mL, with inter- and intra-assay variability always under 6%. The mean voriconazole recovery rate in undulate skate plasma samples using this protocol resulted 80%, determined by adding known concentrations of voriconazole (Sigma-Aldrich Química SA, Tres Cantos 28,760, Madrid, Spain) to blank undulate skate plasma.

Pharmacokinetic and statistical analysis

The number of animals used in this study was carefully selected using the GRANMO sample size calculator software (version 7.12, REGICOR, IMIM, Barcelona, Spain).

The arithmetic means of the maximum plasma concentration (C_{max}) and the mean time required to attain C_{max} (T_{max}) were directly computed from the plasma concentration profiles acquired during the study.

A non-compartmental analysis was executed using a commercially available software (PK Solutions, version 2.0, Summit Research Services, Montrose, United States) for the estimation of the rest of the PK parameters. The analysis encompassed the determination of several essential pharmacokinetic parameters, notably, the plasma concentration extrapolated to time zero (C_0), the elimination half-life ($t_{1/2\beta}$), the area under the plasma concentration-time curve based on observed data points (AUC_t), the area under the plasma concentration-time curve extrapolated to infinity (AUC_{inf}), and the mean residence time (MRT).

The calculation of absolute IM bioavailability (F) for voriconazole was achieved by comparing the AUC following IM and IV administration. Additionally, two key parameters, the apparent volume of distribution in pseudo-equilibrium conditions (Vd) and the systemic clearance (Cl), were estimated following IV administration. To estimate the Vd and Cl after IM administration, a correction is performed based on the calculated F for this route of administration. The mean absorption time (MAT) was determined as the difference between the MRT for IM administration and the MRT for IV administration.

This article reports plasma concentrations and pharmacokinetic parameters with their corresponding means and standard error of the mean (± SEM). A Mann–Whitney *U* test was run to evaluate statistical differences between both dosing routes, using the statistical software package SPSS Statistics (IBM SPSS Statistics for Windows, Version 25.0. IBM Corp., Armonk, NY, United States). Differences were considered statistically significant when $p < 0.05$.

Results

The administration of voriconazole using IM and IV routes to the undulate skates was well tolerated in all animals and produced plasma concentrations over MIC for the main fungal pathogens affecting elasmobranchs (0.5–2.0 μg/mL) for periods over 12 h for both administration routes.

Voriconazole seemed to be well tolerated following the administration protocols outlined in this study, as all animals exhibited normal levels of activity, appetite, reproductive activity and swimming behavior. No abnormal clinical signs were observed in the animals throughout the studies nor 8 weeks after the conclusion of each study.

Table 1 provides a summary of the pharmacokinetic parameter estimates for voriconazole administration at a dose of 4 mg/kg, both intravenously (IV) and intramuscularly (IM). The average plasma concentrations following IV and IM administration of voriconazole to *R. undulata* are depicted in Figure 2.

Voriconazole showed a rapid absorption after IM administration, with a T_{max} of 1.33 ± 0.37 h, and a MAT of 4.56 ± 1.03 h. Bioavailability for IM administration was 64.67 ± 11.47%. No statistical differences were detected for drug distribution, with a Vd of 1.12 ± 0.14 L/kg for IV and 0.98 ± 0.10 L/kg for IM administration ($p = 0.485$; Mann–Whitney *U* Test); these values are close to 1 L/kg and suggest that the drug has a good distribution across the entire organism, without apparent accumulation in any tissue. Elimination was slow and progressive after both IV and IM administrations, with similar rates for both dosing routes ($t_{1/2\beta}$ = 11.18 ± 1.32 and 9.59 ± 1.38 h, respectively; and MRT = 13.17 ± 2.09 and 14.43 ± 2.19 h, respectively). Furthermore, after incorporating the value of bioavailability into the systemic clearance calculation following IM administration, the values of this parameter did not differ statistically from those estimated for the IV route ($p = 0.394$; Mann–Whitney *U* Test), resulting 69.2 ± 3.0 mL/h/kg for IV and 78.6 ± 11.9 mL/h/kg for IM administration (Figure 3).

Discussion

When it comes to selecting the most appropriate active compound and the dosing regime, veterinary clinicians working with elasmobranchs still face the challenge of lacking reliable and accurate scientific data in the field of pharmacology and pharmacotherapeutics for most of the drugs prescribed in sharks and rays (6, 7). To the authors knowledge, this is the first pharmacokinetic study with voriconazole in fish. The promising pharmacokinetic results obtained in this study, together with the great interspecific drug kinetic differences observed for other medications in teleost and elasmobranchs, even for species with similar biological and ecological characteristics, justify the development of further pharmacokinetic studies with voriconazole in different fish species (23).

As previously mentioned, azole antifungals frequently represent the primary choice for both preventing and treating invasive fungal infections; they are frequently administered for extended durations, spanning from weeks to months. The prolonged use of azoles is linked to adverse effects such as hepatotoxicity, hypokalemia, hyponatremia, hormone-related impacts, and rarely, adrenal insufficiency (34). Given that elevated plasma levels of voriconazole have been associated with an elevation in hepatic enzymes and hepatotoxicity, trough concentrations of voriconazole should be monitored not only to ensure successful antifungal therapy but also to avoid hepatic damage (35). Access to pharmacokinetic testing can be limited in veterinary medicine and especially in the clinical management of elasmobranchs. Having access to pharmacokinetic data in multiple different species can assist in conservatively developing the best regimen for a given species, recognizing that interspecies differences can be significant (7, 36).

A limitation to our study was that in an effort to decrease the total blood volume to be collected from the animals during the pharmacokinetic study (only 0.4 mL per sample), no complete blood analysis was performed. Further studies evaluating the pharmacokinetics of voriconazole in elasmobranchs should include routine blood tests (eg. hematology, plasma chemistry, plasma protein electrophoresis) to assess for subclinical impacts on organ function and animal health. It is important to note that blood analyses in a single dose study such as the one performed, while offering valuable insights into potential adverse effects of concurrently administered drugs and aiding in the evaluation of acute toxicity alongside pharmacokinetic studies, do not comprehensively evaluate the impact of voriconazole on hepatic function (34, 35, 37).

Despite the great interindividual and interstudy differences observed with oral drug administration in sharks and rays, oral dosing is still the most common administration route for voriconazole in elasmobranchs (21). Results provided by this study are relevant for aquatic animal veterinarians and researchers because they present novel data on the PK properties of voriconazole in elasmobranchs, evaluating two less frequent

10.3389/fvets.2024.1376851

TABLE 1 Pharmacokinetic parameters of voriconazole administered at a single dose of 4 mg/kg IV or IM in undulate skates (*R. undulata*; *n* = 6) maintained under human care.

		IV administration (*n* = 6)	IM administration (*n* = 6)			
Parameter	Unit	Mean	SEM	MEAN	SEM	*p*
C_0	μg/ml	27.19	7.15	–	–	–
T_{max}	h	–	–	1.33	0.17	–
C_{max}	μg/ml	–	–	2.98	0.28	–
$t_{½β}$	h	11.18	1.32	9.59	1.38	0.485
AUCt*	h•μg/ml	47.46	3.39	27.92	5.06	0.026
AUCinf*	h•μg/ml	58.14	2.79	37.60	6.67	0.041
MRT	h	13.17	2.09	14.43	2.19	1.000
Vd	L/kg	1.12	0.14	0.98	0.10	0.485
Cl	ml/h/kg	69.2	3.0	78.6	11.9	0.394
F	%	–	–	64.67	11.47	–
MAT	h	–	–	4.56	1.03	–

T_{max}, time required to achieve maximum plasma concentration; C_0, extrapolated concentration at 0 h after IV administration; C_{max}, maximum plasma concentration; $t_{1/2}$ β, elimination half-life; AUC_t, area under the plasma concentration curve computed using observed data points only; AUC_{inf}, area under the curve extrapolated to infinity; MRT, mean residence time; Vd, distribution volume in pseudo-equilibrium conditions; Cl, clearance; F, bioavailability; MAT, mean absorption time. * Indicates the presence of statistically significant differences ($p < 0.05$; Mann–Whitney U test) between IV and IM administration protocols.

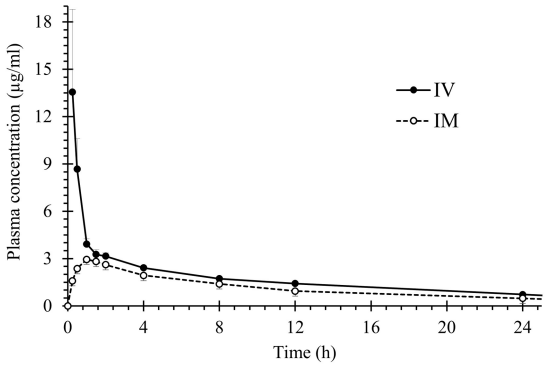

FIGURE 2
Mean ± SEM plasma concentrations of voriconazole in undulate skates (*R. undulata*; *n* = 6) after administration of a single IV (solid circles, continued line) or IM dose (open circles, discontinued line) (4 mg/kg).

administration routes: intravenous and intramuscular administration. This study suggests that the selection of an intramuscular administration route could allow a significant reduction in the dosages of voriconazole needed to achieve effective plasma concentrations when compared to the posology regimes currently recommended for elasmobranchs (6). The relatively elevated plasma concentrations after the IM administration of 4 mg/kg in the undulate skate (2.98 μg/mL) when compared to those obtained after the oral administration of 50 mg/kg every 12 h in the scalloped hammerhead shark (1.2 μg/mL) suggest that oral bioavailability of voriconazole in elasmobranchs could be limited. This phenomenon has been previously described in elasmobranchs following oral administration of other drugs and active compounds. The cause of the great interindividual variation and low plasma concentrations of orally administered compounds in elasmobranchs requires further study (22). This is important as oral administration is the most frequently used dosing route, because it allows treatment but avoids capture, handling and the potential stress response or capture related injuries (38). Treating diseases elasmobranchs intramuscularly instead of orally, would decrease the possibility of under- or overdosing due to the strong interindividual variations observed. Another important factor that may contribute to limited oral bioavailability of different drugs in elasmobranchs, and would be avoided with intramuscular administration, is pre-systemic elimination or hepatic first-pass phenomenon (39). Studies that quantify drug metabolites in plasma and tissues are needed to determine if hepatic first-pass effect plays a role in interindividual and interspecific differences in drug plasma concentrations in elasmobranchs. Our results reveal that voriconazole is rapidly absorbed in the undulate skates after IM administration, with a T_{max} of 1.33 ± 0.17 h and a MAT of 4.56 ± 1.03 h, leading to high plasma concentrations (Cmax of 2.98 ± 0.28 μg/mL). Elimination seems to be more prolonged in time than absorption, with a Cl of 78.6 ± 11.9 mL/h/kg. These auspicious PK results could support the prescription of multiple-dose treatment protocols, in which voriconazole could be administered every 12 h under the studied conditions. Although our results are promising the following factors should be considered with regard to the intramuscular administration of voriconazole in this study.

Drug leakage following intramuscular administration of medications in elasmobranchs is a known issue and must be considered in this study, though manual pressure was applied and no leakage was appreciated. This could have reduced the bioavailability and drug plasma concentrations, as previous studies have reported in teleost and elasmobranch fish (7, 22). Future research goals include quantifying the amount of drug expelled from the injection site and exploring strategies to minimize leakage

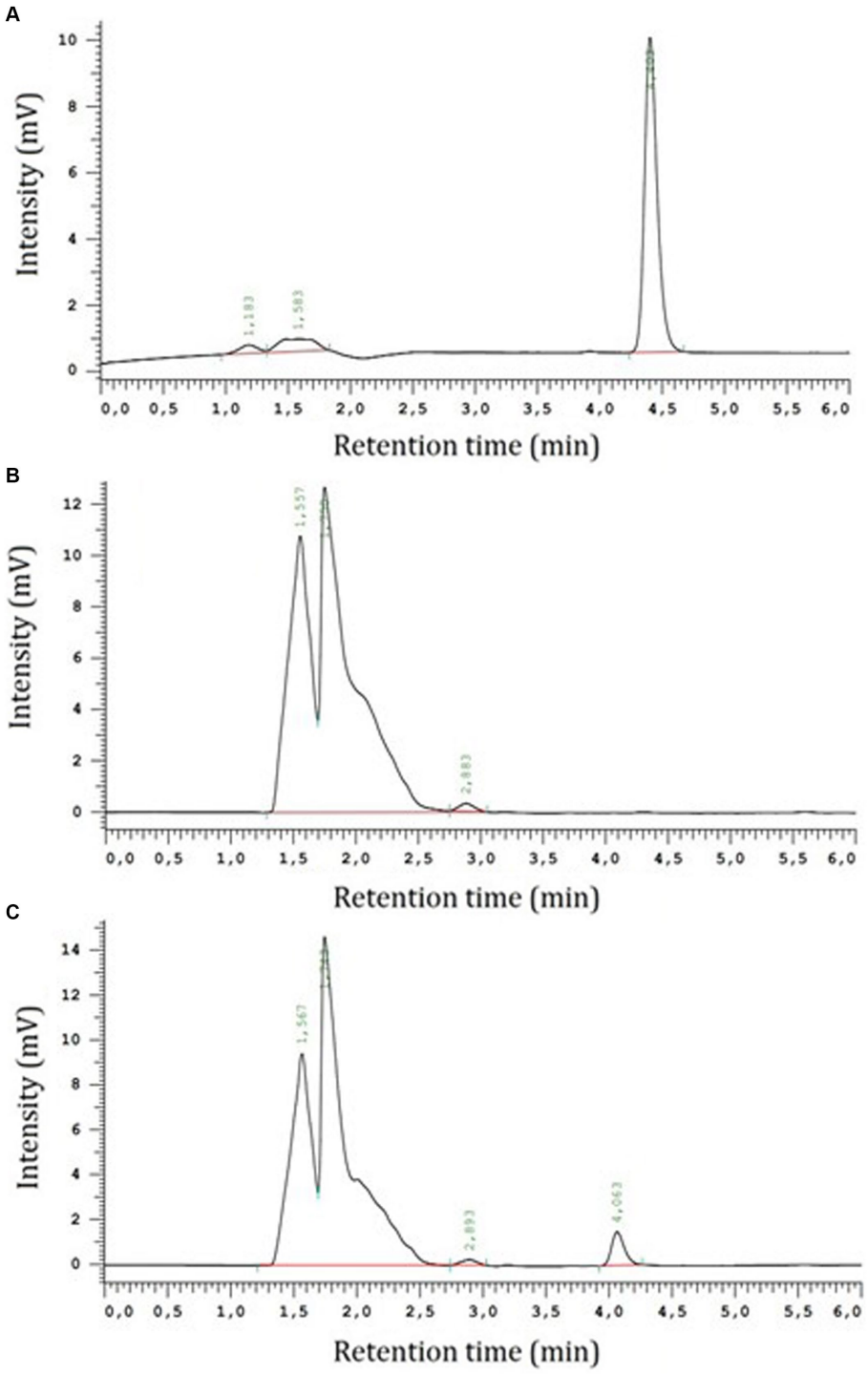

FIGURE 3
Representative chromatograms of voriconazole (Sigma-Aldrich Química SA., Tres Cantos 28,760, Madrid, Spain) at 5 µg/mL concentration in methanol, retention time was 4.40 min and AUC was 67,484 AUFS·min^{-1} **(A)**; blank undulate skate (*R. undulata*) after processing using the methodology described by Blanco Dorado et al. (32) and Zhang et al. (33) **(B)**, plasma and a sample containing voriconazole at 5 µg/mL concentration in undulate skate plasma after processing using the methodology described by Blanco Dorado et al. (32) and Zhang et al. (33); retention time was 4.06 min and AUC was 10,474 AUFS·min^{-1} **(C)**. Hitachi High-Tech Corporation, 08210, Barbera Del Valles, Barcelona.

if detected, such as sealing the injection site, using higher concentration formulations or distributing the dose across multiple injection sites. However, it should be noted that the main goal of this study was to evaluate the PK of voriconazole replicating the current administration protocols for voriconazole in elasmobranch clinical management.

Another pharmacological phenomenon which has been described in fish and which could be also reducing drug bioavailability after

parenteral administration in elasmobranchs is the renal portal system, which collects blood from the caudal fin, which then passes through the kidneys before returning to the heart; this can increase nephrotoxicity or pre-systemic renal excretion and modify their distribution (23, 39). Given that the recommended site for intravenous administration in elasmobranchs is the caudal vessels and for intramuscular administration it is the epaxial musculature lateral to the dorsal fin (also in the caudal half of the animal), this administration may be affected by the renal portal system, and its effect must be taken into account in further studies. Future research goals include the studying the PK differences between the administration in the cranial and caudal halves of sharks and rays. Therefore, future trials would be necessary to rule out a possible interaction of the renal portal system in the distribution and elimination of certain drugs such as voriconazole in this group of animals.

Clinicians should note that in the context of fungi, a robust correlation between *in vitro* minimum inhibitory concentration (MIC) levels and effective *in vivo* drug concentrations is often elusive (6, 27, 35). This discrepancy can be attributed to various factors influencing the complex dynamics of drug interactions within a living organism, making it challenging to predict the *in vivo* effectiveness based solely on *in vitro* MIC values (8). Consequently, comprehensive, and context-specific assessments are essential to better understand and optimize the therapeutic outcomes of antifungal treatments.

Former studies with voriconazole have shown that metabolism can significantly influence the kinetic behavior, revealing a substantial reliance on the functionality of certain cytochrome P450 enzymes, specifically 2C19, 2C9, and 3A4 (40). Earlier studies emphasize the need to carefully explore how drugs are processed by CYP enzymes, cautioning against assuming uniform reactions across various animals. Fish, in particular, exhibit unique responses compared to mammals in this aspect (41). The role of this enzymatic system in elasmobranchs and its influence on drug elimination is currently unknown, but it could serve as a rationale for explaining the substantial kinetic differences observed following oral administration of various drugs in this group of animals. The hepatic characteristics also exhibit great interspecific variability, with elasmobranchs manifesting a liver constituting a substantial proportion, up to 23% of their total body weight, primarily comprised of lipids. In addition, elasmobranchs lack cavitary adipose tissue and opt for hepatocytes as the primary site for lipid storage (42). This distinctive hepatocellular lipid storage, in conjunction with the extent of liver cell exposure and lipid concentration, introduces considerable nuances in drug pharmacology within elasmobranchs (35, 43). The likelihood of a progressive decline in plasma concentrations to suboptimal drug levels during prolonged treatment necessitates systematic monitoring to ascertain and address the implications of enzymatic induction on the drug's metabolism.

Furthermore, it should be considered that the clinical management of fungal diseases in this group of animals must have a multimodal approach (3–6). First, environmental considerations should be implemented to slow down the advancement of the disease and attempt to cure the animals; these environmental interventions include an adjustment of salinity while still maintaining a range compatible with the species survival; temperature regulation; and an increase in oxygen saturation (5). The clinician working with teleost and elasmobranchs should be conscious that variations in water temperature and salinity can produce differences in drug absorption, distribution, metabolization and excretion (7, 44). Given that temperature regulation is a key consideration when treating fungal diseases in fish and that variations in environmental temperature can produce differences in drug PK parameters, further studies should evaluate how temperature affects voriconazole absorption, distribution and elimination in the different elasmobranch species, as this could be key to achieve clinically effective concentrations in plasma and tissues.

Food supplementation with vitamins and immunostimulants is also frequently considered to enhance the animal's immunity when dealing with fungal diseases in elasmobranchs (15). Clinicians should consider that this supplementation together with the use of concomitant medication, such as antimicrobials to treat secondary infections, can lead to pharmacological interactions and also have an influence on antifungal pharmacokinetics (8, 27). Future research goals include evaluating the effect of feeding on the kinetics of orally administered voriconazole, given the unique characteristics of their digestive system and the importance of this route of administration in these animals.

As mentioned throughout this article, voriconazole has provided promising pharmacodynamic data and tolerability in different aquatic animals including elasmobranchs (4, 11, 45). This, together with the fact that azole antifungals have proven great efficacy in the pharmacotherapeutic treatment of mycotic infections in fish, justified the selection of voriconazole to be evaluated in our study (4, 5, 46). The results provided by our study suggest that voriconazole could be a promising antifungal drug to be used intramuscularly in elasmobranchs due to its good kinetic properties and tolerance. The data provided in this study provides the first pharmacokinetic basis for intramuscular and intravenous dosing of voriconazole in elasmobranchs, and continues to build the foundation of scientifically based pharmacotherapeutics in this taxonomic group. Results obtained from this study also highlight the important differences in drug disposition among administration routes in this group of animals and underscores the need for future pharmacokinetic and pharmacodynamic studies evaluating the different drug delivery methods in sharks and rays.

Conclusion

Voriconazole administered intravenously and intramuscularly to undulate skates at a dose of 4 mg/kg achieved higher plasma concentrations compared to those reached in other elasmobranch species after the administration of the same drug at dosages up to 50 mg/kg via oral route, while showing no apparent adverse effects. Both IV and IM routes of administration allowed for plasma levels of voriconazole over the *in vitro* calculated MICs for *Fusarium solani* and *Purpureocilium lilacinus* in elasmobranchs for at least 12 h. These results support the use of voriconazole via parenteral administration in undulate skates and justify the study of intramuscular administration in other shark and ray species. Further pharmacodynamic and toxicologic studies should be performed with voriconazole in other elasmobranch species to ensure the efficacy and safety of this drug and the proposed dosing regime.

Data availability statement

The raw data supporting the conclusions of this article will be made available by the authors, without undue reservation.

Ethics statement

The animal study was approved by Animal Care and Welfare Committee at the Oceanogràfic of Valencia. Project identification code OCE-22-19. The study was conducted in accordance with the local legislation and institutional requirements.

Author contributions

DC-C: Conceptualization, Investigation, Methodology, Writing – original draft, Writing – review & editing. CR-S: Methodology, Writing – review & editing. SR-L: Data curation, Formal analysis, Investigation, Writing – review & editing. DG-P: Funding acquisition, Project administration, Resources, Writing – review & editing. TE: Conceptualization, Data curation, Methodology, Supervision, Writing – review & editing. PM-E: Conceptualization, Data curation, Formal analysis, Investigation, Methodology, Resources, Software, Supervision, Writing – original draft, Writing – review & editing.

Funding

The author(s) declare financial support was received for the research, authorship, and/or publication of this article. Funding for this study was provided by the Fundación Oceanogràfic under the project "UCM/Art. 83 631-2022: Farmacocinética de especies acuáticas."

Acknowledgments

The authors would like to thank the Fundación Oceanogràfic for supporting this study under the project reference number OCE-19-22 and under the project "UCM/Art. 83 631-2022: Farmacocinética de especies acuáticas," Oceanogràfic for providing the researchers with the sharks and infrastructure necessary for developing this study. Also special thanks to the team of aquarists and veterinarians working at Oceanogràfic for their excellent work, support and assistance.

Conflict of interest

The authors declare that the research was conducted in the absence of any commercial or financial relationships that could be construed as a potential conflict of interest.

Publisher's note

All claims expressed in this article are solely those of the authors and do not necessarily represent those of their affiliated organizations, or those of the publisher, the editors and the reviewers. Any product that may be evaluated in this article, or claim that may be made by its manufacturer, is not guaranteed or endorsed by the publisher.

References

1. Dove A, Clauss T, Marancik D, Camus A. Emerging diseases of elasmobranchs in aquaria. In: M Smith, D Warmolts, D Thoney, R Hueter, M Murray and J Ezcurra, editors. *Elasmobranch husbandry manual II: recent advances in the care of sharks, rays and their relatives*. Columbus: Ohio Biological Survey (2017). 263–75.

2. Yanong R. Fungal diseases of fish. *Vet Clin North Am Exot Anim Pract*. (2003) 6:377–400. doi: 10.1016/S1094-9194(03)00005-7

3. Smith AG, Muhvich AG, Muhvich KH, Wood C. Fatal *fusarium solani* infections in baby sharks. *J Med Vet Mycol*. (1989) 27:83–91. doi: 10.1080/02681218980000121

4. Hsu LH, Su CY, Sun PL, Chen YL. *Fusarium solani* species complex infection in elasmobranchs: a case report for rough-tail stingray with valid antifungal therapy. *Med Mycol Case Rep*. (2021) 32:34–8. doi: 10.1016/J.MMCR.2021.02.002

5. Lécu A, Herbert R, Tirmarche D, Coulier L, Hénard S. Fighting with fusariosis disease on hammerhead sharks, *Sphyrna lewini*, Griffith & Smith, 1834. *Drum Croak*. (2018) 3:2–16. Available at: http://drumandcroaker.org/pdf/SharkSupplement2-2018.pdf.

6. Hyatt MW. *Management of fusariosis in Sphyrnidae sharks: the ugly, the bad, and the good – IAAAM 2017 – VIN. IAAAM 2017*. Cancun, Mexico (2017). Available at: https://www.vin.com/apputil/content/defaultadv1.aspx?pId=18363&meta=Generic&catId=98258&id=7977700&ind=40&objTypeID=17 (Accessed November 23, 2023).

7. Mylniczenko N. Pharmacology of elasmobranchs: updates and techniques. In: M Smith, D Warmolts, D Thoney, R Hueter, M Murray and J Ezcurra, editors. *The elasmobranch husbandryn manual II: Recent advances in the care of sharks, rays, and their relatives*. Columbus: Ohio Biological Survey (2017). 289–302.

8. Houšť J, Spížek J, Havlíček V. Antifungal drugs. *Meta*. (2020) 10:106. doi: 10.3390/METABO10030106

9. Jordá T, Puig S. Regulation of ergosterol biosynthesis in *Saccharomyces cerevisiae*. *Genes*. (2020) 11:1–18. doi: 10.3390/GENES11070795

10. Delattin N, Cammue BP, Thevissen K. Reactive oxygen species-inducing antifungal agents and their activity against fungal biofilms. *Future Med Chem*. (2014) 6:77–90. doi: 10.4155/FMC.13.189

11. Marancik DP, Berliner AL, Cavin JM, Clauss TM, Dove ADM, Sutton DA, et al. Disseminated fungal infection in two species of captive sharks. *J Zoo Wildl Med*. (2011) 42:686–93. doi: 10.1638/2010-0175.1

12. Lemetayer JD, Dowling PM, Taylor SM, Papich MG. Pharmacokinetics and distribution of voriconazole in body fluids of dogs after repeated oral dosing. *J Vet Pharmacol Ther*. (2015) 38:451–6. doi: 10.1111/JVP.12208

13. Vishkautsan P, Papich MG, Thompson GR, Sykes JE. Pharmacokinetics of voriconazole after intravenous and oral administration to healthy cats. *Am J Vet Res*. (2016) 77:931–9. doi: 10.2460/AJVR.77.9.931

14. Naples LM, Poll CP, Berzins IK. Successful treatment of a severe case of fusariomycosis in a beluga whale (*Delphinapterus leucas leucas*). *J Zoo Wildl Med*. (2012) 43:596–602. doi: 10.1638/2011-0268R1.1

15. Hyatt MW, Wiederhold NP, Hope WW, Stott KE. Pharmacokinetics of orally administered voriconazole in african penguins (*Spheniscus demersus*) after single and multiple doses. *J Zoo Wildl Med*. (2017) 48:352–62. doi: 10.1638/2016-0160R2.1

16. Innis CJ, Young D, Wetzlich S, Whitcomb AJ, Tell L. Plasma concentrations and safety assessment of voriconazole in red-eared slider turtles (*Trachemys scripta elegans*) after single and multiple subcutaneous injections. *J Herpetol Med Surg*. (2014) 24:28–35. doi: 10.5818/1529-9651-24.1.28

17. Wright TL, Gjeltema J, Wack RF, Woodburn D, Tell LA. Plasma voriconazole concentrations following single- and multiple-dose subcutaneous injections in western pond turtles (*Actinemys marmorata*). *J Zoo Wildl Med*. (2021) 52:538–47. doi: 10.1638/2020-0161

18. Lindemann DM, Allender MC, Rzadkowska M, Archer G, Kane L, Baitchman E, et al. Pharmacokinetics, efficacy, and safety of voriconazole and itraconazole in healthy cottonmouths (*Agkistrodon piscivorous*) and massasauga rattlesnakes (*Sistrurus catenatus*) with snake fungal disease. *J Zoo Wildl Med*. (2017) 48:757–66. doi: 10.1638/2016-0179.1

19. Seitz Herrick K, Papich MG, Clarke EO, Micheals LT, Schmitt TL. Pharmacokinetics of single-dose voriconazole in green sea turtles (*Chelonia mydas*). 50th Annual IAAAM Conference. Durban, SA: VIN (2019)

20. Singh M, Saha H, Saha RK. Comparative pharmacokinetics of the orally administered sub-lethal doses of miconazole nitrate in *Labeo rohita*. *Int J Curr Microbiol App Sci*. (2020) 9:3197–210. doi: 10.20546/ijcmas.2020.912.381

21. Mylniczenko N. Appendix 1: elasmobranch formulary. In: M Smith, D Warmolts, D Thoney, R Hueter, M Murray and J Ezcurra, editors. *The elasmobranch husbandry manual II – recent advances in the care of sharks, rays and their relatives*. Columbus, OH: Ohio Biological Survey (2018). 22.

22. Morón-Elorza P, Rojo-Solís C, Álvaro-Álvarez T, Valls-Torres M, García-Párraga D, Encinas T. Pharmacokinetic studies in elasmobranchs: meloxicam administered at 0.5 mg/kg using intravenous, intramuscular and oral routes to large-spotted catsharks (*Scyliorhinus stellaris*). *Front Vet Sci*. (2022) 9:9. doi: 10.3389/FVETS.2022.845555

23. Morón-Elorza P, Cañizares-Cooz D, Rojo-Solis C, Álvaro-álvarez T, Valls-Torres M, García-Párraga D, et al. Pharmacokinetics of the anti-inflammatory drug meloxicam after single 1.5 mg/kg intramuscular administration to undulate skates (*Raja undulata*). *Vet Sci*. (2022) 9:216. doi: 10.3390/VETSCI9050216

24. Kane LP, O'Connor MR, Papich MG. Pharmacokinetics of a single dose of intramuscular and oral meloxicam in yellow stingray (*Urobatis jamaicensis*). *J Zoo Wildl Med*. (2022) 53:153–8. doi: 10.1638/2021-0123

25. Morón-Elorza P, Rojo-Solís C, Álvaro-Álvarez T, Valls-Torres M, García-Párraga D, Encinas T. Pharmacokinetics of the analgesic and anti-inflammatory drug meloxicam after multiple 1.5 mg/kg administration to nursehound shark (*Scyliorhinus stellaris*). *Vet Anaesth Analg*. (2023) 51:71–9. doi: 10.1016/j.vaa.2023.09.072

26. Bucking C. Feeding and digestion in elasmobranchs: tying diet and physiology together. *Fish Physiol*. (2015) 34:347–94. doi: 10.1016/B978-0-12-801286-4.00006-X

27. Peyton LR, Gallagher S, Hashemzadeh M. Triazole antifungals: a review. *Drugs Today*. (2015) 51:705–18. doi: 10.1358/DOT.2015.51.12.2421058

28. Carneiro De Castro IF, Schmidt V, Das SC, Binoy A, Azmanis PN. Safety of an intravenous formulation of voriconazole as an intramuscular injection in pigeons (*Columba livia f. domestica*). *J Avian Med Surg*. (2022) 36:262–71. doi: 10.1647/20-00006

29. Morón-Elorza P, Steyrer C, Rojo-Solís C, Álvaro-Álvarez T, Valls-Torres M, Encinas T, et al. Hematology and plasma biochemistry reference values of juvenile undulate rays (*Raja undulata*) under human care. *J Zoo Wild Med*. (2022) 53:504–14. doi: 10.1638/2021-0140

30. Coelho R, Bertozzi M, Ungaro N, Ellis J. *Undulate skate (Raja undulata). The IUCN Red List of Threatened Species* (2009). Available at: https://www.iucnredlist.org/species/161425/5420694 (Accessed June 18, 2022).

31. Coelho R, Erzini K. Age and growth of the undulate ray, *Raja undulata*, in the Algarve (southern Portugal). *J Mar Biol Assoc U K*. (2002) 82:987–90. doi: 10.1017/S0025315402006495

32. Blanco Dorado S, Maroñas Amigo O, Latorre-Pellicer A, Rodríguez Jato MT, López-Vizcaíno A, Gómez Márquez A, et al. A multicenter prospective study evaluating the impact of proton-pump inhibitors omeprazole and pantoprazole on voriconazole plasma concentrations. *Br J Clin Pharmacol*. (2020) 86:1661–6. doi: 10.1111/BCP.14267

33. Zhang M, Moore GA, Barclay ML, Begg EJ. A simple high-performance liquid chromatography method for simultaneous determination of three triazole antifungals in human plasma. *Antimicrob Agents Chemother*. (2013) 57:484–9. doi: 10.1128/AAC.00768-12

34. Benitez LL, Carver PL. Adverse effects associated with long-term administration of azole antifungal agents. *Drugs*. (2019) 79:833–53. doi: 10.1007/S40265-019-01127-8

35. Ueda K, Nannya Y, Kumano K, Hangaishi A, Takahashi T, Imai Y, et al. Monitoring trough concentration of voriconazole is important to ensure successful antifungal therapy and to avoid hepatic damage in patients with hematological disorders. *Int J Hematol*. (2009) 89:592–9. doi: 10.1007/S12185-009-0296-3

36. Hunter RP, Isaza R. Concepts and issues with interspecies scaling in zoological pharmacology. *J Zoo Wildl Med*. (2008) 39:517–26. doi: 10.1638/2008-0041.1

37. Bhagat J, Singh N, Nishimura N, Shimada Y. A comprehensive review on environmental toxicity of azole compounds to fish. *Chemosphere*. (2021) 262:128335. doi: 10.1016/J.CHEMOSPHERE.2020.128335

38. Davis R. Quarantine and prophylaxis for elasmobranchs. In: M Smith, D Warmolts, D Thoney and R Hueter, editors. *The elasmobranch husbandry manual: captive care of sharks, rays and their relatives*. Columbus: Ohio Biological Survey (2004). 143–50.

39. Gibaldi M, Boyes RN, Feldman S. Influence of first-pass effect on availability of drugs on oral administration. *J Pharm Sci*. (1971) 60:1338–40. doi: 10.1002/JPS.2600600909

40. Hyland R, Jones BC, Smith DA. Identification of the cytochrome P450 enzymes involved in the N-oxidation of voriconazole. *Drug Metab Dispos*. (2003) 31:540–7. doi: 10.1124/DMD.31.5.540

41. Smith EM. *Cytochrome P450 drug metabolism and protein induction and inhibition in fish liver microsomes*. (2009). Available at: https://macsphere.mcmaster.ca/handle/11375/9496 (Accessed December 16, 2021).

42. Holmgren S, Nilsson S. Digestive system in sharks, skates and rays. In: NC Hamlet, editor. *The biology of elasmobranch fish*. Baltimore: John Hopkins University Press (1999). 144–73.

43. Beernaert LA, Baert K, Marin P, Chiers K, De Backer P, Pasmans F, et al. Designing voriconazole treatment for racing pigeons: balancing between hepatic enzyme auto induction and toxicity. *Med Mycol*. (2009) 47:276–85. doi: 10.1080/13693780802262115

44. Samuelsen OB. Pharmacokinetics of quinolones in fish: a review. *Aquaculture*. (2006) 255:55–75. doi: 10.1016/J.AQUACULTURE.2005.12.008

45. Consigny S, Dhedin N, Datry A, Choquet S, Leblond V, Chosidow O. Successsful voriconazole treatment of disseminated fusarium infection in an immunocompromised patient. *Clin Infect Dis*. (2003) 37:311–3. doi: 10.1086/375842

46. Desoubeaux G, Debourgogne A, Wiederhold NP, Zaffino M, Sutton D, Burns RE, et al. Multi-locus sequence typing provides epidemiological insights for diseased sharks infected with fungi belonging to the *fusarium solani* species complex. *Med Mycol*. (2018) 56:591–601. doi: 10.1093/MMY/MYX089

frontiers | Frontiers in Veterinary Science

TYPE Methods
PUBLISHED 13 June 2024
DOI 10.3389/fvets.2024.1410332

Check for updates

OPEN ACCESS

EDITED BY
Alisa Newton,
Ocearch, United States

REVIEWED BY
Nuno Pereira,
Oceanário de Lisboa, Portugal
Carlos Rodriguez,
Walt Disney Parks and Resorts, United States

*CORRESPONDENCE
Ri K. Chang
✉ rchang@mbayaq.org

RECEIVED 31 March 2024
ACCEPTED 04 June 2024
PUBLISHED 13 June 2024

CITATION
Chang RK and Okihiro MS (2024) A practical guide to necropsy of the elasmobranch chondrocranium and causes of mortality in wild and aquarium-housed California elasmobranchs.
Front. Vet. Sci. 11:1410332.
doi: 10.3389/fvets.2024.1410332

COPYRIGHT
© 2024 Chang and Okihiro. This is an open-access article distributed under the terms of the Creative Commons Attribution License (CC BY). The use, distribution or reproduction in other forums is permitted, provided the original author(s) and the copyright owner(s) are credited and that the original publication in this journal is cited, in accordance with accepted academic practice. No use, distribution or reproduction is permitted which does not comply with these terms.

A practical guide to necropsy of the elasmobranch chondrocranium and causes of mortality in wild and aquarium-housed California elasmobranchs

Ri K. Chang[1]* and Mark S. Okihiro[2]

[1]Monterey Bay Aquarium, Monterey, CA, United States, [2]California Department of Fish and Wildlife, Vista, CA, United States

Elasmobranchs are common, iconic species in public aquaria; their wild counterparts are key members of marine ecosystems. Post-mortem examination is a critical tool for disease monitoring of wild elasmobranchs and for management of those under human care. Careful necropsy of the head, with a focus on clinically relevant anatomy, can ensure that proper samples are collected, increasing the chance of presumptive diagnoses prior to slower diagnostic workup. Immediate feedback from a thorough head necropsy allows for faster management decisions, often identifying pathogens, routes of pathogen entry, and pathogenesis, which are current shortcomings in published literature. This article proposes a protocol for necropsy of the elasmobranch chondrocranium, emphasizing unique anatomy and careful dissection, evaluation, and sampling of the endolymphatic pores and ducts, inner ears, brain, and olfactory system as part of a complete, whole-body necropsy. Extensive use of cytology and microbiology, along with thorough sample collection for histology and molecular biology, has proven effective in identifying a wide range of pathogens and assisting with characterization of pathogenesis. The cause of mortality is often identified from a head necropsy alone, but does not replace a thorough whole-body dissection. This protocol for necropsy and ancillary diagnostic sample collection and evaluation was developed and implemented in the necropsy of 189 wild and aquarium-housed elasmobranchs across 18 species over 13 years (2011–2023) in California. Using this chondrocranial approach, meningoencephalitis was determined to be the primary cause of mortality in 70% (118/168) of stranded wild and aquarium-housed elasmobranchs. Etiology was largely bacterial or protozoal. *Carnobacterium maltaromaticum* bacterial meningoencephalitis occurred in salmon sharks (*Lamna ditropis*), shortfin mako sharks (*Isurus oxyrinchus*), common thresher sharks (*Alopias vulpinus*), and one Pacific electric ray (*Tetronarce californica*). *Miamiensis avidus* was the most common cause of protozoal meningoencephalitis and found almost exclusively in leopard sharks (*Triakis semifasciata*) and bat rays (*Myliobatis californica*) that stranded in San Francisco Bay. Bacterial pathogens were found to use an endolymphatic route of entry, while protozoa entered via the nares and olfactory lamellae. Trauma was the second most common cause of mortality and responsible for 14% (24/168) of wild shark strandings and deaths of aquarium-housed animals.

KEYWORDS

elasmobranch, necropsy, stranding, chondrocranium, *Miamiensis avidus*, *Carnobacterium maltaromaticum*, meningoencephalitis, otitis

Introduction

Post-mortem examination is a critical tool for disease monitoring of wild, stranded elasmobranchs and management of sharks, rays, and skates under human care. Necropsies performed with a thorough understanding of taxa-specific anatomy can ensure that appropriate samples are collected, increasing the chance of presumptive diagnoses prior to slower diagnostic workup (e.g., histology, microbiology, and molecular biology), and allowing for faster management decisions. Wildlife necropsy is also a critical tool for disease surveillance and building our anatomic knowledge for understudied species (1, 2).

Elasmobranchs are a common taxa in aquaria and their wild counterparts are key members of their ecosystems (3). Infectious and inflammatory diseases are the most common cause of mortality of aquarium-housed elasmobranchs, with the gastrointestinal tract, gills, and brain being the most commonly affected sites (4, 5). Infectious meningoencephalitis has been reported in wild, stranded elasmobranchs, notably by the scuticociliate protozoa, *Miamiensis avidus*, and Gram-positive bacterium, *Carnobacterium maltaromaticum*, which have caused epizootic and enzootic strandings (6–8). *Miamiensis avidus* and the closely related *Philasterides dicentarchi* have also been implicated in deaths of aquarium-housed elasmobranchs (9–12). Potential routes of entry for pathogens include the endolymphatic ducts, olfactory system, ampullary system, and hematogenous spread, but are often undetermined in the current literature (8–11, 13–15).

This article proposes a protocol for the necropsy of the elasmobranch chondrocranium, emphasizing careful dissection of the endolymphatic pores/ducts, inner ear, brain, and olfactory system, providing methods for gross necropsy, sample collection for microbiology, cytology, molecular biology, and histopathology, and evaluation of wet-mount and stained cytology. The proposed protocol for necropsy and ancillary diagnostic sample collection and evaluation was developed through work with stranded, wild and aquarium-housed elasmobranchs and has been implemented in the necropsy of over 180 sharks and rays across 18 species from 2011–2023. The aim of this article is to highlight clinically relevant anatomy of the elasmobranch chondrocranium and offer guidance to those performing necropsies of animals both under managed care and free ranging.

Materials and equipment

a. *General necropsy instruments* – exact tools will depend on personal preference, but these authors have found Russian tissue forceps or rat-tooth forceps, Brown-Adson tissue forceps, Miltex dressing forceps, Mayo blunt/blunt scissors, iris scissors, and a #4 scalpel handle to work well. A large supply of sterile disposable #20 scalpel blades is necessary as blades will dull quickly when cutting skin and placoid scales. A #3 scalpel handle and #10 blades may be sufficient for smaller sharks and elasmobranchs without placoid scales. A heavy, fixed blade knife also has utility for some larger animals. A tissue spatula or other flat to slightly curved instrument for removing the brain is helpful. Disinfection materials, such as Clorox™ disinfecting wipes or 70% isopropyl alcohol on gauze, are used to minimize external contaminants prior to culture. General necropsy personal protective equipment, including eye protection, is a must.

b. *Fluid sampling* – these tools are used for the sterile collection of fluids for cytologic, molecular biologic (e.g., PCR and metagenomic next generation sequencing) and microbiologic analysis. Sterile disposable transfer pipettes (1 and 5 mL), with tips small enough to enter the inner ear or sterile syringes (0.5, 1, or 3 mL) and needles (20, 22, or 25 gauge) are essential. Subcutaneous tissues surrounding endolymphatic ducts may not hold enough fluid to be easily collected and a cotton-tipped applicator may be useful in these instances. One mL cryovials are needed to store, freeze, and ship molecular biology samples.

c. *Cytology and light microscopy* – a high quality binocular light microscope, with 4, 10, 20, and 40× plan achromatic dry objectives, is recommended. An ocular micrometer (to measure pathogen size), 60× dry, and 100× oil immersion objectives are also desirable. Dark-field condensers are extremely useful for identifying host cells and microorganisms in wet-mount cytology preparations. If a dark-field condenser is unavailable, the standard microscope condenser can be lowered to help visualize pathogens and host cells. Phase contrast may also highlight cells and pathogens, but is often less useful and more confusing than dark-field. Cytology samples are prepared on conventional 25 × 75 mm glass slides with glass coverslips.

d. *Wright-Giemsa or modified Wright-Giemsa stains* (e.g., Dip Quick Stain by Jorgensen Laboratories, Stain Dip Quick by Covetrus, RAL Diff-Quik™ by Siemens, or HEMA 3® by Protocol/Fisher Scientific) – although not strictly necessary, staining air-dried slides will help identify host cell types, better visualize bacteria and other microorganisms, and allow slides to be archived.

e. *Bacterial and fungal culture* – there are many ways of identifying microbiologic agents. The most inexpensive is to prepare agar plates in-house and submit plates with growth for identification. Tryptic soy agar with 5% sheep red blood cells (blood agar) is typically used for bacterial pathogens and Sabouraud-Dextrose (Sab-Dex) agar for suspect fungal pathogens (16, 17). Blood agar and Sab-Dex are widely available commercially, at minimal expense. For most elasmobranch necropsies, both Sab-Dex and blood agar are used. While plate incubation at the appropriate ambient (i.e., ocean or display enclosure) water temperature is ideal, culture at room temperature has proven adequate for commonly

encountered elasmobranch pathogens in these authors' experience. Although colony morphology, combined with cytology, can often be used to classify and characterize pathogens, isolates are usually sent to outside diagnostic labs for precise identification. Diagnostic labs typically use matrix assisted laser desorption ionization-time of flight mass spectrometry (MALDI-TOF), 16S rRNA PCR, or conventional biochemical identification methods to determine pathogen genus and species.

f. *Histology* – submission of histology samples to a laboratory well-versed in elasmobranch pathology will help to define normal, confirm gross and cytological findings, and provide additional details on pathogens, pathology, and pathogenesis. Supplies include 10% neutral buffered formalin, leakproof containers, and histology cassettes.

g. *Photography equipment* – although digital single-lens reflex (DSLR) cameras may show the greatest detail, with adequate lighting and sample preparation, cell phone cameras and inexpensive point-and-shoot cameras (e.g., Sony Cybershot) are more than sufficient for documenting findings. Small lightweight compact cameras can be used one-handed and are often preferable to heavy DSLRs when the subject matter requires dynamic manipulation (e.g., reflecting the skin or calvarium) to expose a lesion or display a specific anatomic feature. This way manipulation can be done with one hand while taking photos with the other. Emphasis should be on taking high quality photos by (1) clearing the field of interest of debris, (2) blotting dry any pooled liquid (e.g., blood or extradural fluid), (3) using white paper or poster board as a nonreflective matte background, and (4) using diffuse indirect lighting (e.g., avoiding direct sunlight and artificial spotlights). Photos should be taken with and without a metric scale bar, so that the size of lesions and anatomy can be determined. Regardless of ambient lighting, photos should be taken with and without flash, to ensure proper exposure.

Methods

Specimen collection and preparation

Ideally specimens are necropsied as fresh as possible. If there is less than a 72 h delay, keeping the carcass on ice or in a walk-in cold room, but not frozen, is recommended. A longer delay will lead to significant autolysis. If immediate necropsy is not possible, consider freezing the specimen. Although freezing may preclude histopathology interpretation, diagnoses based on cytology, molecular techniques, and microbiology may still be possible.

Prior to necropsy, the animal should be thoroughly cleaned. This is especially important with stranded animals that are often covered by sand, mud, and debris. Spraying with clean saltwater or tap water will remove extraneous material from external skin surfaces, nares, the oral cavity, and gills. Cleaning the animal allows wounds to be accurately assessed and for normal anatomic features to be identified and photographed.

Complete morphometric data should be taken. For sharks, this includes body weight, total and fork lengths, and girth at a minimum. For rays, body weight, total length, disc length and width should be determined. External lesions and parasites should be counted, described, and parasites preserved in 95% ethanol.

Elasmobranch species should be determined by examination of (1) overall body size and shape, (2) dentition, (3) size, shape, and location of fins, and (4) skin pigmentation. Should questions remain as to species identity, a DNA sample (i.e., piece of fin or muscle) can be taken and frozen or preserved in 75–90% ethanol. Determine sex by the presence (male) or absence (female) of claspers. Thorough use of photography during the necropsy is critical for documenting anatomy and lesions. Anatomy varies widely among elasmobranchs and documenting anatomy for each species will help better distinguish normal from abnormal in future necropsies.

Overall necropsy approach

Although emphasis here is on careful dissection of the head and chondrocranium, this is not to imply that the rest of the animal should be ignored. Prioritization of the head is necessary because a full necropsy is time consuming, often requiring more than 8 h to complete, and evaluation of chondrocranium has proven to be diagnostic more often than not. To minimize autolysis, the head can be detached from the trunk and examined separately while the rest of the animal is iced or refrigerated.

Following completion of the chondrocranial dissection, the rest of the animal can be examined in depth. This would include assessment of the branchial cavity and gills, heart, and major coelomic cavity organs. Details of a complete elasmobranch necropsy are beyond the scope of this paper, but the extent of trunk, cardiac, and coelomic cavity exam are usually dictated by finding in the head. If no cause of morbidity and mortality is found in the head, then there is greater emphasis on careful necropsy of the remainder of the animal. In contrast, if a definitive cause of death is found in the head, then more time can be spent on documenting normal anatomy and ancillary lesions or parasites.

Chondrocranial approach

Prior to the start of the chondrocranial dissection, it is first necessary to identify key landmarks: nares, eyes, spiracles, Ampullae of Lorenzini, endolymphatic fossa, and endolymphatic skin pores (ELP; Figures 1–3). Focus should be on location of the endolymphatic fossa (Figure 2), which defines the cranial vault, and the ELPs, which are openings for the endolymphatic ducts (ELD; Figures 3, 4) (18).

The most ergonomic approach is to sit in front of the head facing caudal. Locate the ELPs (Figures 3, 4), which connect to the inner ears via the ELDs (Figures 4, 5). These paired pores sit just off midline, typically caudal to the eyes, and dorsal to the spiracles. Morphology and location vary widely across species, but the ELPs are typically quite small (e.g., <1–2 mm in diameter), especially in sharks (Figure 3) (18). Skin pores for Ampullae of Lorenzini and the cephalic lateral line system are often similar in size and must be distinguished.

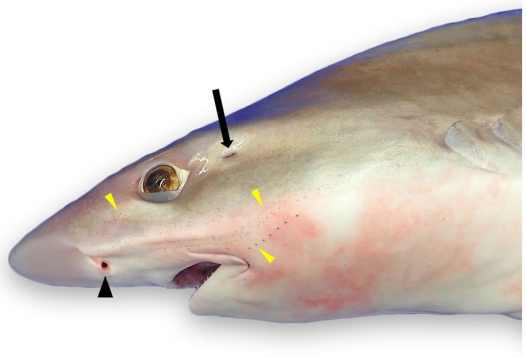

FIGURE 1
External landmarks for chondrocranial necropsy of a tope shark (*Galeorhinus galeus*): naris (black arrowhead), spiracle (black arrow), and numerous ampullae of Lorenzini and/or pores of the cephalic lateral line system (yellow arrowheads).

Identification of ELPs in species with variable skin pigmentation (e.g., leopard sharks, *Triakis semifasciata*) may be difficult or impossible (Figure 3).

If endolymphatic skin pores cannot be visually identified, locate the endolymphatic fossa, a shallow midline oval depression situated dorsally, between the eyes (Figure 2) (18, 19). The endolymphatic fossa is at the apex of the chondrocranium and bounded laterally by the orbits. ELPs are always located at the caudal margin of the fossa. There is no subcutaneous fat or muscle overlying the dorsal aspect of the chondrocranium, so digital pressure can be used to identify the hard margins of the concave endolymphatic fossa. Digital pressure may also cause endolymph with otoconia (crystals in the inner ear that aid in vestibular and auditory sensing) (20, 21) to be expressed from the pores. This will confirm identification of ELPs but does not reliably occur in most species.

Once the ELPs have been identified, the entire dorsal aspect of the head should be cleaned and disinfected using Lysol™ or Clorox™ wipes, or gauze soaked with 70% isopropyl alcohol. Wipes should be moved rostral to caudal, covering the entire endolymphatic fossa and skin pores with large ~4–6 cm margins. At a minimum, disinfect three times, using a new wipe or gauze pad each time.

To maintain an aseptic approach, don new gloves, clean gloves with disinfecting wipes, and use sterile instruments and a new sterile scalpel blade. Make a stab incision lateral to the ELP. Once through the skin, invert the scalpel blade to incise from "inside out" to reduce blade dulling and make a rectangle around the ELPs (~1–2 cm margins around both ELPs) (Figure 6A). Reflect the skin and assess subcutaneous tissues surrounding the endolymphatic ducts (Figure 5). Periductal inflammation is common among stranded sharks; a hemorrhagic subcutis often consistent with trauma. Sample tissues around the ducts for cytology and microbiology. If there is sufficient fluid, collect and freeze for future evaluation. Fix the rectangle of tissue with ELPs and ELDs for histopathology.

Next, extend the skin incisions in all directions to expose the dorsal aspect of the chondrocranium (Figure 6B). The ELPs typically lie directly over the inner ears, which demarcate the caudal aspect of the cranial vault. The goal is to expand the dissection caudally (to the level of the spinal cord) to expose both otic capsules (housing the inner ears) and then laterally and dorsally to expose left and right orbits and midline endolymphatic fossa. The caudal margin of the fossa is characterized by four small foramina (1–3 mm; Figures 2, 4) (18, 19). Connective and/or inflammatory tissue may obscure these openings in the chondrocranium. The smaller rostral pair of round endolymphatic foramina are termination points for the endolymphatic ducts (Figure 4). Ducts are fragile and often severed during the dissection (Figure 5). The larger caudal pair of oval perilymphatic foramina are associated with sound conduction and do not have attached external ducts (Figure 4) (18). Excising the dorsal aspect of the orbits and retrobulbar connective tissue is optional but often simplifies the approach to the brain and inner ears, particularly in smaller animals.

Once the top of the chondrocranium is fully exposed (Figure 6B), repeat the disinfection procedure. Additional disinfection is necessary because of potential microbial contamination from inflamed periductal tissues, and the orbital and branchial cavities. Instruments should be similarly disinfected, a new scalpel blade used, and gloves cleaned or changed. In smaller sharks and rays, the calvarium, including the entire endolymphatic fossa and dorsal aspects of both otic capsules, can often be removed in one piece. Holding the scalpel parallel to the table, make a deep 360-degree coronal incision around the periphery of the fossa and through the caps of both otic capsules. The dissection requires cutting through multiple layers of the robust cartilaginous labyrinth of the inner ears (Figure 4) and may involve significant effort and more than one scalpel blade. With larger sharks, the calvarium and otic capsules may be exposed more gradually by shaving off thin slices of chondrocranium until the cranial vault is open and otic capsules exposed (Figure 6C). Collect samples of the extradural fluid (EDF) overlying the brain for cytology, bacterial, and fungal cultures. Typically, the cranial vault is entered before the inner ears are exposed, but the exact order of sampling is irrelevant. Repeat the aseptic sampling for inner ear perilymph (clinically indistinguishable from endolymph and will be subsequently referred to as perilymph).

After sterile samples have been collected, continue shaving down cartilage to cleanly expose the entire brain, inner ears, and olfactory lamellae (Figure 6D). Use nares as landmarks for locating the olfactory capsule and lamellae and ensure that olfactory bulbs and tracts are exposed. The olfactory tracts and bulbs are often quite deep, diving ventral from the olfactory lobes; patience and precision are needed for this deep dissection. Sample the rostral EDF, adjacent to olfactory lobes, tracts, and bulbs, as inflammatory cells and pathogens often settled during prolonged storage prior to necropsy. Rostral EDF and meninges will typically have more inflammation when pathogens use a nasal route of entry.

With all relevant structures exposed (Figures 7–9), examine each for pathology. Inner ear perilymph and endolymph should be clear to slightly straw colored; meninges should be thin and clear, and the brain visible through them. Meningeal and parenchymal vasculature should be non-congested; extradural fluid clear to slightly serosanguinous. The parenchyma of the brain should be pale tan and homogeneous, with a smooth surface, and olfactory lamellae a uniform salmon pink to pale red.

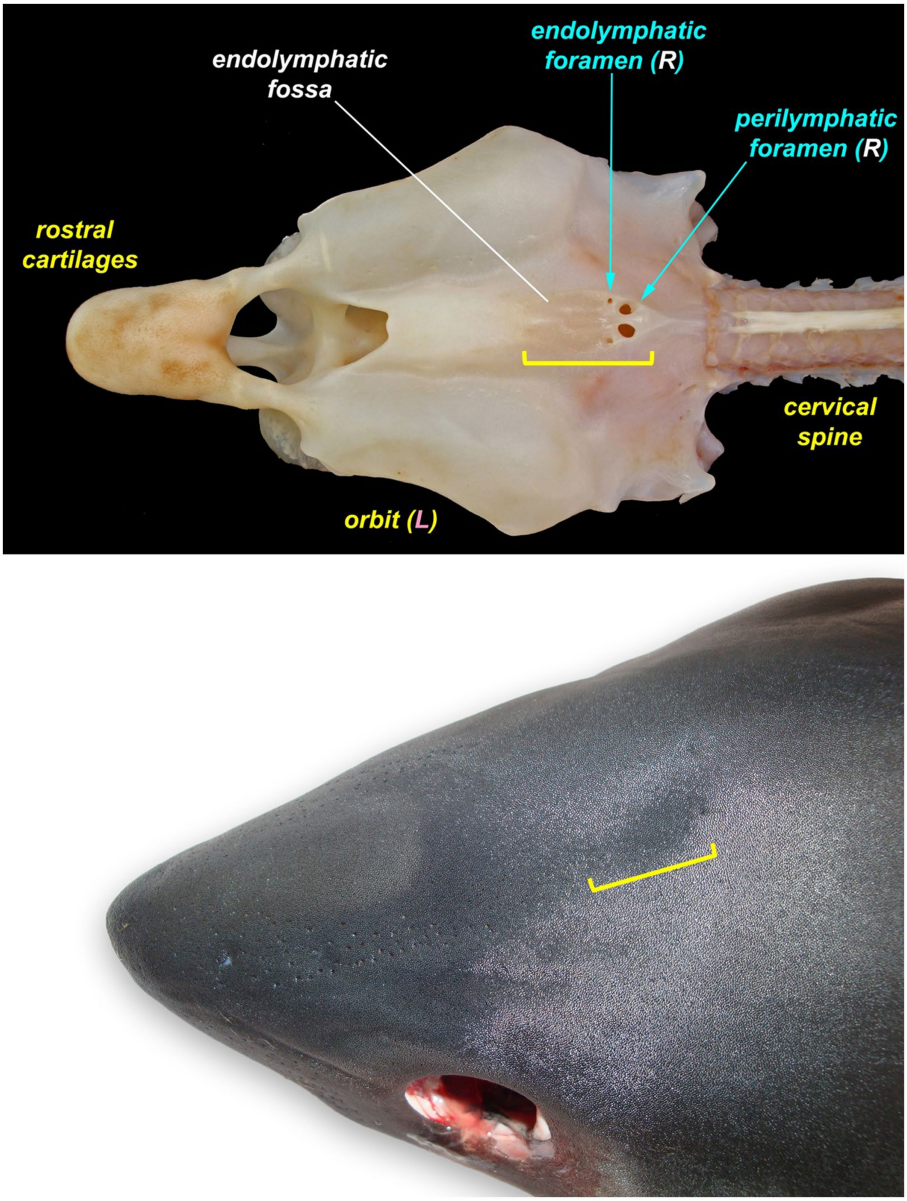

FIGURE 2
The endolymphatic fossa (yellow bracket) of a juvenile salmon shark (*Lamna ditropis*). The endolymphatic fossa is a palpable depression on the dorsal chondrocranium with endolymphatic pores located at the caudal margin. The fossa can be used to identify the location for the initial incision around the endolymphatic pores even when the pores are not visible.

Eyes

After a thorough external ocular exam (assessing conjunctiva, cornea, and third eyelid if present), remove copious gelatinous, retrobulbar connective tissue to expose the six extraocular muscles (22). Evaluate the extraocular muscles for hemorrhage and surrounding tissue for inflammation and hemorrhage. Sever extraocular muscles one-by-one and then apply tension on the globe to expose the optic nerve and optic pedicle. Palpation may be needed to locate and distinguish the optic nerve from the pedicle, a hard cartilaginous extension from the chondrocranium. Cut the optic nerve and optic pedicle to remove the eye. Make a circumferential incision of the globe to evaluate the lens, vitreous and aqueous humor, and retina.

Thymus

The thymus is a bilateral, flattened, red-brown tissue that most commonly lies dorsomedial to the first gill slit (Figure 10) (23). Incise the dermis dorsal to the first gill slit. Removal of the dermis in a larger area may be necessary to locate the unencapsulated organ. The thymus may not be readily apparent, and tends to lie deeper in mature animals (23).

Jaws and oral cavity

Evaluate lips, gingiva, teeth, and oral cavity for trauma or other lesions. This is particularly relevant for wild sharks, as hook injuries

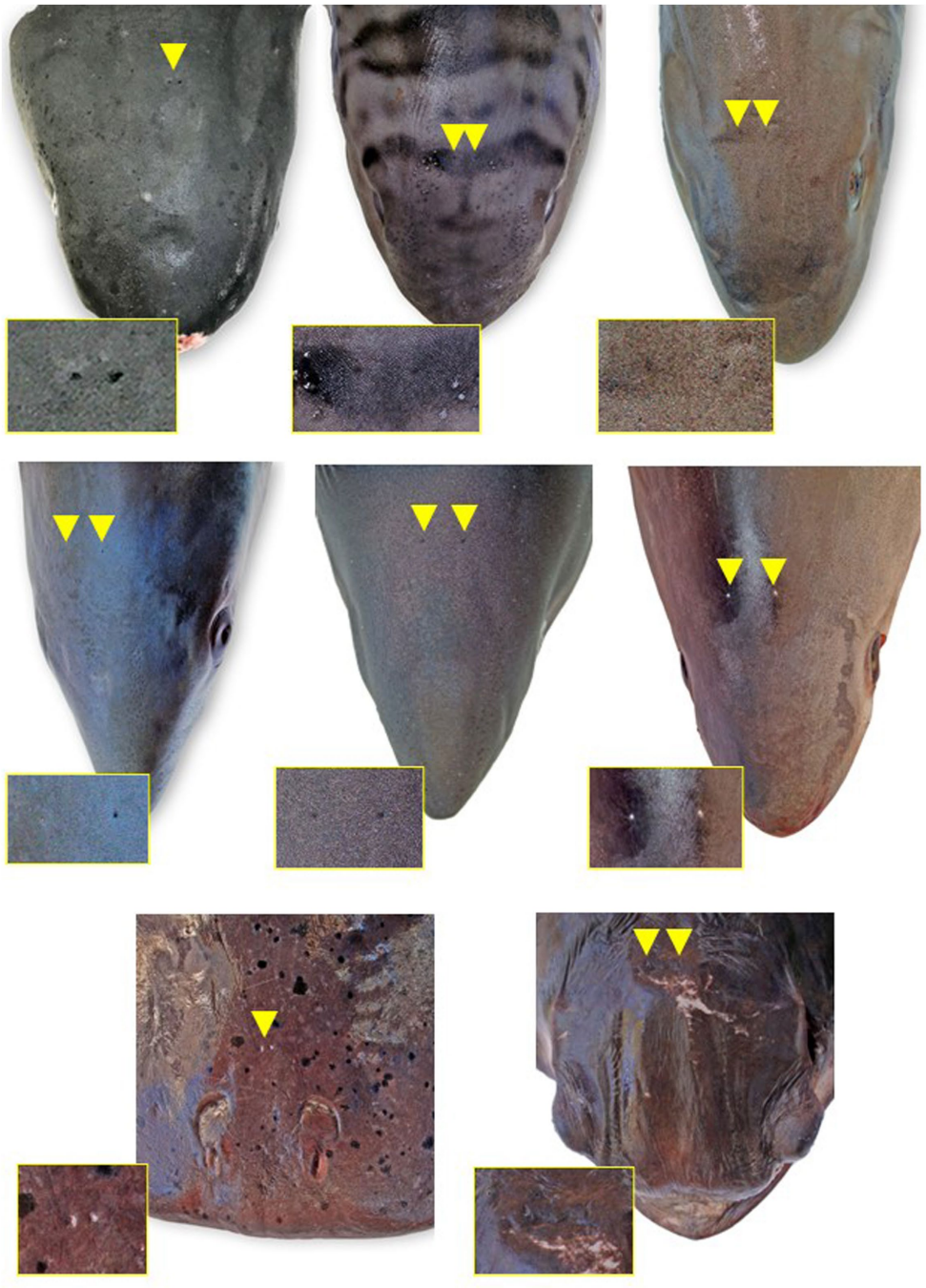

FIGURE 3
Endolymphatic pores (arrowheads and insets) location and morphology across select elasmobranch species. The pores tend to be located just caudal to the eyes and endolymphatic fossa on either side of midline. **(A)** Broadnose sevengill shark (*Notorynchus cepedianus*), **(B)** leopard shark (*Triakis semifasciata*), **(C)** brown smooth-hound shark (*Mustelus henlei*), **(D)** shortfin mako shark (*Isurus oxyrinchus*) (photo angle distorts bilateral symmetry), **(E)** salmon shark (*Lamna ditropis*), **(F)** common thresher shark (*Alopias vulpinus*), **(G)** Pacific electric ray (*Tetronarce californica*), and **(H)** bat ray (*Myliobatis californica*) (photo angle distorts bilateral symmetry).

are common, especially at the commissures. Note any broken or missing teeth.

Thyroid

With the head in dorsal recumbency, make a stab incision along the medial aspect of Meckel's cartilage (lower jaw) and follow the cartilage to make a "V" incision along the cartilage. Incise the interhyoideus, intermandibularis, and coracomandibular muscles, which should expose the thyroid if grossly visible. The thyroid is located within the loose connective tissue between the ventral coracohyoid muscles and the dorsal aspect of the coracomandibular muscles (Figure 11) (24, 25).

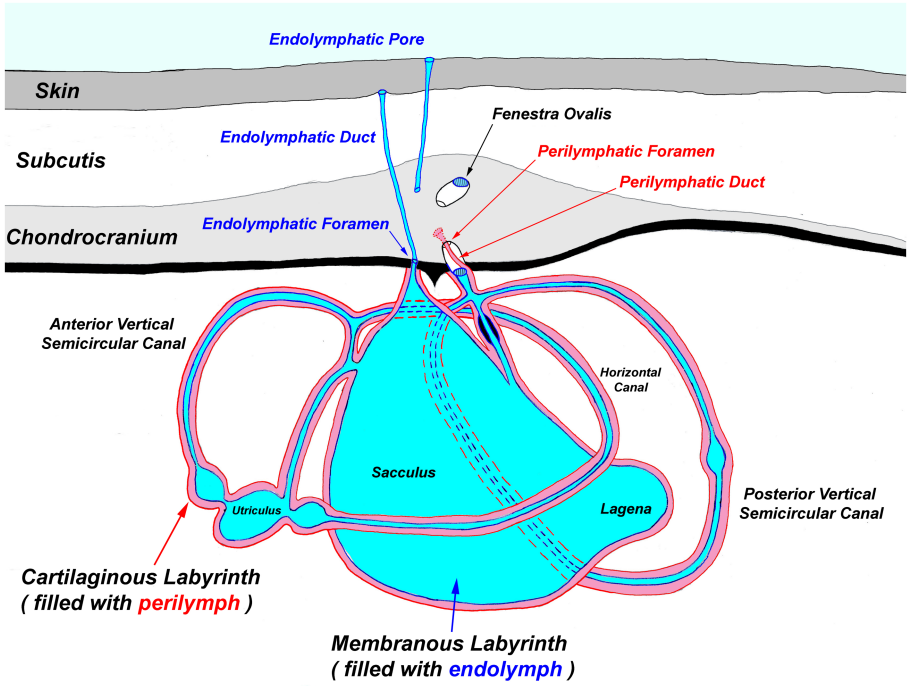

FIGURE 4
Generalized diagram of the elasmobranch inner ear. Notably, the endolymphatic pores and ducts provide direct entry from the external environment to the inner ear.

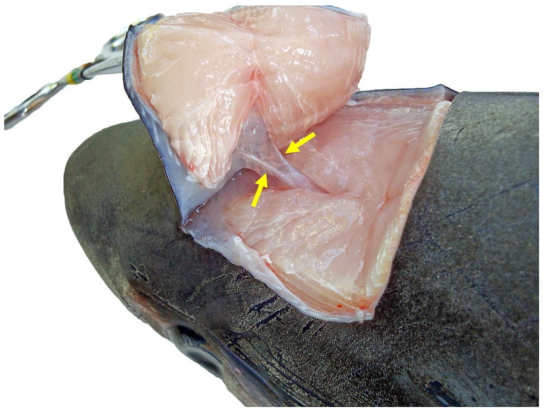

FIGURE 5
Dorsocaudal view of the paired endolymphatic ducts of a common thresher shark (*Alopias vulpinus*) that connect the outside environment and endolymphatic pores to the sacculus of the inner ears.

Microbiology

Three sites are routinely cultured for bacterial and fungal pathogens: (1) subcutaneous tissues surrounding endolymphatic ducts, (2) EDF and meninges overlying the brain, and (3) inner ear perilymph. Cultures are always done first to minimize microbial contamination. If pursuing in-house culture, streak blood agar and Sab-Dex plates following standard microbiological techniques and maintain at room temperature, checking plates daily for growth (17). Colony morphology (e.g., size, shape, color, margins, hemolysis etc.) should be characterized grossly; cellular composition (i.e., microbial size, shape, and motility) assessed via cytology (17). If there is mixed growth, describe major colony types, estimate abundance, and streak unique colonies onto new plates. Pure growth plates or those with minimal contaminants can be submitted for identification, typically via matrix-assisted laser desorption/ionization-time of flight [MALDI-TOF] and/or 16 s rRNA PCR. Alternatively, Amies agar gel transport swabs (e.g., BD BBL™ CultureSwab™ Plus) can be inoculated and submitted for culture at appropriate diagnostic labs.

Cytology

The same three sites cultured for microbial pathogens should also be assessed cytologically. Primary fluid samples include (1) subcutaneous fluid around ELDs, (2) EDF overlying the brain, and (3) inner ear perilymph. As stated above, it is often advantageous to take multiple EDF samples (i.e., an initial dorsal aspirate of fluid overlying the cerebellum and a second rostral/ventral sample from the base of the olfactory lobes). Optional cytology samples include the perichondrial surface of the calvarium (often holding inflammatory exudate), inner ear otoconia from the sacculus (to characterize normal otoconia), and meninges (which may hold larger pathogens, like nematodes).

Fluid cytology aspirates are taken with transfer pipettes or syringes, with or without needles. Thicker exudates are sampled via scraping with a spatula or dull scalpel; tissue samples (e.g., meninges) taken with scissors. Wet mount cytology samples should be mounted onto glass slides and then coverslipped for dark-field exam. Fluid and

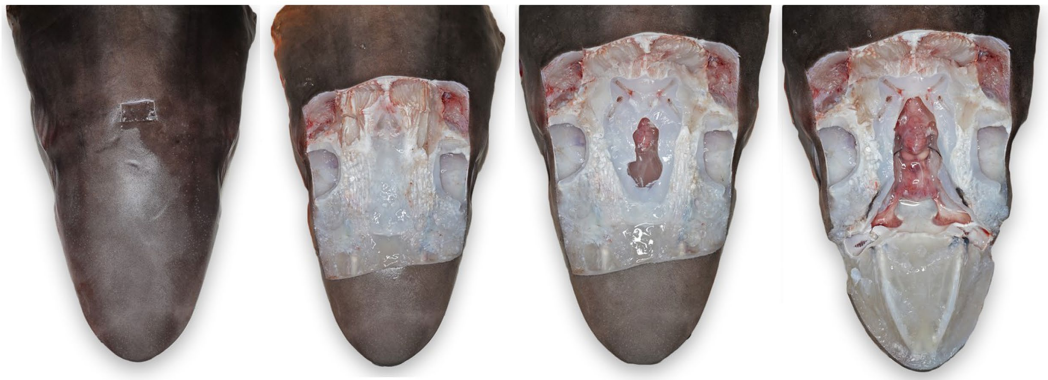

FIGURE 6
Progressive exposure of chondrocranium and brain vault of a tope shark (*Galeorhinus galeus*). **(A)** Initial incision made around endolymphatic pores to sample the tissue surrounding the endolymphatic ducts. **(B)** Extended exposure of dorsal aspect of the chondrocranium, brain vault is not yet exposed. **(C)** Initial exposure of brain and inner ears for sterile sampling of extradural fluid and inner ear perilymph. **(D)** Complete exposure of main chondrocranial structures, including rostral bars, ampullae of Lorenzini, olfactory capsule, brain, and inner ears.

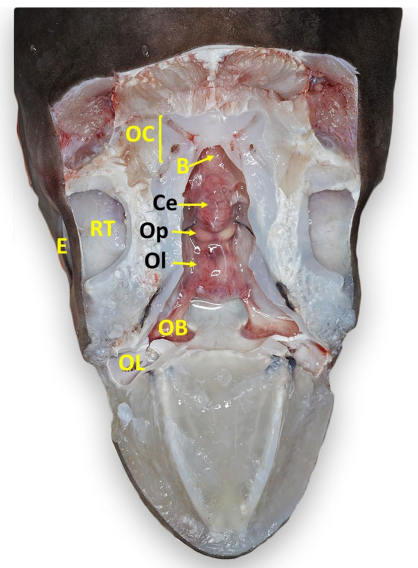

FIGURE 7
Labeled clinically relevant chondrocranial structures in a tope shark (*Galeorhinus galeus*). OL, olfactory lamellae (right); OB, olfactory bulb (right); Ol, olfactory lobe (fused); Op, optic lobe (fused); Ce, cerebellum; B, brainstem; OC, otic capsule (right); E, eye (right); RT, retrobulbar connective tissue (right).

tissue samples should be thin enough to allow identification of inflammatory cell types and unicellular pathogens. Thicker exudates, and microbial colonies from plate agar, can be diluted with saline, prior to coverslipping, to allow for separation of cellular components and easier identification. Allowing clear fluids to settle in cryovials for 10–15 min, prior to sampling, can help maximize detection of pathogens and inflammatory cells.

If dark-field microscopy is unavailable, wet mount preparations can still be assessed by lowering the microscope condenser, closing the condenser aperture, and decreasing available light until cellular detail is discerned. Phase contrast can also be used to help visualize cells and pathogens if dark-field is not available. Wet mount exams allow for immediate assessment of inflammatory response and presence of etiologic agents, especially motile pathogens (e.g., motile bacteria, ciliated or flagellated protozoa).

Cytology preparations (e.g., push or pull smears, tissue imprints, and squash preps) can also be air-dried and stained to provide additional diagnostic material using standard (26). After a small drop is placed on one end of a glass slide, a second slide is used at a 45-degree angle to "push" and spread the fluid over the slide. "Pull smears" are made by placing a fluid sample between two slides and pulling in opposite directions. Tissue imprints are made by gently blotting a tissue dry, then lightly touching tissue samples onto a glass slide multiple times. Squash preps are made by crushing a tissue sample between two slides.

Slides should be thoroughly air-dried or lightly heated prior to alcohol fixation and staining. Use of modified Wright-Giemsa stains allows for greater cell identification, clearer visualization of bacteria and fungi, and creates a durable record if stained slides are dried and coverslipped with permanent mounting media (e.g., Permount®). Stained, coverslipped cytology slides can also be examined with oil immersion objectives (1,000X magnification), increasing diagnostic accuracy.

Histology

For histological sampling of smaller sharks and rays, the entire brain, pituitary gland, inner ears, and olfactory lamellae should be immersion fixed in 10% formalin, along with the ventral aspect of the chondrocranium. Fixing the brain whole, with inclusion of supporting chondrocranial elements (i.e., olfactory capsules, palate, pituitary fossa, and otic capsules), requires extensive dissection, often with a heavy knife, but minimizes excisional damage. This method is also ideal for those animals with friable brains due to autolysis. All tissues should be fixed with at least a 10:1 formalin to tissue ratio.

For larger elasmobranchs, the brain should be separated from the chondrocranium prior to histologic fixation. The decision on whether

FIGURE 8
Comparative elasmobranch chondrocraniums with clinically relevant structures exposed; animals have varying degrees of gross pathology. **(A)** Leopard shark (*Triakis semifasciata*), **(B)** brown smooth-hound shark (*Mustelus henlei*), **(C)** blue shark (*Prionace glauca*), **(D)** common thresher shark (*Alopias vulpinus*) with right rostrum and globes removed, **(E)** shortfin mako shark (*Isurus oxyrinchus*) with eyes removed, **(F)** white shark (*Carcharodon carcharias*), **(G)** Pacific electric ray (*Tetronarce californica*) with olfactory bulbs and lamellae not exposed, **(H)** bat ray (*Myliobatis californica*).

to excise the brain with or without olfactory bulbs is dependent on cerebral anatomy and size. In species with short, thick olfactory tracts (e.g., Triakidae houndsharks), it is best to keep the olfactory bulbs with the rest of the brain. In contrast, animals with long thin olfactory tracts (e.g., white sharks [*Carcharodon carcharias*] and broadnose sevengill sharks [*Notorynchus cepedianus*]), the preferred method is to sever the olfactory tracts, prior to removal of the brain, and leave the olfactory bulbs with the olfactory lamellae (Figure 8).

To remove brains with attached olfactory bulbs, first separate the olfactory bulbs from adjacent lamellae using a scalpel to cut short olfactory nerves bridging the two organs (27). Olfactory nerves are not grossly visible, so incisions are made blindly, leaving the entire olfactory bulb attached to the tract. Once left and right olfactory bulbs are free, the cervical spinal cord can be transected distal to the brainstem. Holding the spinal cord with forceps, and/or using a tissue spatula to support the brain, elevate the brain dorsally to expose cranial nerves. Use scissors or a scalpel to transect cranial nerves close to the chondrocranial cartilage. Inverting the head, or turning it to the side, will allow gravity to expose cranial nerves and ease removal of the brain.

For brains where olfactory tracts are cut and olfactory bulbs left attached to the lamellae, the procedure is essentially the same. The only

FIGURE 9
Labeled clinically relevant chondrocranial structures in a scalloped hammerhead shark (*Sphyrna lewini*) **(A)** gross necropsy and **(B)** drawn representation of cartilaginous and key soft tissue structures. OL, olfactory lamellae (right); C, cerebrum (predominately fused olfactory lobes); Ce, cerebellum; B, brainstem; OC, otic capsule (right); E, eye (right); RT, retrobulbar connective tissue (right).

difference is that olfactory bulbs need to be excised separate from the rest of the brain. In this scenario, olfactory bulbs are excised together with attached olfactory lamellae. A scalpel is used to cut through the olfactory capsule, separating it from the rest of the chondrocranium. The brain, olfactory bulb and lamellae are then fixed in formalin. Large brains may benefit from injecting 10% formalin into the parenchyma or sectioning lobes to expose ventricles and improve fixation (7).

Following removal of the brain, the inner ears and olfactory lamellae can be sampled for histology. Inner ears (semicircular canals and membranous sacs) are sampled using sharp dissection to excise otic capsules (cartilaginous and membranous labyrinths combined) using deep vertical cuts to chop out rough cube-shaped sections of the chondrocranium. In similar fashion, olfactory lamellae are removed via carving out the entire olfactory capsule prior to immersion fixation in formalin.

Trimming tissues for histopathology

Fixed tissues can be trimmed into histology cassettes 48 h after immersion in 10% formalin. Cut tissues into 2–5 mm thick pieces with a sharp, single-edged razor blade following standard protocols for tissue trimming (28, 29). Orient tissues with the side of interest face down in the cassette. Tissues of similar consistency may be included within the same cassette but avoid overcrowding. Small or friable samples should be sandwiched between tissue sponges to prevent loss. Mineralized tissues, such as the endolymphatic pores with surrounding dermal denticles, may require decalcification prior to sectioning.

Skin containing endolymphatic pores and ducts should be trimmed adjacent to one or both pores. Cutting skin with the dermis and subcutis face up will reduce artifacts. To section the brain, we recommend including a sagittal section of each olfactory bulb and olfactory tract (Figure 12, cut 1a and 1b); rostral telencephalon (Figure 12, cut 2); mid telencephalon (Figure 12, cut 3); caudal telencephalon (Figure 12, cut 4); diencephalon and optic chiasm (Figure 12, cut 5); optic lobe and pituitary gland (Figure 12, cut 6); rostral cerebellum, mid optic lobe, and pituitary gland (Figure 12, cut 7); cerebellum, caudal optic lobe, and fourth ventricle (Figure 12, cut 8); cerebellum and brainstem (Figure 12, cut 9); and caudal cerebellum and brainstem (Figure 12, cut 10) (27, 30). Exact sections will vary with different brain morphology.

If olfactory lamellae were fixed together with olfactory bulbs, use sagittal cuts so that trimmed pieces include both organs. If lamellae

FIGURE 10
Thymus (Tm) location in a scalloped hammerhead shark (*Sphyrna lewini*) with brain and eyes removed, from a left dorsal view. The thymus is generally bilateral and dorsomedial to the gills, but exact location varies widely by species and age. The thymus in this shark was more cranial than in other species examined.

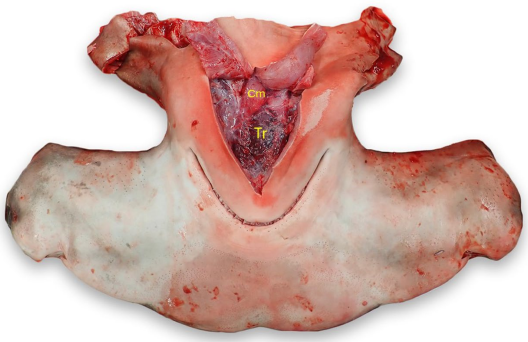

FIGURE 11
Thyroid (Tr) location in a scalloped hammerhead shark (*Sphyrna lewini*). The thyroid is located in loose connective tissue between the coracohyoid muscles (Cm) dorsally and the coracomandibular and interhyoideus muscles laterally and ventrally (reflected).

are fixed separately, either sagittal or transverse sections will work. Inner ear samples should be trimmed to include the sacculus and surrounding otic cartilage. Tissue sponges may be needed to prevent loss of inner ear samples during processing.

Artifact interpretation

Elasmobranchs, particularly stranded animals, often have some degree of autolysis and/or scavenging damage. Both can complicate interpretation of necropsy findings. Scavenging of moribund and dead sharks and rays most commonly affects the gills, globes, and cloaca. Despite scavenging, the chondrocranium, brain, and inner ears are often intact.

Autolysis (i.e., postmortem degradation associated with endogenous and exogenous bacteria, as well has host enzymes and bile) is another common artifact, particularly in stranded and warm water elasmobranchs that are not collected for many hours after death. Autolysis of the brain manifests as tissue softening, loss of integrity, and eventual liquefaction. If cytology and/or culture from an autolyzed brain reveal heavy, mixed bacterial growth, then postmortem bacterial overgrowth can be assumed, which can preclude a definitive diagnosis (31, 32).

Results

Relevant anatomy

All elasmobranch species examined had identifiable ELPs, although they were larger and easier to locate in rays versus sharks (Figure 3). ELPs were often pinpoint and difficult to find in small sharks, particularly tope and leopard. When skin pores could not be readily found, the palpable median endolymphatic fossa was a reliable landmark, providing an initiation point for the dissection and exposure of paired ELDs (Figure 2). Unique to elasmobranchs, these ducts are often overlooked by mammalian and teleost pathologists. Tracing ELDs and careful exposure of the dorsal chondrocranium provided access to both inner ears and brain.

Chondrocranial anatomy was conserved between species, with the endolymphatic fossa defining the apex of the calvarium, and paired perilymphatic and endolymphatic foramina defining the dorsal aspect of the otic capsules. Brain morphology was generally consistent, with all examined shark and ray species having large cerebellums, a relatively small optic tectum, and large fused olfactory lobes (i.e., telencephalon/cerebrum; Figures 7, 8) (33). The primary difference between shark species was with the arrangement of olfactory tracts and bulbs. In broadnose sevengill and white sharks, olfactory tracts were long and thin, with olfactory bulbs located at considerable distance from the rest of the brain. Hound sharks (i.e., leopard, brown smooth-hound [*Mustelus henlei*], and gray smooth-hound [*Mustelus californicus*]), in contrast, had short robust olfactory tracts and olfactory bulbs near olfactory lobes. Differing central nervous system anatomy dictated slightly different approaches to histological sampling.

Causes of mortality

The described chondrocranial approach as the first step of a whole-body dissection was implemented in the necropsy of 189 elasmobranchs, representing 18 shark and ray species, over a 13 year period from 2011 through 2023 (Table 1). Included were necropsies of 156 wild stranded animals, 12 under managed care at five California institutions, and 21 caught by fisherpeople. Meningoencephalitis was found in 70% (118/168) of stranded and aquarium-housed elasmobranchs and was the most common cause of mortality in this study (Table 1). The vast majority of meningoencephalitis cases were due to bacteria (*Carnobacterium maltaromaticum*) or protozoa (*Miamiensis avidus*) (Chang and Okihiro, manuscript in preparation).

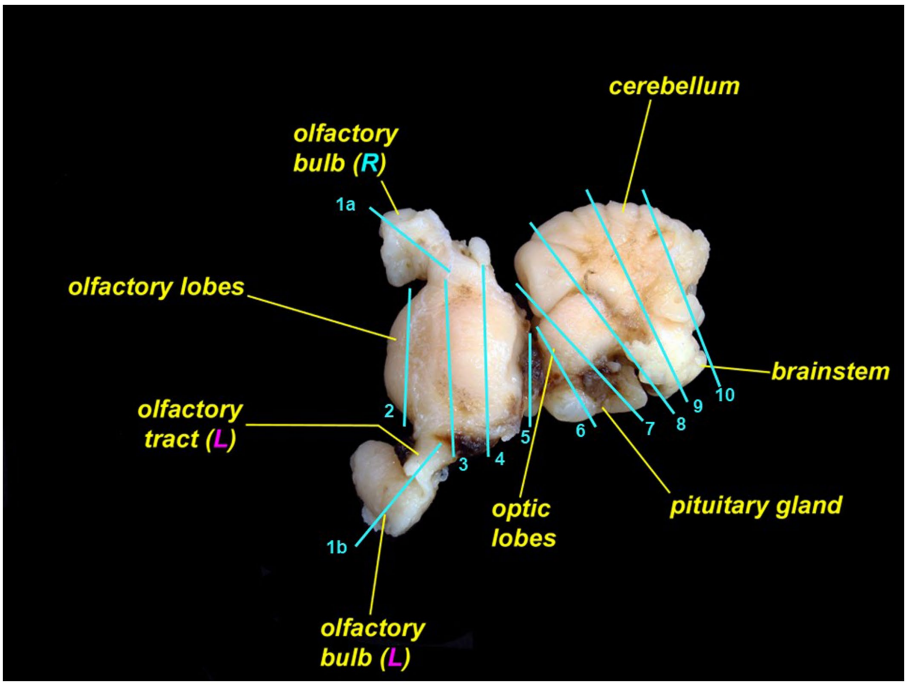

FIGURE 12
Leopard shark (*Triakis semifasciata*) brain with suggested locations to trim for histopathologic evaluation. The rostral brain (rostral to cut 5) is pictured from the dorsal aspect; the caudal brain (caudal to cut 5) is rotated and is pictured from the lateral aspect.

Carnobacterium maltaromaticum meningoencephalitis occurred in salmon sharks (*Lamna ditropis*), shortfin mako sharks (*Isurus oxyrinchus*), common thresher sharks (*Alopias vulpinus*), and one Pacific electric ray (*Tetronarce californica*). *Carnobacterium maltaromaticum* was consistently identified via cytology and bacteriology (culture on blood agar followed by identification with PCR and/or MALDI-TOF) in subcutaneous tissues around ELDs, inner ear perilymph, and EDF. The pathogen was extremely hardy and could be isolated from animals that had been frozen for months or years.

Miamiensis avidus, a scuticociliate parasite, was the most common cause of protozoal meningoencephalitis in stranded elasmobranchs. *Miamiensis avidus* meningoencephalitis was found in 48 leopard sharks, 4 bat rays (*Myliobatis californica*), one common thresher shark, and one brown smooth-hound shark. *Miamiensis* infections were typically characterized by mixed inflammation of rostral EDF, without visualization of motile protozoa because stranded animals were usually dead for 1–3 days prior to necropsy. Except for the thresher shark infection, all *M. avidus* cases occurred in and around San Francisco Bay, CA. Protozoal infection was confirmed via histology and/or PCR in many instances but was also a presumptive diagnosis based on cytology during large epizootics. Less common types of meningoencephalitis in stranded sharks and rays were verminous, fungal, and streptococcal (Chang and Okihiro, manuscript in preparation).

Excluding gill net by-catch and those intentionally caught via hook-and-line or spear, trauma, most often anthropogenic, was the second most common cause of mortality among stranded sharks and rays, and responsible for 14% (24/168) of reported deaths (Table 1). Types of traumatic injuries included: (1) crush and propeller wounds from boat strikes; (2) abrasions, lacerations, and internal hemorrhage from commercial nets; (3) spinal fracture and hemorrhagic puncture wounds from gunfire; (4) tooth loss, jaw damage, gastric perforation, and deep fin lacerations from fishing hooks and line; and (5) collision from an enclosure-mate. Trauma was the cause of stranding and mortality in white sharks, blue sharks (*Prionace glauca*), thornback guitarfish (*Platyrhinoidis triseriata*), and common thresher sharks.

Among elasmobranchs under human care, causes of death included meningoencephalitis (*M. avidus* and nematodes), granulomatous nephritis, enclosure-mate trauma, and capture and transport stress with chronic meningitis of unknown etiology (Chang and Okihiro, manuscript in preparation).

Pathogenesis of chondrocranial infections

The location and severity of inflammation observed via cytology reliably suggested the route of pathogen entry and pathogenesis of infections in many animals and was supported by microbiologic and histologic findings. With etiologic agents likely gaining entry via ELPs and ELDs (e.g., *Carnobacterium maltaromaticum*), inflammation and bacteria were present in subcutaneous tissue around ELDs, inner ear perilymph, and EDF overlying the brain (Figures 4, 5). In contrast, pathogens entering via the nares and olfactory lamellae [e.g., *Miamiensis avidus*; (6, 34)] tended to cause the most significant inflammation in rostral meninges and EDF surrounding the olfactory bulbs, with little or no inflammation of subcutaneous tissues surrounding ELDs or inner ear. Sharks and rays without significant nasal, endolymphatic, or inner ear inflammation, are presumed to

TABLE 1 Primary causes of mortality in stranded wild and aquarium-housed elasmobranchs necropsied from 2011–2023.

Species	Total necropsy	Meningo-encephalitis	Trauma	Other	Healthy (caught)	Etiology not determined
Leopard Shark *Triakis semifasciata*	67	48	5	1	6	7
Salmon Shark *Lamna ditropis*	40	37	0	0	1	2
Common Thresher Shark *Alopias vulpinus*	18	12	5	0	0	1
White Shark *Carcharodon carcharias*	9	1	7	1	0	0
Tope Shark *Galeorhinus galeus*	9	6	0	2*	0	1
Bat Ray *Myliobatis californica*	7	4	1	0	0	2
Broadnose Sevengill Shark *Notorynchus cepedianus*	7	2	0	5	0	0
Shortfin Mako Shark *Isurus oxyrinchus*	6	4	0	0	1	1
Blue Shark *Prionace glauca*	6	0	3	0	3	0
Grey Smooth-hound Shark *Mustelus californicus*	5	0	0	0	5	0
Shovelnose Guitarfish *Rhinobatos productus*	4	1	0	0	3	0
Round Stingray *Urobatis halleri*	3	0	0	1	2	0
Pacific Electric Ray *Tetronarce californica*	3	1	0	2	0	0
Brown Smooth-hound Shark *Mustelus henlei*	1	1	0	0	0	0
Prickly Shark *Echinorhinus cookei*	1	0	0	1	0	0
Thornback Guitarfish *Platyrhinoidis triseriata*	1	0	1	0	0	0
Scalloped Hammerhead Shark *Sphyrna lewini*	1	0	1	0	0	0
Pacific Angel Shark *Squatina californica*	1	1	0	0	0	0
TOTAL	189	118	24	12	21	14

Included are necropsy data from some healthy elasmobranchs caught by fisherpeople. *Primary cause of mortality was capture/transport stress, but an underlying meningoencephalitis and otitis interna was considered contributory.

10.3389/fvets.2024.1410332

have been infected via hematogenous spread, or possibly by a direct route of entry (e.g., penetrating foreign body).

Discussion

This approach to necropsy of the elasmobranch chondrocranium was developed and refined over a 13 year period and has proven applicable to a wide variety of elasmobranch species. In contrast to postmortem protocols which focus on the coelomic and branchial cavities, leaving the head exam to last, we have found that reversing the order of investigation to significantly increase the odds of making a definitive diagnosis, identifying pathogens, and determining pathogenesis. Although the brain does not necessarily autolyze faster than other tissues (35), hours can make the difference between interpretable cytology and histology and post-mortem overgrowth and autolysis (36). Prioritization of the head, together with knowledge of unique features of elasmobranch cranial anatomy, will allow cause of death and likely route of pathogenesis to be determined in more wild elasmobranchs and those under human care. Without an in-depth, methodical approach to the head necropsy, the endolymphatic route of pathogenesis for *C. maltaromaticum* and the olfactory route for *M. avidus* would have been missed.

Although there are distinct anatomic differences between many elasmobranch species (Figures 8, 9), particularly across different superorders, the described protocol utilizes conserved cranial landmarks and can be applied to most elasmobranchs. Awareness of unique elasmobranch anatomy minimizes the chances of overlooking significant lesions and potential routes of pathogen entry into the chondrocranium. The underlying problem is that no formal training is available for elasmobranch necropsy. Although the importance of assessing the central nervous system is well established among mammalian and teleost fish pathologists, only a small percentage will extend dissection and sampling to include the ELDs, inner ears, olfactory bulbs, and olfactory lamellae when working with sharks and rays. Limiting cranial examination to just the brain also limits understanding of pathogen entry and pathogenesis, which are major shortcomings in published reports of infectious meningoencephalitis in elasmobranchs (8–11, 13, 15).

Paired ELPs and ELDs are one of many unique anatomic features of elasmobranchs. Fully developed during late gestation and patent throughout the life of sharks and rays (37, 38), ELPs and ELDs provide a direct route for microbial entry into the otic capsules (18, 39, 40). Once established in the inner ear, pathogens are largely shielded from host immune surveillance and can readily spread to the adjacent cranial vault, meninges, and brain. *Carnobacterium maltaromaticum*, the most common cause of bacterial meningoencephalitis in stranded California elasmobranchs (Chang and Okihiro, manuscript in preparation), almost certainly uses an endolymphatic route of entry based on our findings.

Necropsy of the elasmobranch head should always begin with an aseptic approach to the ELPs and ELDs, with continued use of sterile technique until all three primary sites of potential infection—periductal subcutaneous tissue, inner ear perilymph, and EDF overlying the brain—have been sampled. The assumption is that these three sites are infected until proven otherwise. We encourage the use of as many ancillary diagnostic techniques as possible to identify pathogens and characterize the inflammatory response. The layered use of multiple diagnostic tools—cytology, microbiology, histology, and molecular biology—increases the odds of making a definitive diagnosis.

Cytology and microbiology are two inexpensive, rapid diagnostic highly useful for elasmobranch necropsy. Cytological exam of wet mount and stained preparations provide immediate feedback on inflammation, pathogen presence, and disease pathogenesis, factors which could influence or dictate quarantine and treatment options if animals under managed care share their systems with other animals. Critical decisions on whether to isolate (and treat) or euthanize animals often hinge on pathogen identification because infectivity, speed and mode of replication, as well as virulence, vary widely. Discovery of verminous meningitis in a tope shark carries with it markedly fewer consequences than uncovering necrotizing protozoal encephalitis in a leopard shark. Verminous meningitis is often a chronic, slowly developing disease which may be species specific and treatable; while invasive scuticociliates are highly virulent, lethal, nearly untreatable pathogens with little to no host specificity (41–43). Nematodes have a complex life cycle requiring an intermediate host (44), while scuticociliates are water-borne, highly transmissible, and can multiply via binary fission (45, 46).

Miamiensis avidus is a prolific killer of elasmobranchs and teleost fishes and is responsible for repeated epizootics of leopard shark stranding in San Francisco Bay (6) (Okihiro and Chang, manuscript in preparation). In the elasmobranchs included in this study, *M. avidus* was the most common cause of leopard shark strandings. It can, however, be surprisingly difficult to identify with cytology and histology because protozoal numbers are often small, parasites autolyzed quickly, and motility lost with delays associated with slow recovery of stranded animals. Problems with visual detection can also arise because protozoa use a nasal route of entry and involvement may be restricted to just olfactory lamellae and bulbs.

Definitive evidence for *Miamiensis* involvement in the 2017 epizootic only occurred when EDF samples were assessed via mNGS and PCR in 2017 (6). Parasites were subsequently found in tissue sections, but only after extensive histological sampling. This emphasizes the benefits of a layered approach and archival storage of histology samples (in formalin and paraffin blocks) and molecular biology samples (via freezing).

In summary, prioritization of the head during the elasmobranch necropsy, with knowledge of unique anatomy and emphasis on an aseptic approach to dissection and sampling of the endolymphatic system, inner ears, and brain, will greatly increase the odds of making definitive diagnoses, identifying pathogens, and characterizing pathogenesis. Knowledge gained will assist with monitoring the health of wild stocks, as well as providing valuable information to those involved with making decisions for animals under human care.

Data availability statement

The datasets presented in this article are not readily available because expanded mortality data will be included in a subsequent publication. Requests to access the datasets should be directed to RC rchang@mbayaq.org.

Ethics statement

Ethical approval was not required for the study involving animals in accordance with the local legislation and institutional requirements because data were collected opportunistically during routine diagnostic submissions.

Author contributions

RC: Conceptualization, Data curation, Investigation, Methodology, Visualization, Writing – original draft, Writing – review & editing. MO: Conceptualization, Data curation, Investigation, Methodology, Visualization, Writing – original draft, Writing – review & editing.

Funding

The author(s) declare that no financial support was received for the research, authorship, and/or publication of this article.

Acknowledgments

Thank you to Justine Lee Hirten for the scalloped hammerhead shark illustration. Thank you to the countless individuals who have helped recover, hold, and transport stranded sharks. Special thanks to Maureen Anders (Alameda, California) who has documented shark and ray strandings for over a decade in San Francisco Bay, along with collecting and shipping many valuable specimens. Thank you to all those who have assisted with necropsies and to California Department of Fish and Wildlife Marine Wildlife Veterinary Care and Research Center, Shark Lab at California State University Long Beach, University of California Davis School of Veterinary Medicine, Monterey Bay Aquarium, Pelagic Shark Research Foundation, and California Department of Parks and Recreation who have provided space and resources for necropsies.

Conflict of interest

The authors declare that the research was conducted in the absence of any commercial or financial relationships that could be construed as a potential conflict of interest.

Publisher's note

All claims expressed in this article are solely those of the authors and do not necessarily represent those of their affiliated organizations, or those of the publisher, the editors and the reviewers. Any product that may be evaluated in this article, or claim that may be made by its manufacturer, is not guaranteed or endorsed by the publisher.

References

1. Artois M, Bengis R, Delahay RJ, Duchêne MJ, Duff JP, Ferroglio E, et al, Wildlife disease surveillance and monitoring. RJ Delahay, GC Smith and MR Hutchings, (Eds.), *Management of Disease in wild mammals*. Tokyo: Springer Japan; (2009). 187–213.

2. Warns-Petit E, Morignat E, Artois M, Calavas D. Unsupervised clustering of wildlife necropsy data for syndromic surveillance. *BMC Vet Res*. (2010) 6:56. doi: 10.1186/1746-6148-6-56

3. Ferretti F, Worm B, Britten GL, Heithaus MR, Lotze HK. Patterns and ecosystem consequences of shark declines in the ocean. *Ecol Lett*. (2010) 13:1055–71. doi: 10.1111/j.1461-0248.2010.01489.x

4. Garner MM. A retrospective study of disease in elasmobranchs. *Vet Pathol*. (2013) 50:377–89. doi: 10.1177/0300985813482147

5. Stidworthy MF, Thornton SM, James R. A review of pathologic findings in elasmobranchs: A retrospective case series. *The Elasmobranch Husbandry Manual II—Recent Advances in the Care of Sharks, Rays and their Relatives*. (2017).

6. Retallack H, Okihiro MS, Britton E, Sommeran SV, DeRisi JL. Metagenomic next-generation sequencing reveals Miamiensis avidus (ciliophora: scuticociliatida) in the 2017 epizootic of leopard sharks (Triakis semifasciata) in San Francisco Bay, California, USA. *J Wildl Dis*. (2019) 55:375–86. doi: 10.7589/2018-04-097

7. Steele LM, Okihiro MS, Berlemont R, Dillon JG, Young KA, Hesami S, et al. Carnobacterium maltaromaticum associated with meningoencephalitis and otitis in stranded common thresher sharks (Alopias vulpinus). *Vet Pathol*. (2022) 59:850–9. doi: 10.1177/03009858221102600

8. Schaffer PA, Lifland B, Van Sommeran S, Casper DR, Davis CR. Meningoencephalitis associated with Carnobacterium maltaromaticum-like bacteria in stranded juvenile salmon sharks (Lamna ditropis). *Vet Pathol*. (2013) 50:412–7. doi: 10.1177/0300985812441033

9. Li WT, Lo C, Su CY, Kuo H, Lin SJH, Chang HW, et al. Locally extensive meningoencephalitis caused by Miamiensis avidus (syn. Philasterides dicentrarchi) in a zebra shark. *Dis Aquat Org*. (2017) 126:167–72. doi: 10.3354/dao03166

10. Jalenques M, Lair S, Schmidt-Posthaus H, Jufer M, Lamglait B. Scuticociliate (Philasterides dicentrarchi) infection cluster in a multispecies marine aquarium system. *Dis Aquat Org*. (2021) 144:107–15. doi: 10.3354/dao03580

11. Stidworthy MF, Garner MM, Bradway DS, Westfall BD, Joseph B, Repetto S, et al. Systemic scuticociliatosis (Philasterides dicentrarchi) in sharks. *Vet Pathol*. (2014) 51:628–32. doi: 10.1177/0300985813492800

12. de Felipe A, Lamas J, Sueiro R, Folgueira I, Leiro JM. New data on flatfish scuticociliatosis reveal that Miamiensis avidus and Philasterides dicentrarchi are different species. *Parasitology*. (2017) 144:1394–411. doi: 10.1017/S0031182017000749

13. Dagleish MP, Baily JL, Foster G, Reid RJ, Barley J. The first report of disease in a basking shark (Cetorhinus maximus). *J Comp Pathol*. (2010) 143:284–8. doi: 10.1016/j.jcpa.2010.02.001

14. Barnett JEF, Novotny L, Astley K, Deaville R, Fox RI, Ham C, et al. The first report of meningitis in a Greenland shark (Somniosus microcephalus). *J Comp Pathol*. (2023) 203:31–5. doi: 10.1016/j.jcpa.2023.04.004

15. Morick D, Davidovich N, Bigal E, Rosenbluth E, Bouznach A, Rokney A, et al. Fatal infection in a wild sandbar shark (Carcharhinus plumbeus), caused by Streptococcus agalactiae, type Ia-ST7. *Animals*. (2020) 10:284. doi: 10.3390/ani10020284

16. Acharya T, Hare J. Sabouraud agar and other fungal growth media. VK Gupta and M Tuohy, (Eds.) *Laboratory protocols in fungal biology: Current methods in fungal biology*. Cham: Springer International Publishing; (2022) 69–86.

17. Balows A. Manual of clinical microbiology 8th edition. *Diagn Microbiol Infect Dis*. (2003) 47:625–6. doi: 10.1016/S0732-8893(03)00160-3

18. Evangelista C, Mills M, Siebeck UE, Collin SP. A comparison of the external morphology of the membranous inner ear in elasmobranchs. *J Morphol*. (2010) 271:483–95. doi: 10.1002/jmor.10812

19. Maisey JG, Springer VG. Chondrocranial morphology of the salmon shark, Lamna ditropis, and the porbeagle, L. nasus (Lamnidae). *Copeia*. (2013) 2013:378–89. doi: 10.1643/CG-12-130

20. Mills M, Rasch R, Siebeck UE, Collin SP. Exogenous material in the inner ear of the adult port Jackson shark, Heterodontus portusjacksoni (Elasmbranchii). *Anat Rec*. (2011) 294:373–8. doi: 10.1002/ar.21338

21. Mulligan KP, Gauldie RW. The biological significance of the variation in crystalline morph and habit of otoconia in elasmobranchs. *Copeia*. (1989) 1989:856–71. doi: 10.2307/1445969

22. Gilbert SG. *Pictorial anatomy of the dogfish* University of Washington Press (1973).

23. Luer CA, Walsh CJ, Bodine AB, Wyffels JT, Scott TR. The elasmobranch thymus: anatomical, histological, and preliminary functional characterization. *J Exp Zool*. (1995) 273:342–54. doi: 10.1002/jez.1402730408

24. Crow GL. Ch 28. Goiter in Elasmobranchs. *The elasmobranch husbandry manual: Captive Care of Sharks, rays and their relatives*. (2004).

25. Iuliis GD, Pulerà D. *The dissection of vertebrates* Elsevier Science (2019). 416 p.

26. Meinkoth JH, Cowell RL. Sample collection and preparation in cytology: increasing diagnostic yield. *Vet Clin North Am Small Anim Pract*. (2002) 32:1187–207. doi: 10.1016/S0195-5616(02)00049-9

27. Smeets WJAJ, Nieuwenhuys R, Roberts BL. *The central nervous system of cartilaginous fishes: Structure and functional correlations*. Berlin, Germany: Springer Science & Business Media (2012). 270 p.

28. Slaoui M, Fiette L. Histopathology procedures: from tissue sampling to histopathological evaluation. JC Gautier, (Ed.). *Drug safety evaluation: Methods and protocols*. Totowa, NJ: Humana Press; (2011). 69–82.

29. How to submit tissues for embedding | Research Histology Services | University of Pittsburgh. Available at: https://rhslab.pitt.edu/drop-info/how-submit-tissues-embedding

30. Ashley LM, Chiasson RB. *Laboratory anatomy of the shark*. New York, NY, USA: W.C. Brown Company Publishers (1988). 104 p.

31. Mesli V, Neut C, Hedouin V. Postmortem bacterial translocation. *Forensic microbiology*. John Wiley & Sons, Ltd.; (2017). 192–211.

32. Maujean G, Guinet T, Fanton L, Malicier D. The interest of postmortem bacteriology in putrefied bodies. *JFS*. (2013) 58:1069–70. doi: 10.1111/1556-4029.12155

33. Klimley AP. Brain organization and intelligence. PA Klimley and S Oerding, (Ed.) *The biology of sharks and rays*. University of Chicago Press; (2013).

34. Moustafa EMM, Tange N, Shimada A, Morita T. Experimental scuticociliatosis in Japanese flounder (Paralichthys olivaceus) infected with Miamiensis avidus: pathological study on the possible neural routes of invasion and dissemination of the scuticociliate inside the fish body. *J Vet Med Sci*. (2010) 72:1557–63. doi: 10.1292/jvms.10-0214

35. George J, Van Wettere AJ, Michaels BB, Crain D, Lewbart GA. Histopathologic evaluation of postmortem autolytic changes in bluegill (Lepomis macrohirus) and crappie (Pomoxis anularis) at varied time intervals and storage temperatures. *PeerJ*. (2016) 4:e1943. doi: 10.7717/peerj.1943

36. Wenzlow N, Neal D, Stern AW, Prakoso D, Liu JJ, Delcambre GH, et al. Feasibility of using tissue autolysis to estimate the postmortem interval in horses. *J Vet Diagn Invest*. (2021) 33:825–33. doi: 10.1177/10406387211021865

37. Byrum SR, Frazier BS, Grubbs RD, Naylor GJP, Fraser GJ. Embryonic development in the bonnethead (Sphyrna tiburo), a viviparous hammerhead shark. *Dev Dyn*. (2024) 253:351–62. doi: 10.1002/dvdy.658

38. Quiring DP. The development of the ear of Acanthias vulgaris. *J Morphol*. (1930) 50:259–93. doi: 10.1002/jmor.1050500109

39. Popper AN, Fay RR. Structure and function of the elasmobranch auditory system. *Am Zool*. (1977) 17:443–52. doi: 10.1093/icb/17.2.443

40. Pereira NP, Nunes GD, Baylina N, Peleteiro MC, Rosado L. Fusarium solani infection of the eye, brain, otic capsule, and endolymphatic tubes in captive port Jackson sharks (Heterodintus porusjacksoni). In: IAAAM Archive, (2015), Available at: https://www.vin.com/doc/?id=6696240

41. Poulin R, Mouillot D. Host specificity and the probability of discovering species of helminth parasites. *Parasitology*. (2005) 130:709–15. doi: 10.1017/S0031182004007218

42. Hadfield CA, Clayton LA. *Clinical guide to fish medicine*. *1st* ed John Wiley & Sons Ltd. (2021).

43. Stidworthy MF, Bellamy K, Thornton S, Monreal-Pawlowsky T. *Scuticociliate management philosophy in public aquaria*. (2018); 14–27.

44. Thompson RM, Mouritsen KN, Poulin R. Importance of parasites and their life cycle characteristics in determining the structure of a large marine food web. *J Anim Ecol*. (2005) 74:77–85. doi: 10.1111/j.1365-2656.2004.00899.x

45. Long H, Zufall RA. Diverse modes of reproduction in the marine free-living ciliate Glauconema trihymene. *BMC Microbiol*. (2010) 10:108. doi: 10.1186/1471-2180-10-108

46. Lee JH, Park JJ, Choi JH, Kang SY, Kang YJ, Park KH. Effects of clioquinol on the scuticociliatosis-causing protozoan Miamiensis avidus in olive flounder Paralichthys olivaceus. *J Fish Dis*. (2018) 41:451–62. doi: 10.1111/jfd.12741

frontiers | Frontiers in Veterinary Science

TYPE Case Report
PUBLISHED 19 June 2024
DOI 10.3389/fvets.2024.1401141

Check for updates

OPEN ACCESS

EDITED BY
Alexa Delaune,
Mississippi Aquarium, United Kingdom

REVIEWED BY
Michael James Murray,
Monterey Bay Aquarium, United States
Sean Michael Perry,
Mississippi Aquarium, United States
Shane Boylan,
Georgia Sea Turtle Center, United States

*CORRESPONDENCE
April Beatty
✉ beatty.274@osu.edu

RECEIVED 14 March 2024
ACCEPTED 10 June 2024
PUBLISHED 19 June 2024

CITATION
Beatty A, Gemensky-Metzler A, Newbold G, Aplasca AC and Seeley KE (2024) Case report: Management and long-term ophthalmic sequelae of monogenean ocular infestation in cownose rays (*Rhinoptera bonasus*). *Front. Vet. Sci.* 11:1401141. doi: 10.3389/fvets.2024.1401141

COPYRIGHT
© 2024 Beatty, Gemensky-Metzler, Newbold, Aplasca and Seeley. This is an open-access article distributed under the terms of the Creative Commons Attribution License (CC BY). The use, distribution or reproduction in other forums is permitted, provided the original author(s) and the copyright owner(s) are credited and that the original publication in this journal is cited, in accordance with accepted academic practice. No use, distribution or reproduction is permitted which does not comply with these terms.

Case report: Management and long-term ophthalmic sequelae of monogenean ocular infestation in cownose rays (*Rhinoptera bonasus*)

April Beatty[1]*, Anne Gemensky-Metzler[1], Georgina Newbold[1], Andrea C. Aplasca[2] and Kathryn E. Seeley[3]

[1]Department of Clinical Sciences (Ophthalmology), The Ohio State University College of Veterinary Medicine, Columbus, OH, United States, [2]The Maryland Zoo in Baltimore, Baltimore, MD, United States, [3]Department of Animal Health, The Columbus Zoo and Aquarium, Powell, OH, United States

Monogenean ectoparasitic flatworm infestations, particularly in closely confined populations, can result in severe epizootic disease that is often devastating and occasionally fatal. This case series describes a population of cownose rays (*Rhinoptera bonasus*) ($n = 52$) housed in an aquarium touch-tank exhibit that presented with severe ocular disease due to infestation with monogeneans, presumably *Benedeniella posterocolpa* of the Capsilidae family. The most severely affected individuals ($n = 9$), including several cases with bilaterally ruptured corneas, underwent serial examinations prior to and following treatment with praziquantel, systemic antibiotics, and corticosteroids. The entire population underwent frequent therapeutic water changes with a scheduled decrease in salinity, increase in temperature, and a series of seven praziquantel tank treatments. At the last follow up examination (3.75 years), the most common ocular findings were corneal fibrosis (18/18 eyes; 100%), cataract formation (13/18 eyes; 72.2%), synechia (8/18 eyes; 44.4%), and dyscoria (5/18 eyes; 27.8%). Despite severe corneal disease, including corneal rupture, all examined eyes (18/18; 100%) showed remarkable corneal remodeling and a largely clear visual axis. There are very few reports describing corneal disease in aquarium housed elasmobranchs, and no reports describe ophthalmic implications of monogenean infestation in these animals. This further underscores the importance of this case series in demonstrating the capacity for healing of elasmobranch eyes and can provide further guidance regarding prognosis and treatment in cases of severe corneal disease.

KEYWORDS

cownose ray, capsalid monogenean, elasmobranch, veterinary ophthalmology, case report

1 Introduction

Cownose rays (CNR), (*Rhinoptera bonasus*), are a species of cartilaginous fish belonging to the subclass, Elasmobranchii, alongside sharks, skates, and other ray species. Elasmobranchs are often included in large aquarium touch pools and CNR are the most commonly housed species in these exhibits (1). A documented condition

affecting elasmobranchs, including CNR, is monogenean infestation. Monogeneans are host-specific parasitic flatworms that use hook-like structures, haptors, for attachment prior to feeding on mucus and epithelial cells resulting in a wide range of clinical implications (2). Clinical signs vary widely but commonly include skin and gill lesions, lethargy, and decreased appetite (1, 3, 4). The condition is often associated with high morbidity and mortality (2). While described in tilapia (*Oreochromis mossambicus*) (5), ocular involvement secondary to monogenean infestation has not been previously reported in elasmobranchs. There are a growing number of reports describing ocular disease in aquarium-housed CNR. In these studies, the etiology was not determined, however many rays were diagnosed with historic or current infestation of the skin and gills with *Benedeniella posterocolpa*, a monogenean of the Capsilidae family (6, 7). *Benedenellia posterocolpa* is considered the most likely causative agent of ocular infestation in this case series. These ectoparasites are reported to be large, oviparous monogeneans with a predilection for the ventral skin surface of CNR. Eggs are shed into the water column and can form an egg bank within the tank substrate. The 3–5 week life cycle (egg to egg), in addition to oviparity, renders treatment of tank infestations challenging (1). This represents the first report of confirmed monogenean ocular infestation in a population of aquarium-housed CNR, and includes information regarding treatment, long-term ocular implications, and prognosis.

2 Case description

2.1 Animals

Nine adult CNR (8 male, 1 female) housed in a touch tank exhibit were evaluated throughout this case series. Individuals were amongst a larger population of 52 CNR and 29 southern stingrays (*Hypanus americanus*) housed in a 9,000-gallon tank with sand substrate that is tightly controlled for temperature (75°F-80°F) and salinity (27-30 ppt). Saltwater is created in-house using commercially available sea salt mix (Instant Ocean® Sea Salt, United Pet Group, Inc., Cincinnati, OH, United States), and a 25% water change is performed weekly. Water quality is maintained by a life support system including a sand filter, protein skimmer and ozone. In Spring 2020, a wild caught group of 20 (16 male, 4 female) CNR from the Florida Keys, FL was introduced into the tank. All rays underwent quarantine treatments prior to transport (Figure 1). Transport occurred overnight in a temperature-controlled truck. There were no notable concerns during quarantine

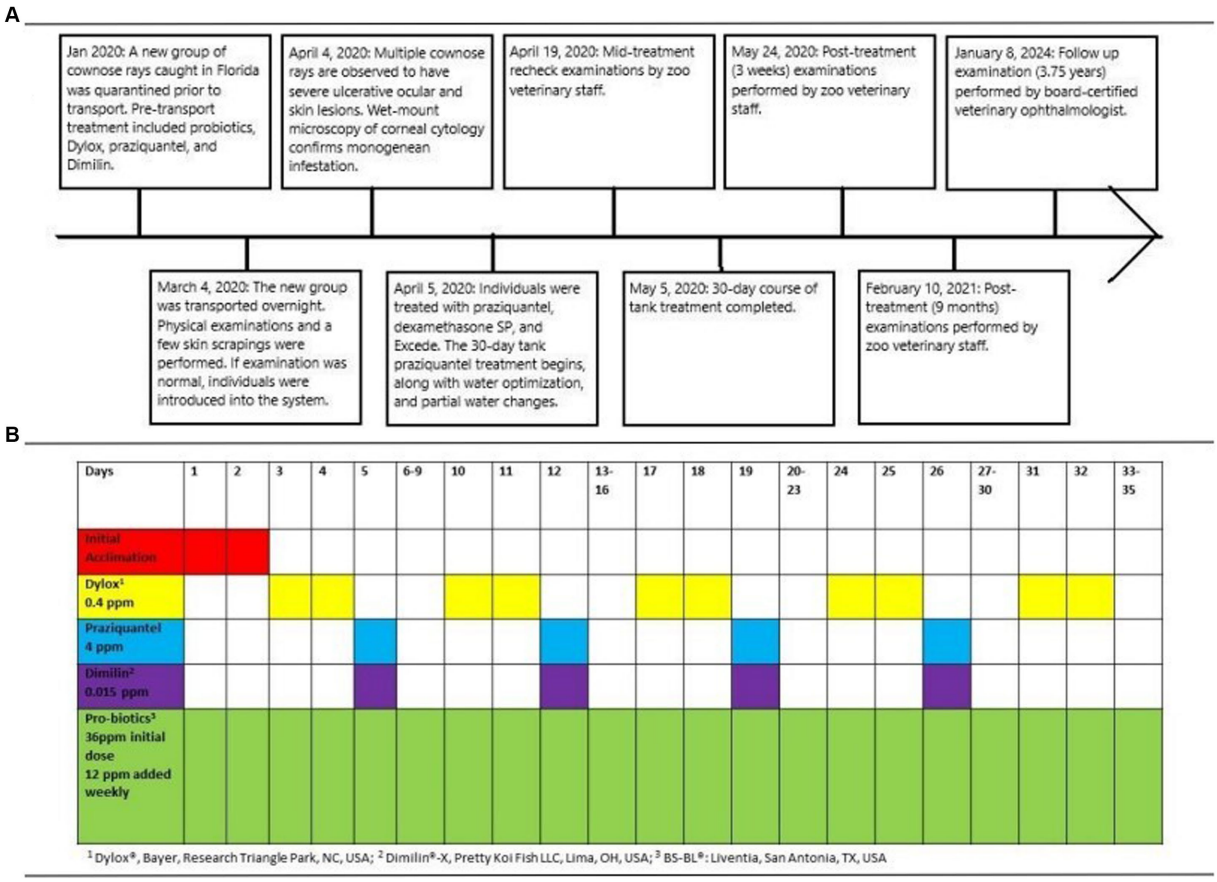

FIGURE 1
A timeline describing the history, diagnosis, treatment, and follow-up period of a confirmed ocular infestation by monogeneans in nine cownose rays (*Rhinoptera bonasus*) **(A)**, as well as a chronogram of treatments administered to incoming rays during the 35-day quarantine period prior to transport **(B)**.

FIGURE 2
Photographs of the right eye of a cownose ray (*Rhinoptera bonasus*) at the time of confirmed monogenean ocular infestation **(A)** and at follow-up examinations halfway through treatment **(B)**, at completion of treatment **(C)**, and 3.75 years following completion of treatment **(D)**. **(A)** Axial corneal perforation with associated prolapsed hemorrhagic uveal tissue. **(B)** Axial conical fibrosis with severe dyscoria and presumed anterior synechia in location of previous perforation. **(C)** Improving corneal clarity and dyscoria. **(D)** Mild axial fibrosis, resolution of previous anterior synechia and dyscoria, focal posterior synechia at 1 o'clock position, incipient axial anterior cortical cataract (not pictured).

or transport. Individuals were examined by a veterinarian under manual restraint upon arrival and eight of 20 rays (40%) had skin scrapes performed. All examinations were within normal limits and no parasites were noted on wet mounts of the skin scrapes.

2.2 Clinical signs and diagnosis

One month following introduction, numerous CNR were observed to have severe ocular and ulcerative skin lesions and were netted for examination. Eight of nine rays in this case series belonged to the recently introduced group. Examination by veterinary staff under manual restraint revealed corneal rupture in 14 eyes (14/18; 77.8%) (Figure 2). Of those not ruptured (4 eyes), four (4/4; 100%) were affected by corneal opacity resembling edema and one (1/4; 25%) had presumed ulceration and stromal loss. Fluorescein stain was not performed given logistical difficulty and severity of ocular changes. Of note, there were additional CNR affected, but only those with the most severe signs were netted for examination. All co-housed southern stingrays appeared clinically normal with no evidence of observable ocular or skin lesions. Given the high morbidity rate and recent introduction of new animals, an infectious condition was presumed. A sterile swab was used to collect corneal cytology from one individual and used for wet-mount preparation (8). Microscopy revealed an oncomiracidium, the ciliated larval form of a monogenean ectoparasite, with distinguishing characteristics of two pairs of eyespots and two pairs of anchor hooks (Figure 3) consistent with a diagnosis of capsalid monogenean infestation, most likely *Benedeniella posterocolpa* (1, 2, 9).

2.3 Treatment

Given the severity of clinical signs and fastidious nature of monogeneans, aggressive medical therapy was planned to target individuals, as well as the entire system. To reduce the burden of adult monogeneans quickly, individuals with visible ophthalmic lesions, including the nine in this study, were netted and placed in a praziquantel medicated bath [20 ppm, once, 30 min (praziquantel powder, Everything Aquatic, Medford, OR, United States)] the day following diagnosis (10–12). Supplemental oxygen was provided using an airstone and dissolved oxygen (DO) maintained between 90 and 100%. While in hand, individuals received dexamethasone sodium phosphate intramuscularly [0.25 mg/kg, once (Dexamethasone-SP,

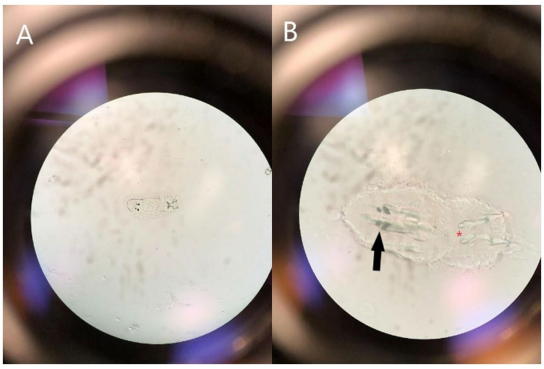

FIGURE 3
Photograph demonstrating the microscopic appearance of a ciliated oncomiracidium capsalid monogenoid, most likely *Benedeniella posterocolpa*, at 40X **(A)** and 100X **(B)** magnification collected via swab cytology from the corneal surface of a cownose ray (*Rhinoptera bonasus*). Distinguishing characteristics include two pairs of eye spots (black solid arrow) and two pairs of anchor hooks (red asterisk).

Bimeda-MTC Animal Health Inc., Ontario, Canada)] to reduce inflammation and ceftiofur crystalline free acid intramuscularly [80 mg, once (Excede, Zoetis Inc., Kalamazoo, MI, United States)] to prevent secondary bacterial infection. Following the bath, they were returned to the general population, but were isolated with baby gates for further monitoring. A water change was performed replacing at least 25% of the water, and a gradual concurrent decrease in salinity from 27 ppt to 18-22 ppt and increase in temperature from 77°F to 80°F was initiated. Water quality was measured daily, and animals were monitored to ensure tolerance of environmental changes. It was not feasible to treat all rays in the system with individualized bath treatments. Therefore, the entire system underwent episodic praziquantel administration in order to treat the less affected individuals and sand substrate, which could not be removed. Based on recommendations in the literature and consultation with colleagues, a lower dose of 8 ppm of praziquantel was dissolved into the system using rubber gloves and mesh stocking hose material every 4 days for a total of seven doses (28-day course) (12). Chemical and physical filtration were removed, and water quality was maintained by performing a 25% water change prior to each treatment cycle. Supplemental oxygen was added to the system to maintain DO. Praziquantel levels were tested to ensure therapeutic levels of >2 ppm were reached (Georgia Aquarium, Atlanta, GA, United States) (13). Immediately prior to redosing, the praziquantel level was 4.4 ppm and increased to 8.2 ppm following repeat dosing. Lastly, enrofloxacin [100 mg/g food (Baytril, Elanco US Inc., Shawness, KS, United States)] was added to the gel food for treatment and prevention of secondary bacterial infections and fed for a total of 30 days.

2.4 Follow up

Examinations occurred 2 weeks following initiation of treatment, then 3 weeks, 9 months, and 3.75 years (45 months) after treatment was completed (Figure 1). Examinations 3 weeks following completion of treatment were performed without sedation by the zoo's staff veterinarian, and all eyes (18/18; 100%) were documented to have healed corneal ulceration and signs of remodeling (Figure 2). The latest examinations were performed by veterinarians with specialty training in ophthalmology under sedation with 175 ppm tricaine methanesulfonate (Syncaine, Syndel, Ferndale, WA, United States) buffered 2:1 with sodium bicarbonate (Arm and Hammer baking soda, Princeton, NJ, United States). Depth of sedation was such that animals allowed handling but maintained voluntary respirations. All animals were recovered in non-medicated tank water and resumed swimming within 5 min. Ophthalmic examination included evaluation of the adnexa and anterior segment with a handheld slit-lamp biomicroscope (KOWA SL-17, Torrance, CA 90502, United States) and indirect ophthalmoscopy using a headset (Keeler, Malvern, PA, 19355, USA) and 30D lens (Volk Optical Inc., Mentor, OH, United States). Examination findings are listed in Supplementary Table 1. The most common findings were corneal fibrosis (18/18 eyes; 100%), cataract formation (13/18 eyes; 72.2%), synechia (8/18 eyes; 44.4%), and dyscoria (5/18 eyes; 27.8%) (Figure 4). Corneal fibrosis was graded as trace (1/18 eyes; 5.6%), mild (5/18 eyes; 27.8%), moderate (8/18 eyes; 44.4%), or severe (4/18 eyes; 22.2%). Cataracts were graded as incipient (10/13 eyes; 76.9%) or early immature (3/13 eyes; 23.1%), and the majority were in the axial anterior cortex. The fundus was successfully visualized in all 18 eyes and no posterior segment abnormalities were detected. All eyes (18/18; 100%) appeared functional, and all individuals continued to exhibit normal social and feeding behaviors.

3 Discussion

This report details the clinical presentation, treatment, and outcome of monogenean ocular infestation in aquarium-housed CNR. Normal anterior segment examination consists of a clear cornea, a relatively shallow anterior chamber devoid of aqueous flare or cellular infiltrate, an immobile vertically ovoid pupil aperture with individual variation in iris color from light tan to brown-black, and a clear lens. CNR lack eyelids, and their corneas are in constant contact with their aquatic environment (6). While ocular trauma has been reported (14), an infectious process was suspected given the percentage of individuals affected, recent introduction of new individuals, and absence of lesions in co-housed southern stingrays. Monogeneans are highly host specific which suggests why only CNR were affected (4). They have a direct life cycle increasing the risk of outbreak following introduction of infected animals because no intermediate host is necessary for infection to occur (2). Incoming individuals were likely infected prior to transport. It is possible they did not have substantial enough parasitic load to demonstrate clinical lesions as monogeneans can persist at low levels, and often do in wild settings, without clinical signs (2). Stress of transport may have exacerbated the condition, particularly given eight of nine animals were part of the incoming group. Additionally, Capsalidae species reproduce quickly, are oviparous, and eggs are resistant to treatment (10). Therefore, despite treatment with praziquantel during quarantine, it is possible a very small number of individuals or eggs could persist and quickly propagate to cause clinical disease (1, 3, 8).

Diagnosis of monogenean infestation is often made using wet-mount microscopy. Gross evaluation of morphologic features aid in determining which family of monogenean is present. Identification

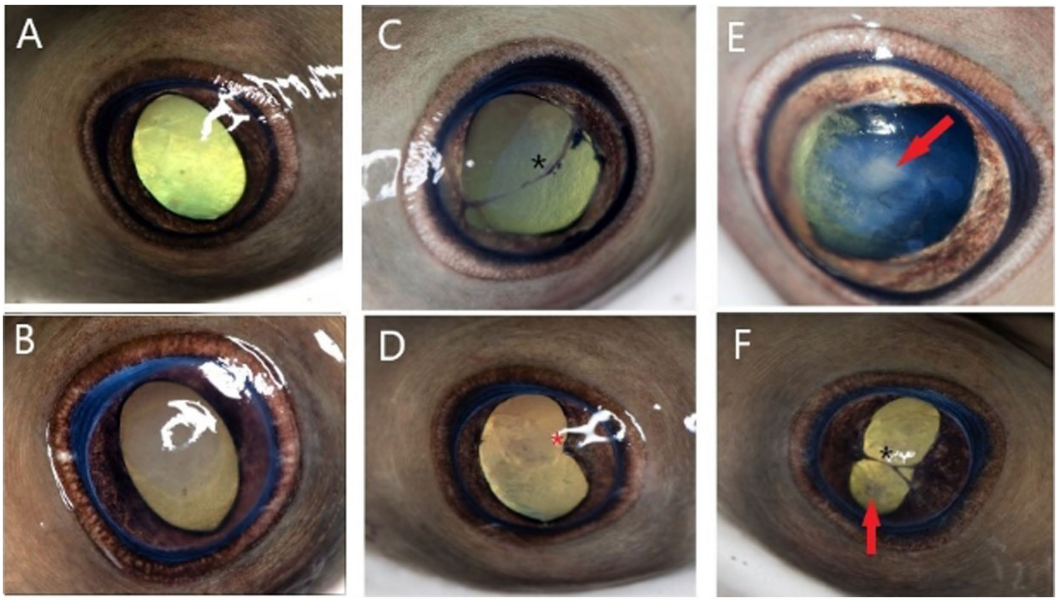

FIGURE 4
Photographs representing ophthalmic examination findings 3.75 years following monogenean ocular infestation in cownose rays (*Rhinoptera bonasus*). Findings are broadly classified as mild **(A,B)**, moderate **(C,D)**, and severe **(E,F)**. Examination findings are described as follows: **(A)** Mild axial corneal fibrosis, otherwise normal examination including ovoid pupil aperture; **(B)** Focal moderate axial corneal fibrosis, otherwise normal examination; **(C)** Moderate diffuse corneal fibrosis, slight dyscoria, multifocal endothelial pigment deposits, axial anterior synechia spanning the pupil aperture (black asterisk), incipient axial anterior cortical cataract (not pictured); **(D)** Moderate axial corneal fibrosis, dyscoria, focal posterior synechia nasally (red asterisk), axial incipient anterior cortical cataract (not pictured); **(E)** Severe axial corneal fibrosis, dyscoria, early immature axial anterior cortical cataract (red arrow); **(F)** Severe axial corneal fibrosis, severe dyscoria, anterior synechia spanning pupil aperture (black asterisk), incipient axial anterior cortical cataract (red arrow).

to the family level, specifically whether the reproductive strategy is oviparous or viviparous, is considered sufficient for management decisions. Further classification requires assessment of haptor and reproductive morphology or DNA sequencing, which was not performed in this study (8). Although species identification was not definitive, based on previous publications and presence of a capsalid oncomiracidium on cytology, *Benedeniella posterocolpa* was considered most likely (1). Once infestation with an oviparous monogenean was confirmed, a treatment strategy was determined. Individuals with severe lesions were considered likely to have the highest parasite burden and were therefore separated for individualized praziquantel medicated baths (2, 10). Group treatment aimed to eliminate all eggs and adult parasites within the environment given sand substrate could not be removed or replaced. The time required for maturation from eggs to adults is temperature dependent, lasting only a few days at higher temperatures. In contrast, cooler temperatures can result in an extended generation time up to 6 months (2). Therefore, water temperature was increased to promote quicker hatching of the eggs, and a 30-day treatment course of cyclical praziquantel administration planned every 4 days to target larvae hatching at varying time points. Praziquantel does not typically impact water quality, however can result in bacterial blooms that decrease DO and increase ammonia. Therefore, it is essential to monitor water quality during immersion treatment (8). Bacteria can begin to utilize praziquantel as a food source and cause degradation over time, necessitating higher doses to maintain therapeutic levels (8, 10). Since each system is unique and praziquantel is unpredictable, levels should be measured throughout treatment. This was not feasible in this case due to staffing and logistical limitations created by the outbreak of SARS-CoV-2. Freshwater dips have been described as a possible treatment in marine species, however a case report involving CNR suggests they may not systemically tolerate this dramatic decrease in salinity (15). Therefore, salinity was gradually decreased to a level deemed tolerable, but which may play a positive role in parasite elimination (16, 17). While a complete water change was not logistically possible, partial and frequent changes were performed throughout treatment.

To date, no reports have definitively confirmed ocular involvement of monogenean infestation in CNR (1, 2, 18). An abstract by Seyer et al. (7) describes ulcerative keratopathy in 11 captive CNR in which all had corneal lesions of varying severity. Interestingly, the Atlantic stingray (*Hypanus sabina*) examined in this report had no evidence of corneal disease. A species-specific etiology was suspected, but not determined. Additionally, Foote et al. (6) reports ophthalmic findings in 63 CNR from three separately housed groups. Nearly every ray (62/63) was diagnosed with ocular pathology including corneal abnormalities (opacity, ulceration, rupture), cataracts, and inactive intraocular changes (synechia). There was a significant association between active disease and which of the three facilities animals were housed. The aquarium with the most affected individuals had recently confirmed *Benedeniella posterocolpa* infestation on the skin of their CNR. A second aquarium had previously managed an outbreak of monogeneans confirmed using skin and gill scrapes. Multiple individuals were noted to have signs of active keratitis throughout the

outbreak (6). While causation cannot be proven, it is probable the ocular changes described were related to a monogenean infestation with *Benedeniella posterocolpa*. These reports, in conjunction with this case series, support the use of corneal cytology and wet-mount microscopic evaluation in cases of keratitis in CNR.

Pathogenesis of corneal infestation and subsequent rupture in these cases is unknown. Monogeneans are found in mucus-laden environments and utilize haptors for epithelial attachment (1, 4). Corneal rupture may be a direct consequence of tissue destruction by monogeneans. It is also plausible the organism's attachment to the cornea results in small ulcerations that become secondarily infected with bacteria, leading to keratomalacia and subsequent perforation (19). Alternatively, attachment may result in a foreign body sensation, and promote excess rubbing and self-trauma. Pathogenesis is likely multifactorial, and further research is warranted to determine the mechanism of corneal degradation and rupture in cases of monogenean ocular infestation as this information will guide future treatment strategies.

Long-term ophthalmic implications and prognosis following monogenean ocular infestation in CNR was previously unknown. Previous reports describe ocular disease secondary to monogenean infestation in tilapia (5), as well as other parasitic organisms such as copepods, (*Lepeophtheirus acutus*) in elasmobranchs (20). In tilapia, surviving individuals commonly had significant scarring and blindness (5), whereas elasmobranchs demonstrated significant healing and presumed functional globes following treatment similar to CNR described in this case series (20). While ocular lesions were noted in all 18 eyes, all were presumed visual at last examination given a relatively clear visual axis and normal fundus. Aquatic species rely on spherical lenses as the major refractive organ of the eye (21), likely rendering residual corneal opacities and fibrosis (18/18 eyes; 100%) in these individuals even less significant in terms of impacting visual acuity. While cataract was relatively common (13/18 eyes; 72.2%), the majority were incipient and did not impede visualization of the posterior segment. Elasmobranch corneas are considered the most primitive of all vertebrates and contain sutural fibers in the stroma as an adaptation to prevent swelling in cases of epithelial disruption (22). This distinct structural difference, in addition to documented wound-healing capabilities of elasmobranchs, likely contributes to exceptional healing following severe ocular disease, including corneal perforation (23, 24). Corneal angiogenesis is a nonspecific response to inflammation in most species (25). Interestingly, corneas of CNR remained relatively avascular throughout follow-up suggesting either an alternative response to keratitis that does not involve significant angiogenesis or rapid regression of vessels to restore translucency. While it may be tempting to consider enucleation or euthanasia in cases of advanced ocular disease, this case series suggests medical therapy may be successful for both healing and preserving long-term vision in CNR.

A limitation of this case series is that baseline and subsequent ophthalmic exams were only performed in nine CNR. Additional individuals were documented to have inactive ocular lesions on future examinations, but were not examined at initial diagnosis. This may overestimate severity of lesions as those evaluated prior to treatment were those with the most observable lesions. Furthermore, rays not examined at initial diagnosis did not receive individual treatment but were subject to treatments of the entire system making interpretation of the necessity of individualized treatments difficult. An additional limitation is that the species of monogenean was not identified. While family classification is sufficient for guiding treatment and *Benedeniella posterocolpa* is considered most likely, interpretation about which species of monogeneans plays a more significant role in ocular disease cannot be definitively stated. Lastly, interpretation of functional vision was based on presence of a clear visual axis, absence of posterior segment abnormalities, and normal behavior. Future investigation may include a prospective case series evaluating all individuals, species identification, pathogenesis, and objective vision assessment to further understand this complex condition of elasmobranchs.

This report is the first to describe clinical implications associated with confirmed ocular monogenean infestation in CNR. Signs of keratitis appear to be associated with monogenean infestation and can be as severe as corneal perforation. Corneal cytology and wet-mount microscopy should be considered in cases of ocular disease in elasmobranch species. Treatment of both individuals and the system using praziquantel, antibiotics, anti-inflammatories, water changes, and optimization of water salinity and temperature may be a successful strategy for eliminating parasites. Despite the severe presentation, CNR demonstrated exceptional healing capacity of ocular structures and all eyes were presumed to retain vision 3.75 years following diagnosis supporting the notion that aggressive medical therapy should be considered in cases of ocular monogenean infestation.

Data availability statement

The original contributions presented in the study are included in the article/Supplementary material, further inquiries can be directed to the corresponding author.

Ethics statement

The animal study was approved by the Columbus Zoo and Aquarium Research Committee. The study was conducted in accordance with the local legislation and institutional requirements.

Author contributions

AB: Conceptualization, Data curation, Formal analysis, Investigation, Writing – original draft, Writing – review & editing. AM: Conceptualization, Investigation, Methodology, Supervision, Writing – original draft, Writing – review & editing. GN: Writing – original draft, Writing – review & editing. AA: Data curation, Investigation, Writing – original draft, Writing – review & editing. KS: Conceptualization, Data curation, Investigation, Methodology, Resources, Supervision, Writing – original draft, Writing – review & editing.

Funding

The author(s) declare that no financial support was received for the research, authorship, and/or publication of this article.

Acknowledgments

The authors of this report would like to thank the husbandry staff of the Columbus Zoo and Aquarium who helped care for these animals, Stephen A. Bullard from Auburn University's School of Fisheries, Aquaculture and Aquatic Sciences, for his assistance with visual parasite identification, and Amanda Carberry, Media Productions Specialist of Columbus Zoo, for photography assistance.

Conflict of interest

The authors declare that the research was conducted in the absence of any commercial or financial relationships that could be construed as a potential conflict of interest.

Publisher's note

All claims expressed in this article are solely those of the authors and do not necessarily represent those of their affiliated organizations, or those of the publisher, the editors and the reviewers. Any product that may be evaluated in this article, or claim that may be made by its manufacturer, is not guaranteed or endorsed by the publisher.

Supplementary material

The Supplementary material for this article can be found online at: https://www.frontiersin.org/articles/10.3389/fvets.2024.1401141/full#supplementary-material

References

1. Smith M, Warmolts D, Thoney D, Hueter R, Murray M, Ezcurra J. *The elasmobranch husbandry manual II: Recent advances in the Care of Sharks, rays, and their relatives*. Columbus, OH: Ohio Biological Survey Inc. (2017). 113–135.

2. Reed P, Francis-Floyd R, Klinger R, Petty D. *Monogenean parasites of fish: FA28/FA033, rev. 6/2012. EDIS*, vol. 8 University of Florida Gainesville, FL (2012).

3. Thoney DA, Hargis WJ. Monogenea (Platyhelminthes) as hazards for fish in confinement. *Annu Rev Fish Dis*. (1991) 1:133–53. doi: 10.1016/0959-8030(91)90027-H

4. Whittington ID, Cribb BW, Hamwood TE, Halliday JA. Host-specificity of monogenean (platyhelminth) parasites: a role for anterior adhesive areas? *Int J Parasitol*. (2000) 3:305–20. doi: 10.1016/S0020-7519(00)00006-0

5. Kaneko JJ, Yamada R, Brock JA, Nakamura RM. Infection of tilapia, *Oreochromis mossambicus*, by a marine monogenean, *Neobenedenia melleni*, Yamaguti, 1963 in Kaneohe Bay, Hawaii, USA, and its treatment. *J Fish Dis*. (1988) 11:295–300. doi: 10.1111/j.1365-2761.1988.tb01225.x

6. Foote BC, Seyer LD, Martinelli L, Betbeze C, Newkirk K, Terio K, et al. Clinical and histopathologic ocular findings in aquarium-housed cownose rays (*Rhinoptera bonasus*). *J Zoo Wildl Med*. (2023) 54:692–703. doi: 10.1638/2023-0006

7. Seyer LD, Moore DP, Barrett C, Solangi M, Betbeze C. Ulcerative keratopathy in 11 captive cownose rays (*Rhinoptera bonasus*) In: *International Association for Aquatic Animal Medicine 2021 proceedings, virtual conference* Veterinary Information Network (VIN) (2021). 23–6.

8. Hadfield CA, Clayton LA. *Clinical guide to fish medicine*. New Jersey: John Wiley and Sons Inc. (2021). 522 p.

9. Campbell TW, Grant KR. Sample collection for wet mounts and Cytodiagnosis in fish In: *Exotic animal hematology and cytology*. *5th* ed. New Jersey: John Wiley and Sons Inc. (2022). 593.

10. Thoney DA. The effects of trichlorfon, praziquantel, and copper sulphate on various stages of the monogenean, *Benedeniella posterocolpa*, a skin parasite of the cownose ray. *Rhinoptera bonasus J Fish Dis*. (1990) 13:385–9. doi: 10.1111/j.1365-2761.1990.tb00797.x

11. Chisholm L, Whittington ID. Efficacy of praziquantel bath treatments for monogenean infections of the *Rhinobatos typus*. *J Aquat Anim Health*. (2002) 14:230–4. doi: 10.1577/1548-8667(2002)014<0230:EOPBTF>2.0.CO;2

12. Noga EJ, editor. *Fish disease: Diagnosis and treatment*. Hoboken: Wiley-Blackwell (2011). 412–413.

13. Thomas A, Dawson MR, Ellis H, Stamper MA. Praziquantel degradation in marine aquarium water. *PeerJ*. (2016) 4:e1857. doi: 10.7717/peerj.1857

14. Gabriel AA, Yee-Nin ST, Adamu L, Hassan HMD, Wahid AH. Enucleation in a cownose ray (*Rhinoptera bonasus*). *Case Rep Vet Med*. (2018) 2018:1–6. doi: 10.1155/2018/5048948

15. Lum AM, Miller SN, Clauss TM, Anderson CE. Physiologic responses of cownose rays (*Rhinoptera bonasus*) following freshwater dips for treatment of capsalid monogeneans. *J Aquat Anim Health*. (2023) 36, 128–135. doi: 10.1002/aah.10210

16. Boylan SM, Daniel W, Matthews C. Prolonged hypo-salinity to control Neobenedenia spp. monogenean infection in large display aquaria. *Zoo Biol*. (2021) 40:584–7. doi: 10.1002/zoo.21633

17. Ellis EP, Watanabe WO. The effects of hyposalinity on eggs, juveniles and adults of the marine monogenean, *Neobenedenia melleni* treatment of ecto-parasitosis in seawater-cultured tilapia. *Aquaculture*. (1993) 117:15–27. doi: 10.1016/0044-8486(93)90119-J

18. Chisholm LA, Whittington ID, Fischer ABP. A review of Dendromonocotyle (Monogenea: Monocotylidae) from the skin of stingrays and their control in public aquaria. *Folia Parasitol*. (2004) 51:123–30. doi: 10.14411/fp.2004.017

19. Tsvetanova A, Powell RM, Tsvetanov KA, Smith KM, Gould DJ. Melting corneal ulcers in dogs: a 5-year clinical and microbiological study (2014-2018). *Vet Ophthalmol*. (2021) 24:265–78. doi: 10.1111/vop.12885

20. Kik MJL, Janse M, Benz GW. The sea louse Lepeophtheirus acutus (Caligidae, Siphonostomatoida, Copepoda) as a pathogen of aquarium-held elasmobranchs. *J Fish Dis*. (2011) 34:793–9. doi: 10.1111/j.1365-2761.2011.01295.x

21. Edelhauser HF. The balance between corneal transparency and edema. *Invest Ophthalmol Vis Sci*. (2006) 47:1755–67. doi: 10.1167/iovs.05-1139

22. Alanazi SA, Almubrad T, Ibrahim AIA, Khan AA, Akhtar S. Ultrastructure Organization of Collagen Fibrils and Proteoglycans of stingray and shark corneal stroma. *J Ophthalmol*. (2015) 2015:686914. doi: 10.1155/2015/686914

23. Womersley F, Hancock J, Perry CT, Rowat D. Wound-healing capabilities of whale sharks (*Rhincodon typus*) and implications for conservation management. *Conserv Physiol*. (2021) 9:1–16. doi: 10.1093/conphys/coaa120

24. McGregor F, Richardson AJ, Armstron AJ, Armstrong AO, Dudgeon CL. Rapid wound healing in a reef manta ray masks the extent of vessel strike. *PLoS One*. (2019) 14:e0225681. doi: 10.1371/journal.pone.0225681

25. Whitley RD, Hamor RE. Diseases and surgery of the canine cornea and sclera In: KN Gelatt, editor. *Veterinary ophthalmology*. Hoboken, NJ: John Wiley and Sons Inc (2021). 1091.

frontiers | Frontiers in Veterinary Science

TYPE Methods
PUBLISHED 22 July 2024
DOI 10.3389/fvets.2024.1410421

Check for updates

OPEN ACCESS

EDITED BY
Natalie D. Mylniczenko,
Walt Disney World, United States

REVIEWED BY
Jennifer Dagostino,
Oklahoma City Zoo, United States
Carlos Rojo-Solis,
Fundación Oceanogràfic de la Comunitat Valenciana, Spain

*CORRESPONDENCE
Jennifer T. Wyffels
✉ wyffels@ripleys.com

RECEIVED 01 April 2024
ACCEPTED 21 June 2024
PUBLISHED 22 July 2024

CITATION
George RH, Buckner C, Baine K, Steeil J, White S, Handsel T and Wyffels JT (2024) Surgical outcomes and complications associated with ovariectomy in the southern stingray *Hypanus americanus*. *Front. Vet. Sci.* 11:1410421. doi: 10.3389/fvets.2024.1410421

COPYRIGHT
© 2024 George, Buckner, Baine, Steeil, White, Handsel and Wyffels. This is an open-access article distributed under the terms of the Creative Commons Attribution License (CC BY). The use, distribution or reproduction in other forums is permitted, provided the original author(s) and the copyright owner(s) are credited and that the original publication in this journal is cited, in accordance with accepted academic practice. No use, distribution or reproduction is permitted which does not comply with these terms.

Surgical outcomes and complications associated with ovariectomy in the southern stingray *Hypanus americanus*

Robert H. George[1], Chris Buckner[2], Katherine Baine[2], James Steeil[2,3], Stacia White[1], Tim Handsel[4] and Jennifer T. Wyffels[4]*

[1]Ripley's Aquarium of Myrtle Beach, Myrtle Beach, SC, United States, [2]Ripley's Aquarium of the Smokies, Gatlinburg, TN, United States, [3]Smithsonian's National Zoo and Conservation Biology Institute, Washington, DC, United States, [4]Ripley's Aquariums, Orlando, FL, United States

Southern stingrays (*Hypanus americanus*) are relatively large rays that are common and popular in public aquariums because of their size and gentle nature. In aquariums, as well as in the wild, female southern stingrays are fecund. They have a short gestation cycle and can sustain multiple pregnancies each year, each culminating with 2–10 young. This reproductive rate could quickly outpace capacity in managed care and result in a ray surplus. To prevent overpopulation, many aquaria have resorted to single sex groups with a preference for female-only populations. This is an effective way to control population growth, but forces the maintenance of two separated populations of rays; for females this interrupts normal reproductive cycling and replaces it with a protracted non-pregnant condition. An additional consideration is development of reproductive disease in females which is recognized by an enlarged, misshapen, and congested ovary with an abundance of cystic structures and an enlarged uterus with a thickened wall that is often filled with histotroph despite a non-pregnant status. There are no effective long-lasting medical treatments for this type of reproductive disease and mortality is often the result. This report describes a surgical technique for ovariectomy in southern stingrays including outcomes and complications. Ovariectomy as a surgical method prevents unwanted reproduction and has the benefit of reducing reproductive pathologies commonly observed in southern stingrays as they age. Seven stingrays 1–5.2years old and 42–83.5cm disc width underwent ovariectomy. After anesthesia, the ovary and a small amount of epigonal was excised via a left para-lumbar incision. Four of the seven rays survived five or more years post-procedure. Two rays died acutely of coelomitis and one ray died of complications unrelated to the procedure. This report details a surgical procedure for ovariectomy in southern stingrays including outcomes, complications, and recommendations.

KEYWORDS

ovary, cyst, histotroph, dystocia, reproductive disease, contraception

Introduction

Southern stingrays (*Hypanus americanus*) are relatively large rays that are common and popular in public aquariums because of their size and gentle nature. They are often maintained in shallow exhibits that offer guests a chance to touch and interact with them through guest interaction programs. In aquariums, as well as in the wild, female southern stingrays are

long-lived (1) and fecund (2). Females have a functional left ovary and uterus, rudimentary and likely non-functional right ovary, and vestigial right uterus (3–5). Southern stingrays in managed care have a relatively short gestation cycle and can sustain multiple pregnancies in any given year, each culminating with 2–10 young (2). The average gestation calculated from the interval between successive parturition dates for seven females at Ripley's Aquarium of Myrtle Beach is 140 ± 9 days (Table 1). The number of young scales with female size so as rays grow their fecundity effectively increases (2, 3). This reproductive rate could quickly outpace capacity in managed care and result in a ray surplus. To prevent overpopulation, many aquariums have resorted to single sex exhibits with a preference for female-only populations. This can be attributed to the larger size of females compared to males (1) but also because of the potential for injuries from conspecific male sexual aggression.

Southern stingrays in the wild reproduce asynchronously with ovulation and parturition observed throughout the year (3). However, for southern stingrays in a single sex population, there is a protracted period of non-pregnancy that may contribute to the development of reproductive disease (5). During this non-pregnant period, the left ovary continues to mature follicles. Continuous follicle production without a corresponding rate of ovulation results in the accumulation of follicles and ovarian mass over time (personal observation). The ovary often becomes cystic and can achieve huge dimensions, weighing up to a kilogram (5). Ovarian tissues are thin and friable, and when ovaries attain such a large size, they are prone to tearing which can lead to catastrophic hemorrhage and death.

Reproductive disease also affects the uterus which often continues to produce histotroph meant to supplement the nutrition of developing embryos. Ultrasonography often reveals a large hypoechoic histotroph-filled uterus (5). The vestigial right uterus may also be similarly affected. Since the ray's coelom may become distended ventrally as well as dorsally from the swollen uteri, rays sometimes develop pressure sores when resting on the exhibit floor. For several southern stingrays, the pressure sores became severe and weakened the coelomic wall which ruptured. The loss of coelomic integrity was followed by the development of severe coelomitis that was nonresponsive to antibiotic therapy and resulted in death (personal observation). The accumulation of histotroph may be symptomatically treated by cannulating the cervix and evacuating the uterus but the fluid accumulation often recurs after only a few months (personal observation). There are no known chemical contraceptive methods effective for elasmobranchs and therefore surgical methods were explored (6). As an alternative to pharmacological contraception, ovariectomy controls unwanted reproduction and has the benefit of reducing reproductive pathologies commonly observed in southern stingrays as they age. To manage the population size and prevent development of reproductive disease, ovariectomy was pursued.

Materials and methods

Animals

Southern stingrays ($n = 7$) were considered candidates for ovariectomy if they were less than 85 cm disc width (DW), not pregnant, and did not have evidence of reproductive disease.

Surgical procedure

Candidate rays were captured and placed in a holding tank containing oxygenated seawater from their exhibit. A second tank with oxygenated seawater from the same source was treated with tricaine methanesulphonate (MS-222) (70 ppm; Syndel, Ferndale, Washington, United States) buffered 4:1 with sodium bicarbonate. Once the MS-222 and bicarbonate had dissolved, a ray was added to the anesthetic solution. Anesthesia was deemed sufficient when the ray was minimally responsive to touch while still maintaining spiracular respiration. The ray was lifted out of the anesthetic tank and placed on a pre-moistened towel covering the surface of a custom and portable stingray medical treatment cart adjacent to the holding tanks. A submersible pump, placed in the anesthetic tank pumped seawater through a ½ inch polypropylene hose to a T adapter from which ½ inch hoses were placed into the ray's spiracles (Figure 1A). Anesthetic seawater flowed through the spiracles, cascaded over the gills and drained from the ray's gill slits as well as its mouth. The anesthetic seawater drained from the top tray of the medical cart into a catching basin on the bottom tray of the cart and was recycled back into the anesthetic holding tank.

A rolled and pre-moistened cotton towel was laid caudal to the spiracles to block potential overflow of anesthetic seawater from contaminating the surgical site. The left para-lumbar area was sanitized using gauze soaked in povidone iodine surgical prep solution and applied using light pressure starting at the incision site and circling outward. The povidone application was repeated twice more and a clear plastic, sterile, surgical drape was sutured in position to isolate the surgical area (Figure 1B). A 6–8 cm incision was made using a number 10 blade parallel to the spinal column and 2–4 cm lateral to the dorsal lumbar muscles. The skin incision was initiated just caudal to where the fin rays (ceratotrichia)

TABLE 1 Parturition dates and gestation time for southern stingrays at Ripley's Aquarium of Myrtle Beach.

Ray ID	Successive parturition dates				Total days	Average gestation ± SD
	1	2	3	4		
091*602*093	05/25/08	10/18/08			146	146
088*262*550	04/03/08	08/18/08			137	137
091*612*103	01/06/08	05/24/08	09/25/08		263	132 ± 11
055*823*843	06/05/08	10/02/08	02/12/09		252	126 ± 10
056*572*292	12/20/07	05/15/08	09/25/08	02/21/09	429	143 ± 9
056*802*312	12/15/07	05/07/08	10/29/08	03/23/09	464	155 ± 18
056*101*838	01/24/08	05/28/08	10/08/08	03/22/09	423	141 ± 21

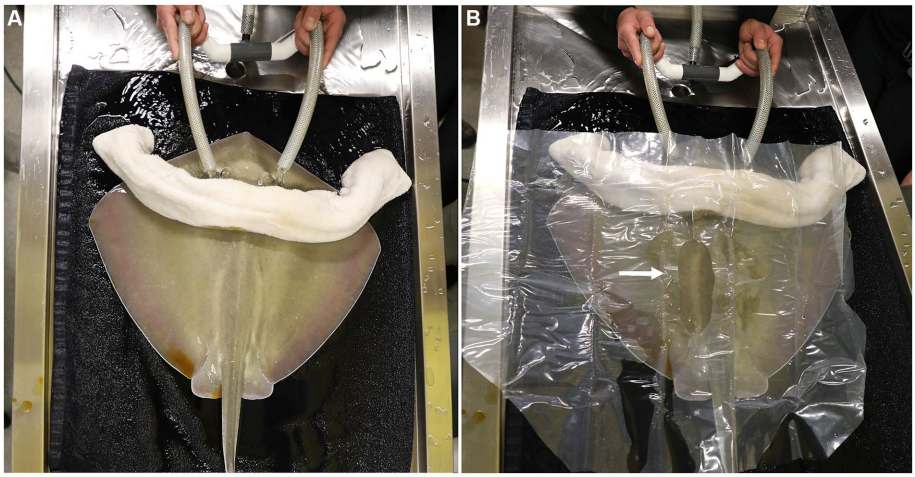

FIGURE 1
(A) The anesthetized southern stingray is placed on a prewetted towel on the surgical surface of the portable medical cart. Seawater was pumped from the anesthetic tank through a ½ inch polypropylene hose to a T adapter from which 1/2 inch hoses are placed into the ray's spiracles. A rolled and pre-wetted cotton towel was laid caudal to the spiracles to block potential overflow anesthetic water from contaminating the surgical site. **(B)** A clear plastic, sterile drape was sutured in position and the surgical area exposed (arrow) for a 6–8 cm incision initiated just caudal to where the fin rays (ceratotrichia) join with the epaxial muscles parallel to the spinal column and 2–4 cm lateral to the dorsal lumbar muscles.

join with the epaxial muscles. Even though the incision is parallel to the spine, it is unavoidable to incise nerves that run medio-laterally all along the incision site. This does not impair normal swimming patterns post-surgery. After incising the muscle and the peritoneum, the cranial portion of the ovary and the oviduct were dissected free from the dorsal suspensory ovarian ligament (Figure 2A). Two 6-inch curved Kelly hemostat clamps were placed around the freed tissue anterior to the ovary. Using 3-0 polydioxanone suture (PDS) material, a single encircling ligature was placed anterior to the two clamps (Figure 2B) and the tissue between them was incised. A second tie was then placed around the clamped blood supply. The thick anterior pedicle appeared to supply most of the blood to the ovary. A thin suspensory ovarian ligament ran along the ray's dorsal midline between the ovary and the body wall. It was transected with scissors or blunt dissection and was relatively avascular. Mosquito forceps were applied for hemostasis as necessary. The caudal pole of the ovary was broadly attached to the cranial end of the epigonal organ. A clamp was placed across the epigonal organ caudal to the junction (Figure 2C), an encircling suture was placed around the epigonal organ, and the ovarian tissue was transected and removed along with a small amount of epigonal tissue (Figure 2D).

The peritoneal membrane was sutured with 3-0 PDS material on a half round taper needle in a simple interrupted pattern. The muscular layers were not directly sutured as the tissues were too weak to hold sutures. At this time, 1–2 mL of 2% lidocaine were dripped into the incision for post-surgical analgesia. The skin was sutured with 3-0 PDS material on a cutting needle in a simple interrupted pattern (Figure 3A). It was important to get good tissue apposition to prevent saltwater intrusion so care was taken to place the sutures relatively close together and tighter than would be done for mammals. Intramuscular injection of NSAIDs (ketoprofen 2 mg/kg or meloxicam 2 mg/kg) and antibiotics (ceftiofur 8 mg/kg) were administered, the spiracular hoses removed, and the ray moved to the adjacent holding or recovery tank. Once the ray responded to touch by swimming away in a normal manner it was returned to the original exhibit. The surgery site did not require post-operative care and sutures were removed after 1 month.

Results

During the development of this surgical procedure, 3 rays (54–65 cm DW, 6.5–8.8 kg, 3–3.9 years old) underwent successful exploratory laparotomies with the intent to evaluate the detailed anatomy of the ovary and associated epigonal tissue and assess the practicality of an ovariectomy but were not ovariectomized, and 7 rays were subsequently ovariectomized (Table 2). Average surgery time was 30 ± 11 min ($n = 6$, average ± standard deviation) and ranged from 17–49 min. Of the ovariectomized rays, one died 22 days post procedure from coelomitis, one died 21 days post-procedure from coelomitis, and a third in poor body condition at the time of surgery died 21 days post-procedure of unrelated health complications. Four rays survived long-term after surgery, two surviving 5.1 and 6.0 years, and two were alive at the time of writing, 5.2 and 10.9 years post-procedure. Among this relatively small cohort of ovariectomized southern stingrays, none became pregnant, and no evidence of regeneration of functional ovarian tissue or rudimentary and likely non-functional vestigial ovarian tissue has been observed at necropsy (Figure 3B) or ultrasonographically during annual wellness exams.

Discussion

Ovariectomy of southern stingrays is a practical technique that can be employed to prevent unwanted reproduction and has the added benefit of reducing reproductive pathologies commonly observed in southern stingrays as they age. Mature stingrays with a well-developed ovary make it challenging to safely complete the surgery because of the large ovarian mass and corresponding blood supply compared to immature or maturing rays. The smallest and most immature ray also complicated the surgery because of the difficulty to identify the margins of the ovary from the epigonal organ. To help choose the ideal surgical candidate, ovary and ovarian follicle size may be evaluated pre-operatively by ultrasonography for

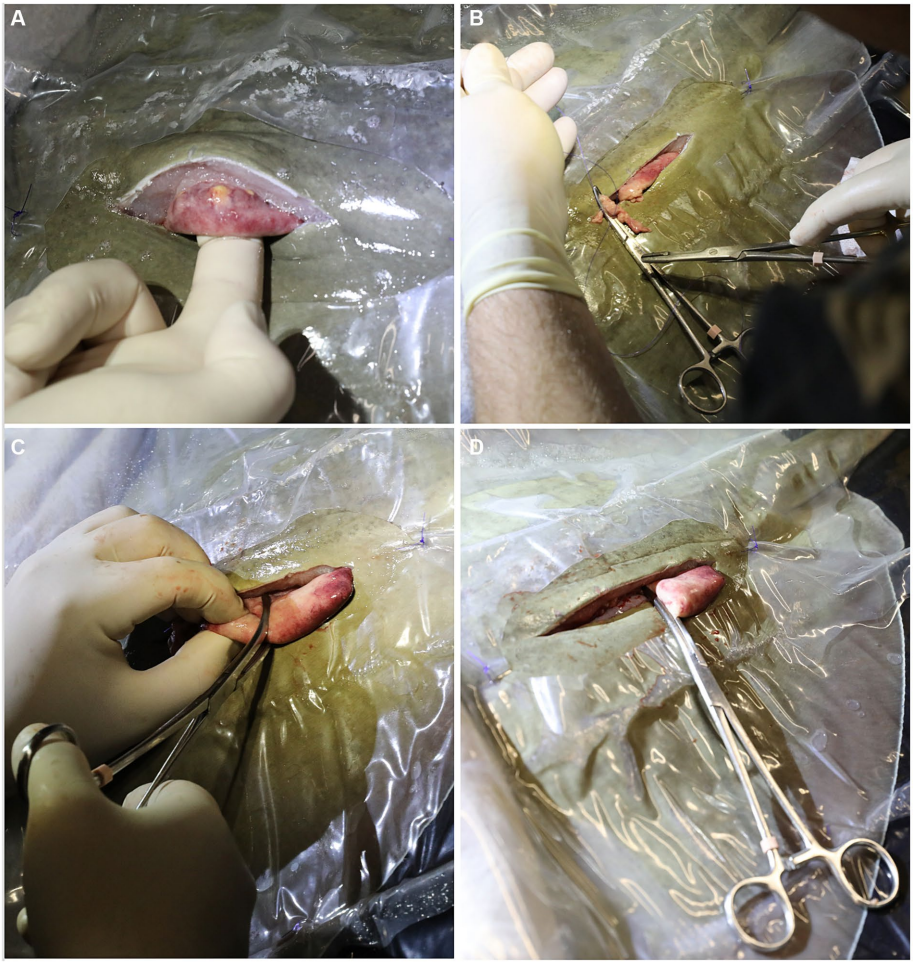

FIGURE 2
(A) After incising the muscle and the peritoneum, the cranial portion of the ovary and the oviduct were dissected free from the dorsal suspensory ovarian ligament. **(B)** Two 6 inch curved Kelly hemostat clamps were placed around the freed tissue anterior to the ovary. Using 3-0 polydioxanone suture (PDS) material, a single encircling ligature was placed anterior to the two clamps and the tissue between them was incised. A second tie was then placed around the clamped blood supply. **(C)** A clamp was placed across the epigonal organ caudal to the junction, an encircling suture was placed around the epigonal organ. **(D)** The ovarian tissue was transected and removed along with a small amount of epigonal tissue.

rays nearing maturity based on disc width. Ultrasonography also informs ovarian position to help guide incision location. Too large (mature) a stingray may have a large ovary with several cohorts of developing follicles making extraction more difficult and increasing the chance of hemorrhage during removal. Based on the authors' experience, too small (immature) a stingray may increase the chance of leaving tissue that can become a functional ovary. Ultimately, the ideal stingray size was approximately 60–70 cm DW, at the onset of maturity, when ovarian margins are visually distinct from the epigonal and ovarian follicle development is minimal with the largest follicles 1 cm or less in diameter.

There were two mortalities among the first series of ovariectomies, both due to coelomitis. Both the procedure and equipment were refined with each procedure, and no further mortalities directly attributed to the surgery have occurred. During one of the initial procedures, an anesthetic hose popped out of the stingray's spiracle and injected seawater into the surgery site. To prevent this problem during future procedures, anesthetic seawater pressure was decreased and a pre-moistened, rolled cotton towel was placed across the ray's body just caudal to the spiracles. The towel should be pre-moistened to avoid stripping the stingray's epithelial mucus and rolling the towel creates a protective barrier to block water reflux from the spiracle. Despite antibiotic therapy this animal died due to coelomitis. Southern stingrays did not appear to be adversely affected by the procedure and returned to normal swimming and eating behaviors the same day as the surgery.

Ovariectomy of southern stingrays is feasible within the realm of any experienced veterinary surgeon. Surgical time should be 45 min or less and with experience the procedure time should decrease to 30 min or less. Other institutions have used this procedure and successfully ovariectomized southern stingrays under their care to limit future reproduction (Dr. Shane Boylan, personal communication, 31 February 2024). Hysterectomy of the functional uterus and/or vestigial uterus was not considered for any ray because the primary purpose was to prevent reproduction which is accomplished via ovariectomy. Further, pathologies of the uterus related to reproductive disease are secondary to ovarian pathologies (5) and have not been observed for ovariectomized southern stingrays.

This surgical procedure can be extended for use in other ray species increasing the utility and impact of the procedure (7). It

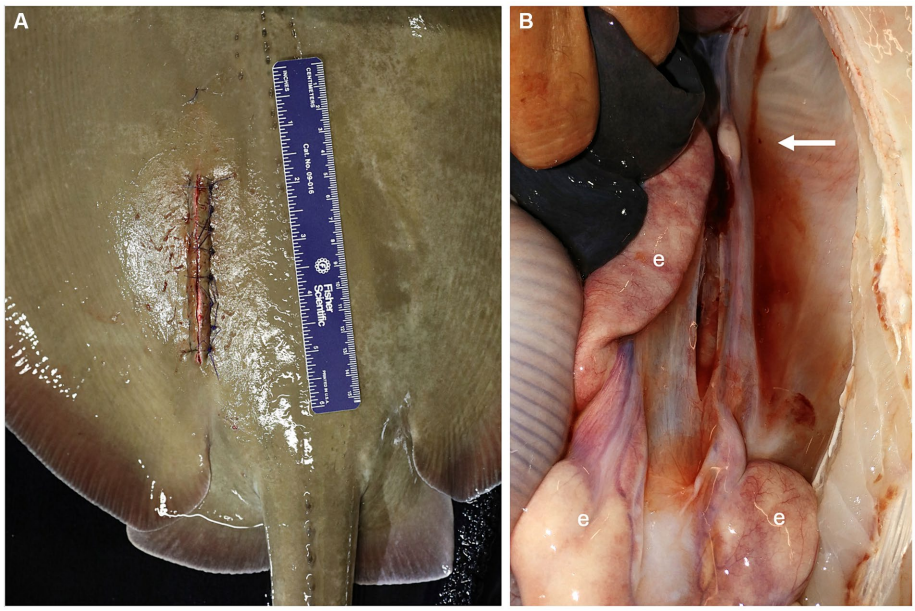

FIGURE 3
(A) The peritoneum was sutured with 3-0 PDS material on a half round taper needle in a simple interrupted pattern and the skin was sutured with 3-0 PDS material on a cutting needle in a simple interrupted pattern. **(B)** Lack of ovarian tissue was confirmed during necropsy 5.1 years after surgical ovariectomy. The right epigonal organ (e) extends cranial to caudal in the coelom but is reduced on the left side where the ovary was removed (arrow).

TABLE 2 Southern stingray age and size at ovariectomy with survivorship post-ovariectomy ordered by ray disc width and body weight.

Ray ID	Age (years)	Disc width (cm)	Body weight (kg)	Survivorship post-ovariectomy
MB-DA-18-13-F	1	42	2.1	Alive, 5.2 years
MB-DA-10-03-F	4.6	53	4.3	22 days
MB-DA-10-10-F	4.5	54	4.7	21 days
MB-DA-08-28-F	4.8	54	7.8	Alive, 10.9 years
MB-DA-09-19-F	4.2	64	8	5.1 years
MB-DA-07-03-F	5.2	70.3	10.73	21 days
GB-DA-08-05-F	4.9	83.5	20.5	6.0 years

also could be used as a treatment to be employed successfully in older rays of various species with ovarian disease (Dr. Natalie Mylniczenko, personal communication, 19 March 2024). However, despite all rays being viviparous and histotrophic, their reproductive anatomy cannot be generalized. Rays have species-specific combinations of bilateral and unilateral ovarian and uterine functionality. In addition, ovarian location, attachment to peripheral organs and differences in vascular supply to the organ itself require confirmation before attempting ovariectomy. Further complicating the species-specific anatomy is potential ovarian plasticity, some ray species have asymmetric or even vestigial ovaries that may become functional if the dominant ovary is removed (not observed for southern stingrays) (7). Bilateral ovariectomy would require epigonal organ resection for at least one of the two paired myelopoietic organs making the procedure considerably more difficult to perform. Ovariectomy of southern stingrays is a safe and reliable method and management tool for husbandry professionals to control reproduction among their population.

Data availability statement

The original contributions presented in the study are included in the article/supplementary material, further inquiries can be directed to the corresponding author.

Ethics statement

The animal studies were approved by Ripley's Aquariums Research Review Committee. The studies were conducted in accordance with the local legislation and institutional requirements.

Author contributions

RG: Writing – original draft, Methodology, Conceptualization. CB: Writing – review & editing, Methodology. KB: Writing – review & editing, Methodology. JS: Writing – review & editing,

Methodology. SW: Writing – review & editing, Data curation. TH: Writing – review & editing, Supervision. JW: Writing – original draft, Conceptualization.

Funding

The author(s) declare that financial support was received for the research, authorship, and/or publication of this article. Development of this method and dedicated time for authors to complete a manuscript was supported by Ripley's Aquariums.

Acknowledgments

The authors thank the entire animal care team at Ripley's Aquariums for their support and expertise and Nathan Barnes and Mary Phillips from Ripley's Aquarium of the Smokies who provided images and video of various ovariectomy procedures.

Conflict of interest

The authors declare that the research was conducted in the absence of any commercial or financial relationships that could be construed as a potential conflict of interest.

Publisher's note

All claims expressed in this article are solely those of the authors and do not necessarily represent those of their affiliated organizations, or those of the publisher, the editors and the reviewers. Any product that may be evaluated in this article, or claim that may be made by its manufacturer, is not guaranteed or endorsed by the publisher.

References

1. Henningsen AD, Leaf RT. Observations on the captive biology of the southern stingray. *Trans Am Fish Soc*. (2010) 139:783–91. doi: 10.1577/T09-124.1

2. Henningsen AD. Notes on reproduction in the southern stingray, *Dasyatis americana* (Chondrichthyes: Dasyatidae), in a captive environment. *Copeia*. (2000) 2000:826–8. doi: 10.1643/0045-8511(2000)000[0826:NORITS]2.0.CO;2

3. Ramírez-Mosqueda E, Pérez-Jiménez JC, Mendoza-Carranza M. Reproductive parameters of the southern stingray *Dasyatis americana* in southern Gulf of Mexico Latin. *Lat Am J Aquat Res*. (2012) 40:335–44. doi: 10.3856/vol40-issue2-fulltext-8

4. Schwert HL. (1967). The reproductive system of the female sting ray, *Dasyatis americana*. MSc thesis. Ithaca, NY: Zoology Department, Cornell University

5. Mylniczenko ND, Sumigama S, Wyffels JT, Wheaton CJ, Guttridge TL, DiRocco S, et al. Ultrasonographic and hormonal characterization of reproductive health and disease in wild, semiwild, and aquarium-housed southern stingrays (*Hypanus americanus*). *Am J Vet Res*. (2019) 80:931–42. doi: 10.2460/ajvr.80.10.931

6. Sailler A, Laidebeure S, Lécu A. Effects of a GnRH vaccine and deslorelin acetate implants in male freshwater stingrays (*Potamotrygon* sp.). *J Zoo Wildl Med*. (2023) 54:40–8. doi: 10.1638/2022-0090

7. Anderson CE, Gillis JD, Miller SN, Davis MR. Production of live offspring following unilateral (left) ovariectomized Potamotrygon rays (*Potamotrygon castexi, Potamotrygon leopoldi,* and *Potamotrygon motoro*). *J Am Vet Med Assoc*. (2023) 261:1–4. doi: 10.2460/javma.23.01.0031

frontiers | Frontiers in Veterinary Science

TYPE Original Research
PUBLISHED 30 July 2024
DOI 10.3389/fvets.2024.1410377

Check for updates

OPEN ACCESS

EDITED BY
Nucharin Songsasen,
Center for Species Survival, Smithsonian Conservation Biology Institute (SI), United States

REVIEWED BY
Budhan Pukazhenthi,
Smithsonian Conservation Biology Institute (SI), United States
Jen Flower,
The Walt Disney Company, United States

*CORRESPONDENCE
Lance Adams
ladams@lbaop.org

RECEIVED 01 April 2024
ACCEPTED 11 July 2024
PUBLISHED 30 July 2024

CITATION
Adams L, Wyffels JT, Goodwin B, Munson R, LeBorgne L, Feldheim KA and Lyons K (2024) Monitoring egg fertility, embryonic morbidity, and mortality in an oviparous elasmobranch using ultrasonography.
Front. Vet. Sci. 11:1410377.
doi: 10.3389/fvets.2024.1410377

COPYRIGHT
© 2024 Adams, Wyffels, Goodwin, Munson, LeBorgne, Feldheim and Lyons. This is an open-access article distributed under the terms of the Creative Commons Attribution License (CC BY). The use, distribution or reproduction in other forums is permitted, provided the original author(s) and the copyright owner(s) are credited and that the original publication in this journal is cited, in accordance with accepted academic practice. No use, distribution or reproduction is permitted which does not comply with these terms.

Monitoring egg fertility, embryonic morbidity, and mortality in an oviparous elasmobranch using ultrasonography

Lance Adams[1]*, Jennifer T. Wyffels[2,3], Brittney Goodwin[1], Rachel Munson[1], Louise LeBorgne[1], Kevin A. Feldheim[4] and Kady Lyons[5]

[1]Aquarium of the Pacific, Long Beach, CA, United States, [2]Ripley's Aquariums, Orlando, FL, United States, [3]Delaware Biotechnology Institute, Center for Bioinformatics and Computational Biology, University of Delaware, Newark, DE, United States, [4]Pritzker Laboratory for Molecular Systematics and Evolution, The Field Museum, Chicago, IL, United States, [5]Center for Species Survival, Georgia Aquarium, Atlanta, GA, United States

Ultrasonography is widely used to monitor pregnancy in viviparous species, but it is underutilized as a tool to characterize embryonic development in oviparous species. Currently, a multi-institutional effort is underway to re-wild the endangered zebra shark (*Stegostoma tigrinum*) to locations where this species was previously extirpated by leveraging the reproductive efforts of aquarium sharks as a source of brood stock. Zebra sharks are oviparous and fecund, but a large percentage of their yolked eggs do not result in hatchlings. Therefore, ultrasonography represents a potential tool for distinguishing fertile eggs with developing embryos from degrading eggs, and to diagnose changes in early embryonic development predictive of poor outcomes. The objectives of the current study were to use ultrasonography to assess egg fertility, monitor early embryonic development, and identify morphological indicators that may be predictive of early embryonic mortality. Freshly laid eggs from four female zebra sharks were collected and inventoried daily at Aquarium of the Pacific. Eggs were incubated undisturbed for 2 to 4 weeks and subsequently examined weekly via ultrasound to assess fertility and monitor embryo development. Among 120 fertile eggs, embryos were identified as early as 8 days post-oviposition, with average (±SD) time to first observation at 30 ± 7 days. Morphological and behavioral abnormalities were observed for most embryos ($n = 84$, 70%) as early as 16 days and up to 95 days post-oviposition. Common abnormalities included: bent or curled tails, vesicle(s) at the base of the yolk stalk, and slow or weak movement. Only one embryo survived to hatch during the study and was genetically-confirmed parthenogenetic, suggesting hatching success for parthenotes is low (<1%). Ultrasonography was demonstrated to be an effective and non-invasive method to determine egg fertility, identify embryos with developmental abnormalities, and monitor embryo growth.

KEYWORDS

embryonic development, growth, abnormality, parthenogenesis, ultrasound

1 Introduction

Characterization of reproductive cycling and associated life history parameters is important for management of both domesticated and non-domesticated animals (1, 2). Non-invasive ultrasonography has been a crucial tool in a variety of reproductive applications. For example, gonadal changes can be monitored to determine peak periods of reproductive activity in both males and females (3, 4), information that can then inform livestock production (5, 6) or characterize natural breeding cycles of wild mammals (7–9) and reptiles (10) in human care. Ultrasound has also been used to estimate fecundity and to determine sex of teleost fish (11) as well as monitor reproductive maturity, reproductive cycles and pregnancy or egg laying of both viviparous (12–15) and oviparous (16, 17) elasmobranchs, negating the need for lethal sampling which is especially advantageous for species of conservation concern.

Monitoring embryonic development through non-lethal techniques is another aspect where ultrasonography has advanced the field of reproductive science, both in humans and animals. In little-studied species, ultrasonography has been used to establish developmental baselines (18, 19), particularly for species where lethal sampling is not possible or advisable. For example, in elephants (*Loxodonta africana* and *Elephas maximus*) ultrasound was used to monitor early embryonic development from conception to implantation and determined that these species have delayed implantation (20). Understanding developmental timelines during early elephant development allowed the authors to more accurately stage embryonic development described in previous studies where gestational time was unknown. For species with well-described embryonic developmental timelines (e.g., humans, livestock, etc), ultrasound monitoring is important for confirming if (or when) embryos reach significant landmarks at the appropriate time during their gestation (21, 22). As such, ultrasonography has been used as a diagnostic tool to detect and predict signs of congenital problems during embryo development. For example, in humans, ultrasonography has been used to detect prenatal cleft deformities (23) and improper development of the central nervous system (24). In livestock, ultrasonography was used to monitor for embryonic malformations induced as a result of dams ingesting poisonous plants, information that alerted ranchers of potential hazards on farm lands (25).

As most applications have occurred in viviparous species, ultrasonography as a tool to characterize embryonic development in oviparous species is underutilized. In the chicken (*Gallus gallus*), ultrasonography allowed real-time monitoring of heart formation in developing chicks, representing a non-lethal way to study organogenesis in this model species (26, 27). Also in chickens, ultrasonography has enabled biomedical researchers using the chorioallantoic-membrane assay to track *in ovo* tumor growth and size over time (28). Nevertheless, the use of ultrasonography to track aspects of embryonic development in other oviparous species has been limited.

Among elasmobranch fishes (sharks, skates, and rays), approximately 40% of species are oviparous and their embryonic development has traditionally been monitored in two ways. Embryos can be identified and monitored through a process called "candling," where a bright backlight is shown through the egg case. Candling is used to confirm fertility in early incubation and check for viability throughout incubation, but elucidating detailed information on embryo morphology (beyond gross morphometrics) is limited for most species by the opacity of their egg shell/case. Similar techniques are used to monitor avian and reptilian embryonic development (29, 30). Changes in embryo morphology can also be tracked by "windowing" the egg case (i.e., cutting an opening) to expose the embryo for viewing. In elasmobranchs, windowing is less risky to the embryo after it has gone through eclosion, the process whereby the egg case respiratory fissures naturally open and seawater circulates through the egg case which occurs after approximately 40% of their total incubation (31). However, by this point in incubation a significant portion of development is complete, excluding most embryonic stages from direct observation. Windowing prior to eclosion often results in mortality due to iatrogenic infections, even when egg cases are resealed with a transparent barrier (Wyffels, pers. obs).

Other, more advanced, techniques have also been applied to study embryo morphogenesis *in ovo*, but present their own limitations. For example, magnetic resonance imaging (MRI) was recently used to characterize early development in chickens (embryonic day 1–20) longitudinally (32). Likewise, micro-computed tomography (micro-CT) has been applied to study chick cardiac organogenesis (33). While both of these methods are promising, equipment access, expertise, and monetary constraints may limit the use of these techniques in non-model species. Ultrasonography can overcome some of these limitations and allows a non-destructive internal view at any time during development but is especially advantageous for early development. Use of ultrasonography to examine embryo development has been applied to two Heterodontus species, which lay rather thick egg cases that render candling rather ineffective (34). Therefore, ultrasonography fills a significant gap in non-lethal longitudinal monitoring techniques for the earliest stages of embryonic growth and development in oviparous elasmobranch species.

Ultrasonography may also help fill outstanding needs in the conservation community where methods to more easily access fertility in species of concern are required (18, 35). Within the field of elasmobranch conservation, a multi-institutional effort is underway to re-wild the endangered zebra shark (*Stegostoma tigrinum*) to locations where this species was previously extirpated by leveraging aquarium collections as a source of brood stock (36). Through this workplan, eggs from genetically appropriate adults will be shipped to Indonesia where developing embryos will be hatched and reared prior to release. However, while zebra sharks are fecund (37), a large percentage of yolked eggs degrade within the first few weeks post-oviposition (38). Therefore, ultrasonography represents a potential tool that could be used to accurately distinguish fertile from non-fertile eggs, monitor early embryonic development, and diagnose changes in the egg and embryo predictive of poor outcomes. Because the resources that can be invested in each individual egg for potential re-wilding are limited, developing a diagnostic "early warning system" via ultrasound will help guide efforts to achieve the goals of this conservation initiative. The objectives of this study were to use ultrasonography to (1) assess egg fertility, (2) monitor early embryonic development and progress after fertility is confirmed, and (3) identify developmental indicators that may be predictive of early embryonic mortality.

2 Methods

2.1 Husbandry

Four adult female zebra sharks were maintained at Aquarium of the Pacific where egg laying activities were monitored. Two females were housed in an approximately 1.4 million liter mixed-tropical fish indoor exhibit with artificial lighting (12 h light:12 h dark) supplemented by natural light via skylights. The other two females were housed separately in an outdoor ~0.41 million liter exhibit exposed to natural light. All exhibits were filled with natural, filtered seawater kept at 23.8–25°C. Diet consisted of thawed seafood including clam, squid, mackerel and herring fed at ~7% percent of body weight weekly, along with a multivitamin supplement tablet (Mazuri Vita-Zu Shark/Ray; formula 5 M24). Throughout the study, a concurrent, but separate, effort was underway to conduct artificial insemination trials with these females.

2.2 Egg collection and incubation

Exhibits were monitored daily, and freshly laid eggs were removed by aquarists during routine cleaning. Egg cases were labeled with sequentially numbered tags attached through the non-hatching end of the egg case (Supplementary File 1), and the date of oviposition was recorded along with purported female, which was determined based on collection exhibit, egg shape and routine physical examinations to identify females that were actively laying. Eggs were relocated to an independent system maintained with continuously-moving seawater (23.8–25°C). Eggs were incubated horizontally and, on a platform, elevated off the bottom to allow water to circulate around the entire case.

2.3 Ultrasound monitoring

Eggs were incubated undisturbed for up to 4 weeks (~28–32 days) and afterwards underwent weekly checks to monitor for fertility and embryo development. Pre-ecolosion eggs were briefly exposed to air during transfer from the incubation system to a 4 L acrylic rectangular container (Kritter Keeper, Lees Aquarium & Pet Products, San Marcos, CA) with seawater, while eggs that had undergone eclosion were removed from the incubation system completely submersed to prevent air intrusion. Eggs were maintained in the same general orientation as incubation throughout the procedure to minimize movement of the animal pole, making it easier to locate embryos on the upper surface of the yolk via ultrasound. Eggs were examined using a Sonosite Edge II ultrasound and a 15–6 MHz linear transducer (HFL50, Fuifilm Sonosite Inc., Bothell, WA) with general resolution and small parts settings selected. The transducer was submerged in the water which served as the coupling agent between the transducer and the egg. Each egg was imaged in both transverse and sagittal views moving from the non-hatching end to the hatching end or from either lateral keel (lateral margin) towards the other until the entire content of the egg case was imaged (Supplementary File 2).

At each exam, eggs were evaluated for yolk integrity, presence/absence of an embryo, and echogenicity of perivitelline fluid (anechoic or particulate; Supplementary File 3). If the yolk was intact and no embryo was observed, eggs were allowed to incubate further. Eggs that fouled (i.e., formation of a slimy film on the external egg case with particulate perivitelline fluid) prior to confirmation of an embryo were discarded. Once eggs were confirmed fertile, embryos were measured weekly using the ultrasound's caliper tool for total length (cm) and the appearance of developmental features (e.g., external gills, heartbeat, etc.) was noted. The first appearance of morphological abnormalities was documented and subsequently monitored at each exam. Embryo movement was categorized as steady, slow, or none (Supplementary File 4). Non-motile embryos were allowed to incubate 1 week further to recheck and confirm mortality. After weekly exams, eggs were returned to their incubation enclosures.

2.4 Genetic testing

Embryo mortality was assessed through egg fouling, loss of embryo motility or heart beat, or observed disintegration of the yolk. When possible, necropsies were performed to sample embryonic tissue for genetic testing to determine parentage. DNA was extracted from samples using a salting-out method employed in other studies (39, 40). Embryos were genotyped using 14 previously published microsatellite markers (41). In addition, two new microsatellite loci (Sfa325 and Sfa371) were developed from the enriched library of Dudgeon et al. (41) (Supplementary Table 1). PCRs of the 14 published loci were carried out as previously described. For Sfa325 and Sfa371, PCRs were performed in 10 µl volumes with 1x PCR buffer (10 mM Tris–HCl, 50 mM KCl, pH 8.3), 0.12 mM of each dNTP, 10x BSA, 1.5 mM $MgCl_2$, 1 U Taq polymerase, 0.04 µM forward primer tagged with an M13 sequence on the 5′ end (42), 0.16 µM of both the species-specific reverse primer, and a fluorescently labeled M13 primer. Thermal cycling proceeded as follows: an initial denaturation step of 94°C for 4 min was followed by 30 cycles of 94°C for 15 s, 58°C for 15 s, and 72°C for 45 s, followed by 8 cycles of 94°C for 15 s, 53°C for 15 s, and 72°C for 45 s. A final elongation step of 72°C for 10 min concluded each PCR. All PCR products were run with an internal ladder [ALEXA-725, (43)] and on an ABI 3730XL DNA Analyzer (Thermo Fisher Scientific, Waltham, Massachusetts). Individuals were genotyped using Geneious v.10.0.3[1] (44).

2.5 Data analysis

Descriptive statistics (mean ± standard deviation) were used to characterize early life history parameters including: time to first embryo observance (days between oviposition and first identification of an embryo), time to first identification of developmental landmarks or other morphological characteristics, and lifespan (days between oviposition and embryo expiration). Embryo length was measured from still images and growth monitored by taking the mean length of embryos at the same incubation time point grouped by week. Embryos were evaluated for the presence/absence and frequency of morphological abnormalities, and lifespan was compared between groups (i.e., those with an abnormality versus those without) using a Wilcoxon U-test.

1 http://www.geneious.com

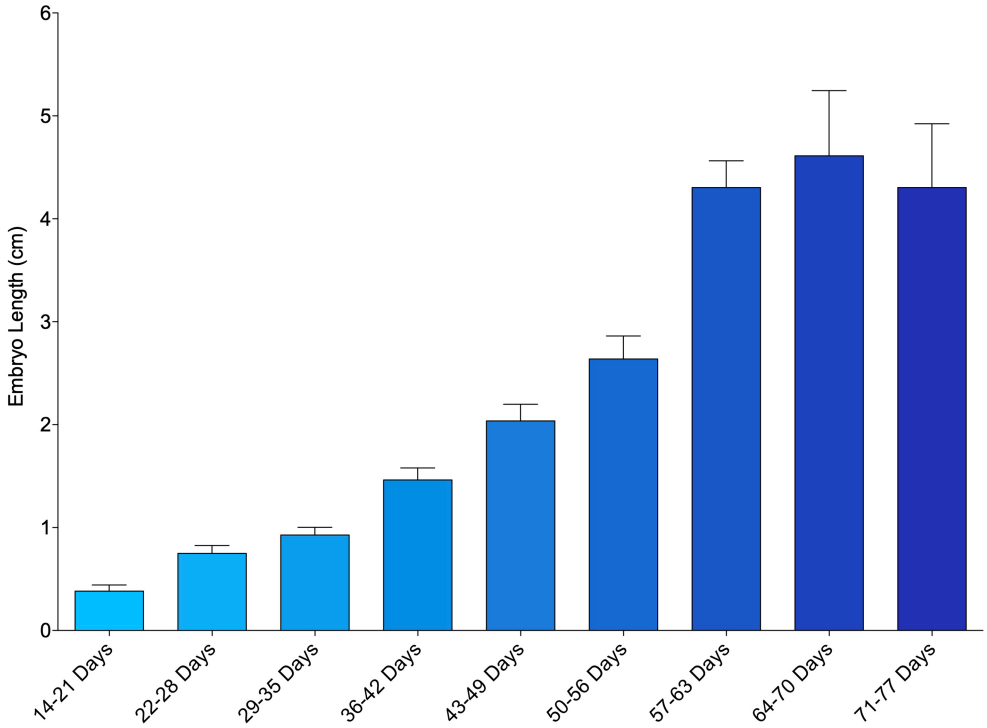

FIGURE 1
Mean length of zebra shark (*Stegostoma tigrinum*) embryos as measured via ultrasound using the caliper tool. Embryos were grouped by week of development.

3 Results

Weekly ultrasonography of incubating eggs commenced in November 2021 and concluded in December 2023. During that time, the embryonic development of 120 embryonated eggs was examined longitudinally using ultrasonography. Embryos were visually identifiable on the surface of the yolk with viability confirmed by their sinusoidal movements, which began early in development (Supplementary File 5). Initially, a subset of eggs ($n = 13$) was examined weekly after oviposition to determine the earliest time point an embryo could be detected. For this subset of eggs, embryos were observed as early as 8 days post-oviposition, with mean time to first observation occurring at 18 ± 3 days (~2.5 weeks). However, most eggs ($n = 107$, 89%) were incubated for 3 to 5 weeks before their first ultrasound examination. With all eggs included, embryos were observed by 30 (±6) days post-oviposition (~4 weeks). The longest incubation time before an embryo was observed was 47 days post-oviposition.

During examinations, the appearance of the perivitelline fluid surrounding the developing embryo was noted as either anechoic fluid or heterogeneous fluid containing particulates (Supplementary File 6). On ultrasound, presence of particulate material gives the visual appearance of a "snow globe." Particulate material was observed in 50 cases (42% of all eggs), with first observation ranging from 26 to 74 days post-oviposition (median = 41 days).

3.1 Growth and developmental landmarks

The smallest measured embryo was 0.18 cm and observed from an egg that incubated 23 days before its first examination. Mean embryo length generally increased over the course of the study from week to week (Figure 1; Supplementary File 7). In a small number of instances (27 out of 224 measurements taken, 12%), embryo length decreased between successive time points and these inconsistencies tended to occur earlier in development. Embryo length was measurable from first detection to about 64–70 days post-oviposition (~9 weeks), after which obtaining an accurate measurement became too difficult due to their size and positioning within the egg case (Figure 1).

Time to first observance of easily recognized developmental features via ultrasonography were recorded. External gill filaments were observed 66 ± 19 ($n = 14$) days post-oviposition (9.5 weeks; Figure 2). A heartbeat was detectable in two embryos at (or between) 61 and 114 days post-oviposition and the mouth could be seen between 103 and 114 days (Supplementary Table 2). As early as 177 days post-oviposition, the embryo was large enough that its movement was restricted so that the pelvic fins could be visualized in an attempt to determine sex. As claspers were not clearly identifiable, the embryo was presumed to be female and later confirmed female at hatching; however, no male embryos were available for comparison in this study. In the latter half of development, post-eclosion, the liver was observable and heart and buccal pump rate could be quantified via ultrasound (Figure 2; Supplementary File 8).

3.2 Embryo abnormalities

Several developmental anomalies were commonly observed including embryos with a sharp bend or coil in the tail, anechoic fluid pockets or vesicles on the yolk sac at the base of the yolk stalk, and more rarely those with a disproportionate or oddly shaped cranium

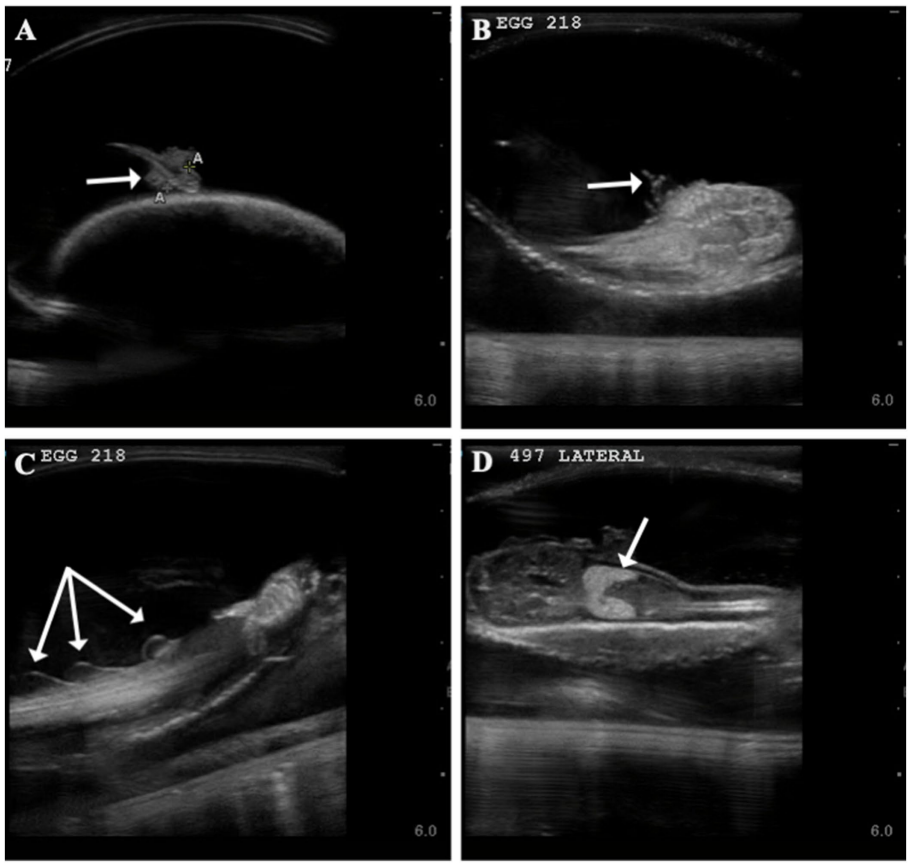

FIGURE 2
Developmental landmarks (denoted with white arrow) identified on ultrasound for two zebra shark (*Stegostoma tigrinum*) embryos (Egg # 218 and 497) at two different time points. Change in external gills from 60 days post-oviposition **(A)** to 93 days post-oviposition **(B)**, note that embryos featured are two different individuals. Fin folds **(C)** seen on an embryo 100 days post-oviposition and liver **(D)** identified on an embryo 116 days post-oviposition.

and/or underdeveloped gill filaments. When possible, abnormalities were physically confirmed at the time of egg dissection. Out of 120 embryonated eggs, 84 embryos (70%) had a deformity detectable using ultrasonography. In general, abnormalities were detected early in development (43 ± 15 days post-oviposition, ~6 weeks). The most frequently observed deformity ($n = 65$, 54%) was a bend or coil in the tail (Figure 3; Supplementary File 9), followed by a vesicle at the base of the umbilicus ($n = 41$; Figure 4). The least common abnormality observed was related to head shape and proportion ($n = 6$). Multiple deformities were observed in approximately 50% of embryos (Figure 5A), and often they were detected within 2 to 3 weeks of the first observance of the embryo (bent/coiled tail = 13 ± 12 days; vesicles = 18 ± 14 days; oddly-shaped cranium = 20 ± 9 days). When a developmental anomaly was observed, it did not resolve with time. For example, once a yolk sac vesicle was detected on ultrasound, the diameter of it either increased or stayed the same size on subsequent exams (Supplementary Files 10, 11).

3.3 Embryo morbidity and mortality

Of the 120 embryonated eggs tracked in this study, only one survived to hatching (0.83%) and it was manually assisted out of the egg case after 205 days of incubation, ~45 days after its predicted hatching date (45). For embryos without an observed abnormality, lifespan ranged from 28 to 91 days (median 42 days) compared to 34 to 142 days (median = 63 days) for embryos with an identifiable abnormality (Figure 6A). Lifespan was significantly shorter for embryos where no abnormality was observed during ultrasound monitoring compared to those with an identifiable morphological issue (Wilcoxon U-test, $W = 572$, $p < 0.0001$). Incidence of mortality was particularly high between 35 to 56 days post-oviposition for embryos where no abnormality was observed. Cumulative mortality increased from 20 to 91.4% in this 21-day period of incubation (Figure 6B). Cumulative mortality increased more gradually for embryos with an observed abnormality with 90% mortality reached at 105 days post-oviposition. No abnormalities were detected via ultrasonography for the lone embryo that survived to hatching.

Flocculent material in the perivitelline fluid had a mean onset time of 45 ± 13 days post-oviposition and was also indicative of poor prognosis. In eggs where flocculent material manifested ($n = 41$, 34%), the result was 100% embryo mortality within 13 ± 16 days of its first observation. In half (50%) of these eggs, the embryos had one or more morphological abnormality identified (Figure 5B).

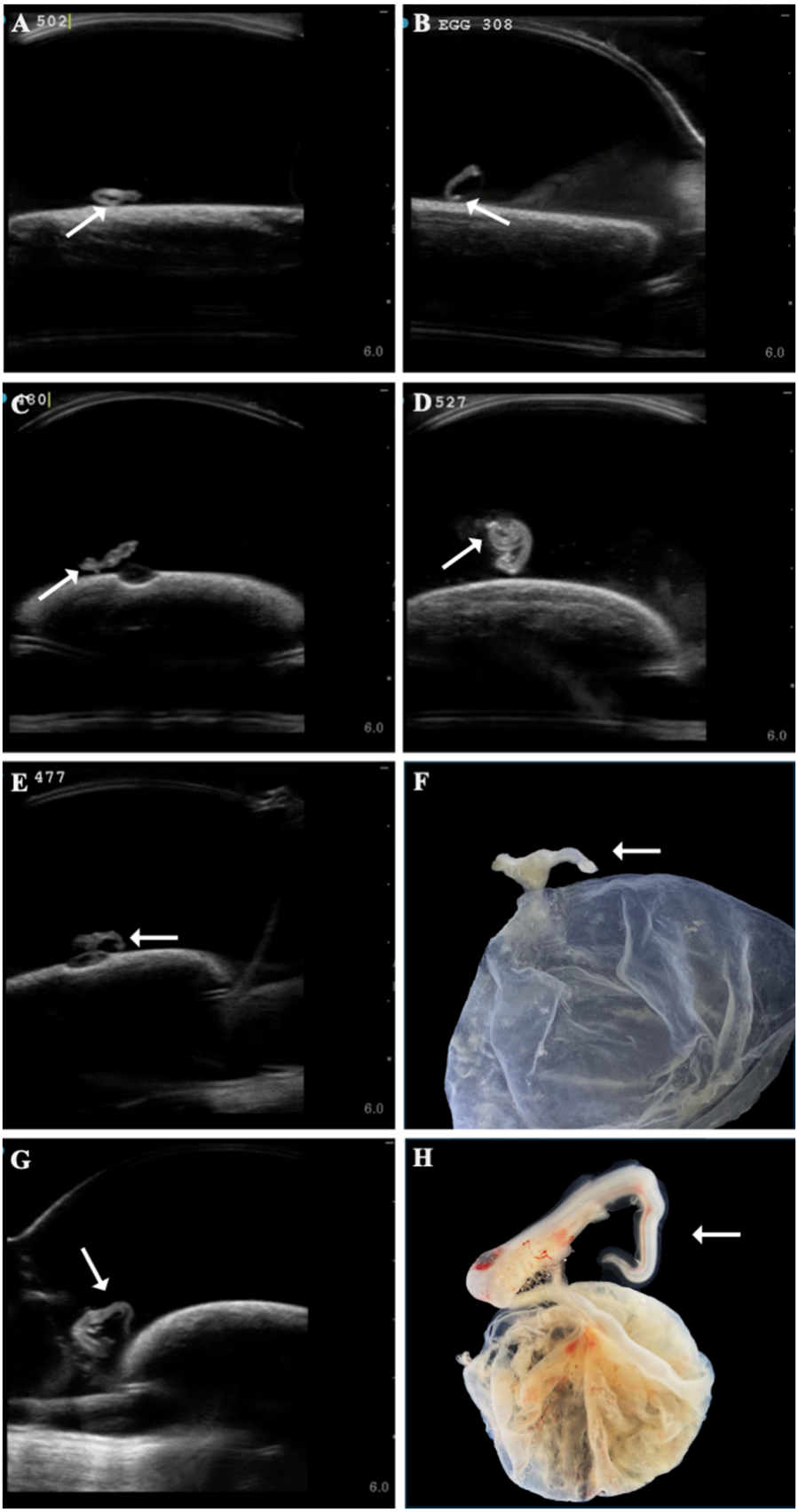

FIGURE 3
A range of different zebra shark (*Stegostoma tigrinum*) embryo abnormal tail morphologies (white arrows) were observed over the course of the study on ultrasound at 37, 47, 64, and 79 days post-oviposition, respectively **(A–D)**. In a subset of eggs, tail abnormalities were confirmed on dissection (**E,F**, 45 days post-oviposition; **G,H**, 69 days post-oviposition).

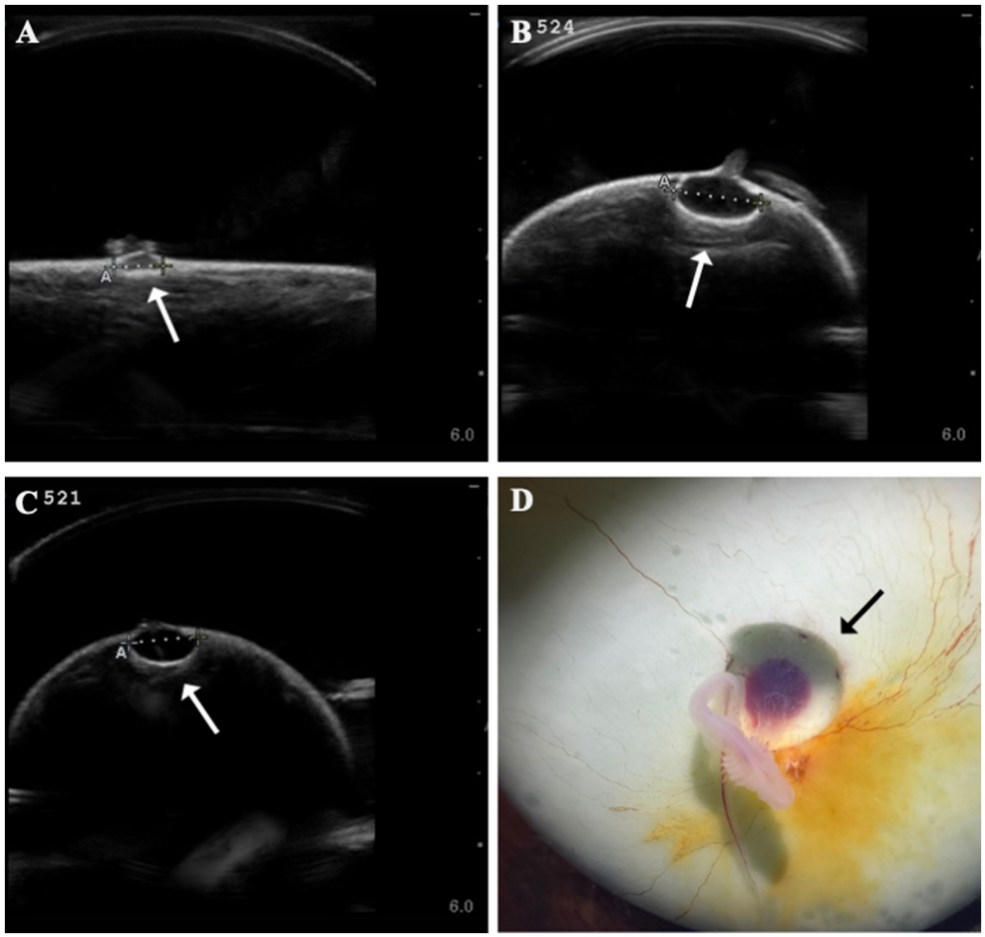

FIGURE 4
Formation of anechoic fluid-filled vesicles (arrows) at the base of the yolk stalk as seen on ultrasound in zebra shark (*Stegostoma tigrinum*) eggs **(A–C)**. The vesicle was documented to expand in the same egg (#524) from 44 days post-oviposition **(A)** to 79 days post-oviposition **(B)**. Vesicles were confirmed at necropsy **(D)**.

3.4 Genetic assignment

Of the 120 embryos, samples from 65 (54%) were sent for genetic testing to determine parentage. Of those, 17 had inconclusive results (i.e., amplification failed due to DNA degradation or too few markers amplified to conclusively determine parentage) and 48 were confirmed parthenotes, including the embryo that successfully hatched. At least one parthenote was produced by each of the four females. Parthenotes included embryos both with ($n = 28$) and without developmental deformities ($n = 19$).

4 Discussion

While its application in reproductive biology is widespread, in this study, ultrasonography was demonstrated to also be useful for monitoring embryo development and morbidity in an oviparous species. Ultrasonography allowed egg fertility to be assessed earlier in incubation and provided an alternative technique to monitor embryo growth and development compared to traditional methods to monitor embryonic development *in ovo*. Ultrasonography enabled a detailed view of the egg yolk, perivitelline fluid, and morphological features of the embryo, which yielded egg and embryo features that can be used as developmental thresholds of fertility and characteristics that were prognostic of morbidity when observed.

4.1 Ultrasonography as a tool to monitor embryonic development

Detection of early-stage embryos through ultrasonography was aided by conscientious egg handling and consistent egg orientation throughout the ultrasound exam procedure. Eggs were incubated and maintained in the same orientation when transferring between incubation and examination systems. This consistent gravitational force on the yolk preserves the animal-vegetal axis and maintains the animal pole and its germinal disc (or developing embryo) on the upper surface of the yolk mass. The predictable location for a developing embryo reduces the ultrasonography search space and facilitates discovery of small embryos.

Ultrasonography aided in earlier embryo identification when compared to a previous study where zebra shark eggs were candled weekly post-oviposition at the same facility' [ultrasound: mean 30 ± 7 days; candling: 45 ± 12 days reported in Adams et al. (38)]. Most

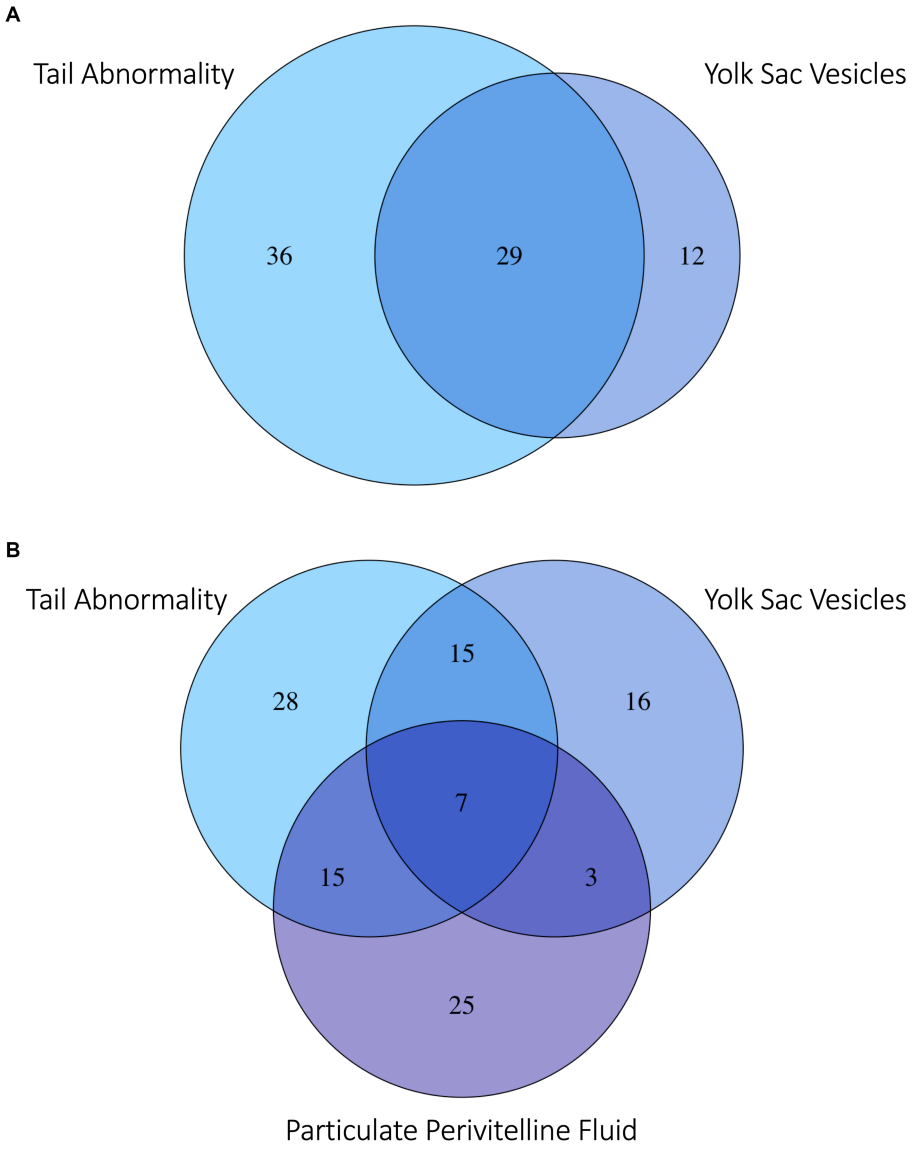

FIGURE 5
Venn diagram of **(A)** zebra shark (*Stegostoma tigrinum*) embryos with the top two abnormalities observed: Abnormal tail deformities tails (blue) and anechoic yolk sac vesicles (violet). **(B)** Embryos with the top two most frequently observed abnormalities and/or flocculent perivitelline fluid (purple) observed during development. Numbers in each bubble or overlap region are numbers of embryos with one or more abnormalities observed.

eggs in the present study were incubated for 3 to 4 weeks before the first fertility check, but through examination of a subset of eggs, it was demonstrated that embryos could be identified as early as 8 days post-oviposition. The longest time from oviposition to identification of an embryo was 47 days and occurred during the Covid-19 pandemic when schedule disruptions delayed regular ultrasound screening. Using 47 days as the upper threshold for determining egg fertility, facilities incubating zebra shark eggs at ~25°C should consider reserving resources after 7 week's time. If no embryo has been identified by that point, it is likely that the egg is infertile, or suffered early embryonic death.

Ultrasonography was useful in monitoring embryonic growth. However, there were several limitations that prevent using the recorded measurements to calculate accurate growth rates. Capturing a true straight-line measurement of embryo length accurately and consistently was challenged by their nearly constant, active movements. For example, there were several instances where embryos decreased in length between time periods (i.e., they were measured "shorter" at a subsequent exam taken 1 week later), which highlights the limitations of this methodology. In addition, once embryos grew to a certain length (~8 cm), they were larger than the field of view of the ultrasound, preventing an accurate total length measurement. As an alternative, growth of embryos larger than ~8 cm could be monitored using head diameter (e.g., maximum distance between the eyes) or other features that can be more easily seen/captured in the frame of the ultrasound transducer (e.g., mouth gape). However, from a monitoring perspective, gross changes in growth from week to week were observable via ultrasonography.

In this study, ultrasonography was used to confirm fertility and identify egg and embryo characteristics that predicted morbidity

10.3389/fvets.2024.1410377

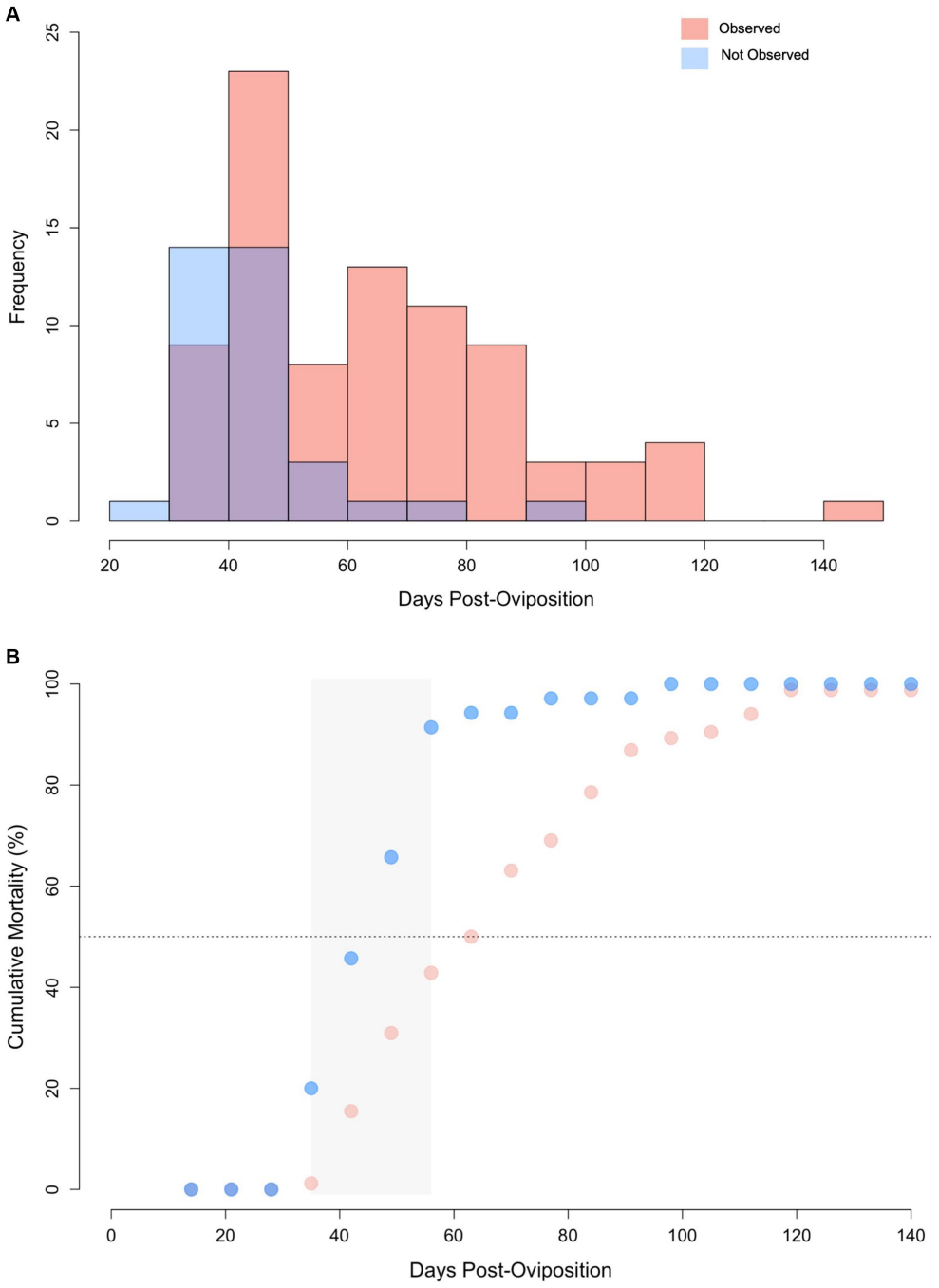

FIGURE 6
(A) Histogram of lifespan for zebra shark (*Stegostoma tigrinum*) embryos with abnormalities observed (pink) and those without abnormalities observed (blue) via ultrasound. Purple color denotes regions of overlap. **(B)** Cumulative mortality curves for embryos via ultrasound with and without abnormalities. Grey box represents the 2-week period where mortality increased at the fastest rate. Note, data from the singular hatchling is omitted from this figure.

when observed. However, there are other applications of this tool that could aid future studies on oviparous elasmobranch early life history and development in a non-invasive manner. Although not a focus, this study demonstrated how ultrasonography could be used to track heart rate and monitor changes in external gill filaments. Maternal provisioning could be inferred through ultrasonic measurements of the yolk mass as well as quantifying embryo yolk consumption across development. In a viviparous, lecithotrophic snake (*Vipera aspis*), ultrasound revealed development-related changes in embryonic volume that were largely attributed to mothers' ability to meet embryonic hydration demands (46). Quantifying maternal-fetal relationships through use of non-invasive tools has implications for predicting how species may respond to climate change and/or resource limitation. Other applications of ultrasonography include quantifying aspects of embryo behavior during development. For example, ultrasonography revealed that late-term copperhead snakes

(*Agkistrodon contortrix*) began performing caudal luring behaviors before birth (47), while embryos of the tawny nurse shark (*Nebrius ferrugineus*) were found to swim between the left and right uterus (48). Although these behaviors were documented in viviparous species, it demonstrates the utility that ultrasonography provides to characterize multiple aspects of the earliest stages of life, which can be applied to oviparous elasmobranch species as well.

4.2 Ultrasonography as a screening tool

Ultrasonography allowed for early identification of morphological abnormalities. These abnormalities were visually confirmed via necropsy in a subset of eggs to validate the ultrasound observations. Tail deformities were the most common abnormality and their prevalence among embryos, all which were confirmed parthenogenetic, suggests that this feature may be used as a biomarker of parthenogenesis and an early warning sign of embryonic mortality when observed. Development of this tool could have applications for conservation projects aiming to maintain genetically diverse populations of this endangered species. By having a method to screen for parthenotes at an early age, ultrasonography can enable resources to be directed towards embryos with greater chances of being heterozygotes resulting from sexual reproduction. However, absence of an observed abnormality on ultrasound does not preclude embryos from being unisexually produced, as demonstrated through the successful hatching of a parthenote in this study with no abnormalities noted on ultrasound.

Other common abnormalities, such as vesicles at the base of the yolk stalk, were equally prognostic of mortality. It is hypothesized that the vesicles visible as one or more anechoic foci during ultrasound exams are the result of focal delamination of the outer ectoderm from the inner enveloping layers of the yolk. Fluid accumulates in the foci and the pressure on the mesoderm, which include blood vessels, eventually restricts blood flow and cuts off circulation, which could account for the high mortality rate soon after a vesicle(s) was first observed.

A third commonly observed morbidity hallmark was the development of particulate material in the perivitelline fluid surrounding the embryo in the egg case. Embryos develop a hatching gland during early incubation that functions to effect eclosion through liquifaction of the semi-solid matrix that initially supports and surrounds the fragile yolk (31). As a result of this matrix breakdown, seawater can enter through the respiratory fissures and circulates through the egg case during the latter half of development (31). Eclosion is developmentally synchronized with the increase in size of the rapidly growing embryo and is proposed necessary to meet its increased oxygen demands. It is hypothesized that this particulate material is a result of incomplete breakdown of the semisolid matrix, due to improper or lack of development of the hatching gland. The particulate material makes the perivitelline fluid appear heterogeneous with small hyperechoic foci resembling "snow" in a snow globe when ultrasounding the egg. Failure to fully liquify the supporting internal matrix jelly would prevent eclosion and, in turn, could interfere with the ability of embryos to receive adequate oxygenation and likely lead to asphyxiation (49). Thus, like the other indicators of morbidity, an egg with streaming heterogeneous perivitelline fluid with particulate material on ultrasonography was confirmed at dissection and indicative of mortality.

While initially counterintuitive, embryos with no observed morphological abnormalities had shorter lifespans than embryos with an observed morphological abnormality. However, the median time to detect an abnormality (43 days post-oviposition) coincided with the median lifespan of embryos without a detectable morphological abnormality (42 days). Therefore, it is likely that many of these embryos perished before a morphological abnormality could be detected because of their small size. In particular, the two-week window around this time period (i.e., 43 ± 7 days) had the highest rates of mortality observed, suggesting that there is a key developmental checkpoint during this time frame that embryos must overcome for development to proceed. If an embryo is not able to overcome this barrier, embryonic death and autolysis proceeds relatively quickly with eggs fouling in less than 1 week. This key time period also aligns with a previous study in this same population of zebra sharks that reported a high degree of egg fouling (i.e., broken yolks) for the first 45 days post-oviposition (38). During that window, fertility was assigned as "unknown" since embryos could not be reliably observed via candling with the naked eye until day 45 post-oviposition. By contrast, eggs that were confirmed infertile maintained their yolk integrity for many weeks after oviposition (38). In light of the new information produced by this study, it is proposed that the broken yolks in Adams et al. (38) were the result of early embryo mortality. To support this hypothesis, a few eggs with broken yolks were examined outside the time frame of this study to determine if any signs of early embryonic development could be identified. Upon close examination embryos 1-3 mm total length were observed suggesting zebra shark eggs with broken yolks after 2–6 weeks of incubation may represent embryonic mortality rather than infertility (Supplementary File 12).

While all embryos with an observed abnormality died, the absence of an abnormality after 42 days post-oviposition did not guarantee long-term viability or sexual reproduction as demonstrated by the successful development and hatching of one parthenogenetically-produced offspring. This embryo developed completely and the egg and embryo morbidity hallmarks described above were not observed; however, incubation was protracted and it was manually extracted from the egg case to prevent hatching-associated mortality. Due to the lack of heterozygous offspring in this study, the timeline and progression of normal development was not available for direct comparison. Studies on zebra shark growth post-hatch have shown that parthenogenetic offspring do not grow equally (both in length and mass) as their heterozygous counterparts (45). Although no clear differences in hatchling morphometrics were reported, it is possible that parthenogenetic embryos exhibit the same delayed growth rate during embryonic development as was demonstrated for homozygous hatchlings. Understanding if parthenotes develop at a slower rate *in ovo* would allow for embryo size and yolk utilization thresholds to be used as biomarkers of parthenogenesis and could reduce the need for genetic confirmation. Access to sexually-developing, heterozygous embryos is needed to describe normal stages of embryonic development and their developmental timeline for comparison to parthenogenetically-developing embryos incubated at the same temperature.

Parthenogenesis, as a phenomenon, has generally been studied in aquariums by accident and through singular events because of

unexpected births when females are kept in single-sex populations. Although not an original goal of the study, the data collected demonstrate that the probability that a parthenote successfully develops to hatching is extremely small (0.83%) and is comparable to parthenogenesis hatch rates in another oviparous species, the whitespotted bamboo shark *Chiloscyllium plagiosum* (0.71%) (50). This rate for zebra sharks is calculated with the assumption that all untested embryos in the study were parthenotes. Although small, this is likely an overestimation as our dataset included only the eggs where embryos were large enough to be identified using ultrasonography (i.e., not all eggs of all females were included in this dataset). This low hatching rate aligns with the seemingly low reports of parthenote births observed across taxa, that often occur as only single observations per species (51–53). Despite the low probability of successful development to hatch, many of the observed embryos were confirmed parthenotes, indicating this mode of reproduction occurs more frequently than previously thought in the zebra shark. A previous study with a singleton female zebra shark documented a parthenogenesis hatch rate higher than our study (~12%) (54). Due to the high mortality rate for parthenotes (especially in early development), future studies should assess all eggs during this period to more accurately determine the prevalence of this phenomenon.

Data availability statement

The raw data supporting the conclusions of this article will be made available by the authors, without undue reservation.

Ethics statement

The requirement of ethical approval was waived by Aquarium of the Pacific Research Advisory Committee for the studies involving animals because study data was obtained from routine care. The studies were conducted in accordance with the local legislation and institutional requirements. Written informed consent was obtained from the owners for the participation of their animals in this study.

Author contributions

LA: Conceptualization, Investigation, Methodology, Project administration, Supervision, Writing – review & editing. JW: Conceptualization, Investigation, Methodology, Project administration, Supervision, Writing – original draft, Writing – review & editing. BG: Data curation, Investigation, Project administration, Visualization, Writing – review & editing. RM: Data curation, Investigation, Project administration, Visualization, Writing – review & editing. LL: Data curation, Methodology, Visualization, Writing – review & editing. KF: Data curation, Formal analysis, Resources, Validation, Writing – review & editing. KL: Conceptualization, Data curation, Formal analysis, Investigation, Methodology, Project administration, Writing – original draft, Writing – review & editing.

Funding

The author(s) declare that financial support was received for the research, authorship, and/or publication of this article. Funding for this project was provided by Aquarium of the Pacific and Georgia Aquarium.

Acknowledgments

We thank all the husbandry and animal care professionals at Aquarium of the Pacific who cared for the zebra sharks over the course of this study.

Conflict of interest

The authors declare that the research was conducted in the absence of any commercial or financial relationships that could be construed as a potential conflict of interest.

Publisher's note

All claims expressed in this article are solely those of the authors and do not necessarily represent those of their affiliated organizations, or those of the publisher, the editors and the reviewers. Any product that may be evaluated in this article, or claim that may be made by its manufacturer, is not guaranteed or endorsed by the publisher.

Supplementary material

The Supplementary material for this article can be found online at: https://www.frontiersin.org/articles/10.3389/fvets.2024.1410377/full#supplementary-material

References

1. Brown JL. Comparative ovarian function and reproductive monitoring of endangered mammals. *Theriogenology*. (2018) 109:2–13. doi: 10.1016/j.theriogenology.2017.12.004

2. Medan MS, Abd El-Aty AM. Advances in ultrasonography and its applications in domestic ruminants and other farm animals reproduction. *J Adv Res*. (2010) 1:123–8. doi: 10.1016/j.jare.2010.03.003

3. Schurich M, Aigner F, Frauscher F, Pallwein L. The role of ultrasound in assessment of male fertility. *Eur J Obstet Gynecol Reprod Biol*. (2009) 144:S192–8. doi: 10.1016/j.ejogrb.2009.02.034

4. Rostal DC, Robeck TR, Owens DW, Kraemer DC. Ultrasound imaging of ovaries and eggs in Kemp's Ridley Sea Turtles (*Lepidochelys Kempi*). *J Zoo Wildl Med*. (1990) 21:27–35.

5. Quintela LA, Barrio M, Peña AI, Becerra JJ, Cainzos J, Herradón PG, et al. Use of ultrasound in the reproductive management of dairy cattle. *Reprod Domest Anim*. (2012) 47:34–44. doi: 10.1111/j.1439-0531.2012.02032.x

6. Smith RF, Oultram J, Dobson H. Herd monitoring to optimise fertility in the dairy cow: making the most of herd records, metabolic profiling and ultrasonography (research into practice). *Animal*. (2014) 8:185–98. doi: 10.1017/S1751731114000597

7. Sontakke SD. Monitoring and controlling ovarian activities in wild ungulates. *Theriogenology*. (2018) 109:31–41. doi: 10.1016/j.theriogenology.2017.12.008

8. Hildebrandt TB, Göritz F, Hermes R. Ultrasonography: an important tool in captive breeding management in elephants and rhinoceroses. *Eur J Wildl Res*. (2006) 52:23–7. doi: 10.1007/s10344-005-0012-4

9. Russell AF, Brotherton PNM, McIlrath GM, Sharpe LL, Clutton-Brock TH. Breeding success in cooperative meerkats: effects of helper number and maternal state. *Behav Ecol*. (2003) 14:486–92. doi: 10.1093/beheco/arg022

10. Cheng Y-Y, Chen T-Y, Yu P-H, Chi C-H. Observations on the female reproductive cycles of captive Asian yellow pond turtles (*Mauremys Mutica*) with radiography and ultrasonography. *Zoo Biol*. (2010) 29:50–8. doi: 10.1002/zoo.20265

11. Whiteman EA, Jennings CA, Nemeth RS. Sex structure and potential female fecundity in a *Epinephelus Guttatus* spawning aggregation: applying ultrasonic imaging. *J Fish Biol*. (2005) 66:983–95. doi: 10.1111/j.0022-1112.2005.00653.x

12. Wyffels JT, George R, Christiansen EF, Clauss TM, Newton AL, Hyatt MW, et al. Reproductive cycle and periodicity of in situ and aquarium female sand tiger sharks *Carcharias Taurus* from the Western North Atlantic. *Front Mar Sci*. (2022) 9:9. doi: 10.3389/fmars.2022.925749

13. Wyffels JT, George R, Adams L, Adams C, Clauss T, Newton A, et al. Testosterone and semen seasonality for the sand tiger shark *Carcharias Taurus*. *Biol Reprod*. (2020) 102:876–87. doi: 10.1093/biolre/ioz221

14. Daly J, Gunn I, Kirby N, Jones R, Galloway D. Ultrasound examination and behavior scoring of captive *Broadnose Sevengill* sharks, *Notorynchus Cepedianus* (Peron, 1807). *Zoo Biol*. (2007) 26:383–95. doi: 10.1002/zoo.20155

15. Anderson B, Belcher C, Slack J, Gelsleichter J. Evaluation of the use of portable ultrasonography to determine pregnancy status and fecundity in Bonnethead shark Sphyrna Tiburo. *J Fish Biol*. (2018) 93:1163–70. doi: 10.1111/jfb.13831

16. Whittamore JM, Bloomer C, Hanna GM, McCarthy ID. Evaluating ultrasonography as a non-lethal method for the assessment of maturity in oviparous elasmobranchs. *Mar Biol*. (2010) 157:2613–24. doi: 10.1007/s00227-010-1523-4

17. Nau MR, O'Brien JK, Schmitt TL, Nollens HH, Robeck TR. Diagnostic assessment of reproductive status in white-spotted bamboo sharks (Chiloscyllium Plagiosum). *Anim Reprod Sci*. (2018) 197:48–57. doi: 10.1016/j.anireprosci.2018.08.005

18. Hildebrandt TB, Brown J, Hermes R, Goritz F. Ultrasound for analysis of reproductive function in wildlife species In: WV Holt, A Pickard, J Roger and D Wildt, editors. Reproductive science and integrated conservation. Cambridge, UK: Cambridge University Press (2003). 166–82.

19. Radcliffe RW, Eyres AI, Patton ML, Czekala NM, Emslie RH. Ultrasonographic characterization of ovarian events and fetal gestational parameters in two southern black rhinoceros (Diceros Bicornis Minor) and correlation to fecal progesterone. *Theriogenology*. (2001) 55:1033–49. doi: 10.1016/S0093-691X(01)00464-2

20. Drews B, Hermes R, Göritz F, Gray C, Kurz J, Lueders I, et al. Early embryo development in the elephant assessed by serial ultrasound examinations. *Theriogenology*. (2008) 69:1120–8. doi: 10.1016/j.theriogenology.2008.01.026

21. Whitworth M, Bricker L, Mullan C. Ultrasound for fetal assessment in early pregnancy. *Cochrane Database Syst Rev*. (2015) 2015:CD007058. doi: 10.1002/14651858.CD007058.pub3

22. Tonni G, Martins WP, Guimarães Filho H, Araujo Júnior E. Role of 3-D ultrasound in clinical obstetric practice: evolution over 20 years. *Ultrasound Med Biol*. (2015) 41:1180–211. doi: 10.1016/j.ultrasmedbio.2014.12.009

23. Heinrich A, Proff P, Michel T, Ruhland F, Kirbschus A, Gedrange T. Prenatal diagnostics of cleft deformities and its significance for parent and infant care. *J Cranio-Maxillofacial Surg*. (2006) 34:14–6. doi: 10.1016/S1010-5182(06)60004-8

24. Zhang N, Dong H, Wang P, Wang Z, Wang Y, Guo Z. The value of obstetric ultrasound in screening fetal nervous system malformation. *World Neurosurg*. (2020) 138:645–53. doi: 10.1016/j.wneu.2020.01.014

25. Bunch TD, Panter KE, James LF. Ultrasound studies of the effects of certain poisonous plants on uterine function and fetal development in livestock. *J Anim Sci*. (1992) 70:1639–43. doi: 10.2527/1992.7051639x

26. Lansford R, Rugonyi S. Follow me! A tale of avian heart development with comparisons to mammal heart development. *J Cardiovasc Dev Dis*. (2020) 7:7. doi: 10.3390/jcdd7010008

27. McQuinn TC, Bratoeva M, DeAlmeida A, Remond M, Thompson RP, Sedmera D. High-frequency ultrasonographic imaging of avian cardiovascular development. *Dev Dyn*. (2007) 236:3503–13. doi: 10.1002/dvdy.21357

28. Eckrich J, Kugler P, Buhr CR, Ernst BP, Mendler S, Baumgart J, et al. Monitoring of tumor growth and vascularization with repetitive ultrasonography in the chicken chorioallantoic-membrane-assay. *Sci Rep*. (2020) 10:18585. doi: 10.1038/s41598-020-75660-y

29. Beggs K, Young J, Georges A, West P. Ageing the eggs and embryos of the pig-nosed turtle, Carettochelys Insculpta (Chelonia: Carettochelydidae), from northern Australia. *Can J Zool*. (2000) 78:373–92. doi: 10.1139/z99-214

30. Ernst R, Bradley F, Delany M, Abbott U, Craig R. Egg candling and breakout analysis, animal science department, University of California Davis, publication 8134 Oakland, California: UCANR Publications (2004).

31. Wyffels JT. Embryonic development of chondrichthyan fishes - a review In: Y Kunz, CA Luer and B Kapoor, editors. Development of non-teleost fishes. Enfield, NH: Science Publishers Inc (2009)

32. Chen L, Wang Z, Fu X, Wang S, Feng Y, Coudyzer W, et al. Dynamic 3D morphology of chick embryos and allantois depicted nondestructively by 3.0T clinical magnetic resonance imaging. *Poult Sci*. (2023) 102:102902. doi: 10.1016/j.psj.2023.102902

33. Henning AL, Jiang MX, Yalcin HC, Butcher JT. Quantitative three-dimensional imaging of live avian embryonic morphogenesis via micro-computed tomography. *Dev Dyn*. (2011) 240:1949–57. doi: 10.1002/dvdy.22694

34. Daly J, Jones R. The use of reproductive technologies in breeding programs for elasmobranchs in aquaria In: The elasmobranch husbandry manual II: recent advances in the care of sharks, rays and their relatives. In: M Smith, D Warmolts, D Thoney, R Heuter, M Murray and J Ezcurra, editors. Columbus, Ohio: Special Publication of the Ohio Biological Survey (2017). 363–74.

35. Kuchling G. Ultrasound scanning as an effective tool in the conservation of chelonians. *Int Zoo Yearb*. (2015) 49:22–30. doi: 10.1111/izy.12081

36. Traylor-Holzer K. Population viability analysis (PVA) report for population augmentation of Zebra sharks (Stegostoma Tigrinum) in Raja Ampat. MN: Indonesia; Apple Valley (2021).

37. Watson L, Janse M. Reproduction and husbandry of Zebra sharks, *stegostoma fasciatum*, in aquaria In: The elasmobranch husbandry manual II. In: M Smith, D Warmolts, D Thoney, R Heuter, M Murray and J Ezcurra, editors. Columbus, Ohio: Ohio Biological Survey, Inc. (2017). 421.

38. Adams L, Lyons K, Larkin E, Leier N, Monday J, Plante C, et al. Artificial insemination and parthenogenesis in the Zebra shark *Stegostoma Tigrinum*. *Front Mar Sci*. (2022) 9:886616. doi: 10.3389/fmars.2022.886616

39. Feldheim KA, Gruber SH, Ashley MV. Reconstruction of parental microsatellite genotypes reveals female polyandry and Philopatry in the lemon shark, *Negaprion Brevirostris*. *Evolution (N Y)*. (2004) 58:2332–42. doi: 10.1111/j.0014-3820.2004.tb01607.x

40. Miller D, JE B, EL M, Ghiorse W. Evaluation and optimization of DNA extraction and purification procedures for soil and sediment samples. *Appl Environ Microbiol*. (1999) 65:4715–24. doi: 10.1128/AEM.65.11.4715-4724.1999

41. Dudgeon CL, Feldheim K, Schick M, Overden JR. Polymorphic microsatellite loci for the Zebra shark *Stegostoma Fasciatum*. *Mol Ecol Notes*. (2006) 6:1086–8. doi: 10.1111/j.1471-8286.2006.01442.x

42. Schuelke M. An economic method for the fluorescent labeling of PCR fragments. *Nat Biotechnol*. (2000) 18:233–4. doi: 10.1038/72708

43. Maddox JD, Feldheim KA. A cost-effective size standard for fragment analysis that maximizes throughput on five dye set platforms. *Conserv Genet Resour*. (2014) 6:5–7. doi: 10.1007/s12686-013-0019-1

44. Kearse M, Moir R, Wilson A, Stones-Havas S, Cheung M, Sturrock S, et al. Geneious basic: an integrated and extendable desktop software platform for the organization and analysis of sequence data. *Bioinformatics*. (2012) 28:1647–9. doi: 10.1093/bioinformatics/bts199

45. Adams L, Lyons K, Monday J, Larkin E, Wyffels J. Costs of parthenogenesis on growth and longevity in ex situ Zebra sharks *Stegostoma Tigrinum*. *Endanger Species Res*. (2023) 50:81–91. doi: 10.3354/esr01224

46. Lourdais O, Lorioux S, Dupoué A, Wright C, DeNardo DF. Embryonic water uptake during pregnancy is stage- and fecundity-dependent in the Snake *Vipera Aspis*. *Comp Biochem Physiol Part A Mol Integr Physiol*. (2015) 189:102–6. doi: 10.1016/j.cbpa.2015.07.019

47. Smith CF, Schuett GW. Tail movements by late-term fetal pitvipers resemble caudal luring: prenatal development of an ambush predatory behaviour. *R Soc Open Sci*. (2022) 9:220218. doi: 10.1098/rsos.220218

48. Tomita T, Murakumo K, Ueda K, Ashida H, Furuyama R. Locomotion is not a privilege after birth: ultrasound images of viviparous shark embryos swimming from one uterus to the other. *Ethology*. (2019) 125:122–6. doi: 10.1111/eth.12828

49. Richards SW, Merriman D, Calhoun L. Studies on the marine resources of southern New England, IX: the biology of the little skate, Raja Erinaecea Mitchell. *Bull Bingham Ocean Coll*. (1963) 18:1–68.

50. Wyffels JT, Adams LM, Bulman F, Fustukjian A, Hyatt MW, Feldheim KA, et al. Artificial insemination and parthenogenesis in the Whitespotted bamboo shark *Chiloscyllium Plagiosum*. *Sci Rep*. (2021) 11:9966. doi: 10.1038/s41598-021-88568-y

51. Ryder OA, Thomas S, Judson JM, Romanov MN, Dandekar S, Papp JC, et al. Facultative parthenogenesis in California condors. *J Hered*. (2021) 112:569–74. doi: 10.1093/jhered/esab052

52. Booth W, Levine BA, Corush JB, Davis MA, Dwyer Q, De Plecker R, et al. Discovery of facultative parthenogenesis in a New World crocodile. *Biol Lett*. (2023) 19:20230129. doi: 10.1098/rsbl.2023.0129

53. Bester-van der Merwe A, Lyons K, Kacev D, Feldheim K. Elasmobranch mating systems In: JC Carrier, CA Simpfendorfer, MR Heithaus and KE Yopak, editors. Biology of sharks and their relatives. Florida: CRC Press: Boca Raton (2022). 203–29.

54. Robinson DP, Baverstock W, Al-Jaru A, Hyland K, Khazanehdari KA. Annually recurring parthenogenesis in a Zebra shark *Stegostoma Fasciatum*. *J Fish Biol*. (2011) 79:1376–82. doi: 10.1111/j.1095-8649.2011.03110.x

frontiers | Frontiers in Veterinary Science

TYPE Methods
PUBLISHED 04 September 2024
DOI 10.3389/fvets.2024.1411769

Check for updates

OPEN ACCESS

EDITED BY
Alisa Newton,
Ocearch, United States

REVIEWED BY
Tao Wang,
University of Maryland, United States
Mariajesus Soula,
Kansas State University, United States

*CORRESPONDENCE
Jennifer T. Wyffels
✉ wyffels@ripleys.com
Chris Buckner
✉ buckner@ripleys.com

RECEIVED 03 April 2024
ACCEPTED 07 August 2024
PUBLISHED 04 September 2024

CITATION
Buckner C, George RH, Bulman F, Durrett J, Handsel T and Wyffels JT (2024) Cesarian section and long-term outcomes for cownose rays (*Rhinoptera bonasus*). *Front. Vet. Sci.* 11:1411769. doi: 10.3389/fvets.2024.1411769

COPYRIGHT
© 2024 Buckner, George, Bulman, Durrett, Handsel and Wyffels. This is an open-access article distributed under the terms of the Creative Commons Attribution License (CC BY). The use, distribution or reproduction in other forums is permitted, provided the original author(s) and the copyright owner(s) are credited and that the original publication in this journal is cited, in accordance with accepted academic practice. No use, distribution or reproduction is permitted which does not comply with these terms.

Cesarian section and long-term outcomes for cownose rays (*Rhinoptera bonasus*)

Chris Buckner[1]*, Robert H. George[2], Frank Bulman[1], Jared Durrett[1], Tim Handsel[3] and Jennifer T. Wyffels[3]*

[1]Ripley's Aquarium of the Smokies, Gatlinburg, TN, United States, [2]Ripley's Aquarium of Myrtle Beach, Myrtle Beach, SC, United States, [3]Ripley's Aquariums, Orlando, FL, United States

Cownose rays (*Rhinoptera bonasus*) are schooling rays commonly displayed in large groups in public aquariums. They are long-lived, have an annual reproductive cycle, and readily breed in managed care with most pregnancies culminating with the unaided and successful birth of a single neonate. Occasionally, females are observed to have prolonged pregnancies or suffer dystocia during parturition and intervention via a cesarian section (C-section) is required to deliver the neonate. Monthly reproductive monitoring at Ripley's Aquarium of the Smokies using ultrasound to stage pregnancies allows for the prediction of anticipated due dates and guides the decision to assist with delivery. Recognizing when to assist birth and best practices for performing C-section are important for the reproductive health, sustainability, and longevity of this species in managed care. This report describes a surgical technique for C-section in cownose rays and includes short-term complications and long-term outcomes for females.

KEYWORDS

dystocia, reproduction, elasmobranch, parturition, histotroph

Introduction

Cownose rays (*Rhinoptera bonasus*) have been part of the elasmobranch assemblage at Ripley's Aquarium of the Smokies since its opening in December 2000. Male and female cownose rays are maintained together in an 86,000-gallon exhibit that includes a shallow 2-ft-deep touch pool to facilitate guest interaction with the rays through enrichment programs, connected to a 20-ft-deep pool. The rays are housed with southern stingrays (*Hypanus americanus*), spotted eagle rays (*Aetobatis narinari*), bonnethead sharks (*Sphyrna tiburo*), whitespotted bamboo sharks (*Chiloscyllium plagiosum*), and epaulette sharks (*Hemiscyllium ocellatum*).

Cownose rays are long-lived and reproduce annually. Females have a functional left ovary and uterus (1–3) and, except in rare cases (4), give birth to a single neonate after a nearly year-long gestation (1–3). Collectively, this combination of life history traits makes cownose rays particularly susceptible to exploitation from fishing pressure and habitat loss or degradation (5). Maintaining healthy and self-sustaining populations of cownose rays in managed care is a goal of the aquarium that also supports the conservation of this species. The cownose rays in Ripley's Aquarium of the Smokies breed readily, and their reproductive status has been monitored monthly via ultrasonography since 2005. Females are assigned a reproductive stage (stages 0–5) based on the contents and appearance of the uterus as has been previously described: (0) uterus is not visualized indicating an immature

ray; (1) uterus with or without fluid and without an embryo or solid material; (2) uterus with undifferentiated material present in the fluid in the uterus and without organized motion; (3) differentiated embryo floating in uterine fluid with or without organized motion; (4) differentiated embryo present in the uterine fluid, embryo larger than the ultrasound field of view and organized motion detected including the movement of the gill arches indicating respiration and heart valve; and (5) large fetus with hyperechoic folded wings causing displacement and misshaping of the spiral valve (6). When females reach stage 5, late-term pregnancy, they are transferred from the main exhibit to a 20-ft diameter round holding pool for parturition. Occasionally, females stagnate in stage 5 and develop dystocia, requiring surgical intervention to deliver the young by cesarian section (C-section). This procedure is lifesaving for the female and when the timing is correct, also for the neonate. A review of the past 20 years of cownose ray reproduction has allowed for the development and refinement of a C-section procedure for the species and tracking of long-term reproductive outcomes for female cownose rays ($n = 7$) that underwent C-sections.

Materials and methods

Animals

A retrospective review of husbandry and medical records extracted the number of pregnancies and C-sections for resident cownose rays from 2005–2024 at Ripley's Aquarium of the Smokies. Clinical signs of dystocia, stage of pregnancy (0–5), surgical procedure, and postoperative and long-term outcome information up to 20 years were noted for females requiring intervention.

Case selection

A normal pregnancy culminates with reproductive stage 5, with the fetus filling the uterus, which in late pregnancy extends across the ray's midline, causing displacement and crowding of the spiral intestine (6). Females are are normally observed in stage 5 for 1–2 months at the end of their 11–12 months of gestation (6). The parturition date for the previous pregnancy—in combination with exposure to males postpartum—was used to estimate the subsequent parturition date because females were often mated soon after giving birth. Females that persisted longer than 2 months in stage 5 or that had surpassed their expected parturition date were considered at risk of dystocia. The normal position of the fetus within the uterus was a caudal presentation, with the wings folded dorsally and the tail folded in a cranial direction over the body. Incorrect orientation of the fetus may contribute to clinical signs of dystocia.

Pregnant cownose rays were examined monthly via ultrasonography to confirm that their young were viable and to monitor their size and orientation relative to the female's coelom. The decision to perform a C-section was based on both maternal and fetal factors. Externally, females may have exhibited external signs of dystocia characterized by marked coelomic distention, pelvic fin edema, and cloacal protrusion, edema, and/or bruising (Figure 1). Ultrasound of the dam was used to evaluate the fetus for a heartbeat and the presence or absence of movement of the gill arches, indicating respiration and/or fetal movement.

Surgical procedure

A pregnant ray requiring intervention is removed from her exhibit using dip nets and placed in a holding tank containing oxygenated saltwater from her exhibit. A second anesthetic tank with water from the same source is then treated with tricaine methanesulphonate (MS-222) (75–100 ppm, Syndel, Ferndale, Washington, United States) buffered 4:1 with sodium bicarbonate. Pure oxygen is delivered to the anesthetic tank via an airstone. Once the MS-222 and bicarbonate have dissolved, the ray is added. The anesthetic plane is deemed sufficient when the ray is minimally responsive to touch while maintaining spiracular respiration, the intake of water into the dorsal spiracles, which flows over the gill arches and out of the gill slits ventrally.

The ray is lifted out of the anesthetic tank and placed in ventral recumbency on premoistened towels covering the surgical surface of a custom and portable stingray medical treatment cart adjacent to the holding tank (Figure 2A). A submersible pump placed in the anesthetic tank pumps water through a ¾-inch polypropylene hose to a T adapter from which ¾-inch hoses are placed into the ray's spiracles. A ball valve allows for adjustment of the flow rate. Anesthetic water flows through the spiracles, cascades over the gills, and drains from the ray's gill slits as well as her mouth. The anesthetic water drains from the top tray of the medical cart into the anesthetic tank on the bottom tray of the cart and is recycled back into the anesthetic holding tank. Anesthetic concentration during the procedure is maintained at 75 ppm MS-222. The ray's respiratory rate is monitored throughout the procedure. If the rate decreases 25% from the baseline determined before respiratory rate recover, fresh water is added gradually to reduce the MS-222 concentration until the anesthetic-free seawater.

A premoistened cotton towel is laid caudal to the spiracles to block potential overflow anesthetic water from contaminating the surgical site. The left paralumbar area is sanitized using gauze soaked in povidone-iodine surgical prep solution and applied using light pressure starting at the incision site and circling outward. The povidine-iodine application is repeated twice more, and a sterilized plastic drape is sutured to the skin with a single, simple interrupted suture at the cranial and caudal end of the fenestration (Figure 2B). A left paramedian incision, 6–10 inches depending on the size of the neonate, through the skin, musculature, and peritoneum is made into the dorsal coelom in the left paralumbar fossa, over the uterus using a number 10 blade (Figure 2C). Care should be taken when extending the incision caudally, as the kidneys are in the caudodorsal portion of the coelom. Ultrasonography can be used to locate the cranial tip of the kidneys for reference. The uterus is directly under the body wall in this area (Figure 2D), and stay sutures are placed at the cranial and caudal ends using a 3–0 polydioxanone suture (PDS). Using the sutures and applying gentle traction, the uterus is partially exteriorized (Figure 3A). This position minimizes the spillage of uterine contents into the coelom.

A stab incision is made into the uterus using a number 10 blade, and the incision is extended with Mayo scissors to a length that will

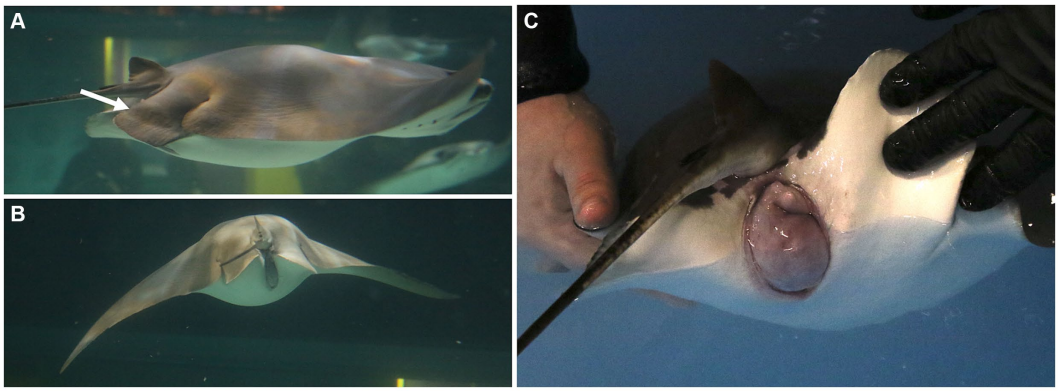

FIGURE 1
Females may exhibit external signs of dystocia characterized by **(A)** pelvic fin edema (arrow), **(B)** marked coelomic distention, and/or **(C)** cloacal protrusion, edema, and/or bruising. These signs are helpful for deciding the timing to intervene and deliver young by C-section.

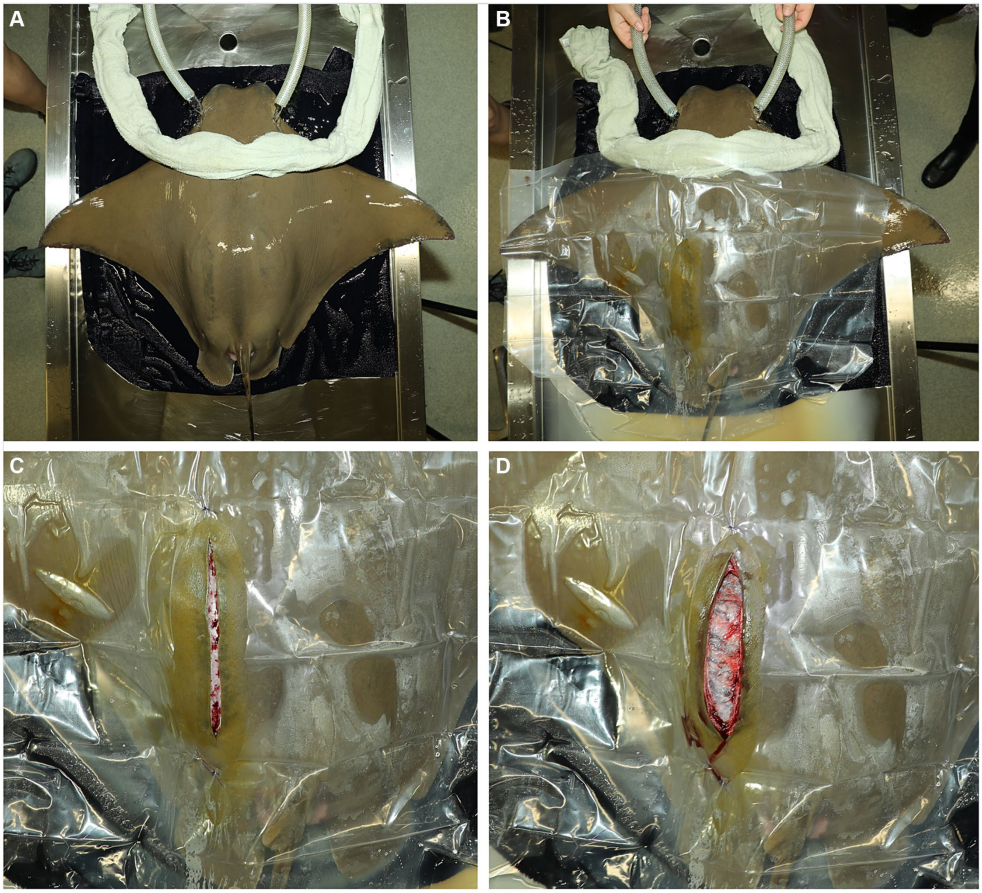

FIGURE 2
(A) An anesthetized ray in ventral recumbency on premoistened towels covering the surgical surface of a custom and portable stingray medical treatment cart. Anesthetic water is pumped through the ray's spiracles. A premoistened cotton towel is laid caudal to the spiracles to block potential overflow anesthetic water from contaminating the surgical site. **(B)** The surgery site is prepped with dilute iodine. The ray is covered with a sterilized plastic drape that is sutured to the skin with a single, simple interrupted suture at the cranial and caudal end of the fenestration. **(C)** A left paramedian incision is made into the dorsal coelom in the left paralumbar fossa over the uterus using a number 10 blade. **(D)** The uterus is directly under the body wall.

allow extraction of the neonate. The neonate is grasped gently by a wing (Figure 3B), rotated to be oriented head first, and extracted manually using gentle traction on the dorsal rim of the spiracle openings (Figure 3C). The visible uterine blood vessels that may be severed when making the incision do not require ligation, thanks to uterine wall contracture.

FIGURE 3
(A) Stay sutures are placed at the cranial and caudal terminus of the uterus using 3–0 PDS. Using the sutures and applying gentle traction, the uterus is partially exteriorized. **(B)** A stab incision is made into the uterus and extended with scissors. The neonate is quickly identified and removed from the uterus manually using gentle traction on a wing to rotate the fetus to be oriented as needed to **(C)** grasp the dorsal rim of the spiracle openings.

FIGURE 4
(A) The uterus is partially exteriorized using the stay sutures, and residual uterine fluid (histoptroph) is removed in preparation for closing the incision. **(B)** The uterus is closed, and the stay sutures are removed. **(C)** The skin is closed with 2–0 PDS on a cutting needle in a horizontal mattress pattern.

The uterus is held up and slightly out of the body wall opening using the stay sutures, residual uterine fluid (histoptroph) is removed using gentle suction, and the lumen is lavaged with sterile lactated ringer's solution (Figure 4A). Fluid is immediately removed via suction, and 1.0 mL small animal enrofloxacin 2.27% is instilled prophylactically into the uterine lumen before commencing closure. The uterus is sutured with a double layer closure with the mucosal layers closed with 3–0 PDS on a taper needle in a continuous fashion and then oversewn with a Lembert pattern incorporating the muscularis/serosal layers. The stay sutures are then removed, and the uterus is lowered back into coelom (Figure 4B). The body wall is closed via a simple interrupted or simple continuous pattern using 2–0 PDS with a tapered needle to prevent fraying of the peritoneum, the holding layer of the coelom (Figure 4B). The skin is closed with 2–0 PDS on a cutting needle in a horizontal mattress pattern (Figure 4C). This suture pattern is chosen because it is an everting and tension-relieving technique.

Rays receive single perioperative intramuscular (IM) injections of meloxicam (0.2 mg/kg), vitamin C (12.5 mg/kg), vitamin B complex (5 mg/kg), and broad-spectrum, long-acting antibiotics [either ceftiofur (6.6 mg/kg) or florfenicol (40 mg/kg)] after closure. The spiracular hoses are removed, and the ray is transferred to an unmedicated holding pool with system seawater for recovery (Figure 5B). Once the ray is responsive to touch, usually 20–30 min, she is returned to exhibit.

The neonate(s) is transferred to a holding tank of anesthetic-free water from the same original source as the female to facilitate recovery (Figure 5A). Supporting the neonate in the water without ventilating and manually and slowly flexing the wings up and down promotes independent swimming (personal observation), which should be observed within 10 min of extraction. The female's sutures are removed 4–6 weeks after surgery (Figure 5C), and sedation is typically not needed. Removal of sutures earlier than 4 weeks may be possible but was not attempted in this study.

Results

Animals

Fourteen female cownose rays served as founders and have successfully reproduced at Ripley's Aquarium of the Smokies since it was opened in 2000. In that time, half ($n = 7$) of founder females have undergone one or more C-section procedures. Monthly reproductive monitoring of the cownose ray population has been in place since 2005, and most (60%, 9 of 15) C-sections have occurred in the last 4 years, which represents 20% of the study duration (Figure 6). Among these seven founder rays, there have been 69 parturition events, with 15 (22%) culminating in C-sections. Five of the seven females underwent multiple C-sections: one female had four C-sections, one female had three C-sections, and three females had two C-sections. A brief reproductive history for each female is given in Table 1. The first C-section was performed in 2005; however, detailed medical

FIGURE 5
The female **(A)** and neonate **(B)** are transferred to a holding tank with clean, anesthetic-free saltwater for recovery. **(C)** Sutures are removed 4–6 weeks after surgery. The healed incision is characterized by hyperpigmentation that gradually fades.

records for retrospective analysis were not available until 2020, and results are reported accordingly.

The majority (75%, 9 of 12) of C-sections resulted in live fetuses. The clinical presentation of females that underwent C-sections resulting in live fetuses included partial or marked pelvic fin edema and cloacal prolapse (78%, 7 of 9), which were consistently observed in concert. The urogenital papilla was noted to be prominent for one of the seven females with marked edema and prolapse. She was also observed to be increasingly lying on the bottom of the enclosure in the days before her C-section, highlighting a behavior change presumed to be related to her reproductive condition. The duration of stage 5, late pregnancy, was 3 months or more for for 6 C-sections including 5 females suggesting over gestation and 2 of these females developed a pressure ulcer on their ventral coelom. In addition to maternal concerns as a reason for C-section, the uterine fluid transitioned from a normal hypoechoic and homogeneous appearance on ultrasound to a very hyperechoic and heterogeneous appearance for two females and pregnancies (22%, 2 of 9), which was a health concern for the fetus that prompted C-section.

Neonates usually swam under their own power shortly after birth. They were transferred either to a nursery enclosure or a holding pool with other neonate rays to isolate them from large rays in the exhibit, thereby preventing injury and predation. Rays delivered naturally or by C-section commenced feeding on their own approximately 5–7 days after birth (personal observation). After the initial period of inappetence, they ate readily using general broadcast feeding methods. Cownose ray neonates were individually identified with passive integrated transponders (PIT) when 3–4 months old. At this age, they were large enough to be released into the exhibit with other fish without risk of predation.

Complications

No mortalities were associated with C-section procedures, but surgical site complications were observed for two of nine procedures involving two out of seven females. Both complications, one minor and the other major, were dehiscence. The minor complication was partial dehiscence near the center of the C-section incision and was observed 5 days post-C-section. On day seven postprocedure, the body wall was still intact, and malachite green was applied to the central open area. Weekly rechecks confirmed healing progression, and no further treatment was required.

The major complication was provoked by tankmates and occurred for a ray that was returned post-C-section to its habitat, which included other rays and porkfish (*Anisotremus virginicus*). After 5 days, the porkfish aggravated the surgical site by chewing out the skin sutures. The porkfish were immediately removed to a different tank to prevent further irritation of the surgical wound. The size of the ray's defect prevented reclosing the skin, and the lesion was irrigated with copious amounts of iodine and malachite green. After 2 days, a complete wound dehiscence occurred. The ray was anesthetized, and the wound was irrigated and prepped with iodine. The remaining body wall sutures were removed, and the edge was debrided. The body wall was closed with 2–0 PDS in a simple interrupted pattern. The cranial 2/3 of the skin was successfully reapposed with 2–0 PDS in a horizontal mattress pattern. The caudal 1/3 was partially closed with 2–0 PDS in a horizontal mattress pattern.

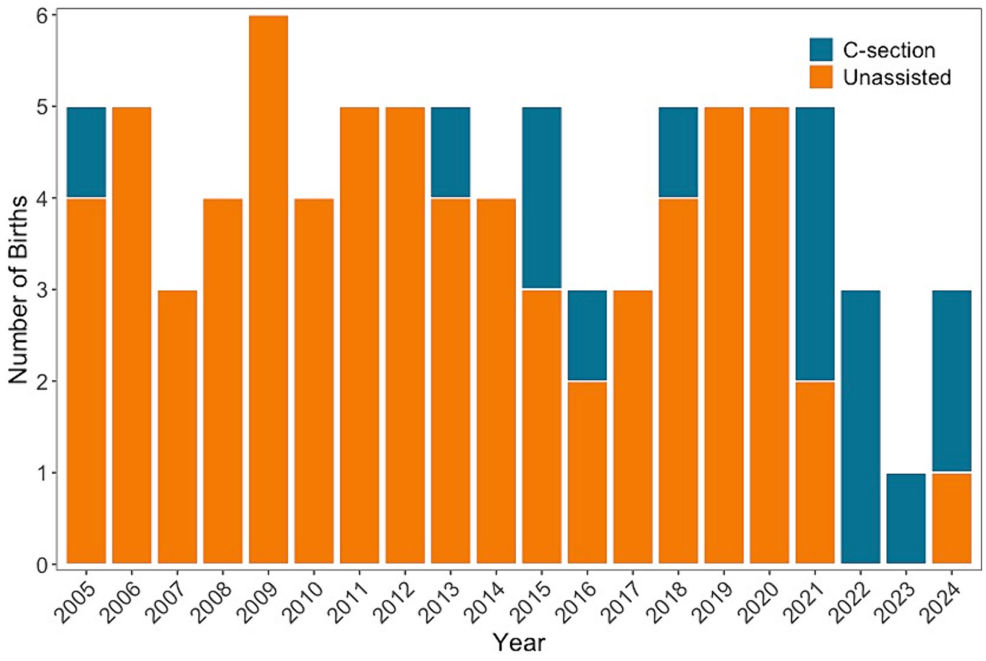

FIGURE 6
The number of births each year that are unassisted (orange) and C-sections (teal) for seven cownose rays that have had one or more C-sections and are founder rays individuals at Ripley's Aquarium of the Smokies. Cownose rays are examined monthly to monitor reproductive status, and the number of pregnancies that have required C-sections has increased since 2020.

TABLE 1 Reproductive history for cownose rays that have had one or more C-sections.

Female	Reproductive history
GB-RB-00-01-F	Unassisted birth in 2006, 2007, 2008, 2009, 2010, 2011, and 2014; C-section in 2015; Unassisted birth in 2017; C-section in 2018; Unassisted birth in 2019, 2020; C-section in 2021
GB-RB-00-04-F	Unassisted birth in 2005, 2007, 2009, 2010, and 2012; C-section in 2013, C-section in 2015; Unassisted birth in 2016, 2018, and 2020; C-section in 2021 and 2023
GB-RB-00-05-F	C-section in 2005; Unassisted birth in 2011 and 2013
GB-RB-00-06-F	Unassisted birth in 2005, 2006, 2008, 2009, 2011, 2012, 2013, 2015, 2018, 2019, and 2020; C-section in 2022 and 2024
GB-RB-00-10-F	Unassisted birth in 2005, 2006, 2008, 2009, 2011, 2012, 2013, 2014, 2015, 2017, 2018, 2019, 2020, and 2021; C-section in 2022 and 2024
GB-RB-00-11-F	Unassisted birth in 2005, 2006, 2009, 2010, 2011, 2012, 2013, and 2014; C-section in 2016; Unassisted birth in 2019; C-section in 2021
GB-RB-00-12-F	Unassisted birth in 2006, 2007, 2008, 2009, 2010, 2012, 2014, 2015, 2016, 2017, 2018, 2019, 2020, and 2021, C-section in 2022; Unassisted birth in 2024

Ceragyn® Wound and Skin spray (Purishield Life Sciences, LLC, CA, United States) was applied, followed by malachite green, Cavilon™ No Sting Barrier Film (3 M, Medical Solutions Division, MN, United States), and finally, liquid bandage. Perioperative IM injections of vitamin C (12.5 mg/kg) and ceftiofur (6.6 mg/kg) were given. Beginning 5 days after the reclosure, malachite green was applied, and enrofloxacin (10 mg/kg) was dosed daily for 5 days. The wound was rechecked on day 7 after reclosure and showed continued improvement. Malachite green and enrofloxacin (10 mg/kg) were dosed again daily for 5 days. The wound was rechecked on day 14 after reclosure and showed continued improvement. Malachite green, enrofloxacin (10 mg/kg), and vitamin C (12 mg/kg) were dosed daily for 5 days. On day 21 postreclosure, there was significant skin regeneration over the wound bed, and a final course of enrofloxacin (10 mg/kg) was continued daily for 5 days. The sutures were removed 28 days after reclosure.

In the long term, none of the rays exhibited complications related to C-sections. One female (GB-RB-00-11) died a year after her procedure of an unrelated cause. Rays were not isolated after C-section and instead returned to their exhibit. They resumed normal swimming patterns, activity, and appetite the same day as their C-section procedure. The surgical site entirely healed within 4–6 weeks, but the incision was still visible as a hyperpigmented scar for at least a year post-surgery.

Outcomes

Females ($n = 7$) were in managed care for an average [±standard deviation (SD)] of 15.4 ± 6.3 years before their first C-section was performed. Five of seven females who had C-sections were able to deliver normally and unassisted in future pregnancies. Two females

(GB-RB-00-06 and GB-RB-00-12) had a long history of unassisted births beginning in 2005 and 2006, and for both, only their most recent two pregnancies (2022 and 2024) required assistance via C-section. Most births (78%, 53 of 69) occurred before a female's first C-section. The average number of unassisted births prior to C-section was 8 ± 4 (range 0–14), and the average number of unassisted births after a female's first C-section was 1 ± 1 (range 1–3).

No mortalities have occurred among pregnant females because of dystocia, but 25% (3 of 12) of procedures were conducted secondary to fetal death. Death was confirmed using ultrasonography, characterized by lack of fetal heartbeat, lack of movement of gill arches indicative of respiration, absence of fetal movement, turbid uterine fluid, and a uterine mucosa with trophonema of variable lengths and thickness. No complications were noted in the short-term period for delivered neonates. One male newborn was remarked to be large and had difficulty unfolding his wings after extraction. Passive range of motion exercises were completed thrice daily to increase his range of motion.

Because cownose rays reproduce readily, there was almost always a group of neonates isolated within the main exhibit or in a holding tank of the exhibit. The isolation was for protection from other adult rays that share the exhibit, and it also facilitates monitoring feeding. The long-term outcome of C-section neonates was hampered by the delay in individual identification using PIT tags except for a 2015 C-section where the neonate is known unequivocally and alive at the time of publication, nearly 10 years post-procedure.

Discussion

Reproduction in managed care is a requirement and responsibility for achieving self-sustaining populations and supporting conservation and education initiatives. Not all species reproduce readily in aquariums, but for those that do, a thorough understanding of the reproductive anatomy and cycle is paramount to developing procedures to circumvent complications arising from reproductive efforts. For pregnant cownose rays suffering from over-gestation, dystocia, or fetal death, a C-section, as described in this report, is a lifesaving procedure. Most females that underwent C-sections had a history of successful reproduction with unassisted births both before and after their C-section procedure(s). Females that underwent C-sections were already mature and had been in managed care for an average of more than 15 years before their first C-section. Two females had delivered unassisted since 2005, but their two most recent pregnancies required C-sections. The monitoring efforts of female cownose rays at Ripley's Aquarium of the Smokies have not changed since 2005, but C-sections have increased in frequency during the last 4 years. This suggests that complications with gestation may be more prevalent as rays age, which may be an important consideration for the reproductive management of older rays. However, dependency on assisted birth is not necessarily a long-term problem because females are able to deliver naturally after C-section.

Determining when to intervene and assist with delivery is important because waiting too long may result in the loss of the neonate and potentially the female. Ideally, this decision is data-driven and based on knowledge of the female's reproductive history and status. The cownose rays at Ripley's Aquarium of the Smokies breed readily, and their reproductive status has been monitored monthly via ultrasonography since 2005. Females are assigned a reproductive stage (stages 0–5) based on the contents and appearance of the uterus (6). In the first cases of dystocia observed (2005 and 2013), a C-section was performed retroactively to remove stillborn young. Later, C-sections were performed proactively, largely due to monthly reproductive monitoring of the population, resulting in live young being extracted. For C-sections to be used proactively, a commitment to routine reproductive and health monitoring is needed to understand when gestation began and accurately predict the delivery date, which can then be used to help decide when intervention is warranted.

Adapting a procedure for use with a new species requires flexibility, attention to detail, and a willingness to recognize the pitfalls of a procedure and document how to avoid them. Customized equipment and lessons learned from procedure complications enabled the refinement of the surgical technique and recovery requirements to ensure favorable outcomes for future procedures. A portable procedure table was built for stingray medical procedures that included a surgery area and recirculating water to maintain anesthesia until the end of the procedure by delivering water to both spiracles with the rate of delivery infinitely adjustable using valves in the water lines. The surgical drape was a non-permeable, sterilized plastic barrier instead of a standard paper surgical drape. Keeping recovering rays with sutures isolated from fish that may irritate or disrupt the healing suture line was essential to prevent infection and enlargement of the wound.

This report details the procedure and long-term outcomes of C-sections for cownose ray females. This demonstrates that the procedure does not impact the rays' future reproduction. C-sections were increasingly required as females aged, which is important in monitoring gestation length and clinical signs of dystocia and may be a consideration for managing mixed populations in aquariums.

Data availability statement

The original contributions presented in the study are included in the article/supplementary material, further inquiries can be directed to the corresponding authors.

Ethics statement

The animal studies were approved by Ripley's Aquariums Research Review Committee. The studies were conducted in accordance with the local legislation and institutional requirements.

Author contributions

CB: Conceptualization, Investigation, Methodology, Writing – original draft. RG: Conceptualization, Writing – original draft, Investigation, Methodology. FB: Resources, Writing – review & editing. JD: Resources, Writing – review & editing. TH: Resources,

Supervision, Writing – review & editing. JW: Conceptualization, Data curation, Formal analysis, Writing – original draft.

Funding

The author(s) declare financial support was received for the research, authorship, and/or publication of this article. Development of this method was supported by Ripley's Aquariums.

Acknowledgments

The authors thank the entire animal care team at Ripley's Aquariums for their support and expertise. The authors also thank Nathan Barnes, Grayson McReynolds, and Mary Phillips from Ripley's Aquarium of the Smokies who expertly documented various C-section procedures using still images and video.

Conflict of interest

CB, FB, and JD are employed by Ripley's Aquarium of the Smokies. RG is employed by Ripley's Aquarium of Myrtle Beach. TH and JW are employed by Ripley's Aquariums.

The authors declare that the research was conducted in the absence of any commercial or financial relationships that could be construed as a potential conflict of interest.

Publisher's note

All claims expressed in this article are solely those of the authors and do not necessarily represent those of their affiliated organizations, or those of the publisher, the editors and the reviewers. Any product that may be evaluated in this article, or claim that may be made by its manufacturer, is not guaranteed or endorsed by the publisher.

References

1. Smith JW, Merriner J. Observations on the reproductive biology of the cownose ray, *Rhinoptera bonasus*, in Chesapeake Bay. *Fish Bull.* (1986) 84:871.

2. Neer JA, Thompson BA. Life history of the cownose ray, *Rhinoptera bonasus*, in the northern Gulf of Mexico, with comments on geographic variability in life history traits. *Environ Biol Fish*. (2005) 73:321–31. doi: 10.1007/s10641-005-2136-5

3. Poulakis GR. Reproductive biology of the cownose ray in the Charlotte Harbor estuarine system, Florida. *Marine Coastal Fish*. (2013) 5:159–73. doi: 10.1080/19425120.2013.795509

4. Fisher RA, Call GC, McDowell JR. Reproductive variations in cownose rays (Rhinoptera bonasus) from Chesapeake Bay. *Environ Biol Fish*. (2014) 97:1031–8. doi: 10.1007/s10641-014-0297-9

5. Fisher RA, Call GC, Dean Grubbs R. Age, growth, and reproductive biology of Cownose rays in Chesapeake Bay. *Marine Coastal Fish*. (2013) 5:224–35. doi: 10.1080/19425120.2013.812587

6. Sheldon JD, Allender MC, George RH, Bulman F, Abney K. Reproductive hormone patterns in male and female cownose rays (Rhinoptera bonasus) in an aquarium setting and correlation to ultrasonographic staging. *J Zoo Wildl Med*. (2018) 49:638–47. doi: 10.1638/2017-0247.1

frontiers | Frontiers in Veterinary Science

TYPE Original Research
PUBLISHED 02 October 2024
DOI 10.3389/fvets.2024.1470052

Check for updates

OPEN ACCESS

EDITED BY
Natalie D. Mylniczenko,
Walt Disney World, United States

REVIEWED BY
Kenneth Conley,
Independent Researcher, Orlando, Florida, United States
Ayoze Castro Alonso,
University of Las Palmas de Gran Canaria, Spain
Tracie Seimon,
Wildlife Conservation Society, United States

*CORRESPONDENCE
Alvin C. Camus
✉ camus@uga.edu

†These authors share senior authorship

RECEIVED 24 July 2024
ACCEPTED 18 September 2024
PUBLISHED 02 October 2024

CITATION
Powell AL, Camus AC, Leary JH, Miller SN, Bell CM and Ng TFF (2024) Novel adomavirus associated with proliferative skin lesions affecting the dermal denticles of a sand tiger shark (*Carcharias taurus*). *Front. Vet. Sci.* 11:1470052. doi: 10.3389/fvets.2024.1470052

COPYRIGHT
© 2024 Powell, Camus, Leary, Miller, Bell and Ng. This is an open-access article distributed under the terms of the Creative Commons Attribution License (CC BY). The use, distribution or reproduction in other forums is permitted, provided the original author(s) and the copyright owner(s) are credited and that the original publication in this journal is cited, in accordance with accepted academic practice. No use, distribution or reproduction is permitted which does not comply with these terms.

Novel adomavirus associated with proliferative skin lesions affecting the dermal denticles of a sand tiger shark (*Carcharias taurus*)

Ashley L. Powell[1], Alvin C. Camus[1*†], John H. Leary[1], Sarah N. Miller[2], Cynthia M. Bell[3] and Terry Fei Fan Ng[1†]

[1]Department of Pathology, College of Veterinary Medicine, University of Georgia, Athens, GA, United States, [2]Georgia Aquarium, Atlanta, GA, United States, [3]Specialty Oral Pathology for Animals, Geneseo, IL, United States

A captive sand tiger shark (*Carcharias taurus*) presented with progressive, hard, raised, miliary skin lesions localized to the lateral trunk and peduncle. Histopathologic evaluation of biopsy samples revealed dysplastic proliferation of odontogenic epithelium with the production of collagenous material. Inclusion bodies and viral particles were not observed with light or transmission electron microscopy, respectively. However, using next generation sequencing with Illumina MiSeq and PCR followed by Sanger sequencing, the complete genome of a novel adomavirus, tentatively named sand tiger shark adomavirus (STAdoV), was obtained from the affected tissue. The genome was circular and 18.5 kilobases with bidirectionally transcribed genes, namely EO1, EO2 & 4, EO3, LO4, LO5, LO6, LO7, LO8, and SET. *In situ* hybridization using RNAscope® technology and a STAdoV specific probe localized viral DNA to the nuclei of proliferating epithelial cells. Adomaviruses are an emerging viral group with structural and replicative genes sharing a complex evolutionary history with adenoviruses and small circular DNA tumor viruses including papillomaviruses and polyomaviruses. Adomaviruses are described in a number of fish species in association with both necrotizing and proliferative diseases. BLAST analysis of the viral genome revealed greatest nucleotide identity (71.29%) to guitarfish adomavirus (GAdoV), another elasmobranch virus associated with proliferative (epidermal) skin lesions. Lesions in the index animal persisted for approximately 1 year during which time four conspecifics developed similar proliferations. Ultimately, lesions in all sharks regressed spontaneously without recurrence for 2 years.

KEYWORDS

adomaviridae, genome sequencing, histopathology, denticle, elasmobranch, odontogenic epithelium

1 Introduction

"Adomaviridae" is a proposed family of viruses described in teleost and elasmobranch fishes thought to share a complex evolutionary history with adenoviruses and other small circular DNA tumor viruses, including papillomaviruses and polyomaviruses, based on homologies between their replicative strategies and structural components (1). The adomavirus genome contains a gene encoding a replicase protein with a superfamily 3 (SF3) helicase domain, similar to either the papillomavirus EO1 protein or polyomavirus large T antigen,

which are proposed to delineate "alpha" and "beta" subgroups within the family. Adomaviruses also encode LO6 and LO8 gene arrays, homologous to adenovirus morphogenetic genes pX and adenain, respectively (1). While adomaviruses are currently considered recombinants of these viral groups, their genetic elements are phylogenetically discrete (1).

The first reported adomavirus was associated with endothelial cell necrosis in Japanese eels (*Anguilla japonica*) in 2011 (2), followed by an outbreak of hemorrhagic gill disease in marbled eels (*Anguilla marmorata*) in 2012 (3, 4). Since then, adomaviruses have been described from proliferative skin lesions in a giant guitarfish (*Rhynchobatus djiddensis*) and smallmouth bass (*Micropterus dolomieu*) (5–7). Most recently, a novel adomavirus was associated with necrohemorrhagic gill disease in American eels (*Anguilla rostrata*) cultured in China (8). A growing list of additional adomavirus sequences and genomes have been identified within genomic sequence data of multiple fish species and other vertebrates (1, 9).

Descriptions of viral diseases in elasmobranchs are limited, despite their popularity in public aquaria and concerns over declining wild populations. In a retrospective study of 1,546 elasmobranch diagnostic cases, 15 (0.97%) were attributed to viral etiologies (10). Early diagnoses of herpesvirus and adenovirus infections were based on histopathologic and electron microscopic findings, namely observation of inclusion bodies and morphologically compatible viral particles, while others were entirely presumptive (10–12). Detailed descriptions of viral genomes are limited to the guitarfish polyomavirus-1 (GPyV) (13) and guitarfish adomavirus (GAdoV) (6). Histopathologic descriptions, electron microscopic findings and limited sequence data on an alloherpesvirus induced branchitis in a tiger shark (*Galeocerdo cuvier*) has also been reported (14).

Described herein are gross and histologic changes associated with unique proliferative skin lesions involving the odontogenic epithelium of dermal denticles in an aquarium exhibited sand tiger shark (*Carcharias taurus*). Following histopathologic evaluation of the lesions, the possibility of a viral etiology was considered. Further investigation utilizing electron microscopy, next generation sequencing, and *in situ* hybridization identified a novel alpha adomavirus that was localized to epithelial cells within the lesion, including cells with ameloblast morphology. A description of the associated adomavirus genome is presented.

2 Materials and methods

2.1 Case history and clinical evaluation

An estimated 100 kg, wild-collected, adult sand tiger shark (*Carcharias taurus*) maintained for 17 months in an indoor, 1.2 million-gallon, water-recirculating, mixed species, aquarium exhibit developed progressive skin lesions localized to the left lateral trunk and peduncle (Figure 1A). The irregular, miliary lesions were hard, raised, and light gray to pink with small peripheral ulcerations (Figure 1B). Over a period of several months, the skin lesion expanded locally then manifested on the right side. At this time, the shark, which was behaviorally conditioned to enter a stretcher, was manually restrained tank-side and 3% mepivacaine (1.7 mL total) administered by local injection for biopsy sample collection. A full-thickness, 5 mm-diameter skin punch biopsy and two 4–5 mm superficial skin shaves of the lesion were collected from the right lateral peduncle. Separate samples were immediately placed in 10% neutral buffered formalin and electron microscopy fixative containing 2% glutaraldehyde, 2% paraformaldehyde, and 0.2% picric acid in 0.1 M cacodylate-HCl buffer for submission to the Aquatic Pathology Service, Department of Pathology, College of Veterinary Medicine, University of Georgia. Additional samples were frozen at-80°C. Cell culture was not attempted due to lack of elasmobranch cell lines. Following the approximately 10-min biopsy procedure, a 3-week regimen of oral cefpodoxime proxetil (10 mg/kg) and vitamin C (12.5 mg/kg) three times per week was initiated and daily visual observations for signs of abnormal behavior, feeding responses, and infection were made by veterinary staff. Based on the superficial nature and small size of the biopsy samples, as well as potential detrimental effects associated with repeated restraint, analgesic therapy and topical medications were not administered. During this time, the shark continued to feed and behave normally, and the biopsy sites healed uneventfully.

2.2 Light and electron microscopy

Skin biopsy samples were decalcified overnight in Kristensen's solution, bisected and placed cut surface down in tissue processing cassettes. Routine processing by dehydration and clearing in a series of alcohol and xylene solutions, respectively, was followed by embedding in paraffin, sectioning at 5 µm, and staining with hematoxylin and eosin (H&E) and Masson's trichrome (MT). Comparative evaluation of normal histology and tissues used as controls in immunohistochemical and *in situ* hybridization studies utilized sections of similarly processed sand tiger and silvertip (*Carcharhinus albimarginatus*) shark skin with fully mature and developing dermal denticles. Tissue sections were prepared from paraffin blocks archived at the University of Georgia. For transmission electron microscopy (TEM), fixed tissues were post-fixed in 1% osmium tetroxide, dehydrated in a series of ethanol solutions, stained 'en bloc' with 0.5% uranyl acetate, and embedded in Epon-Araldite (Electron Microscopy Sciences). Ultrathin sections were prepared with a Reichert Ultracut S ultramicrotome (Leica), stained with lead citrate, and examined with a JEM-1011 transmission electron microscope (JEOL USA).

2.3 Immunohistochemistry (IHC)

Immunohistochemical staining for cytokeratin used a standard indirect protocol. Briefly, paraffin-embedded formalin-fixed (FFPE) tissue sections were deparaffinized and subjected to targeted antigen retrieval (Antigen Retrieval Citra, BioGenex) and background blocking (Power Block™, BioGenex). Primary and secondary antibodies consisted of anti-cytokeratin cocktail (AE1/AE3) anti-mouse monoclonal antibody (Cell Marque) and biotinylated horse anti-mouse IgG (Vector Laboratories), respectively. Color development utilized a horseradish peroxidase (HRP) labeled streptavidin (Biocare Medical) and Betazoid DAB

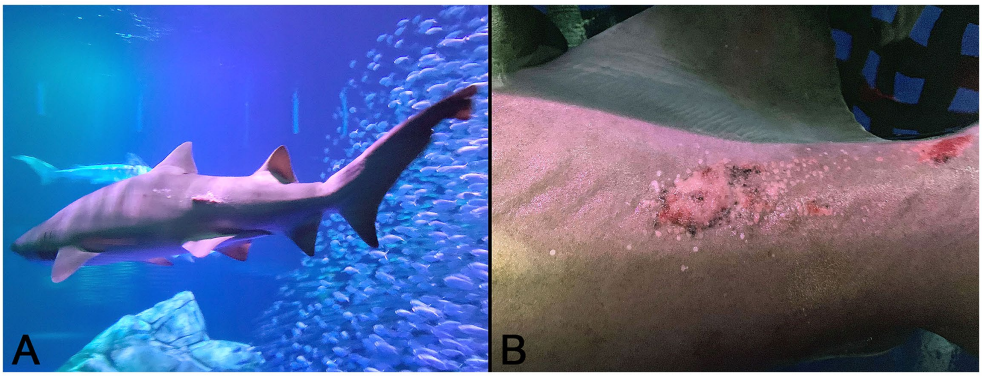

FIGURE 1
Gross images of the affected sand tiger shark (*Carcharias taurus*): **(A)** Irregular, raised, pink skin lesion on the lateral midline of the caudal trunk; **(B)** Close up image of the coarsely granular proliferative skin lesion composed of numerous, small, hard, coalescing nodules radiating multifocally from the central ulcerated mass.

Chromagen kit (Biocare Medical) followed by counterstaining with hematoxylin. For comparative purposes, cytokeratin IHC was performed on a developing denticle in the skin of a silvertip shark.

2.4 Next, generation sequencing and bioinformatics

Total DNA was extracted from previously frozen lesioned skin using the DNAEasy Blood and Tissue Kit (Qiagen) as per manufacturer's instructions. A next generation sequencing (NGS) library was then generated using a Nextera XT DNA Library Preparation Kit (Illumina Inc., USA) and sequenced using Illumina MiSeq with 2× 150-bp paired-end sequencing reagents by GENEWIZ (Azenta Life Sciences). Reads were assembled using the Geneious (Dotmatics; Version Prime 2022.1.1) *de novo* assembly pipeline. Briefly, paired reads were set, trimmed and filtered using default parameters. Trimmed reads were assembled using the Geneious algorithm with the default setting. The contigs were compared to GenBank non-redundant nucleotide database using (BLASTn) and protein (BLASTx) search. Viral contigs were compared and realigned by Geneious assembly for a draft genome to the subsequent analyses below.

2.5 Completion of the viral genome

Closing the circular genome was accomplished using conventional and long-distance PCR methods. For the former, NEB OneTaq reagents (M04080L) were used for standard PCR. Annealing temperatures were determined using NEB Tm calculator for each primer pair. Standard PCR reactions included 30 cycles of the following three steps: 95°C for 30 s, variable annealing temperatures for 30 s, and 68°C for 30–60 s. For long-range PCR, LongAmp Taq DNA Polymerase (NEB M0323S) reagents were used as per manufacturer's protocol to produce the 3,994 bp amplicon used for targeted Sanger sequencing. Cycling conditions utilized 30 cycles of the following three steps: 94°C for 30 s, 60°C for 30 s, and 65°C for 5 min. Primers pairs were designed to flank the putative gap between the 3′ and 5′ ends of the linear sequence generated by NGS assembly (Supplementary Table 1).

2.6 Phylogenetic analysis

Helicase core protein sequences from adomavirus, papillomavirus, and polyomavirus representatives were selected based on a previous study (5) and aligned with STAdoV using MAFFT (15). Certain unpublished adomaviruses in GenBank were not included due to uncertainty of their host and sequence status. Maximum likelihood trees were generated using the PhyML (16), where the best amino acid substitution model was analyzed by Smart Model Selection (17). Tree annotation was performed using FigTree.[1] Mid-point rooting was performed on the adomavirus-only tree as it was constructed without outgroups.

2.7 *In situ* hybridization (ISH)

Localization of viral DNA sequences to affected skin utilized *in situ* hybridization (ISH) with RNAscope® technology (Bio-Techne® Advanced Cell Diagnostics™) performed on FFPE tissue (18). A custom designed target probe pool of 20 ZZ probe pairs was used to hybridize within a 978 bp region (Supplementary Table 2) complimentary to positions 11,387–12,364 (5.3%) of the STAdoV genome (V-Ct-AdoV-C1, Advanced Cell Diagnostics™). Briefly, following the RNAscope® 2.5 HD Detection kit (RED) protocol, unstained histologic sections prepared on charged slides were deparaffinized, dried, treated with hydrogen peroxide, rinsed with distilled water, and immersed in target retrieval solution for 15 min at 99°C. Sand tiger shark adomavirus probe or RNAscope® Negative Control Probe (DapB) was added and incubated for 2 h at 40°C. Detection steps followed the Advanced Cell Diagnostics protocol after which slides were counterstained with

1 http://tree.bio.ed.ac.uk/software/figtree/

hematoxylin followed by nuclear bluing (0.02% ammonium hydroxide) and coverslipping with mounting media (Biocare Medical LLC, Concord, CA). A full-thickness section of microscopically normal skin from the same individual was used as an internal negative control.

3 Results

3.1 Light and electron microscopic findings

In normal control sand tiger shark skin, mature denticles were composed primarily of acellular dentine surrounding an inner pulp cavity. Denticles were anchored in the dermis by a broad base, tapered as they passed through the epidermis, expanded again above the skin surface and were capped by a thin layer of translucent enameloid (Figure 2A). In developing denticles, dermal papillae were topped peripherally by sequential layers of spindloid odontoblasts, dentine and enameloid with an outer margin of columnar ameloblasts located immediately beneath the surface epithelium (Figure 2B).

In decalcified sections of lesioned skin, interspersed among morphologically normal dermal denticles, were lobules of proliferative cells corresponding to the grossly visible hard skin nodules (Figures 3A,B). The abnormal structures were limited by a variably thick, hyalinized eosinophilic basement membrane bordered by a zone of palisading tall, thin columnar cells with indistinct cell borders and small amounts of amorphous to finely vesicular pale eosinophilic cytoplasm. Nuclei were ovoid with vesicular chromatin and often a single small nucleolus. Variably shaped polygonal cells with similar cytoplasmic and nuclear features filled central regions of the lobules. These cells were haphazardly arranged or formed follicular structures that encircled small islands of amorphous, vaguely lamellated eosinophilic material that resembled dentine (Figure 3C). With a Masson's trichrome stain, dentine within normal denticles stained intensely red (Figure 4A). In contrast, thickened basement membranes and the dentine-like material within the proliferative structures stained predominantly blue with only scattered areas of red staining (Figure 4B). This material was interpreted as hyalinized collagen, presumably produced by the proliferative cells but not clearly analogous to either dentine or enamel. The cells had mild nuclear pleomorphism and no mitotic figures were observed. Anisocytosis and anisokaryosis were minimal. Central regions of some affected structures contained cavitated spaces partially filled by necrotic cellular debris (cystic degeneration). Rare lobules of proliferative cells had a small invagination at the base into which streamed elongate mesenchymal cells, resembling pulp mesenchyme. No structures suggestive of inclusion bodies were noted. Dermal collagen immediately adjacent to the affected denticles was infiltrated by small to moderate numbers of lymphocytes (Figure 3B).

Pancytokeratin (AE1/AE3) IHC was used to identify cells of epithelial origin and served as an internal positive control in normal tissue and the case shark. In a histologic section of a normally developing denticle from a silky shark, cytokeratin IHC positively labeled the cytoplasm of cells comprising the stratified epidermis and the palisading epithelial cells (ameloblasts) forming the enamel organ of the denticle. Odontoblasts, which are neural crest derived ectomesenchymal cells, did not label with the antibody (Figure 5A). In lesions from the affected shark, cytokeratin IHC similarly labeled cells palisading peripherally along the basement membrane, as well as proliferative cells associated with the foci of hyalinized collagen (Figure 5B).

Using the RNAscope® ISH probe, no hybridization signal was detected in an emerging denticle from an unrelated sand tiger shark (Figure 5C). In the case shark, viral DNA was localized by strong positive hybridization signals to the nuclei of proliferating odontogenic epithelial cells within the lesion. There was no labeling of nuclei in the adjacent surface epidermis, odontoblasts or other dermal mesenchymal cells (Figure 5D). Despite the positive ISH results, neither inclusion bodies nor free viral particles were observed in the nuclei or cytoplasm of proliferative cells with TEM (Figure 6).

3.2 NGS, genome assembly, and completion

NGS using Illumina MiSeq on extracted skin lesion DNA generated a total of 2,372,727 reads; *de novo* assembly resulted in

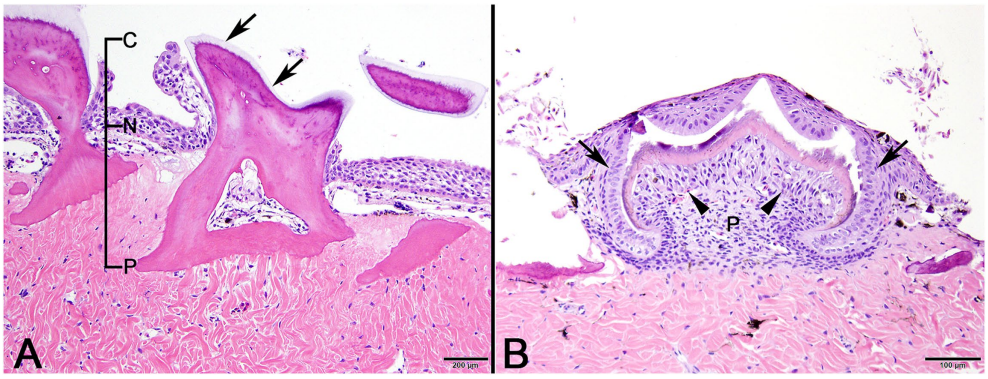

FIGURE 2
Photomicrographic images of normal sand tiger shark (*Carcharias taurus*) skin with stratified squamous epithelium and dermal denticles. **(A)** Mature denticle from a sand tiger shark composed predominantly of eosinophilic dentine with a broad basal plate (P) embedded in the dermis, narrow neck (N) at the skin surface, and crown (C) with superficial layer of enameloid (arrows). A central pulp cavity is present within the dentine (H&E stain, Bar = 200 µm). **(B)** Developing denticle from a sand tiger shark with thin layers of basophilic enameloid and eosinophilic dentine surrounded by palisading ameloblasts (arrows) and subtended by spindle-shaped odontoblasts (arrowheads). Deep to this is pulp (P) and eosinophilic dense dermal collagen (H&E stain, Bar = 100 µm).

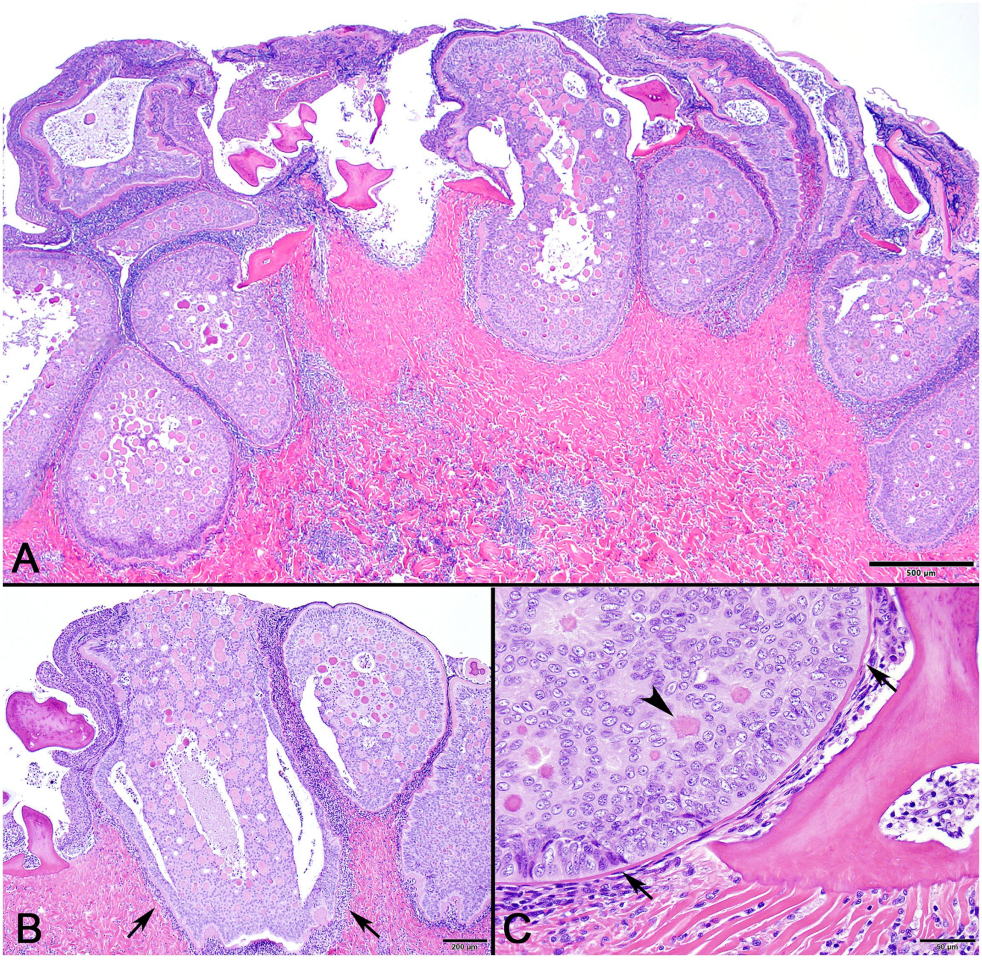

FIGURE 3
Photomicrographs of lesioned skin from a sand tiger shark (*Carcharias taurus*). **(A)** Lower magnification image of normal surface epithelium and denticle fragments interspersed among multiple large, basement membrane limited structures composed of proliferating odontogenic epithelial cells surrounding eosinophilic islands. (H&E stain, Bar = 500 µm). **(B)** Closer examination illustrates a cavitated space partially filled by necrotic debris within the proliferative lesion. The adjacent dermis is diffusely infiltrated by a dark staining band of lymphocytes (arrows). (H&E stain, Bar = 200 µm). **(C)** Higher magnification image of a proliferative lesion and an adjacent morphologically normal denticle. The lesion is limited by a hyalinized basement membrane (arrows) along which proliferating odontogenic epithelial cells palisade. Internally, follicular-like structures surround eosinophilic islands of hyalinized collagen (arrowhead). (H&E stain, Bar = 50 µm).

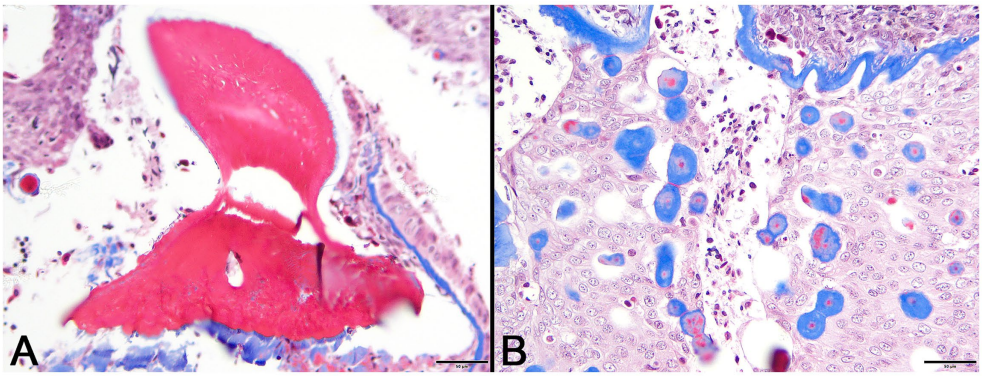

FIGURE 4
Photomicrographs of Masson's trichrome sections from lesioned skin. **(A)** Normal denticle stains intensely red. (Bar = 50 µm). **(B)** Blue staining of basement membrane and multifocal islands of material within the lesion are indicative of their collagenous nature. (Bar = 50 µm).

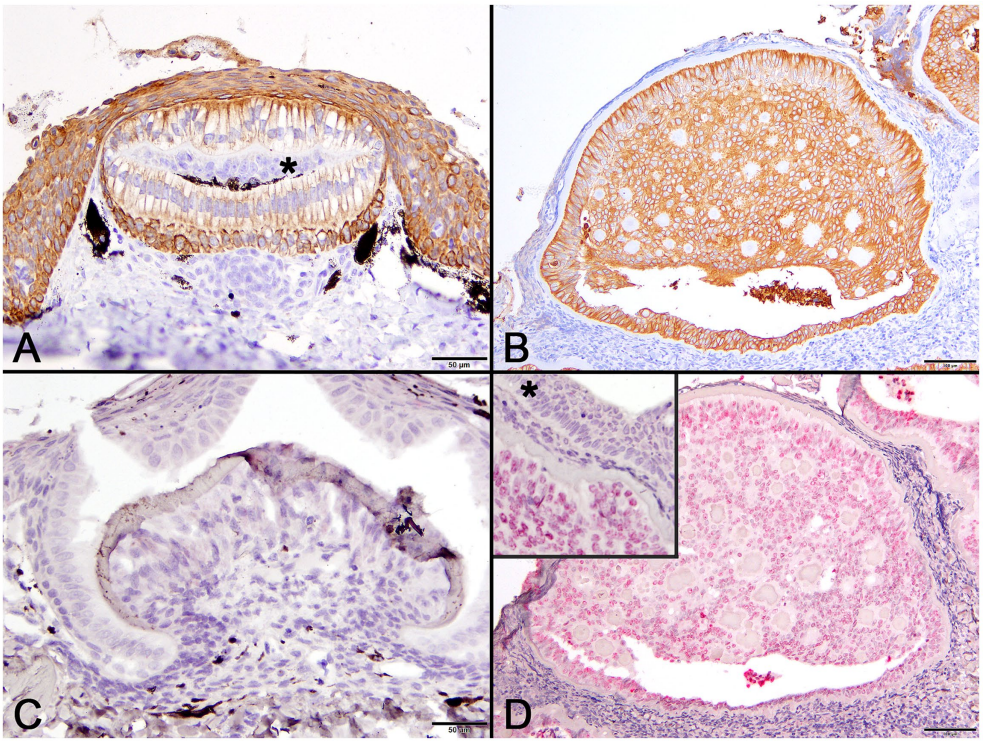

FIGURE 5
Photomicrographs of normal developing denticles (left column) and proliferative skin lesions (right column). **(A)** Control developing denticle from a silvertip sharp demonstrating positive pancytokeratin (AE1/AE3) cytoplasmic immunoreactivity of palisading ameloblasts and surface epithelium. There is no labeling of centrally located odontoblasts (asterisk) beneath the thin layer of dentine (Bar = 50 μm). **(B)** Positive pancytokeratin (AE1/AE3) cytoplasmic immunoreactivity of odontogenic epithelial cells at the lesion periphery and located centrally surrounding collagenous islands in the affected shark (Bar = 100 μm). **(C)** Normal developing sand tiger shark denticle with no hybridization signal following ISH using an RNAscope® adomavirus probe (Bar =50 μm). **(D)** Strong positive hybridization signal from the nuclei of proliferating odontogenic epithelial cells within lesioned skin of the affected shark following ISH using an RNAscope® adomavirus probe (Bar =100 μm). The higher magnification inset image illustrates a positive hybridization signal within nuclei of odontogenic epithelial cells but not surface epithelial cells (asterisk).

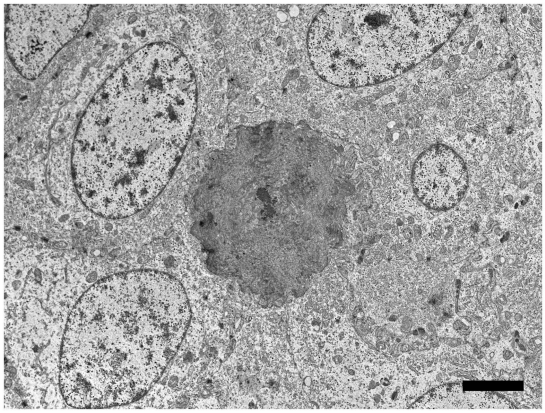

FIGURE 6
Electron microscopic image of lesioned skin from a sand tiger shark (*Carcharias taurus*) with a cluster of cells surrounding an irregular central island of positively contrasting dentine-like material. Identified as odontogenic epithelial cells, the proliferating cells corresponded to cytokeratin IHC positive cells observed histologically and exhibited a positive intranuclear ISH signal with the RNAscope® probe. The polygonal cells had large central ovoid nuclei and moderate amount of cytoplasm with rough endoplasmic reticulum, scattered mitochondria, and prominent desmosomes. (Bar=4μm).

368,335 contigs, of which 33,000 were greater than 1,000 bp. The contigs were used to assemble a near-complete adomavirus-like genome, and PCR followed by Sanger sequencing was used to close the circular genome by resolving a 21 bp GC rich sequence region. Final assembly of the circular genome using both NGS and Sanger sequences confirmed a viral genome size of 18,544 bp (Figure 7). NGS coverage spanned the entire genome except for the 21 bp sequence gap near nucleotide position 15,164, which was resolved by Sanger sequencing with 6X coverage. The complete genome shared 71.29% nucleotide identity with the Guitarfish Adomavirus 1 (GAdoV) genome (GenBank MF946548.1) and has been deposited in GenBank under accession number (PQ069217).

3.3 Genomic characteristics of the sand tiger shark adomavirus (STAdoV)

The viral proteins of STAdoV were divergent to known viral species but were most related to the adomaviruses (Table 1). The genome encodes two cassettes of bidirectionally transcribed genes, namely EO1, EO2 & 4, EO3, LO4, LO5, LO6, LO7, and LO8, as well as a SET [Su(var)3–9 Enhancer-of-Zeste and Trithorax] homolog (Figure 6). These genes are located on the sense strand, except for EO1

(anti-sense), in a genome organization consistent with those of guitarfish adomavirus and marbled eel adomavirus. Most of the viral proteins are highly divergent, sharing only 38–46% amino acid identity (AI) to the closest adomaviral homologs in GenBank (Table 1). The LO5, LO6, LO7, and LO8 genes showed significant protein homology (Blastx/Blastp) to adomaviral capsid subunits, namely penton, core, hexon, and adenain, correspondingly. While the L04 gene has no significant viral homolog, based on its location, it could potentially code for fiber or cement protein (2). The EO3 gene was inferred to be DNA primase-like, and another gene (EO2 & 4) is named for its location but shares no currently known protein homologs.

The most conserved protein for adomaviruses is EO1 helicase which is suitable for inter-and intra-viral family phylogenetic analysis (6). Helicase phylogeny of STAdoV showed that it is most closely related to other fish adomaviruses. Consistent with previous observations (6), these fish adomaviruses are distant relatives of polyomaviruses and papillomaviruses (Figure 8A). Considering the genome organization and helicase phylogeny, STAdoV should be recognized as a taxon within the fish adomavirus group. STAdoV could potentially be considered a novel species once criteria are established for declamation by the International Committee on Taxonomy of Viruses (ICTV).

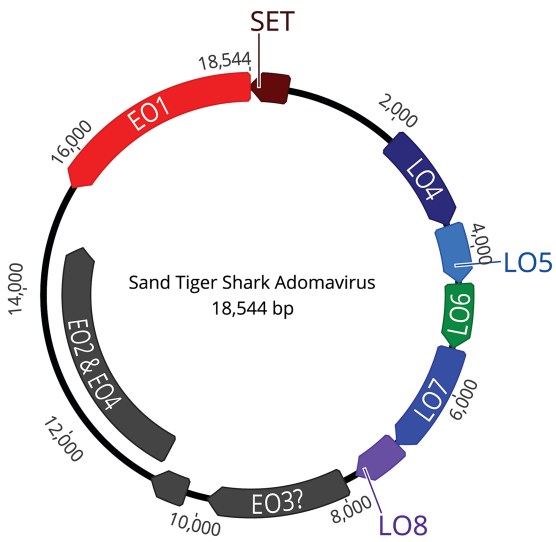

FIGURE 7
The assembled, approximately 18.5 kb, circular, double stranded DNA genome contains 9 open reading frames (ORFs).

4 Discussion

Histopathologic and immunologic examination of the hard, raised skin lesions in the case shark revealed viral associated dysplastic proliferation of cytokeratin-positive epithelial cells, including cells with ameloblast morphology. These lesions represent proliferation of odontogenic epithelium that normally forms dermal denticles in the skin of sharks. Individual lobules within the lesion were limited by a hyalinized basement membrane and these discrete structures likely represent proliferation of the enamel organ epithelium that would have formed a single denticle. Organization of the lesions was reminiscent of ameloblastoma, particularly follicular and dentinoid-associated subtypes as described in humans (19–23). Hyalinization of basement membranes is a common feature of proliferative lesions involving odontogenic epithelium (24). Many small foci of hyalinized collagen were distributed among the proliferating odontogenic epithelium and were presumably mineralized based on hardness of the gross lesions. The precise nature of this material is unclear but suggestive of dentinoid, a poorly understood collagenous material resembling true dentine but having a close association with odontogenic epithelium rather than odontoblasts (25). Hyalinized eosinophilic material within odontogenic epithelial tumors has been variously described as basement membrane, amyloid, glycoprotein, keratin, and enamel matrix (24, 25). In this case, blue staining with Masson's trichrome supports the collagenous nature of the material. Subepithelial hyalinization and hyalinized collagen deposits may represent unsuccessful attempts by odontogenic epithelium to produce dental matrix in the absence of appropriate induction (24, 26).

Next, generation sequencing and additional PCR yielded the complete, 18.5 kb, circular genome of a novel adomavirus tentatively named sand tiger adomavirus (STAdoV). Using RNAscope® technology, a subsequently developed ISH assay localized viral DNA

TABLE 1 Sand tiger adomavirus protein characteristics and their closest related homologs.

Protein	Length (bp)	Direction	Putative functions	Protein identity to the closest virus	Closest virus in GenBank
LO4	1,440	Forward	Unknown	No significant Blastx hit (currently)	N/A
LO5	825	Forward	Penton	38%	Adomaviruses
LO6	918	Forward	Core	38%	Adomaviruses
LO7	1,569	Forward	Hexon/Major Capsid protein	42%	Adomaviruses
LO8	735	Forward	Adenain	30%	Adomaviruses
EO1	3,024	Reverse	Helicase	39%	Adomaviruses
EO2 & EO4	4,026	Forward	Unknown	No significant Blastx hit (currently)	N/A
EO3	2001	Forward	DNA primase-like	41%	Adomaviruses
SET	558	Reverse	Su(var)3–9, Enhancer-of-zeste, Trithorax (SET) domain superfamily, containing lysine methyltransferases	46%	Adomaviruses

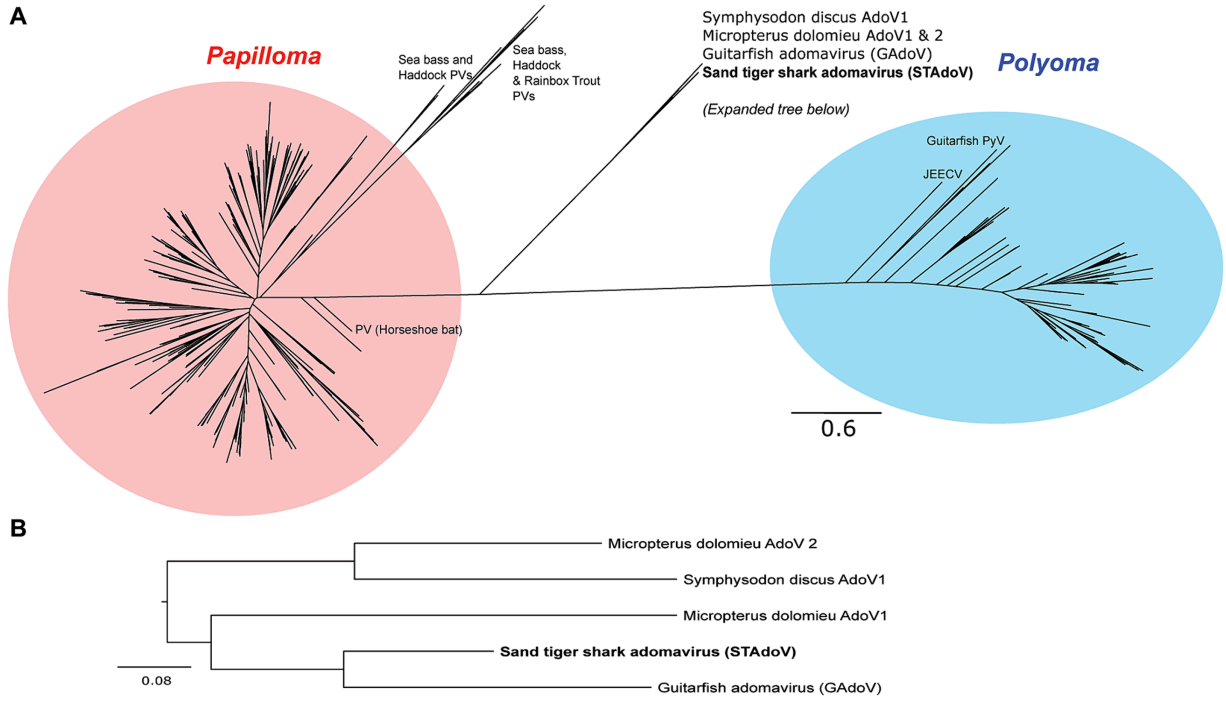

FIGURE 8
Maximum likelihood trees demonstrating relationships between core helicase proteins of adomaviruses and related taxa. **(A)** Helicase protein phylogeny among adomavirus, papillomavirus, and polyomavirus representatives. **(B)**Helicase protein phylogeny among adomaviruses related to STAdoV. JEECV, Japanese eel endothelial cell-infecting virus; PV, papillomavirus; PyV, polymavirus.

to the nuclei of proliferating odontogenic epithelial cells within the abnormal denticle-like structures. This is the second adomavirus genome associated with proliferative epithelial lesions in the skin of an elasmobranch and the first described from a sand tiger shark (5, 6).

Similar to infection with the guitarfish adomavirus, lesions in this sand tiger shark were restricted to epithelial cells, although different specific cell types (epidermal versus odontogenic) were involved. The skin of cartilaginous fishes is covered by a stratified squamous epithelium and contains mineralized dermal denticles (placoid scales) that share the same evolutionary origin (odontodes), gene regulatory network, and histologic developmental stages as mammalian teeth, making them serial homologs (27). Functioning to facilitate laminar flow of water and reduce drag, denticles grow to a definitive size, are shed asynchronously, and are then replaced (28). Histologically, denticles are composed of a calcified basal plate embedded in the dermis, tapering neck region, and crown that rises above the surface epithelium (Figure 2A). A central pulp cavity is enclosed by a thick layer of dentine and thin surface margin of enameloid (28). In the developing denticle, a dermal papilla containing mesothelial cells (odontoblasts) is capped by epithelial cells of the stratum germinativum and pushes outward as the base extends into the dermis. Odontoblasts peripherally line the central pulp, produce the dentine matrix and induce overlying epithelial cells (ameloblasts) to deposit the enameloid matrix (27–29) (Figure 2B).

Prior to this investigation, guitarfish adomavirus (GAdoV) represented the only adomavirus described in an elasmobranch species (6). Helicase phylogeny suggested that STAdoV shared a close relationship to a group of piscine adomaviruses including those found in *Micropterus dolomieu* (smallmouth bass), *Symphysodon discus* (red discus), and giant guitarfish (GAdoV) (Figures 8A,B). This group of piscine adomaviruses have a helicase protein homology that is closer to those of papillomaviruses, thus placing them within the proposed "alpha group" of adomaviruses (1) Among the piscine adomavirus infections for which lesions have been described, members of the "alpha group" appear pathologically more benign and proliferative (5–7). In contrast, the "beta group," which possess a polyomavirus-like LT helicase and include adomaviruses described from cultured Japanese, marbled, and American eels are highly pathogenic and associated with necrohemorrhagic disease (1–3, 8).

Despite genomic similarities to GAdoV and localization of viral sequences to the nuclei of proliferating odontogenic epithelial cells, neither viral inclusions nor virions were observed for STAdoV histologically or with transmission electron microscopy, respectively. This contrasts with lesions induced by GAdoV, where large numbers of intranuclear inclusion bodies corresponded to arrays of 75 nm icosahedral virus particles (5, 6). We speculate that STAdoV virion production is potentially supported by relatively few cells limiting the chances of observing viral particles in a manner similar to papillomavirus infections (30). A lack of histologic and immunohistochemical evidence of papillomavirus infection has been reported in tumors induced by bovine papillomavirus in feline sarcoids and in human papillomavirus infections where viral DNA was localized to proliferating fibroblasts using *in situ* hybridization (31). It is also conceivable that since the lesions persisted for approximately 6 months prior to sampling, the productive stage of the viral infection had ceased and there were no longer detectable viral particles.

As seen with GAdoV infection in the giant guitarfish, STAdoV-associated skin lesions in the sand tiger shark persisted for many

months before regressing spontaneously (5, 6). Histopathologic evidence of regression is presumptively indicated by cavitation with necrotic debris within some lesions and possibly by lymphocytic inflammation in the adjacent dermis (Figure 3). Throughout the course of infection, signs of systemic illness were not observed clinically and residual effects were limited to irregularly shaped areas of depigmented skin. While similar lesions appeared on four conspecifics in the exhibit, they also regressed spontaneously and have not reappeared in over a year indicating the self-limiting infection may produce prolonged immunity. There was no spread to other elasmobranch species in the mixed exhibit, suggesting the virus is species-specific.

Adomaviruses are reported from a variety of fishes (including elasmobranchs), amphibians, and terrestrial and aquatic reptiles with varying clinical significance. Several have been discovered while screening public genomic databanks rather than during investigations of disease, suggesting some may be orphan viruses or nonpathogenic (10, 32). It is speculated that additional adomaviruses will be described as non-biased sequencing methodologies come into more widespread use in routine diagnostics, particularly when applied to the investigation of relatively benign disease processes in uncommonly observed species such as this sand tiger shark. Only a small number of viral diseases are described in elasmobranchs and few reports characterize viral genomes (5, 6, 13, 14). This, however, is changing as molecular diagnostic technologies improve and become more affordable, and interest in elasmobranch conservation and research expands. Cases in which a viral etiology is suspected warrant further attention and investigation, particularly in confined settings conducive to disease transmission.

Data availability statement

The datasets presented in this study can be found in online repositories. The names of the repository/repositories and accession number(s) can be found in the article/Supplementary material.

Ethics statement

Ethical approval was not required for the study involving animals in accordance with the local legislation and institutional requirements because opportunistic research was completed from a diagnostic biopsy submission.

Author contributions

AP: Data curation, Formal analysis, Investigation, Visualization, Writing – original draft, Writing – review & editing. AC: Conceptualization, Formal analysis, Investigation, Methodology, Project administration, Resources, Supervision, Visualization, Writing – original draft, Writing – review & editing. JL: Data curation, Formal analysis, Methodology, Validation, Writing – original draft, Writing – review & editing. SM: Writing – review & editing, Investigation. CB: Formal analysis, Methodology, Validation, Visualization, Writing – review & editing. TN: Data curation, Formal analysis, Methodology, Validation, Visualization, Writing – original draft, Writing – review & editing.

Funding

The author(s) declare that no financial support was received for the research, authorship, and/or publication of this article.

Conflict of interest

CB is employed by Specialty Oral Pathology for Animals.

The remaining authors declare that the research was conducted in the absence of any commercial or financial relationships that could be construed as a potential conflict of interest.

Publisher's note

All claims expressed in this article are solely those of the authors and do not necessarily represent those of their affiliated organizations, or those of the publisher, the editors and the reviewers. Any product that may be evaluated in this article, or claim that may be made by its manufacturer, is not guaranteed or endorsed by the publisher.

Supplementary material

The Supplementary material for this article can be found online at: https://www.frontiersin.org/articles/10.3389/fvets.2024.1470052/full#supplementary-material

References

1. Welch NL, Tisza MJ, Starrett GJ, Belford AK, Pastrana DV, Pang YY, et al. Identification of adomavirus virion proteins. *Bio Rxiv*. (2020) 7:341131. doi: 10.1101/341131

2. Mizutani T, Sayama Y, Nakanishi A, Ochiai H, Sakai K, Wakabayashi K, et al. Novel DNA virus isolated from samples showing endothelial cell necrosis in the Japanese eel, *Anguilla japonica*. *Virology*. (2011) 412:179–87. doi: 10.1016/j.virol.2010.12.057

3. Pao HY, Wu CY, Wen CM. Persistent development of adomavirus and aquareovirus in a novel cell line from marbled eel with petechial skin haemorrhage. *J Fish Dis*. (2019) 42:345–55. doi: 10.1111/jfd.12939

4. Wen CM, Chen MM, Wang CS, Liu PC, Nan FH. Isolation of a novel polyomavirus, related to Japanese eel endothelial cell-infecting virus, from marbled eels, *Anguilla marmorata* (Quoy & Gaimard). *J Fish Dis*. (2016) 39:889–97. doi: 10.1111/jfd.12423

5. Camus A, Dill J, McDermott A, Camus M, Ng TF. Virus-associated papillomatous skin lesions in a giant guitarfish *Rhynchobatus djiddensis*: a case report. *Dis Aquat Org*. (2016) 117:253–8. doi: 10.3354/dao02956

6. Dill JA, Camus AC, Leary JH, Ng TF. Microscopic and molecular evidence of the first elasmobranch adomavirus, the cause of skin disease in a giant guitarfish, *Rhynchobatus djiddensis*. *MBio*. (2018) 9:e00185–18. doi: 10.1128/mBio.00185-18

7. Iwanowicz LR, Young KT, Adams CR, Blazer VS, Smith GD, Cornman RS. Draft genome sequence of an adomavirus associated with raised mucoid skin lesions on smallmouth bass (*Micropterus dolomieu*). *Microbiol Res Announce*. (2020) 9:10–128. doi: 10.1128/MRA.01479-19

8. Yang JX, Chen X, Li YY, Song TY, Ge JQ. Isolation of a novel adomavirus from cultured American eels, *Anguilla rostrata*, with haemorrhagic gill necrosis disease. *J Fish Dis*. (2021) 44:1811–8. doi: 10.1111/jfd.13500

9. Harding EF, Russo AG, Yan GJ, Mercer LK, White PA. Revealing the uncharacterized diversity of amphibian and reptile viruses. *ISME Communications*. (2022) 2:95. doi: 10.1038/s43705-022-00180-x

10. Garner MM. A retrospective study of disease in elasmobranchs. *Vet Pathol*. (2013) 50:377–89. doi: 10.1177/0300985813482147

11. Leibovitz L, Lebouitz SS. A viral dermatitis of the smooth dogfish, *Mustelus canis* (Mitchill). *J Fish Dis*. (1985) 8:273–9. doi: 10.1111/j.1365-2761.1985.tb00943.x

12. Bowman M, Ramer J, Proudfoot J, Stringer E, Garner M, Trupkiewicz J, et al. A novel adenovirus in a collection of wild-caught dusky smooth-hounds *(Mustelus canis)*. In: Proceedings AAZV ARAV joint conference; 2008 Oct 11–17; Los Angeles, CA. American Association of Zoo Veterinarians (2008). p. 208–209.

13. Dill JA, Ng TF, Camus AC. Complete sequence of the smallest polyomavirus genome, giant guitarfish (*Rhynchobatus djiddensis*) polyomavirus 1. *Genome Announc*. (2016) 4:10–128. doi: 10.1128/genomeA.00391-16

14. Armwood AR, Stilwell JM, Ng TF, Clauss TM, Leary JH, Mader D, et al. A novel herpes-like virus inducing branchial lesions in a tiger shark (*Galeocerdo cuvier*). *Vet Pathol*. (2022) 59:348–52. doi: 10.1177/03009858211052662

15. Kuraku S, Zmasek CM, Nishimura O, Katoh K. aLeaves facilitates on-demand exploration of metazoan gene family trees on MAFFT sequence alignment server with enhanced interactivity. *Nucleic Acids Res*. (2013) 41:W22–8. doi: 10.1093/nar/gkt389

16. Guindon S, Dufayard JF, Lefort V, Anisimova M, Hordijk W, Gascuel O. New algorithms and methods to estimate maximum-likelihood phylogenies: assessing the performance of PhyML 3.0. *Syst Biol*. (2010) 59:307–21. doi: 10.1093/sysbio/syq010

17. Lefort V, Longueville JE, Gascuel O. SMS: smart model selection in PhyML. *Mol Biol Evol*. (2017) 34:2422–4. doi: 10.1093/molbev/msx149

18. Wang F, Flanagan J, Su N, Wang LC, Bui S, Nielson A, et al. RNAscope: a novel in situ RNA analysis platform for formalin-fixed, paraffin-embedded tissues. *J Mol Diagn*. (2012) 14:22–9. doi: 10.1016/j.jmoldx.2011.08.002

19. Murphy BG, Bell CM, Soukup JW. "Odontogenic tumors." In: Veterinary Oral and Maxillofacial Pathology. Hoboken, NJ: John Wiley & Sons, Inc. (2020). p. 91–127.

20. Chettiankandy TJ, Sachdev SS, Kende PP, Sardar MA, Saju R. Adenoid ameloblastoma with dentinoid: a rare hybrid odontogenic tumor. *Indian J Pathol Microbiol*. (2024) 67:441–4. doi: 10.4103/ijpm.ijpm_186_22

21. Reesha K, Nair RG, Anusree P, Navajeevraj MN. Ameloblastic fibroma with extensive dentinoid–a rare presentation. *J Oral Maxillofac Pathol*. (2023) 27:760–4. doi: 10.4103/jomfp.jomfp_200_23

22. Narayan B, Kumar P, Priya B, Urs AB, Augustine J. Adenomatoid odontogenic tumor: a histopathologic profile of 43 cases with evidence supporting a mixed odontogenic origin. *Pathol Res Pract*. (2024) 257:155322. doi: 10.1016/j.prp.2024.155322

23. Zeng M, Guo X, Chen X, Shao Z, Yang S. Odontogenic carcinoma with dentinoid: case report and literature review of a rare entity. *BMC Oral Health*. (2024) 24:704. doi: 10.1186/s12903-024-04471-8

24. Augustine D, Rao RS, Patil S. Hyalinization as a histomorphological risk predictor in oral pathological lesions. *J Oral Biol Craniofac Res*. (2021) 11:415–22. doi: 10.1016/j.jobcr.2021.05.002

25. Gardner DG, Farquhar DA. A classification of dysplastic forms of dentin. *J Oral Pathol Med*. (1979) 8:28–46. doi: 10.1111/j.1600-0714.1979.tb01620.x

26. Pillipsen HP, Nikai H. Adenomatoid odontogenic tumor In: L Barnes, JW Eveson, P Reichart and D Sidransky, editors. WHO classification of tumors: Head and neck tumors. Lyon, France: IARC Press (2005). 304–5.

27. Debiais-Thibaud M, Oulion S, Bourrat F, Laurenti P, Casane D, Borday-Birraux V. The homology of odontodes in gnathostomes: insights from dlx gene expression in the dogfish, *Scyliorhinus canicula*. *BMC Evol Biol*. (2011) 11:307. doi: 10.1186/1471-2148-11-307

28. Kemp NE. Chapter 2: integumentary system and teeth In: Hamlett, editor. Sharks, skates, and rays: The biology of elasmobranch fishes. *1st* ed. Baltimore, MD: The Johns Hopkins University Press (1999). 43–65.

29. Gillis JA, Donoghue PC. The homology and phylogeny of chondrichthyan tooth enameloid. *J Morphol*. (2007) 268:33–49. doi: 10.1002/jmor.10501

30. Doorbar J. The papillomavirus life cycle. *J Clin Virol*. (2005) 32:7–15. doi: 10.1016/j.jcv.2004.12.006

31. Schulman FY, Krafft AE, Janczewski T. Feline cutaneous fibropapillomas: clinicopathologic findings and association with papillomavirus infection. *Vet Pathol*. (2001) 38:291–6. doi: 10.1354/vp.38-3-291

32. Costa VA, Ronco F, Mifsud JC, Harvey E, Salzburger W, Holmes EC. Host adaptive radiation is associated with rapid virus diversification and cross-species transmission in African cichlid fishes. *Curr Biol*. (2024) 34:1247–1257. doi: 10.1016/j.cub.2024.02.008

frontiers | Frontiers in Veterinary Science

TYPE Original Research
PUBLISHED 24 October 2024
DOI 10.3389/fvets.2024.1452659

Check for updates

OPEN ACCESS

EDITED BY
Natalie D. Mylniczenko,
Walt Disney World, United States

REVIEWED BY
Steven Nelson,
Mystic Aquarium, United States
Lorrie Gaschen,
VetCT Specialist, United Kingdom
James Johnson,
Denver Zoo, United States

*CORRESPONDENCE
María José Caballero
✉ mariajose.caballero@ulpgc.es

RECEIVED 21 June 2024
ACCEPTED 08 October 2024
PUBLISHED 24 October 2024

CITATION
Montero-Hernández G, Caballero MJ, Curros-Moreno Á, Suárez-Santana CM, Rivero MA, Caballero-Hernández L, Encinoso M, Fernández A and Castro-Alonso A (2024) Pathological study of a traumatic anthropogenic injury in the skeleton of a spiny butterfly ray (*Gymnura altavela*). *Front. Vet. Sci.* 11:1452659. doi: 10.3389/fvets.2024.1452659

COPYRIGHT
© 2024 Montero-Hernández, Caballero, Curros-Moreno, Suárez-Santana, Rivero, Caballero-Hernández, Encinoso, Fernández and Castro-Alonso. This is an open-access article distributed under the terms of the Creative Commons Attribution License (CC BY). The use, distribution or reproduction in other forums is permitted, provided the original author(s) and the copyright owner(s) are credited and that the original publication in this journal is cited, in accordance with accepted academic practice. No use, distribution or reproduction is permitted which does not comply with these terms.

Pathological study of a traumatic anthropogenic injury in the skeleton of a spiny butterfly ray (*Gymnura altavela*)

Gustavo Montero-Hernández[1], María José Caballero[1]*, Ángel Curros-Moreno[1,2], Cristian M. Suárez-Santana[1], Miguel A. Rivero[1], Lucía Caballero-Hernández[1], Mario Encinoso[3], Antonio Fernández[1] and Ayoze Castro-Alonso[1]

[1]Institute of Animal Health and Food Safety (IUSA), College of Veterinary Medicine, University of Las Palmas de Gran Canaria, Las Palmas, Spain, [2]Poema del Mar Aquarium, Loro Parque Fundación, Las Palmas, Spain, [3]Veterinary Hospital, College of Veterinary Medicine, University of Las Palmas de Gran Canaria, Las Palmas, Spain

Introduction: External injuries in elasmobranchs are frequent findings, either due to inter- or intraspecific interactions or as a result of interaction with human activities. However, the resilience of these species to traumatic injury remains poorly understood. This work provides an insight into the clinical presentation, diagnostic imaging, and pathological features of a severe traumatic injury to the cartilaginous skeleton of a spiny butterfly ray (*Gymnura altavela*).

Methods: An adult female was found lethargic in the bottom of the coast of Gran Canaria, with an external incised-contused traumatic lesion of 2 cm diameter in the scapulocoracoid cartilage. It was captured and transferred to the Poema del Mar Aquarium for its clinical evaluation and treatment. Despite these efforts, the animal eventually died and was transfer to the Institute of Animal Health and Food Safety (IUSA) for its pathological diagnosis, including a Computed Tomography (CT) study and necropsy.

Results: The animal presented a marked reduction in hematocrit and hepatosomatic index due a chronic debilitation process. The CT scan revealed a destructive lesion with irregular margins at the level of the right scapulocoracoid cartilage. The main pathological findings were the disorganization of the tesserae layer, appearing as whitish square to rectangular geometric pieces separated from the cartilaginous core. Histologically, these pieces of tesserae were separated from the unmineralized cartilage core and displaced from the adjacent perichondrium, where inflammatory cells infiltrate. Edema and hemorrhages were also observed.

Conclusions: This study reports the first comprehensive description of skeleton trauma in a spiny butterfly ray, including the clinical presentation, diagnostic imaging and the anatomopathological features.

KEYWORDS

***Gymnura altavela*, elasmobranch, clinical presentation, computed tomography, veterinary pathology, cartilage**

1 Introduction

The situation of elasmobranchs is critical, being considered as one of the most endangered groups of animals on the planet (1, 2). Anthropogenic causes, primarily fishing interactions, stand out as the foremost threats and causes of death in sharks and rays (1, 3, 4). Located in the Atlantic Ocean, the Canary Islands are an archipelago of volcanic origin that constitutes a Spanish autonomous community situated off the northwest coast of Africa. Comprising eight inhabited islands (Gran Canaria,

Tenerife, Fuerteventura, Lanzarote, La Palma, La Gomera, El Hierro, and La Graciosa) alongside various uninhabited islets. The distinctive environmental characteristics of this archipelago result in a unique biodiversity, with a high number of endemic species (5–7). This region represents a stronghold for a wide variety of endangered elasmobranchs species, where they form stable populations and have nurseries in locations with high human presence (8–13). The spiny butterfly ray (*Gymnura altavela*) is among the most frequently observed elasmobranchs in the Canary Islands (10). This ray species belongs to the family *Gymnuridae* and is distributed throughout the coastal waters of the Atlantic Ocean, Mediterranean Sea, and Black Sea, where it primarily inhabits sandy substrates ranging from the seashore to depths of 150 meters (14). It is classified as Critically Endangered in Europe and Endangered worldwide in the International Union for Conservation of Nature (IUCN) Red List due to declining populations mainly because of fishing pressure and habitat destruction (15). The vast presence of tourism along the coasts of the Canary Islands, raises significant interest in studying the potential threats by human actions to the marine environment.

Particularly, traumatic injuries in wild elasmobranchs often arise from both intraspecific and interspecific encounters, or because of interactions with human activity (16–24). The remarkable capacity and rapidity of external wound healing in chondrichthyans are widely acknowledged (25–29). For instance, severe injuries consistent with vessel collisions have been documented in a great white shark (*Carcharodon carcharias*) (30), a reef manta ray (*Mobula alfredi*) (31), and whale sharks (*Rhincodon typus*) (32), cases where the monitorization of these animals highlighted the astonishing resilience of these species and the rapid speed of healing. However, the regenerative capacity of cartilage tissue in elasmobranchs has been a subject of debate in different studies. Thus, Ashhurst (33) concluded that chondrichthyans were unable to repair their cartilaginous skeleton based on an experiment involving the cutting of fin rays in dogfishes (*Scyliorhinus* spp.) and the observations made over a 26-week period. In contrast, recent findings have revealed evidence of a spontaneous mechanism of cartilage repair in response to small injuries in rays (34, 35). However, injuries involving extensive and severe damage to the skeleton of elasmobranchs have been poorly documented. The aim of this study is to provide a comprehensive description of the clinical intervention, diagnostic imaging findings, alongside the macroscopic and histological characteristics of a traumatic injury of anthropogenic origin in the scapulocoracoid cartilage of a spiny butterfly ray.

2 Materials and methods

An adult female spiny butterfly ray (*Gymnura altavela*) was spotted nearby the Castillo del Romeral wharf in Gran Canaria (Canary Islands, Spain) laying lethargic in the sandy bottom with an external circular incised-contused traumatic lesion of 2 cm diameter in the scapulocoracoid cartilage (Figure 1). It was captured and transferred to the Poema del Mar Aquarium facilities (Loro Parque Fundación, Gran Canaria) under the appropriate national and regional legal permissions and authorizations to evaluate the animals condition and consider treatment and rehabilitation options. This facility has quarantine tanks suitable for the housing of this animal, and a veterinary team specialized in the handling and health care of this elasmobranch specie. The ray weighed 32 kg, had a disc width of 179 cm and a total length of 114 cm. The animal was placed in a tank of 16.252 m^3 with a mean water temperature of 22°C and mean values of pH and salinity of 8.1 and 36.3%, respectively.

A radiographic study was conducted to assess the affected structures and determine the depth of the incision using a portable direct digital radiography equipment (Portable X-ray Orange 9020F, Mano Medical, Taden, France) and an imaging plate measuring 42.1 × 34.4 cm (ClaroX 1417, CVM Diagnstico Veterinario S.L., Tudela, Spain). The animal was carefully transferred from the tank by several aquarists using a specialized stretcher and placed on the imaging plate, which was wrapped in plastic bags to protect it from exposure to water. Following image acquisition, the ray was immediately returned to the tank. A blood sample was collected from the pectoral fin vasculature for hematological analysis, using a 23G needle attached to a 3 mL syringe. After extraction, blood was transferred into 1.3 mL lithium heparin anticoagulant tubes (Sarstedt® Micro Sample Tube Li-Heparin LH, Nümbrecht, Germany). Blood smears were made using the slide-to-slide technique and stained using a Diff-Quick stain (T.R.H., Maim S.L., Barcelona, Spain).

The initial treatment plan consisted in vitamin C 12.5 mg/kg, ceftazidime 25 mg/kg and dexamethasone 1 mg/kg by intramuscular injection. Despite these efforts, the animal died four days later and was transferred to the Institute of Animal Health and Food Safety (IUSA) of the ULPGC for further analysis.

A Computed Tomography (CT) study was conducted postmortem before starting the necropsy at the University Hospital of the Veterinary College. Sequential slices were acquired using a 16-slice helical CT scanner (Toshiba Astelion, Canon Medical System®, Tokyo, Japan). The animal was symmetrically positioned in dorsal recumbency on the stretcher, with craniocaudal entry, and a standard clinical protocol was used (120 kVp, 50 mA, 512 × 512 acquisition matrix, 1,809 × 834 field of view, pitch of 0.94, and a gantry rotation of 1.5 s), to acquire images of a 1 mm thickness. CT images were acquired in transverse planes from cranial to caudal during dorsal recumbency. Using these transverse images, reconstructions were made in the dorsal and sagittal planes, with the images being displayed using both bone and soft tissue windows. All these images were uploaded to an image viewer (OsiriX MD v. 13.0.2, Apple, Cupertino, CA, USA) in DICOM format to perform data manipulation.

The necropsy was performed at the facilities of the Institute of Animal Health and Food Safety (IUSA) of the ULPGC, through a systematic approach and observation of external and internal organs (36). Samples from the wound and main organs were fixed in 10% neutral buffered formalin for histopathological examination. In addition, to make a comparison between normal and affected cartilage, a sample from the non-affected scapulocoracoid cartilage was taken. Cartilage tissues were placed in a histological decalcifier (Decalcifier DC2, Qpath®, Fontenay-sous-bois, France) for 7 days. Formalin-fixed tissues samples were placed into cassettes and routinely processed. This included dehydration through ascending grades of alcohols, clearing in xylene and finally paraffin wax imbibition. Paraffin blocks were sectioned at 4 μm and stained with hematoxylin and eosin (H&E), periodic acid–Schiff (PAS) and Masson's trichrome (MT).

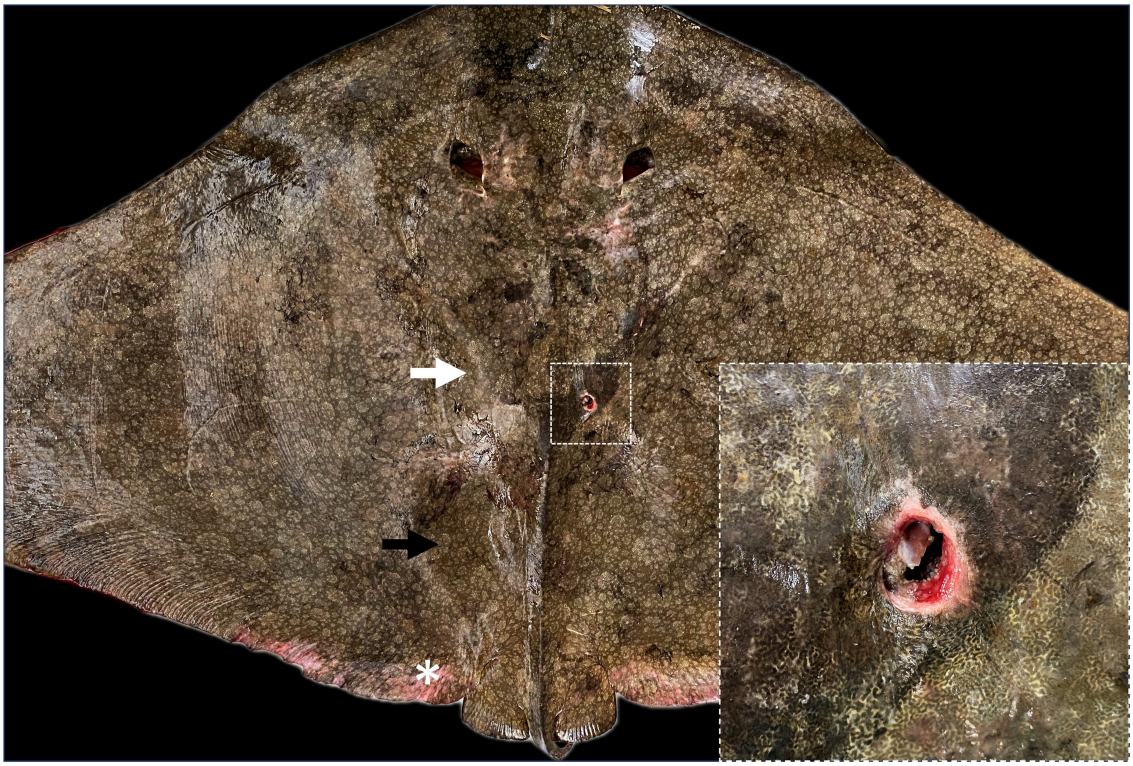

FIGURE 1
Dorsal view of the animal with the penetrating wound. The pectoral arch of the skeleton (white arrow) and the severe concavity on the dorsal coelomic surface (black arrow) are both observed as a result of the animal's cachectic state. Inset: detail of the incised-contused wound of 2 cm diameter and a depth of ~5 cm. It can be appreciated erythema, congestion, and edema at the edges of the lesion. In addition, desquamation and depigmentation could be observed in the caudal region of the dorsal surface of the pectoral fins (*).

The slides were mounted and examined with a light microscope (Olympus BX51, Tokyo, Japan) equipped with a camera software for DP21 (Olympus DP21, Tokyo, Japan).

3 Results

3.1 Clinical examination and hematology

The ray was kept in a quarantine tank since the arrival at the Poema del Mar Aquarium. External examination revealed a low body condition score with marked muscle wastage and severe concavity on the coelomic surfaces (Figure 1). Despite the administered treatment, the animal presented decreased responsiveness and refrained from eating during the days it was kept under human care. A differential leukocyte count was performed on the blood sample obtained, in which lymphocytes were the most abundant leukocyte with 63%, followed by 20% eosinophils or coarse eosinophilic granulocytes, 9% heterophils or fine eosinophilic granulocytes, 7% monocytes and 1% basophils. The packed cell volume (PCV) was measured and the obtained results of 15% revealed a significant decrease of 13.4% compared to an average value of 28.4% PCV gathered from previous clinical experiences for this specie (n = 41), working with wildlife populations in the Canary Islands (CanBio Project).

3.2 Radiographic and computed tomography examination

One single radiography in dorsoventral projection was shot with a 0.9 × 70 mm hypodermic needle with its cap (Sterican® deep intramuscular with long bevel, B. Braun, Melsungen, Germany), introduced inside the incision to determine the depth of the wound (Figure 2). Regarding the radiographic findings, the digital radiograph revealed no affection to any vital organs, but there was severe destruction of cartilage at the level of the scapulocoracoid-synarcual joint.

CT findings unveiled a destructive lesion with irregular margins on the right side, affecting the articular surfaces that establish the pectoral arch of the synarcual cartilage with the scapulocoracoid cartilage, specifically the distal and proximal articular surfaces, as well as cranially the glenoid surface (Figures 3A–C).

3.3 Necropsy

3.3.1 Gross pathology

In the external examination, at the level of the circular wound was observed hyperemic and edematous injured tissue and severe damage of the cartilage at the joint

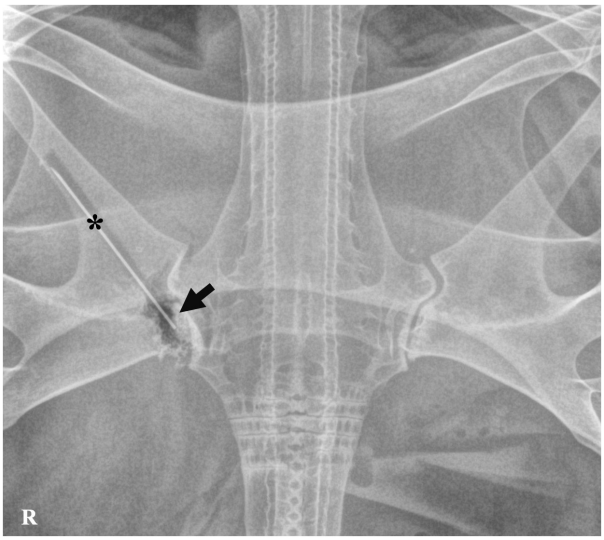

FIGURE 2
Dorsoventral radiography of the spiny butterfly ray (*Gymnura altavela*). Hypodermic needle with a cap (*) inserted into the incised-contused wound. Irregular margins with adjacent gas opacity are observed on the scapulocoracoid-synarcual joint (arrow).

below (inset Figure 1). The lesion reached a depth of ~5 cm, affecting the scapular process of the scapulocoracoid cartilage and the articular surface of the synarcual. Once opened, this area, showed numerous square and rectangular geometric structures of hard consistency and whitish color (Figure 4). The adjacent muscular tissue showed reddened and edematous zones.

In the internal examination, the liver displayed a marked reduction in size (727.5 g) with dark gray coloration, rounded edges of hepatic lobes, readily visible capsule, and a severe distension of the gallbladder (Figure 5A). Also, an empty digestive tract and moderate hemorrhage in the colon was observed (Figure 5A, inset). Body and liver weight, hepatosomatic index and gross appearance of the liver were compared with necropsy reports of other spiny butterfly rays studied by our research group. The hepatosomatic index of this animal was 2.51 representing a 32.89% decrease compared to the average of measured animals (3.74) (Supplementary material). Microscopically, the liver showed low storage of lipid drops in the hepatocytes when it is compared with those observed from livers of non-cachectic spiny butterfly rays (Supplementary Figure 1). Large accumulations of pigments diffusely distributed were also observed in the liver parenchyma, as well as the presence of aggregates of concentric smooth muscle fibers in the liver capsule (Figure 5B).

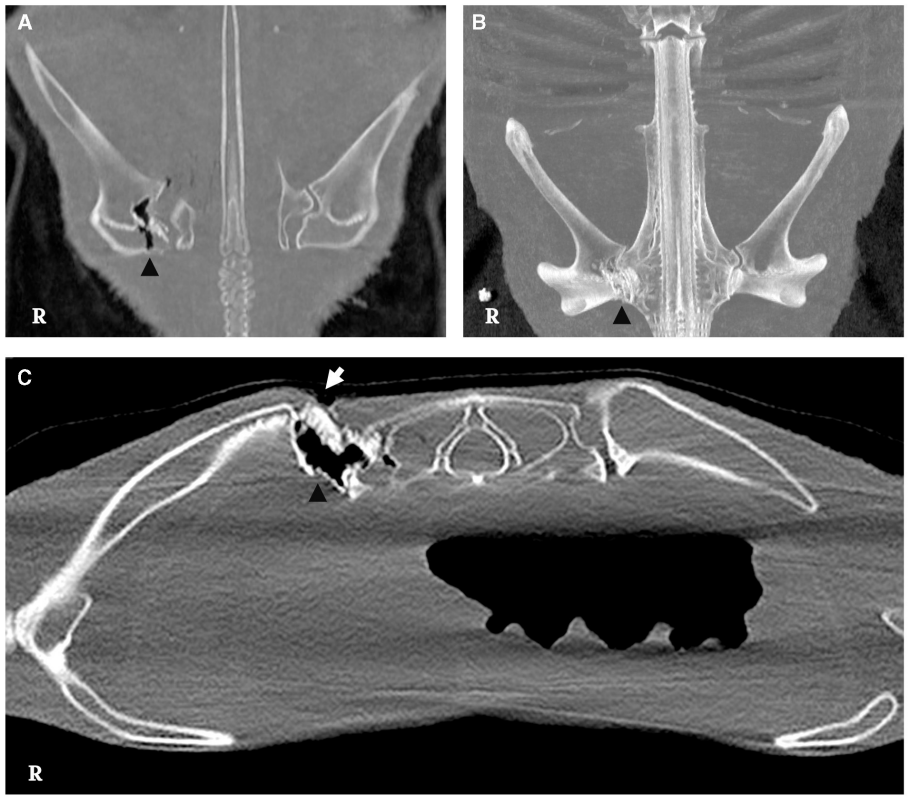

FIGURE 3
CT scan of the lesion. **(A, B)** Irregular borders are observed in the medial aspect of the scapulocoracoid cartilage with presence of slight gas attenuation (arrowhead) [bone window, dorsal multiplanar reconstruction (MPR) and dorsal maximum intensity projection 3D (MIP), respectively]. **(C)** Bone window, cross-sectional image, displaying discontinuity of the skin on the dorsal aspect of the scapulocoracoid-synarcual joint (white arrow), featuring irregular margins and gas attenuation presence (arrowhead).

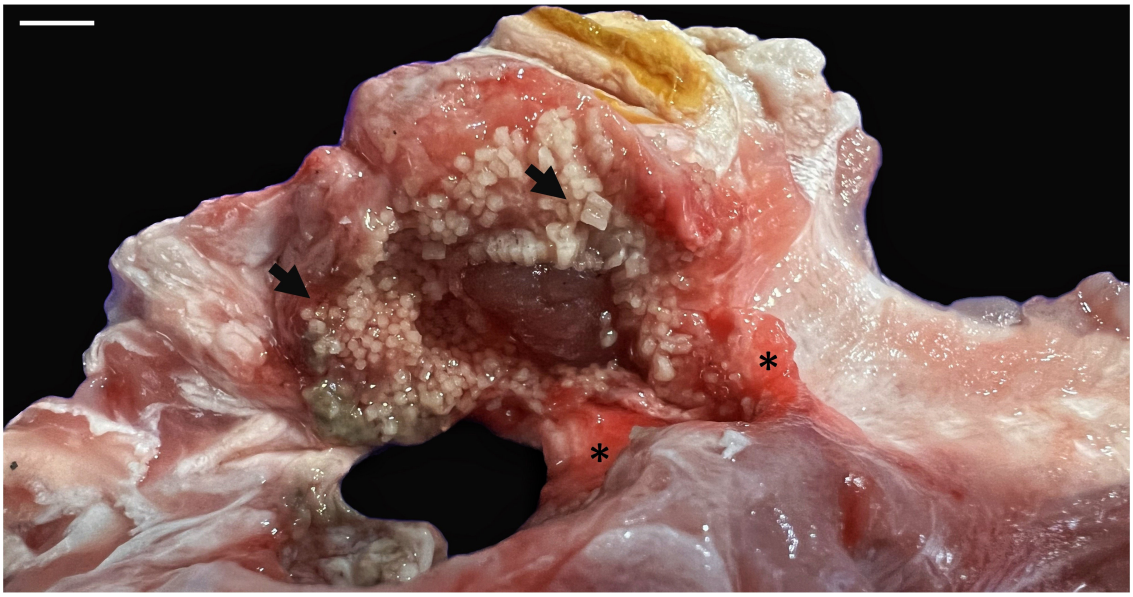

FIGURE 4
Macroscopic aspect of the lesion in the scapular process of the scapulocoracoid cartilage. Numerous square to rectangular geometric structures of hard consistency and whitish color were observed (arrows). The adjacent muscular tissue showed reddened and edematous areas (*). Scale bar = 1 cm.

3.3.2 Histopathology

Within this section we report the comparison of the histological features of the normal cartilage with those of affected tissue. The Figure 6A show the normal structure of the spiny butterfly ray scapulocoracoid cartilage. An outer calcified ring of polygonal tiles (tesserae layer) is observed between the unmineralized cartilaginous core and the fibrous perichondrium. In Figure 6B a magnification of the tesserae layer is shown with the detail of thick Sharpey's fibers penetrating from the perichondrium into the cap zone of each tesserae pieces.

In the normal structure using Masson's Trichrome (MT) staining, the perichondrium layer (connective tissue), is usually marked in blue while the muscle layer can be observed stained in red (Figure 6C). On the peripheral edges of normal tesserae pieces, clear differentiated areas are stained also in red in contrast with an intense blue of the fibrous intertesserae zones (ITZ). According to what have been previously published by other authors, these changes could be related with different collagen compositions (35, 37) (Figure 6D).

The cartilage affected by the traumatic lesion showed the disorganization of the pieces of tesserae, separated from the unmineralized core, and displaced from the adjacent perichondrium (Figure 6E). In the injured area of cartilage, fragmentation and fraying of the Sharpey's fibers were observed in each piece of tesserae leading to the rupture and damage of the perichondrium (Figure 6F). The injured area showed the lack of the normal layers of the different tissues surrounding the joint (Figures 6G, H). The articular muscles are not evident anymore and they have been replaced, in the damaged area, by an abundant fibrous tissue with an intense inflammatory cell population, mostly composed by granulocytes and mononuclear cells (insets in Figures 6G, H).

4 Discussion

Anthropogenic causes of death in elasmobranchs are frequently observed. Overfishing is one of the biggest threats to these species, that together with climate change and habitat degradation have caused a worldwide decline in sharks and rays populations (2, 38, 39). Bycatch is the main cause, particularly in pelagic longline fisheries (40), but also illegal trading or even ship collisions are responsible of large numbers of deaths every year (41, 42). These interactions between human activities and elasmobranchs can lead to a wide range of injuries. The main pathologies resulting from these fishing interactions are hypoxia and trauma, including blunt-force trauma, penetrating trauma from different fishing instruments and the wounds arising from hooks to the oral cavity, digestive tract, and gills (43).

This study describes the clinical presentation, diagnostic imaging evaluation and anatomopathological features of a traumatic lesion in the scapulocoracoid and synarcual cartilages in a spiny butterfly ray. The topography of the incised-contused wound, located dorsally at the level of the right scapulocoracoid cartilage, coupled with the macroscopic characteristics of the lesion and the findings from the CT scan, suggested an anthropogenic origin with some fishing instrument (pike pole, harpoon, or similar). This penetrating wound impacted the juncture of the scapulocoracoid and synarcual cartilages, resulting in significant movement impairment. Other pathological findings included a decreased liver size, hemorrhagic enteritis, and an empty digestive tract. These observations suggest a chronic process of debilitation and a potential compromise of predatory behaviors that could ultimately lead to the death of the animal.

Due to the animal's penetrating wound, pharmacological treatment was immediately initiated to aid recovery upon arrival

FIGURE 5
(A) Liver and gastrointestinal system from spiny butterfly ray. Inset: Detail of the colon, once opened, with moderate hemorrhage (*). **(B)** Microscopic view of the liver parenchyma showing concentric smooth muscle fibers in the liver capsule (arrow). Inset: magnification of the liver showing a low amount of intracellular lipid drops in the hepatocytes and abundant accumulation of pigments. Scale bar = 5 cm.

at the Poema del Mar Aquarium facilities. There is little data on pharmacokinetics and pharmacodynamics for most drugs used in elasmobranch medicine, particularly in some species, so clinicians use treatments that are often extrapolated from taxonomically close species or are based on previous clinical experience (44). Since septicemias are common in batoids with non-healing wounds (45), ceftazidime was chosen as antibiotic coverage. Dexamethasone was administered to control inflammation associated with the wound. Vitamin C was administered due to its role as a cofactor involved in collagen and cartilage synthesis, which is commonly employed as nutritional supplementation in elasmobranchs kept under human care (46). In terms of hematological parameters, although elasmobranchs can have a low hematocrit in comparison to other species (47, 48), our result of 15% was lower compared to unpublished data obtained for the same species.

The marked reduction in liver size suggested that the animal was undergoing a chronic debilitation process, likely resulting due to difficulties in moving and feeding (44, 45, 49). The liver in

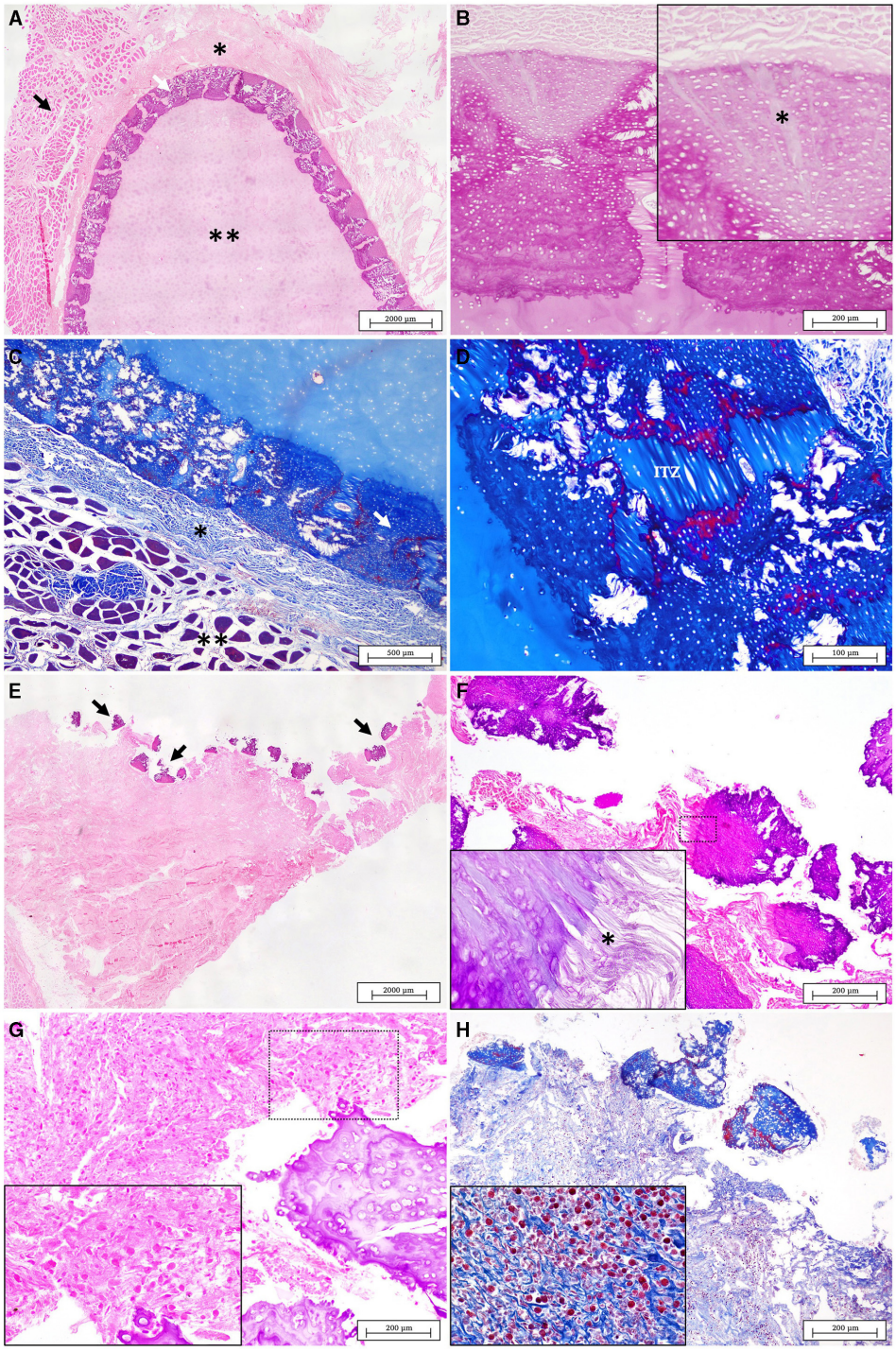

FIGURE 6
(A) Normal structure of healthy cartilage displaying four distinct layers, from the outer to the inner: the muscle layer (black arrow), the perichondrium (*), tesserae layer (white arrow) and the unmineralized cartilage core (**) (H&E). **(B)** Normal tesserae. Sharpey's fibers from the perichondrium are observed penetrating in the cap zone of the tesserae (*) (PAS). **(C)** Normal structure of the healthy cartilage stained with MT. The muscle layer is evident in red (**) while the perichondrium (*) and the mineralized tesserae layer (white arrow) are seen in intense blue (MT). **(D)** A detail of the fibrous intertesserae zone (ITZ) stained in blue with MT. The edges of each tesserae piece are shown marked in red probably due to different types and degrees of maturation of collagen fibers (MT). **(E)** Lesion in the scapulocoracoid cartilage of the affected animal. The injured area is characterized by the disorganization of the tesserae layer (arrows), with the presence of broken tesserae pieces over an abundant fibrous connective tissue (H&E). **(F)** Detailed of fractured pieces of tesserae displaced from the adjacent perichondrium (H&E). (Inset) fraying of the Sharpey's fibers were observed in each piece of tesserae (*) (PAS). **(G)** The fibrous tissue below the broken tesserae layer appears increased and infiltrated by an abundant inflammatory cell population (H&E). **(H)** The MT stain revealed the absence of the muscle layer while it helps to identify granulocytes as the main cells of the inflammatory infiltrate (MT).

elasmobranchs is the primary reservoir of triglycerides and the principal energy source when affected by periods with absence of intake; a decrease in its size may be related to prolonged fasting periods, high energy demand or stressful circumstances (49). In agreement with Neyrão et al. (50) histopathological analysis of the liver revealed characteristics consistent with prolonged fasting, such as diminished lipid content and increased number of melanomacrophages. Similarly, the gallbladder was severely distended, which could also be related to a long period of feeding cessation (51).

The hemorrhages observed in the region of the colon are associated with an inflammatory process of enteritis. This lesion can be frequently observed secondary to other many pathologies in elasmobranchs, such as septicemia or parasitic infections (52–55) and it could also contribute to the overall poor health status observed in this butterfly ray.

The radiographic examination of elasmobranchs is limited due to the lower density of internal structures when compared to other species of animals, yet they offer remarkable detail for the assessment of the cartilaginous skeleton (56). In this work, the utilization of radiography allowed us to inspect the depth of the incision and the affected structures while the animal was alive. Due to the significant dorsoventral flattening of the spiny butterfly ray, alternative radiographic projections with conventional radiographic techniques were impractical for obtaining more detailed information of the lesion. However, this issue was addressed post-mortem by conducting a CT study. The application of this type of advanced diagnostic imaging techniques, provides a more accurate and comprehensive evaluation of lesions in zoological animals (57). The results showed lysis of the right scapulocoracoid cartilage, affecting the articular surfaces that form the pectoral arch connection between the synarcual and scapulocoracoid cartilages. In our best knowledge this is the first CT description of a traumatic lesion of the skeleton in a butterfly ray.

The skeleton of elasmobranchs is composed of cartilaginous tissue consisting of a mineralized layer constituted by minute, polygonal tiles called tesserae that lies in between the cartilage core and the perichondrium (58). In the present study, multiple whitish, disordered geometric structures corresponding to disorganized pieces of tesserae were observed, macroscopically, in the injured cartilage. Likewise, the disruption of the tesserae pieces was evident in the microscopic study. To our knowledge, this is the first complete anatomopathological description of this lesion in the skeleton of a spiny butterfly ray.

There has been controversy in recent decades about cartilage regeneration in elasmobranchs. Ashhurst (33), following a 26-week experiment involving cutting the fin rays cartilages of dogfishes, concluded that, chondrichthyans, were unable to repair their cartilaginous skeleton. Although cartilage-like tissue did develop by 12 weeks, it exhibited poor vascularization and failed to integrate with the injured tissue. However, a more recent study by Seidel et al. (34) in sharks and rays described the aberrant development of mineralized cartilage-like tissue, referred to as endophytic masses (EPMs), exhibiting ultrastructural and chemical characteristics distinct from tesserae. While the formation of EPMs was considered a potential form of attempted cartilage repair, the authors concluded that the most likely cause was a local breakdown of CaP mineralization inhibition processes. Marconi et al. (35) reported, for the first time, the presence of cartilage progenitor cells and chondrogenesis in adults of the little skate (*Leucoraja erinacea*), demonstrating the ability to spontaneously repair injured cartilage. The repair tissue shared characteristics with normal tissue, comprising type II collagen and seamlessly integrating with adjacent tissue to rectify irregularities. Notably, their study involved surgical incisions of <2 cm and the removal of cartilage with a 4 mm biopsy punch, followed by wound suturing and postoperative antibiotherapy. In this study, we observed a chronic injury characterized by the disorganization of the tesserae layer of the cartilage, with an inflammatory reaction and extensive edema and hemorrhage. The severity of the trauma precludes cartilage regeneration, leading to a chronic process that could impair the animal's mobility and complicates feeding. Despite different traumatic injuries have been studied in sharks and rays (16–24), there are scarce detailed descriptions of the pathological features of these lesions on elasmobranchs. To our best knowledge, this study represents the first comprehensive description of the diagnostic imaging findings and the macroscopic and histological characteristics of a traumatic injury of anthropogenic origin in the skeleton of a spiny butterfly ray.

5 Conclusions

This study reports the first comprehensive description of skeleton trauma in a spiny butterfly ray, including the clinical presentation, diagnostic imaging and the anatomopathological features. These three points of view lead to the conclusion that, the incised-contused wound had an anthropogenic origin, probably, by some kind of fishing instrument (pike pole, harpoon, or similar).

Although the animal was found alive and kept in a quarantine tank, under veterinary healthcare and treatments, unfortunately, the establishment of a chronic pathological process with a marked intake reduction, movement reluctancy and the absence or low regenerative processes, on the affected tissues, produced an overall debilitation status that, eventually, might cause the death of the animal.

Together with the clinical signs and administered treatment, our work provides the assessment of hematological parameters on the dying animal, resulting on a notable hematocrit reduction of the 13.4%, when compared with the average of healthy wildlife spiny butterfly ray populations. Furthermore, the clinical evaluation provides, for the first time, a CT study of a critical traumatic lesion, of the right scapulocoracoid cartilage and associated articular surfaces, in this species. The anatomopathological findings also confirmed that the animal was undergoing a chronic debilitation process. The specimen showed a marked reduction of the 32.89% in the hepatosomatic index, when compared to the average value of non-cachectic female spiny butterfly rays. Histological findings demonstrated a remarkable reduction of lipid drops in the cytoplasm of the hepatocytes.

Our work showed, for the first time, the macroscopic and microscopic description of the non-regenerative disorganization of the tesserae layer, and adjacent tissues, of the scapulocoracoid cartilage, due to a traumatic lesion. The main characteristics were the presence of whitish square to rectangular geometric pieces of tesserae, separated among them and torn from the cartilaginous

core. Histologically, some of these pieces kept their connection of the Sharpey's fibers with the perichondrium demonstrating its strong resistance. However, due to the traumatic impact, the surrounding soft tissues showed edema, hemorrhages, and a persistent inflammatory process, composed mainly of granulocytes and fibrous connective tissue. This reaction failed to produce regeneration of the cartilage and the soft tissues around the open wound including the epidermis, dermis, and the periarticular fibrous and muscular tissues.

Finally, there is still an important lack of knowledge on the clinical and diagnostic approaches to elasmobranch species, many of which are affected by anthropogenic impacts and in severe risk of extinction. Our work contributes to reduce this gap and facilitate to the scientific communities new resources to conduct more specific clinical and pathological diagnosis and, therefore, path the way to improve treatments and develop more specific conservation and preservation management plans.

Data availability statement

The raw data supporting the conclusions of this article will be made available by the authors, without undue reservation.

Ethics statement

Ethical approval was not required for the study involving animals in accordance with the local legislation and institutional requirements because the animal was captured with the permission of the competent authority. In addition, non-experimental clinical veterinary practices do not require approval by an Ethics Committee for Animal Experimentation. Further analysis were carried out post-mortem.

Author contributions

GM-H: Conceptualization, Data curation, Investigation, Methodology, Writing – original draft, Writing – review & editing. MC: Conceptualization, Investigation, Methodology, Supervision, Validation, Writing – original draft, Writing – review & editing. ÁC-M: Methodology, Writing – review & editing. CS-S: Investigation, Methodology, Writing – review & editing. MR: Investigation, Methodology, Writing – review & editing. LC-H: Investigation, Methodology, Writing – review & editing. ME: Investigation, Methodology, Writing – review & editing. AF: Investigation, Methodology, Writing – review & editing. AC-A: Conceptualization, Investigation, Methodology, Project administration, Validation, Writing – original draft, Writing – review & editing.

Funding

The author(s) declare financial support was received for the research, authorship, and/or publication of this article. This work was supported by the project "AGN-Project": Strengthening the Angelshark Protection Networks: Increasing the Knowledge and Veterinary Diagnosis of Shark Mortalities in the Canary Islands, funded by Loro Parque Fundación (www.loroparque-fundacion.org) in its 2022 call for projects; Gustavo Montero-Hernández was supported by the "Grant for the financing of predoctoral contracts" program of the University of Las Palmas de Gran Canaria (PIFULPGC-2022-CCSALUD-1).

Acknowledgments

The authors would like to thank Loro Parque Fundación and the Poema del Mar Aquarium for supporting the *in-vivo* clinical and diagnostic work. In addition, we express our gratitude to the team and personnel of The Save Our Seas Foundation, Keystone Grant number 391/2017 and CanBio Project (foundation registration number 269) for their collaboration in accessing to wild spiny butterfly rays.

Conflict of interest

The authors declare that the research was conducted in the absence of any commercial or financial relationships that could be construed as a potential conflict of interest.

Publisher's note

All claims expressed in this article are solely those of the authors and do not necessarily represent those of their affiliated organizations, or those of the publisher, the editors and the reviewers. Any product that may be evaluated in this article, or claim that may be made by its manufacturer, is not guaranteed or endorsed by the publisher.

Supplementary material

The Supplementary Material for this article can be found online at: https://www.frontiersin.org/articles/10.3389/fvets.2024.1452659/full#supplementary-material

References

1. Dulvy NK, Fowler SL, Musick JA, Cavanagh RD, Kyne PM, Harrison LR, et al. Extinction risk and conservation of the world's sharks and rays. *Elife*. (2014) 3:e00590. doi: 10.7554/eLife.00590

2. Pacoureau N, Rigby CL, Kyne PM, Sherley RB, Winker H, Carlson JK, et al. Half a century of global decline in oceanic sharks and rays. *Nature*. (2021) 589:567–71. doi: 10.1038/s41586-020-03173-9

3. Wosnick N, Giareta EP, Leite RD, Hyrycena I, Charvet P. An overview on elasmobranch release as a bycatch mitigation strategy. *ICES J Mar Sci*. (2023) 80:591–604. doi: 10.1093/icesjms/fsac164

4. Sherman CS, Simpfendorfer CA, Pacoureau N, Matsushiba JH, Yan HF, Walls RH, et al. Half a century of rising extinction risk of coral reef sharks and rays. *Nat Commun*. (2023) 14:15. doi: 10.1038/s41467-022-35091-x

5. Martín JL, Cardoso P, Arechavaleta M, Borges PA, Faria BF, Abreu C, et al. Using taxonomically unbiased criteria to prioritize resource allocation for oceanic island species conservation. *Biodivers Conserv*. (2010) 19:1659–82. doi: 10.1007/s10531-010-9795-z

6. Riera R, Becerro MA, Stuart-Smith RD, Delgado JD, Edgar GJ. Out of sight, out of mind: threats to the marine biodiversity of the Canary Islands (NE Atlantic Ocean). *Mar Pollut Bull*. (2014) 86:9–18. doi: 10.1016/j.marpolbul.2014.07.014

7. McIvor AJ, Williams CT, Alves F, Dinis A, Pais MP, Canning-Clode J. The status of marine megafauna research in macaronesia: a systematic review. *Front Mar Sci*. (2022) 9:819581. doi: 10.3389/fmars.2022.819581

8. Meyers EKM, Tuya F, Barker J, Jiménez-Alvarado D, Castro-Hernández JJ, Haroun R, et al. Population structure, distribution and habitat use of the Critically Endangered Angelshark, *Squatina squatina,* in the Canary Islands. *Aquat Conserv*. (2017) 27:1133–44. doi: 10.1002/aqc.2769

9. Jiménez-Alvarado D, Meyers EKM, Caro MB, Sealey MJ, Barker J. Investigation of juvenile angelshark (*Squatina squatina*) habitat in the Canary Islands with recommended measures for protection and management. *Aquat Conserv*. (2020) 30:2019–25. doi: 10.1002/aqc.3337

10. Tuya F, Asensio M, Navarro A. "Urbanite" rays and sharks: presence, habitat use and population structure in an urban semi-enclosed lagoon. *Reg Stud Mar Sci*. (2020) 37:101342. doi: 10.1016/j.rsma.2020.101342

11. Tuya F, Aguilar R, Espino F, Bosch NE, Meyers EKM, Jiménez-Alvarado D, et al. Differences in the occurrence and abundance of batoids across an oceanic archipelago using complementary data sources: implications for conservation. *Ecol Evol*. (2021) 11:16704–15. doi: 10.1002/ece3.8290

12. Espino-Ruano A, Castro JJ, Guerra-Marrero A, Couce-Montero L, Meyers EKM, Santana-del Pino A, et al. Aggregative behaviour of spiny butterfly rays (*Gymnura altavela*, Linnaeus, 1758) in the shallow coastal zones of Gran Canaria in the Eastern Central Atlantic. *Animals*. (2023) 13:1455. doi: 10.3390/ani13091455

13. Mead LR, Alvarado DJ, Meyers E, Barker J, Sealey M, Caro MB, et al. Spatiotemporal distribution and sexual segregation in the critically endangered angelshark *Squatina squatina* in Spain's largest marine reserve. *Endanger Species Res*. (2023) 51:233–48. doi: 10.3354/esr01255

14. Yokota L, White WT, de Carvalho MR. Butterfly rays Family Gymnuridae. In: Last PW, White W, Carvalho MB, Sáet MS, Naylor G, editors. *Rays of the World*. Clayton South: CSIRO Publishing (2016). p. 511–21.

15. Dulvy NK, Charvet P, Carlson J, Badji L, Blanco-Parra MP, Chartrain E et al. *Spiny Butterfly Ray (Gymnura altavela)*. The IUCN Red List of Threatened Species (2021). Available at: https://www.iucnredlist.org/species/63153/3123409 (accessed July 29, 2023).

16. Fierstine HL, Cailliet GM, Neer JA. Shortfin Mako, *Isurus oxyrinchus*, impaled by blue marlin, *Makaira nigricans* (Teleostei: Istiophoridae). *Bull South Calif Acad Sci*. (1997) 96:117.

17. Riley MJ, Harman A, Rees RG. Evidence of continued hunting of whale sharks *Rhincodon typus* in the Maldives. *Environ Biol Fishes*. (2009) 86:371–4. doi: 10.1007/s10641-009-9541-0

18. Penadés-Suay J, Tomás J, Aznar FJ. Deadly impalement of a blue shark *Prionace glauca* by a swordfish *Xiphias gladius*. *Mediterr Mar Sci*. (2017) 18:340–3. doi: 10.12681/mms.1959

19. Penadés-Suay J, García-Salinas P, Tomás J, Aznar FJ. Aggressive interactions between juvenile swordfishes and blue sharks in the Western Mediterranean: a widespread phenomenon? *Mediterr Mar Sci*. (2019) 20:314–9. doi: 10.12681/mms.18102

20. Schoeman RP, Patterson-Abrolat C, Plön S. A global review of vessel collisions with marine animals. *Front Mar Sci*. (2020) 7:292. doi: 10.3389/fmars.2020.00292

21. Jambura PL, Türtscher J, Kriwet J, Al Mabruk SA. Deadly interaction between a swordfish Xiphias gladius and a bigeye thresher shark *Alopias superciliosus*. *Ichthyol Res*. (2021) 68:317–21. doi: 10.1007/s10228-020-00787-x

22. Rangel BS, Viegas R, Bettcher VB, Garla RC. Eye healing in a free-ranging whitespotted eagle ray (*Aetobatus narinari*) following shark-inflicted bite injuries. *J Fish Biol*. (2022) 100:590–3. doi: 10.1111/jfb.14961

23. Strike EM, Harris JL, Ballard KL, Hawkins JP, Crockett J, Stevens GMW. Sublethal injuries and physical abnormalities in Maldives Manta Rays, *Mobula alfredi* and *Mobula birostris*. *Front Mar Sci*. (2022) 9:773897. doi: 10.3389/fmars.2022.773897

24. Womersley FC, Humphries NE, Queiroz N, Vedor M, da Costa I, Furtado M, et al. Global collision-risk hotspots of marine traffic and the world's largest fish, the whale shark. *Proc Nat Acad Sci USA*. (2022) 119:e2117440119. doi: 10.1073/pnas.2117440119

25. Bird PM. Tissue regeneration in three carcharhinid sharks encircled by embedded straps. *Copeia*. (1978) 1978:345–9. doi: 10.2307/1443580

26. Chin A, Mourier J, Rummer JL. Blacktip reef sharks (*Carcharhinus Melanopterus*) show high capacity for wound healing and recovery following injury. *Conserv Physiol*. (2015) 3:cov062. doi: 10.1093/conphys/cov062

27. Borucinska J, Adams DH, Frazier BS. Histologic observations of dermal wound healing in a free-ranging blacktip shark from the Southeastern US Atlantic Coast: a case report. *J Aquat Anim Health*. (2020) 32:141–8. doi: 10.1002/aah.10113

28. Black C. Resilience in the depths: first example of fin regeneration in a silky shark (*Carcharhinus falciformis*) following traumatic injury. *J Mar Sci*. (2023) 2023:1–8. doi: 10.1155/2023/6639805

29. Heim V, Grubbs RD, Smukall MJ, Frazier BS, Carlson JK, Guttridge TL. Observations of fin injury closure in Great Hammerheads and implications for the use of fin-mounted geolocators. *J Aquat Anim Health*. (2023) 35:53–63. doi: 10.1002/aah.10178

30. Towner A, Smale MJ, Jewell O. Boat strike wound healing in *Carcharodon carcharias*. In: Smith M, Warmolts D, Thoney D, Hueter R, Murray M, Ezcurra J, editors. *Global Perspectives on the Biology and Life History of the White Shark*. Boca Raton, FL: CRC Press (2012). p. 77–84.

31. McGregor F, Richardson AJ, Armstrong AJ, Armstrong AO, Dudgeon CL. Rapid wound healing in a reef manta ray masks the extent of vessel strike. *PLoS ONE*. (2019) 14:1–11. doi: 10.1371/journal.pone.0225681

32. Womersley F, Hancock J, Perry CT, Rowat D. Wound-healing capabilities of whale sharks (*Rhincodon typus*) and implications for conservation management. *Conserv Physiol*. (2021) 9:coaa120. doi: 10.1093/conphys/coaa120

33. Ashhurst DE. The cartilaginous skeleton of an elasmobranch fish does not heal. *Matrix Biol*. (2004) 23:15–22. doi: 10.1016/j.matbio.2004.02.001

34. Seidel R, Blumer M, Zaslansky P, Knötel D, Huber DR, Weaver JC, et al. Ultrastructural, material and crystallographic description of endophytic masses—A possible damage response in shark and ray tessellated calcified cartilage. J Struct Biolo (2017) 198:5–18. doi: 10.1016/j.jsb.2017.03.004

35. Marconi A, Hancock-Ronemus A, Gillis JA. Adult chondrogenesis and spontaneous cartilage repair in the skate, Leucoraja erinacea. *eLife*. (2020) 9:e53414. doi: 10.7554/eLife.53414

36. Crow GL, Brock JA. Necropsy methods and procedures for elasmobranchs. In: Smith M, Warmolts D, Thoney D, Hueter R, editors. *The Elasmobranch Husbandry Manual: Captive Care of Sharks, Rays, and Their Relatives*. Columbus, OH: Ohio Biological Survey (2004). p. 467–72.

37. Seidel R, Lyons K, Blumer M, Zaslansky P, Fratzl P, Weaver JC, et al. Ultrastructural and developmental features of the tessellated endoskeleton of elasmobranchs (sharks and rays). *J Anat*. (2016) 229:681–702. doi: 10.1111/joa.12508

38. Dulvy NK, Pacoureau N, Rigby CL, Pollom RA, Jabado RW, Ebert DA, et al. Overfishing drives over one-third of all sharks and rays toward a global extinction crisis. *Curr Biol*. (2021) 31:4773–87.e8. doi: 10.1016/j.cub.2021.08.062

39. Pacoureau N, Carlson JK, Kindsvater HK, Rigby CL, Winker H, Simpfendorfer CA, et al. Conservation successes and challenges for wide-ranging sharks and rays. *Proc Nat Acad Sci USA*. (2023) 120:e2216891120. doi: 10.1073/pnas.2216891120

40. Oliver S, Braccini M, Newman SJ, Harvey ES. Global patterns in the bycatch of sharks and rays. *Mar Policy*. (2015) 54:86–97. doi: 10.1016/j.marpol.2014.12.017

41. Speed CW, Meekan MG, Rowat D, Pierce SJ, Marshall AD, Bradshaw CJA. Scarring patterns and relative mortality rates of Indian Ocean whale sharks. *J Fish Biol*. (2008) 72:1488–503. doi: 10.1111/j.1095-8649.2008.01810.x

42. Prasetyo AP, McDevitt AD, Murray JM, Barry J, Agung F, Muttaqin E, et al. Shark and ray trade in and out of Indonesia: addressing knowledge gaps on the path to sustainability. *Mar Policy*. (2021) 133:104714. doi: 10.1016/j.marpol.2021.104714

43. Newton AL, Ritchie KB. Elasmobranch health, pathology, and the host microbiome. In: Carrier JC, Simpfendorfer CA, Heithaus MR, Yopak KE, editors. *Biology of Sharks and Their Relatives*. Boca Raton, FL: CRC Press (2022). p. 421–85.

44. Mylniczenko ND, Clauss T. Pharmacology of elasmobranchs: updates and techniques. In: Smith M, Warmolts D, Thoney D, Hueter R, Murray M, Ezcurra J, editors. *The Elasmobranch Husbandry Manual II: Recent Advances in the Care of Sharks, Rays, and Their Relatives*. Columbus, OH: Ohio Biological Survey (2017). p. 289–302.

45. Mylniczenko ND. Medical management of rays. In: Miller RE, Fowler ME, editors. *Zoo and Wild Animal Medicine Current Therapy, Vol 7*. St. Louis, MO: Elsevier Saunders (2012). p. 170–6.

46. Hoopes LA. Elasmobranch mineral and vitamin requirements. In: Smith DW, Thoney D, Hueter R, Murray M, Ezcurra J, editors. *The Elasmobranch Husbandry Manual II: Recent Advances in the Care of Sharks, Rays, And Their Relatives*. Columbus, OH: Ohio Biological Survey (2017). p. 135–46.

47. Filho DW, Eble GJ, Kassner G, Caprario FX. Dafré AL, Ohira M. Comparative hematology in marine fish. *Comp Biochem Physiol Part A*. (1992) 102:311–21. doi: 10.1016/0300-9629(92)90141-C

48. Clauss TM, Dove ADM, Arnold JE. Hematologic disorders of fish. *Vet Clin N Am*. (2008) 11:445–62. doi: 10.1016/j.cvex.2008.03.007

49. Grant KR, Campbell TW, Silver TI, Olea-Popelka FJ. Validation of an ultrasound-guided technique to establish a liver-to-coelom ratio and a comparative analysis of the ratios among acclimated and recently wild-caught southern Stingrays, *Dasyatis Americana*. *Zoo Biol*. (2013) 32:104–11. doi: 10.1002/zoo.21014

50. Neyrão IM, Conrado ALV, Takatsuka V, Bruno CEM, de Azevedo VG. Quantification of liver lipid deposition and melano-macrophages in lesser guitarfish *Zapteryx brevirostris* submitted to different feeding cycles. *Comp Clin Pathol*. (2019) 28:805–10. doi: 10.1007/s00580-019-02953-8

51. Wosnick N, Chaves AP, Niella YV, Takatsuka V, Hazin FHV, Nunes JLS, et al. Physiological impairment as a result of bile accumulation in an apex predator, the tiger shark (*Galeocerdo cuvier* Péron & Lesueur, 1822). *Animals*. (2020) 10:30. doi: 10.3390/ani10112030

52. Borucinska J, Caira JN. A comparison of mode of attachment and histopathogenicity of four tapeworm species representing two orders infecting the spiral intestine of the nurse shark. *J Parasitol*. (1993) 79:238. doi: 10.2307/3283514

53. Briones V, Fernández A, Blanco M, Ramiro F, De Vicente ML, García J, et al. Haemorrhagic septicaemia by *Aeromonas salmonicida* subsp salmonicida in a Black-tip Reef Shark (*Carcharhinus melanopterus*). *J Vet Med Ser B*. (1998) 45:443–5. doi: 10.1111/j.1439-0450.1998.tb00814.x

54. Garner MM. A retrospective study of disease in elasmobranchs. *Vet Pathol*. (2013) 50:377–89. doi: 10.1177/0300985813482147

55. Stidworthy MF, Thornton SM, James R. A review of pathologic findings in elasmobranchs: a retrospective case series. In: Smith M, Warmolts D, Thoney D, Hueter R, Murray M, Ezcurra J, editors. *The Elasmobranch Husbandry Manual II: Recent Advances in the Care of Sharks, Rays, and Their Relatives*. Columbus, OH: Ohio Biological Survey (2017). p. 277–87.

56. Mylniczenko ND, Culpepper EE, Clauss T. Diagnostic imaging of elasmobranchs: updates and case examples. In: Smith M, Warmolts D, Thoney D, Hueter R, Murray M, Ezcurra J, editors. *The Elasmobranch Husbandry Manual II: Recent Advances in the Care of Sharks, Rays, and Their Relatives*. Columbus, OH: Ohio Biological Survey (2017). p. 303–24.

57. Mackey EB, Hernandez-Divers SJ, Holland M, Frank P. Clinical technique: application of computed tomography in zoological medicine. J Exot Pet Med. (2008) 17:198–209. doi: 10.1053/j.jepm.2008.05.007

58. Seidel R, Blumer M, Pechriggl EJ, Lyons K, Hall BK, Fratzl P, et al. Calcified cartilage or bone? Collagens in the tessellated endoskeletons of cartilaginous fish (sharks and rays). *J Struct Biol*. (2017) 200:54–71. doi: 10.1016/j.jsb.2017.09.005

frontiers | Frontiers in Veterinary Science

TYPE Original Research
PUBLISHED 26 February 2025
DOI 10.3389/fvets.2025.1504527

Check for updates

OPEN ACCESS

EDITED BY
Francesco Tiralongo,
University of Catania, Italy

REVIEWED BY
Michael James Murray,
Monterey Bay Aquarium, United States
Sean Michael Perry,
Mississippi Aquarium, United States

*CORRESPONDENCE
Natalie D. Mylniczenko
✉ natalie.mylniczenko@disney.com

†These authors have contributed equally to this work and share first authorship

RECEIVED 30 September 2024
ACCEPTED 08 January 2025
PUBLISHED 26 February 2025

CITATION
Wheaton CJ, Sullivan KE, Bassiouny E, Burns CM, Smukall MJ, Hendon JM and Mylniczenko ND (2025) Investigation of serum thyroid hormones, iodine and cobalt concentrations across common aquarium-housed elasmobranchs. *Front. Vet. Sci.* 12:1504527. doi: 10.3389/fvets.2025.1504527

COPYRIGHT
© 2025 Wheaton, Sullivan, Bassiouny, Burns, Smukall, Hendon and Mylniczenko. This is an open-access article distributed under the terms of the Creative Commons Attribution License (CC BY). The use, distribution or reproduction in other forums is permitted, provided the original author(s) and the copyright owner(s) are credited and that the original publication in this journal is cited, in accordance with accepted academic practice. No use, distribution or reproduction is permitted which does not comply with these terms.

Investigation of serum thyroid hormones, iodine and cobalt concentrations across common aquarium-housed elasmobranchs

Catharine J. Wheaton[1†], Kathleen E. Sullivan[1], Enass Bassiouny[2], Charlene M. Burns[1], Matthew J. Smukall[3], Jill M. Hendon[4] and Natalie D. Mylniczenko[1*†]

[1]Disney's Animals, Science and Environment, Animal Programs, Lake Buena Vista, FL, United States, [2]Michigan State University Veterinary Diagnostic Laboratory, College of Veterinary Medicine, East Lansing, MI, United States, [3]Bimini Biological Field Station, South Bimini, Bahamas, [4]The University of Southern Mississippi, Center for Fisheries Research and Development, Ocean Springs, MS, United States

Introduction: Thyroid disease is an important condition to understand in elasmobranchs, with goiters being predominant. To identify dysfunction, measuring serum thyroid hormone levels is a standard of practice for diagnosing disease in most species. Although these levels have been reported in elasmobranch literature, the testing methodology is varied and values are not clinically useful for most aquarium species. In a group of aquarium-housed elasmobranchs, thyroid hormone levels had been persistently low or not detectable in otherwise healthy animals as well as animals with thyroid disease. The concern for reliability of these results to diagnose thyroid disease, prompted a shift to serum iodine levels as a proxy to determine thyroid health.

Methods: This study assesses thyroid hormone and iodine levels as compared to thyroid disease stage in elasmobranchs with and without dietary supplementation, to determine the efficacy of using these serum values to guide clinical decisions.

Results: Serum thyroid hormone results were lower than the readable range of the standard curve in both sharks and rays; thus reported values are usually extrapolated. Including additional standards down to the limit of sensitivity improved detection, however increasing the sample volume tested was determined to be the most important factor for obtaining measurable results in low-value thyroid hormone samples. Serum iodine levels are reported in three groups of southern stingrays (*Hypanus americanus*). Other elasmobranch species maintained in aquaria with and without thyroid disease were used for biological comparisons. Non-goiter, diseased animals reliably had elevated levels (over baseline) of thyroid hormones and iodine; in goiter cases, hormones were not useful. Additionally, it was found that cobalt levels were also elevated in some disease states and correlated positively with serum iodine levels.

Conclusion: Current available thyroid testing may not provide clinically useful values unless methodology is adjusted, or disease is severe. Serum iodine may be a useful marker to investigate thyroid health. Further, while thyroid disease may be identifiable with thyroid hormones, it is not straightforward or substantial enough alone for diagnosis.

KEYWORDS

Total T3, Total T4, free T4, triiodothyronine (T3), tetraiodothyronine (thyroxine; T4), reproductive disease, ultrasound, thyroid disease

1 Introduction

The thyroid gland plays a critical role for fish maturation, reproduction and osmoregulation (1–5). Due to reproductive diseases in elasmobranchs in aquaria (6), investigation into thyroid activity is important as it has been shown that thyroid and reproductive activity parallel each other (1, 4, 5, 7). However, results from the cohorts reported here (from send-out laboratory tests) routinely showed low or undetectable thyroid levels, where 'normal' values were expected (compared with other species ranges, particularly mammals) so it was of interest to determine if normal values were truly low in concentration.

Thyroid disease in elasmobranchs is most commonly associated with goiters (hyperplastic, diffuse colloid or multinodular goiter) but thyroiditis and thyroid carcinoma have also been reported (8, 9). Overall thyroid disease is poorly represented in the elasmobranch pathology literature and this is likely, in part, because the thyroid is frequently not included in the submitted set of tissues (10). Subclinical conditions in the thyroid seem plausible. Additionally, ultrasonographic examination by the authors during diagnostic examinations often showed abnormal thyroids (with multifocal cysts or mineralizations) that did not classify as classic hyperplastic or colloidal goiters (unpublished data).

In the absence of a reliable or validated testing method for thyroids, the use of serum iodine was investigated for elasmobranchs under human care (The Seas with Nemo and Friends®, Lake Buena Vista, Florida, United States) as it has been shown to be correlated with thyroid health in other animals (11–13). Iodine's sole role in the vertebrate is in thyroid hormone synthesis (14, 15) and iodine levels are correlated with thyroid levels and ultimately thyroid disease (16–18), therefore it was expected that iodine values could translate into a meaningful test for elasmobranch thyroid health. Using iodine assays is useful because it does not require species-specific validation that is required with antibody focused assays, does not require sample treatment (like extraction) and there is no interference with sample components (19–21). Initial values in southern stingrays (*Hypanus americanus*) showed some surprisingly high iodine values as compared to mammalian ranges (19–21) and to ranges from other elasmobranchs in the facility and in the wild (22, 23). These rays were in moderate stages of reproductive disease (22, 23). This suggested further investigation and once again revitalized the need to understand thyroid hormones in elasmobranchs, particularly in regard to iodine and how it related to abnormal thyroids as evaluated by high serum iodine and identification of abnormal thyroid glands on ultrasound or postmortem examination.

This paper investigates serum iodine values in two populations of 'thyroid-normal' southern stingrays in natural sea water and compares it to validated thyroid hormone levels in an aquarium-housed population. Additionally, several elasmobranchs with goiters and other thyroid pathology were evaluated and compared to normal animals as a biological validation. Parallel to iodine testing, cobalt (through trace nutrient analysis) was additionally identified with levels above expectation, therefore, was included in this analysis.

2 Materials and methods

This is a retrospective study using banked samples and available ultrasound images through routine examinations or health assessments.

2.1 Animals

2.1.1 Study 1

Southern stingrays (SR) from three habitats (see Supplementary Table S1 for additional details): aquarium-housed ($N = 38$, closed system), lagoon-housed ($N = 22$, managed, semi-wild), and wild ($N = 11$). For all stingrays, disk width was obtained ventrally by measuring the span between the tips of the widest portion of the pectoral fins. Housing, restraint, and sample collection is described elsewhere (6). For lagoon-housed animals, samples were collected prior to 2019 under a permit to conduct scientific research (No. MAF/LIA/22) from the Department of Fisheries of the Commonwealth of the Bahamas. Wild animals included 11 wild adult females from Bimini, Bahamas, collected under protocols from the Bimini Biological Field Station Foundation, and were released after sampling. Sampling was limited to the spring in both cohorts therefore seasonality could not be assessed.

2.1.2 Study 2

Eight aquarium-managed elasmobranch species were included in this cohort [brownbanded bamboo shark (BBBS); cownose ray (CNR); honeycomb ray (HCR); porcupine ray (PR); round ribbontail ray (RRR); spotted eagle ray (SER); southern stingray (SR); and whitespotted bamboo shark (WSBS); see Supplementary Table S1 for size, sex, scientific name, sample collection years and species N]. Banked samples were originally collected during routine examinations under anesthesia (with varied doses and protocols) and included ultrasound evaluations of the thyroid when possible.

Animals were considered to be in normal health based on physical exam and in-house blood work ranges for complete blood count and serum chemistry. The only variation was an obvious thyroid abnormality as evaluated by ultrasound and subsequently categorized. Post-mortem sample: thyroid tissue and blood was opportunistically collected post-mortem from an SR ($N = 1$) caught in a longline survey through The University of Southern Mississippi, Ocean Springs, MS. Thyroid tissue (extracted for HPLC fractioning) and matching cardiac blood was used for initial thyroid assay (TT3, TT4, FT4) biological validations.

2.2 Nutrition

Aquarium-housed elasmobranchs were fed a variety of fish and shellfish (capelin, clam, shrimp, herring, and smelt) based on body weight. Animals were offered an elasmobranch micronutrient supplement (hereafter termed 'supplement') specifically made for Disney's Animal Kingdom (Table 1) at the recommended dose [1 tablet (1.5 g) per ½ lb. of fish; Mazuri Vita-Zu Shark/Ray tabs 5M1Y, Mazuri Exotic Animal Nutrition, St. Louis, MO]. This supplement was altered from the commercial product (5MD8-2011 analysis shown) during the course of this data collection at Disney's request unrelated to this study at the time (Table 1). Supplements were hidden inside target-fed fish, but consumption was variable across species and individuals, and not always able to be clearly tracked. SRs in the aquarium setting had vitamins withheld from 8/1/2015 to 9/28/2016 as a response to elevated levels of iodine.

TABLE 1 Analysis of percent dry matter, cobalt (ppm), and iodine (ppm) levels in a commercially available shark/ray micronutrient supplement tablet (assigned a letter supplement code based on batch analyzed) and aquatic gel, as well as average levels for commonly fed diet items in the aquarium setting, Atlantic capelin, Norwegian herring, cherrystone clams, lake smelt, white shrimp, and squid without heads or pens.

Supplement type	Date of analysis	Dry matter (%)	Cobalt (ppm DM)	Iodine (ppm DM)	Supplement code N (%)[a]
Shark/ray micronutrient supplement tablet (5M1Y; 5MD8)[b]	5/5/2011[b]	86.8	151.4	191,819.9	"A" 10 (5.6)
	10/3/2012	92.6	4.2	202,603.4	"B" 8 (4.5)
	3/9/2015	93.1	3.8	133,658.3	"C" 32 (17.9)
	8/10/2022	83.7	1.4	104,714.6	"D" 66 (36.9)
	1/31/2023	98.6	0.3	51,043.8	"E" 4 (2.2)
	various	N/A	N/A	N/A	"N" 34 (19.0)
Aquatic gel 57W9[b]	4/17/2016	91.4	3.5	2.12[c]	"G" 25 (14.0)
Atlantic capelin[d]	various	18.5	0.004	1.2	N/A
Norwegian herring[d]	various	30.4	0.01	0.1	N/A
Cherrystone clam[d]	various	78.7	2.7	0.9	N/A
Lake smelt[d]	various	19.2	0.03	0.1	N/A
White shrimp[d]	various	21.3	0.4	2.3	N/A
Squid without heads or pen[d]	various	81.8	0.1	0.1	N/A

[a]Number and (%) of total study samples for that micronutrient supplement product. Products are labeled as A, B, C, D, E, N, or G to identify the batch used based on date.
[b]2011 sample is 5MD8 and all others are 5M1Y tablets, except aquatic gel 57 W9; all products: Mazuri Exotic Animal Nutrition, St. Louis, MO analyzed at Dairy One Laboratories, Ithaca, NY.
[c]Estimate from manufacturer, product specifications accurate to 2016.
[d]All analyses performed at Dairy One Laboratory within last 10 years of 2024; for average values; capelin, $N = 26$; clam, $N = 3$; shrimp, $N = 4$; herring, $N = 40$; lake smelt, $N = 11$; squid, $N = 3$.

Lagoon animals were housed in a netted lagoon pen in natural sea water (Castaway Cay, Bahamas). They were fed a daily diet consisting of shrimp with shells but no tails (20% total diet), squid without heads or pens (30% total diet), and an aquatic gel product fed as 50% of the total diet offered (Aquatic gel 57 W9, Mazuri Exotic Animal Nutrition, St Louis, MO).

Wild SR diets were unknown, but diet and stable isotope analysis has been described (24).

2.3 Thyroid hormone analysis: biological and chemical validations

2.3.1 Reagents

All reagents used were LC/MS or HPLC analytical grade quality. Purified hormones used for HPLC reference standards or for testing as potential cross reactants (Sigma Aldrich, St. Louis, MO, or Fisher Scientific, Hampton, NH) include: EtOH (Ethanol 200 proof, #459828), MeOH (Methanol, #A452-1), acetonitrile with 0.1% TFA [v/v, Trifluoroacetic Acid (v/v), Optima™ #6000063], T2 (3,3′-Diiodo-L-thyronine, #719536), T3 (3,3′,5-Triiodo-L-thyronine, #T2877), T4 (L-Thyroxine, #T2376), Iodide (certified reference material #41271, 1,000 mg/L); and the following certified reference materials for thyroid standards [Cerilliant® 100 µg/mLin Methanol: T-073 T4, T-074 T3, and T-075 reverse T3 (rT3)].

2.3.2 Thyroid tissue extraction

Historically, thyroid hormone testing in SR serum samples had produced mostly low or near zero values. As a biological validation, thyroid tissue was retrieved from a wild-caught (bycatch) SR (Hendon) and stored frozen at -80C. Thyroid tissue was thawed, homogenized and 0.25 g was extracted with ice cold MeOH, centrifuged and the supernatant was passed through a syringe filter before HPLC fractionation (25–27).

2.3.3 High performance liquid chromatography

Reverse-phase HPLC was used to separate thyroid hormones of interest, fractioning samples for subsequent RIA evaluation of immunoreactivity within each fraction. HPLC methods followed Sweeting and Eales (28), also see (29, 30), and utilized a Dionex Ultimate 3,000 set up (31) with the following changes for thyroid analyses. Solution A contained water with 0.1% TFA, and solution B contained acetonitrile with 0.1% TFA (v/v, #6000063). Following column equilibration in Solution A, 100 µL of the sample was injected into the column with a flow rate of 0.75 mL min-1. Hormones were collected at a linear gradient of 34 to 45% of solution B over 30 min followed by a pulse of 5 min ACN to clear residual lower polarity steroids. Elution peaks were determined following injection of concentrated Iodide, T2, and analytical reference standards (rT3, T3, T4, 100 µg/mL), monitored at 190, 220, 240 and 254 nm. Singly injected standards often eluted with earlier retention times (RT) than the pooled panel of standards, so the range or medians of RT are reported where appropriate. Fractions (fr) were collected every 60 s from 1 to 29 min into tubes, evaporated, and reconstituted in 1 mL of heat-inactivated, charcoal stripped FBS (fetal bovine serum albumin) as diluent for the RIA. Fractions were shipped frozen overnight along with the FBS diluent, Iodide, rT3 and T2 standards to MSU VDL (Michigan State University, Veterinary Diagnostic Laboratory) for testing and cross-reactivity assessment in the thyroid RIA panel via the standard protocols, using 100 µL for TT3, 200 µL for TT4, and 50 µL for FT4.

2.3.4 Blood samples

Thyroid Radioimmunoassay (RIAs): Optimizations for MSU VDL RIA thyroid panel (#20015).

2.3.5 Preliminary data

Upon initial analysis, only a small percentage of the lagoon or wild animal samples were within the readable range of the standard curve when analyzed using standard protocols and sample volumes. As part of the MSU VDL standard protocol, low concentration samples are provided values following extrapolation from the lowest standard to zero. To improve detection accuracy, samples were rerun with increased serum volumes (where possible), using additional lower concentration standards down to the reported assay sensitivity limit to allow for interpolation of lower sample analyte concentrations (vs extrapolation). Where appropriate, the RIA analysis program was edited to increase decimal units to improve precision (reduce rounding). Banked SR blood samples from (previously determined) high TT3, TT4 sample values were pooled for tests of parallelism of resultant values when testing multiple sample volumes in the RIAs (TT3, TT4, see below for details). Curve fitting was used to interpolate thyroid values using the extended standards with and without the extended volumes to compare against extrapolated values.

2.3.6 Total triiodothyronine (TT3) by RIA

The TT3 assay was run using an in-house RIA. TT3 standards ranged from 0.4 nmol/L to 4.7 nmol/L. TT3 RIA sensitivity was reported as 0.76 µg/dL (or 0.049 nmol/L). Standard sample test volume used in the assay was 100 µL, run in duplicate. For serum samples with resultant values below the lowest provided standard (0.4 nmol/L) a value was estimated through standard extrapolation between 0.4 nmol/L and zero. For assay optimization of TT3 for use in elasmobranchs we tested and compared increased sample volume (100 and 200 µL), and included an additional three lower standards (0.20, 0.10, and 0.05 nmol/L) to compare values obtained by extrapolation vs. interpolation using the expanded standard curve.

2.3.7 Total thyroxine (TT4) by RIA

Total T4 (TT4) was measured using a commercially available radioimmunoassay kit (MP Biomedicals Diagnostics Division). Total T4 standards ranged 25.7 nmol/L to 257.0 nmol/L. Sensitivity was reported as 0.76 ug/dL (or 0.059 nmol/L TT4). Sample volume was 25 µL, run in duplicate. For serum samples with resultant values below the lowest provided standard (25.7 nmol/L) a value was estimated through standard extrapolation between 25.7 nmol/L and zero. For assay optimization, an increased sample volume (100 and 200 µL) was used and 3 additional lower standards (12.9, 6.45, and 3.23 nmol/L) were added to compare extrapolated vs. interpolated results.

2.3.8 Free thyroxine (FT4) by equilibrium dialysis followed by T4 RIA

Free T4 (FT4) was assessed by equilibrium dialysis and was measured by a commercially available radioimmunoassay manufactured by Antech Diagnostics. T4 standards ranged 3.6 to 126 pmol/L. Sensitivity was reported as 0.045 ng/dL (0.58 pmol/L). Sample test volumes were 50 µL, run in duplicate. For serum samples with resultant values below the lowest provided standard (3.6 pmol/L), the value was estimated through standard extrapolation between 25.7 nmol/L and zero. For assay optimization, the sample volume could not be increased due to equilibrium dialysis methods; however, the software was altered to provide two decimals, reducing rounding. Three additional lower standards (1.8, 0.9, and 0.45 pmol/L) were included to compare extrapolated vs. interpolated results.

2.3.9 Thyroxine (T4) for TT4 chemiluminescent immunoassay

Total thyroxine (TT4) was measured with a commercially available solid-phase competitive chemiluminescent enzyme immunoassay (Total T4 Chemiluminescent Immunoassay, Immulite® 2000XPi, Siemens Healthcare, Glyn Rhonwy, Llanberis, United Kingdom). The TT4 CLIA assay protocol was run via an automated instrument. The instrument picks up the volume it requires for the test (100 µL), and therefore sample volume was unable to be modified for testing. A subset of 54 samples were run on the TT4 CLIA to be compared to the optimized TT4 RIA.

2.4 Iodine testing

Serum for total (the sum of inorganic and organic/protein-bound) and inorganic iodine was submitted to the MSU VDL for analysis as per Wahlen et al. (32).

2.5 Elemental analysis including cobalt

Serum was submitted to the MSU VDL for cobalt analysis as part of a trace mineral panel, using inductively coupled plasma-mass spectrometry (ICP-MS). Standards were from Inorganic Ventures. In-house serum pools were used as controls.

2.6 Ultrasound evaluation

Thyroid ultrasounds were reviewed by one author (Mylniczenko). The purpose of using this tool in this study was to identify animals that had grossly different thyroid appearance from known normal animals, suggesting disease as identified by experience from the authors and in comparison to other species. Images were identified retrospectively from exams which were conducted by multiple individuals; they were not always done with uniform technique and quality, thus acquisition of consistent measurement parameters was not possible. There are limited references on ultrasound evaluation of thyroid glands in elasmobranchs (33). The shape and size of the thyroid varies among species and can be difficult to identify (34). A normal thyroid has a symmetrical, homogenous appearance (35, 36) and in elasmobranchs they are smaller or equal in size to adjacent coracohyal and coracomandibular musculature (34, 37). Any variation from this uniformity was documented.

For a basic or 'high level' assessment of thyroid disease, the following criteria were used:

(1) the thyroid was larger than the adjacent musculature.
(2) multiple cysts were present.
(3) there were scattered hyperechoic foci present.

Cysts and foci were not quantified, they were subjectively evaluated and listed as mild, moderate, and severe.

2.7 Statistical analyses

All analyses were performed using R statistical Software v4.3.2 (38) or SigmaPlot (v.14.0), or MedCalc software Ltd. v.23.0.9. All statistical tests were evaluated at an $\alpha < 0.05$.

Quantitative measures (thyroid, cobalt, and iodine) were tested for normality using the Shapiro–Wilk normality test and visual inspection of the data normality using Q-Q plots (quantile-quantile plots) in the R 'stats' package (38). Since most of the data were left skewed and failed tests for normality even after standard transformations, comparisons between habitats and study cohorts were evaluated using non-parametric methods and corrections were applied for multiple *post-hoc* tests as appropriate. Log-transformation was employed on iodine measures during linear and ordinal regression model testing and evaluations. Single pairwise comparisons of serum thyroid, cobalt, or iodine measures evaluating differences between species and habitats used Mann–Whitney Rank Sum Tests. Study cohorts and habitat results were summarized as median ($\tilde{\chi}$) and interquartile range [IQR; 25th and 75th percentile (%)], where appropriate.

2.7.1 Wild and lagoon-housed normal populations

The thyroid and iodine values from "normal" thyroid (as determined by ultrasound) wild and lagoon-housed SRs were compared using Kruskall-Wallis one way ANOVA on ranks, and Dunn's Method for all (*post hoc*) pairwise comparisons. Comparisons between species, habitat, and supplement type were plotted using the web app "PlotsOfData." Data are displayed with underlying distributions, ordered by medians with mean and 95% confidence intervals by bootstrapping [see (39)].

2.7.2 Correlation analyses of serum thyroid, cobalt and iodine measures (cohort 1 and 2)

All pairwise correlations from all thyroid scores between quantitative sample hormone data (iodine (inorganic), iodine (total), cobalt, TT3, TT4, FT4) were evaluated using Spearman's rho statistic (ρ), rank-based correlation tests of all pairwise complete observations using the R packages 'corrplot' and 'Hmisc' to compute the *p* values of the correlations (38, 40–42). Variables for the correlogram were arranged in the angular order of the eigenvectors (AOE) which are ordered to match their corresponding eigenvalues, sorted in ascending order by magnitude (42). Significant correlations are reported as ρ(df) = [ρ value], p = [p-value], where df = N-2.

2.7.3 Regression analysis of thyroid hormone, iodine, and cobalt measures and thyroid disease states (cohort 2)

Principal component analysis and factor analysis were initially used to explore relationships between thyroid iodine and cobalt measures within cohorts to identify important factors (supplementation and thyroid disease severity) and drive model selection (see Supplementary materials). For model selection, serum thyroid hormone, iodine, and cobalt data from aquarium-managed animals were first assessed for violations of model assumptions, multicollinearity, and VIF (variance inflation factor). VIF was also used to aid in model selection, and trim predictor variables. The associations of thyroid hormone, iodine, and cobalt measures with thyroid disease were first investigated using simple linear regression models, followed by ordinal regression (see Supplementary Table S3 for additional details). For this analysis, ultrasound evaluations of the thyroid at the time of blood sample collection were transformed into an ordered-factor (normal, normal/large =1, goiter =2, mild =3, moderate =4, moderate–severe =5) for use in multivariable proportional odds logistic regression modeling. Ordinal regression model output provided coefficients given in units of ordered logits (ordered log odds). For a simpler interpretation, we converted coefficient values into an odds ratio (OR; the inverse log of the estimated coefficients). Significant coefficients in the model are reported as OR and 95% confidence interval (CI).

In a second model, we were interested in the predictive effects of total iodine measures. For this analysis, total iodine data was transformed into a bivariate categorical variable (< or > 400 ng/mL) alongside thyroid hormone, inorganic iodine, and cobalt (reporting probability estimates of each thyroid disease level). Predictor effect plots of significant factors in the model (coefficients) were built using the 'effects' package in R (43, 44).

3 Results

3.1 Thyroid assay optimization and validation

3.1.1 TT3

Detection and accuracy in measurement of thyroid hormones was improved by increased sample volume and use of additional lower standards. Visual inspection confirmed parallelism of calculated values with normal and extended volumes (100 vs. 200 µL, sample TT3 values >1.0 nmol/L) and from normal standards and extended standards. In a subset of test samples ($N = 16$ SR from the wild cohort), only 33% of the samples (5 of 15) fell within the range of the standard curve using the standard protocol (100 µL sample volume), whereas, 81% (13 of 16 samples) were within the readable range of the standard curve with increased volume (200 µL) and extended standards. Sample TT3 values using 100 µL volume obtained by extrapolation (from the lowest standard to zero) were strongly correlated with result values obtained via interpolation using 200 µL sample volume and additional lower standards ($r^2 = 0.985$).

3.1.2 TT4

TT4 detection was improved by increasing sample test volume from the standard 25 µL to 200 µL. No samples (0 of 16) were detected within the readable range of the standard curve using 25 µL sample volume (normal TT4 standards ranged 25.7 nmol/L to 257.0 nmol/L). Increasing sample volume to 200 µL (8x increase), and adding additional lower standards improved detection to 68.8% (11 of 16). Comparison of extrapolated vs. interpolated values for 200 µL sample volume showed a strong positive correlation ($r^2 = 0.99$), indicating that the extrapolation was sufficient, but the extra sample volume was a critical improvement.

3.1.3 FT4

Serum volumes could not be increased at the dialysis step, so FT4 optimization was only evaluated for improved detection based on extended standards. None of the samples (0 of 16) fell within the

readable range of the standard curve using the 50 µL sample volume and regular standards. Adding additional lower standards increased sample detection on the curve to 25% (4 of 16). Ten samples had reported values of 0 pmol/L. However, values determined by extrapolation were strongly correlated with interpolated values ($r^2 = 0.98$).

Overall, strong, positive correlations for extrapolated vs. interpolated values in all three thyroid RIAs indicated that including extra standards could improve detection but were not necessary for improved accuracy for normal elasmobranch serum sample values at or near the sensitivity of these assays. However, higher sample volumes (TT3 and TT4) significantly improved detection of low thyroid concentrations.

3.1.4 CLIA vs. RIA (TT4)

Due to discontinuation of the RIA TT4 kit near the completion of this study, a small subset of samples ($N = 54$) with a range of serum TT4 RIA values (200 µL test volume), across multiple species, were tested in the new TT4 CLIA platform. A 100 µL test volume was used, which could not be increased due to limitations in assay methodology. Most of the CLIA values (44 of 54) were reported with zero values (vs. only 8 from RIA) resulting in both measures to have a non-normal distribution with positive skew (Shapiro–Wilk RIA TT4, $W = 0.8016$, $p < 0.0001$; CLIA TT4 $W = 0.2842$, $p < 0.0001$). The non-zero values ranged from 0.014 to 6.83 nmol/L for RIA vs. 0.193 to 15.2 nmol/L for the CLIA, However, serum TT4 CLIA values did not correlate with the TT4 from RIA (adjusted $r^2 = -0.0148$). Data were next checked for assumptions of normality of differences for Bland–Altman analysis (MedCalc). The difference in TT4 measurements (RIA-CLIA) revealed an overall positive bias with the optimized RIA TT4 method reporting higher values than the CLIA (RIA-CLIA difference mean ± SD was 0.95 ± 2.93 nmol/L). However, since RIA-CLIA differences were not normally distributed (Shapiro–Wilk $W = 0.7801$, $p < 0.001$), further evaluation using Bland–Altman plots could not be conducted. Removal of the zero-reported values to re-analyze the data was not done since the size of the remaining dataset ($N = 10$) would reduce statistical power and limit interpretation. Because of the poor correlation and repeatability between methods, no further testing or analysis of CLIA TT4 with respect to thyroid disease or the other measures were performed.

3.1.5 HPLC

Results from a HPLC chromatogram, including peak RT of the Cerilluant thyroid standards and iodide, and RIA immunoreactivity profile of the thyroid methanolic extract (see Figure 1) was used to characterize immuno-detectable TT3, TT4 and FT4 (see Supplementary Figure S1 for additional details). Two standards (I2 and T2) partially co-eluted with the wavefront and had RTs as follows: iodide (I2) in a wide band at 1–1.83 RT, T2 (2.073–2.683 RT), whereas T3 and T4 separation was more distinct [T3 2.1 RT (single), 3.78–4.033 RT (panel)], rT3 [3.9–4.1 (single), 4.28–4.55 RT (panel)], and T4 [4.18–4.44 (single), 5.6–6.09 RT (panel)]. Thyroid tissue extract produced a wide band of immunoreactivity starting at the wave front in fr1-2 and continuing through fr 3–4. The highest relative percent immunoreactivity in the TT3 assay was found in a wide band starting at the wave front in fr 1–2 and continued, in part, into fr 3. An unexpected and unidentified immunoreactivity peak was observed in fr 2–3 in TT4 and FT4 RIA. Cardiac blood collected from the wild animal at the time of thyroid tissue recovery had low concentrations of TT3, TT4 and FT4 (0.00 nmol/L, 1.13 nmol/L, and 0.00 pmol/L, respectively).

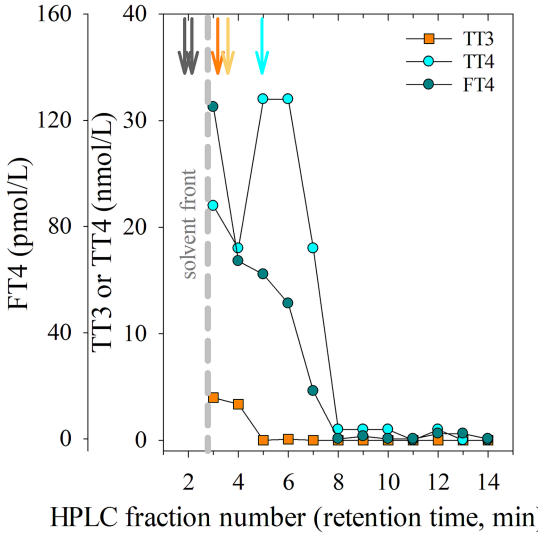

FIGURE 1
High performance liquid chromatography (HPLC) chromatogram including fraction (fr) number and retention time (RT) peaks from injection of methanolic iodide and thyroid standards (denoted by vertical arrows) or immunoreactivity results from fractions collected following injection of a methanolic extract of thyroid tissue (collected from *H. americanus*) run in commercially available RIAs (radioimmunoassay; TT3; total triiodothyronine, nmol/L, orange square); TT4 (total thyroxine, nmol/L, cyan circle; FT4; free thyroxine, pmol/L, dark teal circle). Reference standard RTs are depicted as vertical arrows shown in order from highest to lowest polarity: Iodide and T2 (dark brown), T3 (orange), rT3 (light orange), T4 (cyan). The solvent front is denoted by a vertical gray dashed line.

3.1.6 Assessment of thyroid 'normals' using the optimized thyroid RIAs, cobalt, and iodine

Wild, lagoon- and aquarium-housed thyroid-normal SR did not differ in TT3 (TT3 $\tilde{\chi}$=0.59, 0.70 and 0.46 nmol/L, respectively) or TT4 values (TT4 $\tilde{\chi}$=0.38, 0.85 and 0.47 nmol/L, respectively), however FT4 values were higher in the lagoon (FT4 Lag $\tilde{\chi}$=1.43 pmol/L, IQR = 0.39, 2.12) and aquarium-housed (FT4 Aquar $\tilde{\chi}$=0.00 pmol/L, IQR = 0.00, 1.90) SR compared to the wild SR (FT4 Wild $\tilde{\chi}$=0.0 pmol/L, IQR = 0.0, 0.0; H (2)=11.961; $p = 0.003$; see Figures 2A–C).

SR serum iodine (total, inorganic) and cobalt measures showed more variability. Wild SR had higher serum inorganic iodine relative to lagoon- and aquarium-housed SR (H (2)=28.054, $p < 0.001$), and higher total iodine (I (T) Wild $\tilde{\chi}$=230.0 ng/mL, IQR = 188.0, 292.0, all values <400 ng/mL) than lagoon-housed SR (H (2)=29.765, $p < 0.001$). Lagoon- and aquarium-housed SR had elevated serum cobalt measures compared to wild SR (H (2)=8.342, $p = 0.015$). Cobalt values in the wild SR group ($N = 11$) ranged from 13.41 to 62.20 ng/mL, whereas lagoon- and aquarium-housed SR ranged from 58.98 to 198.60 ng/mL ($N = 25$) and 113.50 to 375.40 ng/mL ($N = 5$), respectively (see Figures 2D–F). Four of the five aquarium-housed SR (all females) were 80 days post-removal of supplement "C" (3.8 ppm DM cobalt).

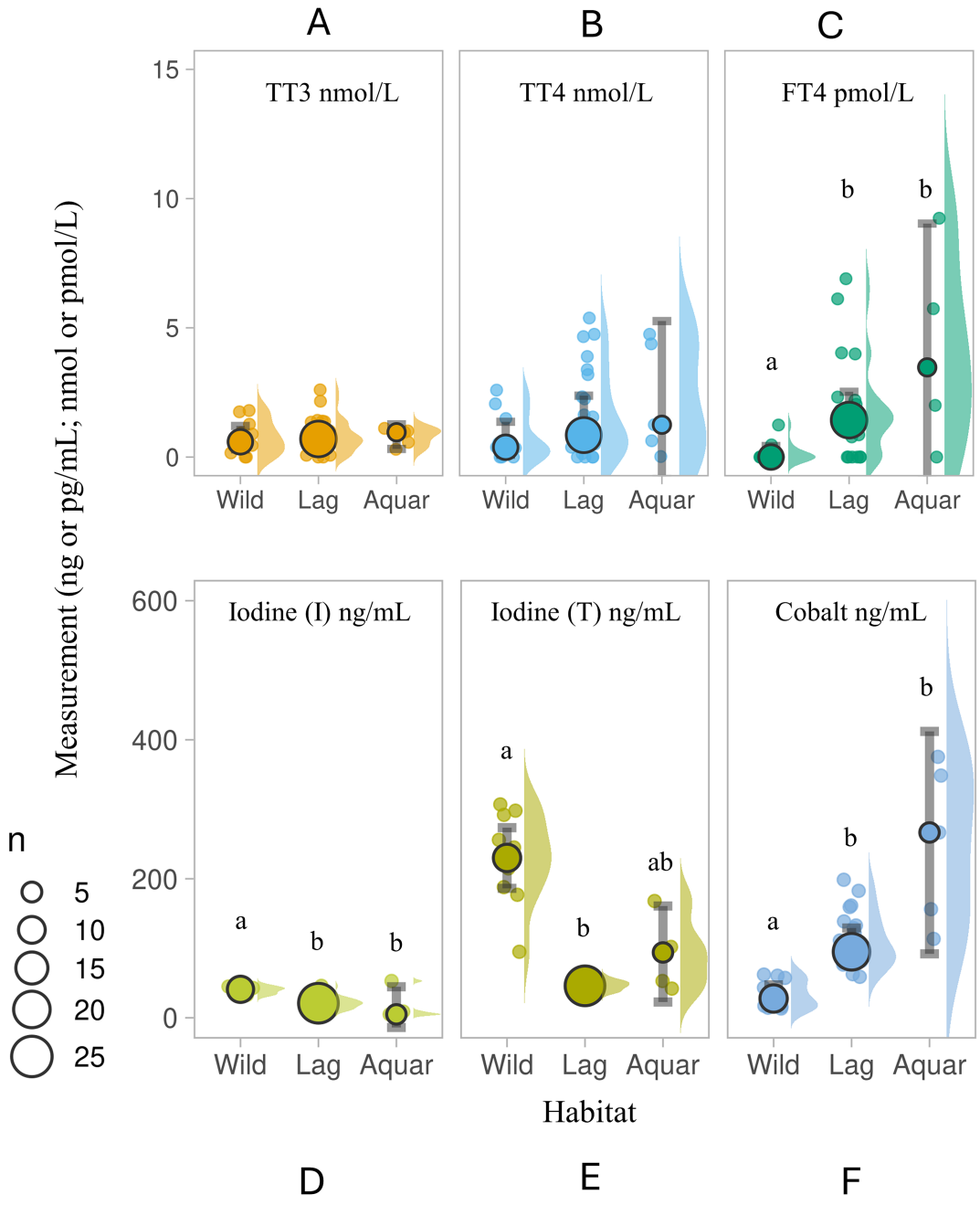

FIGURE 2
Serum **(A)** total triiodothyronine (TT3 nmol/L), **(B)** total thyroxine (TT4, nmol/L), **(C)** free thyroxine (FT4, pmol/L), **(D)** inorganic iodine (I; ng/ml), **(E)** total iodine (T; ng/ml), and **(F)** cobalt (ng/ml) in three populations of wild and housed southern stingrays *Hypanus americanus* with normal presentation of thyroids by ultrasound evaluation (Study 1). Data are displayed as individual sample dot-plots (jittered) with vertical cow-plots to visualize the data distribution for each measure by habitat [(Wild, lagoon (Lag), aquarium (Aquar)]. Medians for each habitat are indicated by the larger outlined circles, with the relative size of the circle indicating the N of that habitat (see key). Error bars represent the 95% confidence interval for the habitat. Letters inside the panels represent significant differences between the habitat ($\alpha < 0.05$). Wild animals ($N = 11$) were unsupplemented. Lagoon animals ($N = 22$) received Aquatic Gel, and 1 of 5 Aquarium animals received supplement "C" (Table 1).

3.2 Iodine and cobalt measures across all cohorts and thyroid disease states

Iodine values measured as high as 606,740 ng/mL [I (I); N = 151 $\tilde{\chi}$=48.0 ng/mL, IQR = 25.00, 130.00] for inorganic iodine, and 493,529 ng/mL [I (T); N = 157, $\tilde{\chi}$=150.0 ng/mL, IQR = 53.00, 495.00] for total iodine in WSBS with moderate to severe thyroid disease. Cobalt ranged from 4.24 to 2,818.91 ng/mL ($N = 146$, $\tilde{\chi}$=112.33, IQR = 27.78, 316.17; see Figure 3). The highest iodine and cobalt values (>1,000 ng/mL) were observed in aquarium-housed animals in 2015 through 2020 ($N = 15$), and primarily in WSBS species (12 of 15 samples, $N = 2$ individuals, samples collected from 2013 to 2020). These high values were obtained when the WSBS were offered (and consumed) supplement "C" and "D" with approximately 100,000 ppm

DM iodine (see Table 1). Highest cobalt values were observed in 2017 and 2018 when animals were offered supplement "D" (5M1Y; 5MD8) approximately 2 years after iodine content had been reduced by over 33% from 202,603 ppm DM down to 133,658 ppm DM, and more than 5 years after cobalt had been reduced from 151.4 ppm DM (supplement "A") down to 4.2 ppm DM (supplement "B") and 3.8 ppm DM (supplement "C"; see Table 1). Only 29 of 53 samples with values <300 ng/mL cobalt were evaluated as thyroid-normal. The remaining samples included 5/53 goiter; 9/53 Normal (LG); 5/53 mild; 5/53 moderate; and 8/53 moderate–severe. There was a mix of thyroid disease scores in the higher cobalt measures (>300 ng/mL), including 7/27 evaluated as normal, 6/27 Normal (LG), 0/27 goiter, 9/27 mild, 1/27 moderate, and 4/27 moderate–severe thyroid disease. The highest cobalt values observed ($N = 13 > 700$ ng/mL) primarily came from HCR, PR, and WSBS species. The lowest iodine and cobalt values were observed in wild and lagoon-housed SR (see Figures 2D–F), where all measured total iodine values were < 400 ng/mL, inorganic iodine values were < 50 ng/mL, and cobalt values were < 200 ng/mL. There was one exception in an aquarium-managed HCR with undetermined thyroid disease status, measuring a low of 14 ng/mL for both inorganic and total iodine.

3.3 Investigation of overall relationships between thyroids, iodines, and cobalt measures

Spearman's rank correlations were computed to assess all available pairwise relationships between quantitative measures.

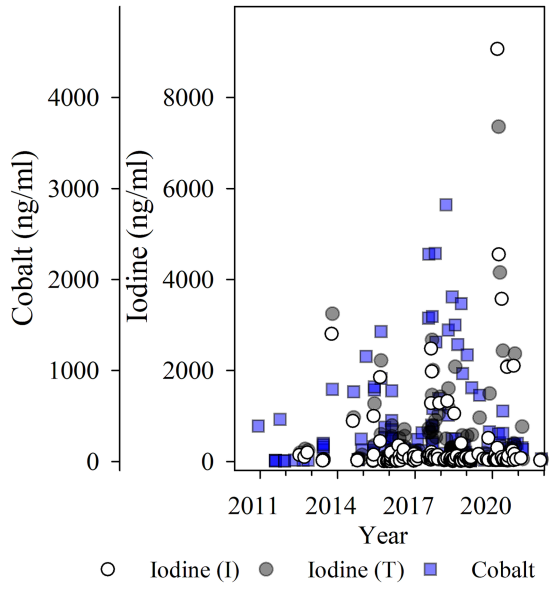

FIGURE 3
Serum iodine [inorganic (I) or total (T) ng/ml] and cobalt (ng/ml) values plotted for study years 2010 to 2022 from both Study cohorts provided the supplementation described in Table 1. Two samples with extremely high iodine values >10,000 ng/mL are not shown ($N = 2$; inorganic iodine: 16,642 and 606,740 ng/mL; total iodine: 17,257 and 493,529 ng/mL). This graph shows that use of supplementation appears to accumulate iodine and cobalt across time.

Overall, there were strong, significant positive relationships between inorganic iodine and total iodine ($\rho(149) = 0.85$, $p < 0.0001$), total iodine and cobalt ($\rho(131) = 0.54$, $p < 0.0001$), TT4 and FT4 ($\rho(112) = 0.69$, $p < 0.0001$). Significant but weaker relationships were also observed between TT3 and TT4 ($\rho(111) = 0.42$, $p < 0.0001$), and TT3 and cobalt ($\rho(45)=0.14$, $p < 0.0001$; see Figure 4). All other correlations were of lower strengths of effect, but it was observed that in this correlation matrix, inorganic iodine had a weak, negative correlation with two of the thyroid measures (TT3 $\rho(46)= -0.05$, and FT4 $\rho(47)= -0.14$, see Figure 4, light red negative ellipses).

3.4 Ultrasound evaluation

3.4.1 Ultrasound evaluation and thyroid disease evaluation score

The most common findings (see Figure 5) were cysts of varying sizes and hyperechoic pinpoint foci, likely representing mineralization (48). Nodular disease with hypoechoic cystic (spongiform/honeycomb) appearance was labeled as moderate disease based on size of the gland and the cyst.

Extent of thyroid disease was broad and evaluation was intended only to assess if there was any correlation with blood data and individuals with a history of reproductive disease ($N = 4$ SR; $N = 2$ WSBS; $N = 4$ HCR). Histopathologic confirmation of thyroid disease was not typically possible in this dataset as biopsies were rarely taken and postmortem thyroid tissue was not always included in the sampling set. A summary of thyroid evaluation scores at the time of blood sampling are provided in Supplementary Table S2.

Samples collected from animals in natural sea water habitats (wild or lagoon-housed) were categorized as normal based on relative size and homogenous symmetrical appearance, whereas aquarium-housed animals provided a range of thyroid disease scores (see Supplementary Table S2). Thyroid, cobalt, and iodine measures differed across thyroid disease evaluation levels, with moderate and moderate/severe thyroid evaluations showing the highest total and inorganic iodine values, but lowest TT3 (see Table 2). Distributions of measured values of TT3, TT4, and FT4 shifted to higher ranges (increased variance; larger interquartile ranges) in supplemented animals (see Figures 6A–C). The pattern was consistent through disease states, with the notable exception of animals in the highest thyroid disease category (thyroid evaluation =5, moderate/severe), which did not show the same pattern of elevated TT3, TT4 or FT4 (Figures 6A–C).

Several of the aquarium-housed individual animals ($N = 38$) in this study were monitored over several years. There was a progression of thyroid disease and an opportunity to see if it resolved. Four SER presenting with hyperplastic goiters resolved with management. One animal was provided supplementation (supplement "A," Tables 1, 3) were given oral lugol's iodine until the goiter resolved and were then put on the supplement. In all other cases, during the course of the study, progression from a normal thyroid evaluation to mild, moderate or moderate–severe was unidirectional.

Challenges with ultrasound evaluation in these cases included a lack of images from examinations, misinterpretation of anatomy, and inability of the ultrasonographer to obtain good quality images (depth, type of transducer, and optimal adjustments of settings).

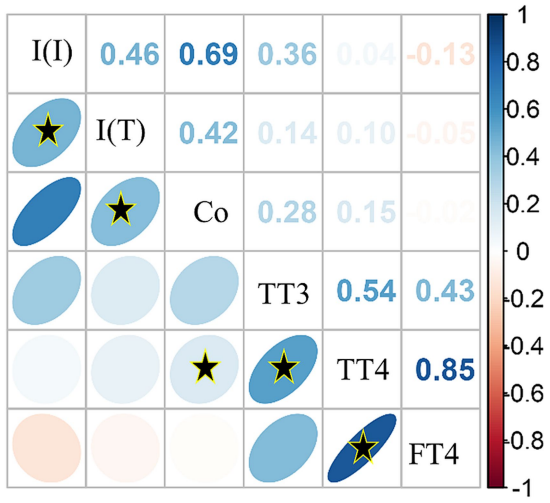

FIGURE 4
Correlation matrix of serum inorganic iodine [I (I)], total iodine [I (T)], cobalt (Co) and thyroid hormone values [total triiodothyronine (TT3); total thyroxine (TT4); free thyroxine (FT4)] using Spearman's correlation method with all pairwise complete observations. Color intensity is proportional to the correlation coefficients. Direction of the ellipses indicates positive or negative relationships. On the right side of the correlogram, the legend color relates to the Spearman correlation coefficient values, with blue indicating positive and red indicating negative correlations. The correlation matrix was reordered according to the correlation coefficient using the angular order of the eigenvectors (AOE) method. Black stars (*) within ellipses indicate significant correlations with $\alpha < 0.01$.

3.4.2 Serum total iodine measures <400 and > 400 ng/mL as a proxy for vitamin/mineral consumption

Since consumption of the supplement varied by species, individual, and time, and was not directly measured, serum total iodine measurements were used to identify animals with likely consistent consumption (animals that consumed their supplement had higher levels than those that did not). This placed their ranges well above values measured in the unsupplemented wild SR (evaluated as having normal thyroids). Using that information, we parsed the dataset using a normal total iodine cutoff of 400 ng/mL and used the two groups (< or > 400 ng/mL total iodine) to compare the relative proportions of samples with or without cysts or abnormal ultrasound echogenicity, and overall thyroid evaluation (normal vs. abnormal, see Table 3A), as well as a comparison of the relative distribution of thyroid evaluation scores, and their thyroid, cobalt, and inorganic iodine values (see Table 3).

Considering all species and habitats, cysts and echogenicity were less likely to be observed in ultrasounds within the <400 ng/mL total iodine group (46% vs. 10%; and 50% vs. 11%, respectively), and a higher percent of observations were scored as normal in the overall thyroid evaluation (45% vs. 10%; see Table 3A). Samples from animals with serum total iodine >400 ng/mL ($N = 62$) had higher rates of observed cysts [18/62 (29%)] and echogenicity [14/62 (22.6%)] compared to the <400 group.

[24/117 (20.5%)] and [17/117 (14.5%), respectively; see Table 3A]. In the aquarium cohort, fewer thyroid ultrasound scans were evaluated as normal in the >400 total iodine group [12/47 (26%)], and a higher percentage of moderate to severe thyroid evaluation scores, were in the >400 total iodine group [13/18 (72%)]. While there were no significant differences in TT3, TT4, or FT4 between the <400 and > 400 total iodine groups (see Table 3B), as expected, inorganic iodine and cobalt were also higher in the >400 group [Table 3B; I (I) <400I(T) $\tilde{\chi}$=35.0, IQR = 21.0, 58.0, vs. I (I) > 400I(T) $\tilde{\chi}$=376.0, IQR = 129.0, 1,883.0; $p < 0.001$; and Cobalt <400I(T) $\tilde{\chi}$=88.0, IQR = 23.0, 160, vs. Cobalt >400I(T) $\tilde{\chi}$=388.0, IQR = 129.0, 365.0; $p < 0.001$].

3.5 Thyroid, iodine and cobalt measures as predictors of thyroid disease in the aquarium-housed SR

Ordinal regression models were determined to be the best fit to evaluate the ability of serum inorganic iodine, total iodine (or total iodine <400 or > 400 ng/mL), cobalt, TT3, TT4, and FT4 to predict thyroid disease evaluation scores in the aquarium cohort. In the first model, iodine values were log-transformed, and total iodine and cobalt were removed due to high VIF, collinearity and best fit. For Model 1 the factors determined to best predict thyroid disease severity (Y) was Y ~ log inorganic iodine + TT3 + TT4 + FT4 (Nagelkerke $R^2 = 0.98$; see Supplementary Table S3). Holding all other predictors constant, samples with 1 unit higher value of log inorganic iodine were 2.7 times more likely to be evaluated in a higher thyroid evaluation score (OR = 2.738, 95% CI = 1.280, 6.833).

Serum TT3 had a more complex association with iodine and thyroid disease score. Serum TT3 values were elevated in many of the samples from supplemented animals with the exception of the highest severity of thyroid disease (see Figure 6A). This negative relationship can also be seen in Figure 7B predictor effects plot as a negative association of TT3 with thyroid disease such that the highest probability of moderate–severe disease was associated with the lowest TT3 values. Holding all other predictor values constant, with every one nmol/L increase in TT3 we would expect a 1.125 decrease in the cumulative probability of thyroid disease evaluation level (log odds scale). Calculating for the OR (OR = 0.325, 95% CI = 0.091, 0.944) the reciprocal (inverse of the odds ratio = 3.077) can be more easily interpreted. In this model, where increased inorganic iodine was correlated with increasing disease severity, there was also a 3.1 times higher odds to be evaluated into a higher thyroid disease category for every 1 nmol/L decrease observed in serum TT3. The cumulative probabilities for each change in thyroid evaluation score are visualized as predictor effects plots in Figures 7A,B (log inorganic iodine, and TT3).

For Model 2 we were specifically interested in the predictive ability of serum total iodine measures <400 or > 400 ng/mL as categorical variables. Using a final model of Y ~ total iodine >400 + TT3 + TT4 + FT4, samples with total iodine >400 ng/mL were 3.6 times more likely to be evaluated as a higher thyroid disease score (OR = 3.591, 95% CI = 1.280, 6.833, $p = 0.012$). Serum TT3 was not significant in this more generalized model ($p = 0.104$), but had similar trends as in Model 1, with lower TT3 values occurring in the highest disease categories. The differences between the highest thyroid disease evaluations for mild/moderate ($p < 0.01$) and moderate/moderate–severe ($p < 0.001$) can be readily distinguished between the <400 and > 400 ng/mL total iodine categories (Figure 7C). In the <400 ng/

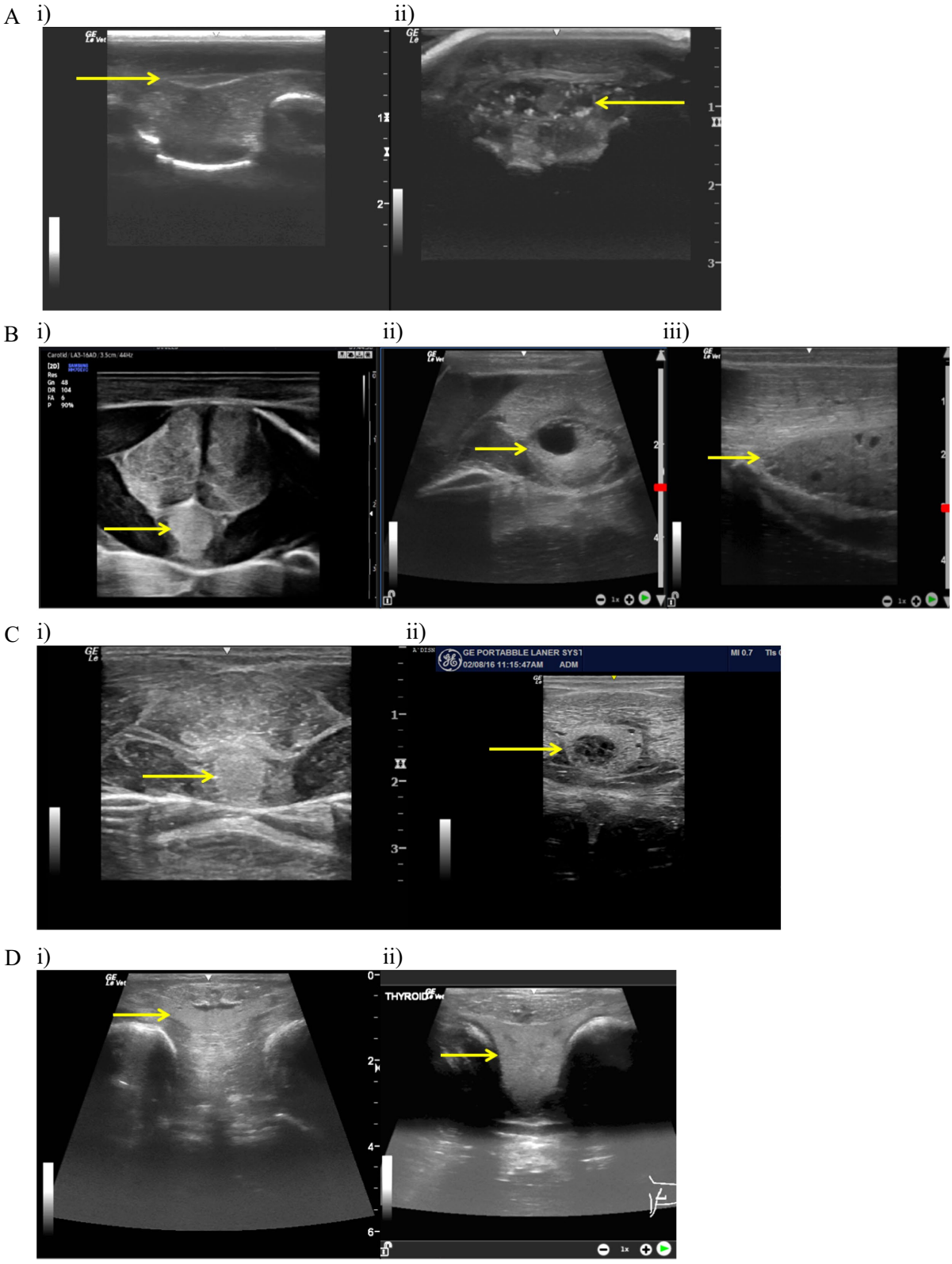

FIGURE 5
Ultrasound evaluations. (**A**: i) Normal bamboo shark (*Chiloscyllium punctatum*) thyroid ultrasound in transverse; arrow scaled to 1 cm. (ii) Abnormal bamboo shark (*Chiloscyllium plagiosum*) thyroid ultrasound in transverse; arrow scaled to 1 cm. Complex multinodular cystic appearance with hyperechoic foci. (**B**: i) Normal honeycomb stingray (*Himantura uarnak*) thyroid ultrasound in transverse; arrow scaled to 1 cm. (ii) Abnormal honeycomb stingray (*H. uarnak*) thyroid ultrasound in transverse; arrow scaled to 1 cm. Note the large cyst present and the overall enlarged size of the thyroid. (iii) Abnormal honeycomb stingray (*H. uarnak*) thyroid ultrasound in sagittal; arrow scaled to 1 cm. Note multiple small cystic structures present

(Continued)

FIGURE 5 (Continued)
throughout the thyroid and larger size compared to adjoining musculature. (**C**: i) Normal southern stingray (*Hypanus americanus*) thyroid ultrasound in transverse; arrow scaled to 1 cm. (ii) Abnormal southern stingray (*H. americanus*) thyroid ultrasound in transverse; arrow scaled to 1 cm. Note the complex cystic nodule with smaller cysts in the parenchyma and the size of the thyroid compared to the ventral musculature. (**D**: i) Normal ocellated eagle ray (*Aetobatus ocellatus*) thyroid ultrasound in transverse; arrow scaled to 1 cm. (ii) Abnormal ocellated eagle ray (*Aetobatus ocellatus*) thyroid ultrasound in transverse; arrow scaled to 1 cm. Note the hyperplasia (goiter).

TABLE 2 **Comparisons of SR thyroid, iodine, and cobalt medians and interquartile range (IQR) across thyroid disease evaluation scores (number) for each study elasmobranch cohort (natural sea water or aquarium habitat).**

Habitat	Thyroid ultrasound evaluation							
	Natural sea water		Aquarium					
Measurement[a] median (IQR[b])	Normal (1) (Wild)	Normal (1) (Lagoon)	Normal (1)	Normal/ Large (1)	Goiter (2)	Mild (3)	Moderate (4)	Moderate/ Severe (5)
TT3 (nmol/L)	0.59 (0.16, 1.27)	0.70 (0.36, 1.18)	0.46 (0.25, 0.95)	0.75 (0.30, 2.34)	0.21 (0.00, 0.57)	0.76 (0.48, 1.09)	0.29 (0.06, 1.34)	0.25 (0.12, 0.44)
TT4 (nmol/L)	0.38 (0.00, 1.49)	0.85 (0.41, 2.98)	0.47 (0.00, 2.23)	1.66 (0.24, 4.43)	0.00 (0.00, 0.94)	3.31 (1.940, 7.07)	2.12 (0.29, 4.34)	0.52 (0.11, 1.62)
FT4 (pmol/L)	0.00 (0.00, 0.00)	1.43 (0.39, 2.12)	0.00 (0.00, 1.90)	2.09 (0.23, 2.69)	0.00 (0.00, 1.03)	0.97 (0.47, 14.14)	0.96 (0.00, 4.51)	0.00 (0.00, 1.62)
Inorganic iodine (ng/ml)	41 (35, 44)	21 (14, 27)	54 (33, 137)	83 (17, 164)	96 (25, 120)	90 (40, 161)	54 (41, 98)	1,306 (38, 4,307)
Total iodine (ng/ml)	230 (188, 292)	46 (40, 56)	99 (55, 267)	323 (42, 698)	224 (58, 283)	258 (54, 960)	112 (86, 216)	1,532 (247, 3,723)
Cobalt (ng/ml)	27.78 (16.23, 57.44)	95.03 (80.87, 135.75)	94.64 (12.10, 247.26)	114.10 (25.90, 1284.06)	10.11 (7.78, 37.07)	423.68 (144.31,740.92)	195.64 (30.36, 254.75)	177.27 (93.01, 306.18)

[a]Total triiodothyronine (TT3; nmol/L); Total tetraiodothyronine (TT4; nmol/L); Free thyroxine (FT4; pmol/L). Sample Ns are provided in Supplementary Table S2.
[b]Interquartile range (IQR) reported here as: (25th, 75th percentile).

mL total iodine category, the probability of a normal thyroid evaluation was 61% (vs. 31% for >400), and only 19% probability of scoring a 4 or 5 (moderate to moderate–severe) in the <400 ng/mL total iodine (vs. 45% probability for >400).

4 Discussion

Thyroid disease is a common concern with elasmobranchs, with hyperplastic or diffuse colloidal ("classic") goiter being the foremost diagnosis. If identified early, morbidity and possible mortality can be prevented. The etiology is frequently linked to iodine, usually as a deficiency originating in low iodine consumption. This occurs because it is unavailable to the animal either from low availability in food or water, ozone treatments of the water, other goitrogenic causes (high nitrates), or a mix of the three (49–53). Diagnosis is made by an obvious enlargement under the jaw. Short of that observation, few studies have shown other methods for diagnosis. Thyroid hormone values have been assessed and reported to be low, when compared to other vertebrates, for both T3 and T4 in goitered sharks (37, 54). As such, thyroid hormone assessment seemed a reasonable test in managed care animals. Interestingly, in the aquarium-managed cohort of animals presented here, the RIA-derived values using standard methodology and sample volumes routinely registered as low or unreadable, even in apparently healthy sharks and rays. There was only one commercial lab with an RIA thyroid assay panel at the time of testing (primarily for canine and feline), prompting a closer investigation of the methodology, assay sensitivity, and testing for validation in elasmobranch species.

4.1 Is the current methodology for blood thyroid hormone assessment appropriate for elasmobranchs?

Commercial laboratory analysis of blood thyroid hormone results consistently showed values in elasmobranchs were markedly below those routinely measured in other non-wildlife, terrestrial vertebrate species at MSU VDL (e.g., *Felis catus* or *Canis familiaris*). This was especially unusual given that clinical cases of thyroid disease (not goiter) still resulted in near undetectable blood thyroid hormone levels. Working with the laboratory (Bousianny), extant RIA methodology was reviewed. First, a direct measurement for known thyroid hormone was necessary. As a biological validation, HPLC performed on homogenized and extracted thyroid tissue showed high concentrations of immunoreactive TT3, TT4 and FT4 (Figure 1), while values from a matched cardiac blood sample were low. These results suggest that thyroid hormones are indeed highly conserved in elasmobranchs (55), and exhibited expected cross reactivity with established commercial RIA antisera. Secondly, serum was evaluated from a subset of 'thyroid-normal' SR and compared to thyroid abnormal SR. Normal values were uniformly quite low, most at or near zero, and in fact, below the readable range of the kit standard curve. Increased sample volume (2x for TT3 and 8x for TT4) and additional

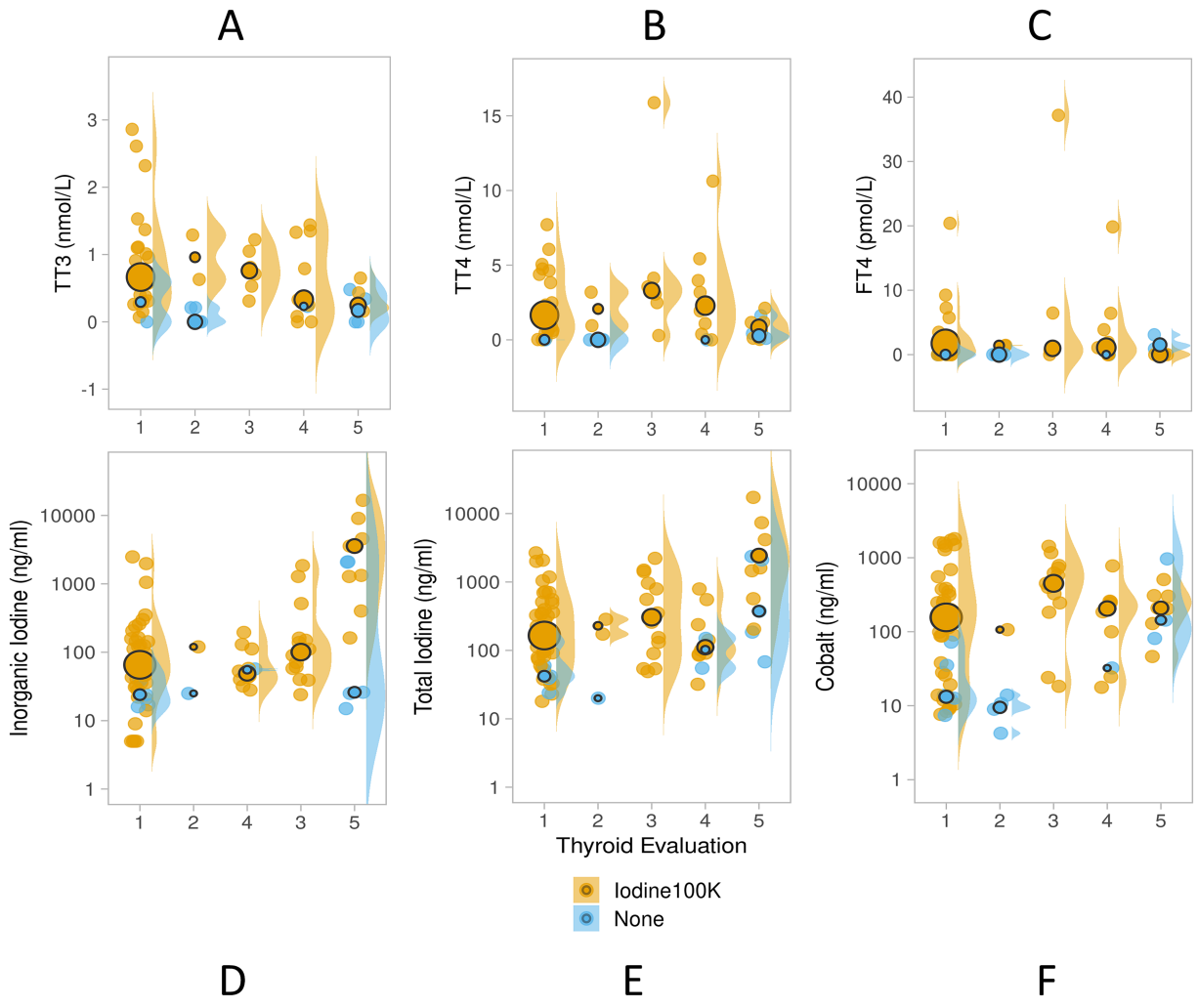

FIGURE 6
Study 2 serum TT3 (nmol/L), TT4 (nmol/L), FT4 (pmol/L; panels **A–C**), inorganic iodine (ng/ml), total iodine (ng/ml) and cobalt (ng/ml; panels **D–F**) values in unsupplemented (blue, *N* = 20) and micronutrient supplemented elasmobranchs (orange, *N* = 82) with total iodine dose ~100,000 ppm DM (Iodine 100 K), and cobalt dose 3.8 or 1.4 ppm DM (Supplements "C" and "D," Table 1.) Serum inorganic, total iodine and cobalt shown here with y-axis in log-scale. Thyroid evaluations obtained by ultrasound during the time of the blood sample collection provided a range of thyroid disease from 1 = normal, or normal/large, 2 = goiter, 3 = mild, 4 = moderate, and 5 = moderate/severe. Data are displayed as individual sample dot-plots (jittered) with vertical cow-plots to visualize the data distribution for each measure. Medians for each group are indicated by the larger outlined circles, with the relative size of the circle indicating the N of that group.

standards (down to the assay lower limit of sensitivity) allowed for improved sample measurement (Tables 2, 3). While both T3 and T4 are found in the thyroid itself, presumably large amounts are not routinely released into circulation resulting in relatively low levels which may not correlate with hypothyroidism.

RIA is generally considered the "gold standard" for thyroid hormone assays. Developed decades before the more current EIAs and CLIAs, RIAs generally had the advantage of improved discrimination and greater sensitivity and could easily be adapted "in-house" to meet the needs of species-specific lower ranges by adjusting working dilutions of the radio-labled tracer or antisera titer (56, 57). In contrast, current commercial labs typically follow a standardized RIA kit protocol using unextracted serum that had been optimized for species with higher thyroid hormone ranges (e.g., canine, feline (21)). Previously published data as well as older research were focused on RIA and likely varied methodology. Many labs may switch to non-RIA assays because of ease and safety (no need for radiation) but since they are often validated for targeted species, they might not be sufficiently sensitive to work well on elasmobranchs. Direct comparison of this study to previously published elasmobranch values is not a simple task. Current commercial labs and assays cannot easily perform historical sample processing or match assay methods (49, 51, 56–61). A further question was which of these values have biologic relevance. Thyroid hormone physiology is reviewed elsewhere (62) but salient content notes that in many species T3 is the biologically active form with T4 being a prohormone that requires conversion (62). Additionally T3 may be produced peripherally in multiple organs, like the liver (in dogfish (*Squalus acanthias*)) and possibly the kidney. Overall, the literature continues to be data-poor for thyroid function in elasmobranchs. What exists is challenging to interpret due to a variety of sample processing and assay methodology, and a potential confound of increased TT3 and

10.3389/fvets.2025.1504527

TABLE 3 (A) Ultrasound evaluation of elasmobranch thyroid gland architecture including presence or absence of cysts and hyperechogenic foci, used to provide an overall measure of overall thyroid normality score during the time of blood sampling in all habitats.

	Total iodine group (ng/ml)		Overall	*p*-value[a,e]
	< 400	>400		
(A) Ultrasound evaluation N(%)				
Cysts				<0.001
Not observed	83 (46%)	18 (10%)	101 (56%)	
Undetermined[b]	10 (5.6%)	26 (15%)	36 (20%)	
Observed	24 (13%)	18 (10%)	42 (23%)	
Echogenicity				<0.001
Not observed	89 (50%)	19 (11%)	108 (60%)	
Undetermined[b]	11 (6.1%)	29 (16%)	40 (22%)	
Observed	17 (9.5%)	14 (7.8%)	31 (17%)	
Overall				<0.001
Abnormal	29 (16%)	27 (15%)	56 (31%)	
Normal	80 (45%)	18 (10%)	98 (55%)	
Undetermined	8 (4.5%)	17 (9.5%)	25 (14%)	
Total, N (%)	117 (65%)	62 (35%)	179 (100%)	
(B) Measurement[c] median (IQR)[d]				
TT3 (nmol/L)	0.59 (0.29, 1.11)	0.31 (0.16, 0.91)	0.55 (0.22, 1.02)	0.089
TT4 (nmol/L)	0.85 (0.10, 2.56)	0.56 (0.01, 2.46)	0.80 (0.04, 2.49)	0.5
FT4 (pmol/L)	0.86 (0.00, 2.02)	0.00 (0.00, 1.32)	0.62 (0.00, 1.86)	0.2
Inorganic iodine (ng/ml)	35.0 (21.0, 58.0)	376.0 (129.0, 1883.0)	48.0 (25.0, 128.0)	<0.001
Total iodine (ng/ml)	79.0 (48.0, 185.0)	962.0 (626.0, 2087.0)	150.0 (53.0, 492.0)	N/A
Cobalt (ng/ml)	88.0 (23.0, 160.0)	388.0 (129.0, 865.0)	112.0 (28.0, 312.0)	<0.001

Ultrasound scores were compared by grouping blood samples into <400 and > 400 ng/mL total iodine, where 400 ng/mL was used as the upper cutoff value in normal, wild SRs. Pearson's chi-squared test was used to determine differences between the expected and observed frequencies in observations between the two total iodine level groups. (B) Thyroid, iodine and cobalt median and interquartile range (IQR) for the <400 and > 400 ng/mL total iodine groups outlined in A.

[a]Pearson's Chi-squared test.

[b]Undetermined or unknown due to absence of ultrasound or quality sufficient to evaluate.

[c]Total triiodothyronine (TT3; nmol/L); Total tetraiodothyronine (TT4; nmol/L); Free thyroxine (FT4; pmol/L).

[d]Interquartile range (IQR) reported here as: (25th, 75th percentile).

[e]Wilcoxon rank sum test.

TT4 in supplemented animals that may also vary in rates of consumption.

Testing methods for TT4 were changed during the timeframe of this research from RIA to CLIA due to assay kit availability. To examine the usefulness of this new test in comparison to the validated RIA, comparisons were conducted on the same samples, where available ($N = 54$). No correlation was found between the two methods ($r^2 = -0.015$). Additionally, CLIA values did not repeat well with the same samples when resubmitted. It is unclear why the repeat samples were not consistent but antisera differences or interference factors within the sample matrix are suspected (6, 63, 64).

These findings overall suggest that only TT4 and TT3 of the current RIA assay have potential value with the assay modifications as described. Using the assay 'as is', TT4 and TT3 (without increased sample volume) low values near zero may not mean hypothyroidism, and values that are readable (e.g., elevated TT4 and FT4), may indicate a problem. When disease progressed to a severe category, TT3 concentrations dropped to near baseline. TT4 CLIA results were questionable, and further research should be conducted to validate it.

4.2 Is serum iodine a good proxy for thyroid health?

Considering that iodide deficiency is the most likely cause of thyroid enlargement and at the time when this study was initiated, with near zero thyroid hormone results in nearly all samples, serum iodine seemed a plausible tool to explore for deficiency and as a proxy potentially for goiters. There are well established connections between acute iodide loads and thyroid inhibition known as the Wolff-Chaikoff effect (65). Total iodine (including unbound and protein-bound forms) and inorganic iodine (unbound only) were run on serum to establish some baselines and also to see if there were changes related to disease. Wild SRs (considered normal) were compared to semi-wild lagoon-housed SR (natural sea water but nutritionally managed) and closed system aquarium-housed SR, that was overrepresented with reproductive disease. In general, serum iodine levels of <20 ng/mL are abnormally low and 20–40 ng/mL questionably low, while 40–400 ng/mL seems to be a range consistent with a healthy animal. The wild SR stood out with iodine values in the 300 ng/mL range and this is likely because of a diet rich in natural iodine [crustaceans, seaweed, etc. (66,

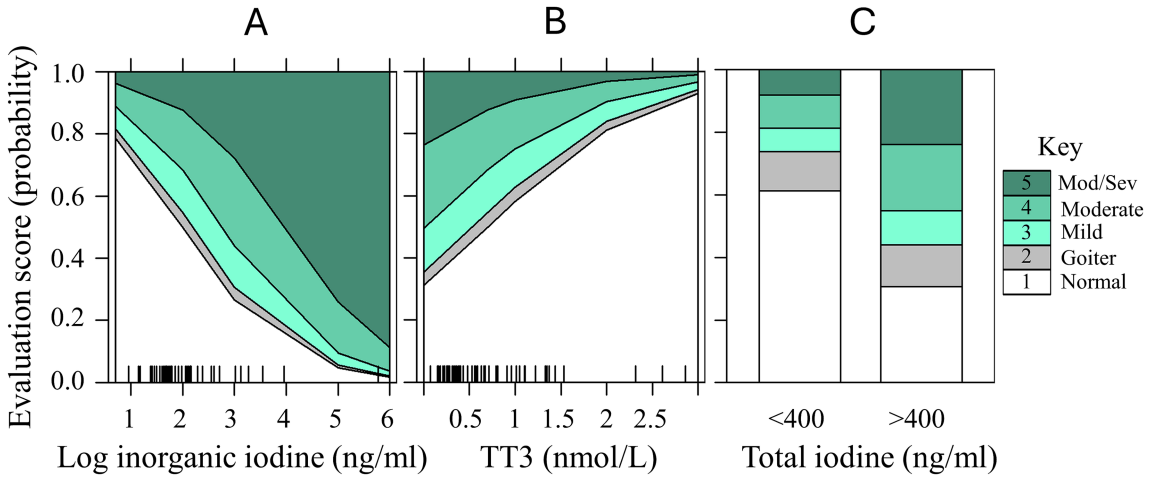

FIGURE 7
Predictor effects plots with cumulative probability estimates for increasing severity in elasmobranch thyroid evaluation disease (scores 1 through 5; normal through moderate/severe) for predictor variables in ordinal regression Model 1: **(A)** log inorganic iodine (ng/ml); **(B)** TT3 (nmol/L); and for Model 2: **(C)** Total iodine <400 and > 400 ng/mL. Rug plots on the x-axes represent the marginal distribution of the numeric predictors (panels **A,B**). Data from aquarium-managed Study 2 cohort only.

67)]. Conversely, lagoon-housed SR did not have access to high volumes of natural foods and were fed a managed diet while living in natural sea water. Their diet however differed from aquarium-housed SR in that they did not receive a supplement and only a gel diet offered with low levels of iodine and cobalt.

High iodine values (>400 ng/mL) were frequently identified and associated with a negative health status and abnormal thyroid appearance. In practice, the authors recommend any serum values above 200 ng/mL prompt an evaluation of the animal and its history, thyroid appearance, and any comorbidities. A possible outcome might be a reduction of supplement in a mg/kg of fish or a reduction of frequency per week. Extant supplements that a majority of aquaria use have a moderate amount of iodide in their formulations although this has decreased over the last several years. Others have suggested that the typical level of iodide offered to elasmobranchs is more than required to balance a deficient diet (37, 68).

Serum total and inorganic iodine values in wild SR ranged from 177 to 307 ng/mL, and 32 to 48 ng/mL (respectively). In the lagoon-housed SR, values were lower than expected. These animals were exposed to natural iodide in natural sea water and minor amounts in the diet, but they were not supplemented. Neither of these groups had any thyroid abnormalities identified on physical exam or ultrasound. In the overall dataset including aquarium held animals, there were some very high values of iodine (Figure 2). Levels of supplement correlated with serum levels: if there were higher levels of dietary iodine, this tended to correlate with greater serum iodine levels. Animals that reliably accepted and consumed supplements were documented with elevated iodine levels compared to individuals that did not (pers experience Mylniczenko). One cohort had reproductive disease and abnormally high levels of iodine (>2000 ng/mL, unpublished) (22). Those individuals had all supplementation removed (oral and water sources) for more than a year to observe serum levels of iodine over time as well as thyroid size and shape. Iodine levels dropped but took several weeks to months, suggesting accumulation and slow excretion rate (69), yet the thyroid never enlarged although showed abnormal architecture. This prompted a smaller investigation in healthy animals given one dose of supplement (70) that showed iodine peaked at 24 h and declined over 72 h. This suggests that repeated dosing at an interval less than 72 h may result in accumulation, helping at least in part to explain higher levels of iodine.

This finding highlighted that accumulated iodine levels take a long period of time to reduce and even with seemingly low levels, not all species develop goiters. In contrast, eagle rays not receiving supplements developed a goiter by 6 months post birth. Similarly, bamboo sharks developed goiters 2 months after removal of supplements (52). The water systems they were in were ozonated, making iodide absorption and use from water improbable (50). This is likely due to the assumption that any iodide that comes in contact with ozonated water, potentially even within the digestive tract, would react to become biologically unavailable in the form of iodate (50, 71).

It is tempting to recommend normal ranges or exact cut-offs for low serum iodine to facilitate diagnosis of goiters. However, lagoon-housed SR had both low serum values and low dietary iodine, with only the natural sea water providing biologically available iodine and they did not develop goiters. Iodine can be both absorbed and excreted through renal clearance at a variable rate dependent on species and the presence of other nutrients such as chloride, so the ocean's bioavailable iodide may be processed differently than in an aquarium setting with faster clearance (12, 72, 73). In the few animals with confirmed goiters, those individuals were not on any supplements prior to diagnosis (pups under observation). Once a goiter was identified, either by gross appearance or ultrasound, supplementation was started and the goiter was resolved.

Hyperiodinism, as shown here, has not really been considered a problem of elasmobranchs. It has been suggested that 'excess' waterborne iodide did not change serum T3 and T4 (RIA) concentrations in white tip reef sharks relative to TT3 and TT4 (EIA) when compared to ranges reported in wild-caught Atlantic stingrays (*H. sabina*) (49, 57, 58) and trout (74). This direct comparison is challenged by the variability in

delivery method, sample processing, antisera, assay methodology and sensitivity (free vs. total T3 or T4: RIA vs. EIA). The authors suggested no negative consequence from high iodide and concluded that they are insensitive to excess iodide. This is contrary to literature across species which does suggest iodine in excess can cause problems. Excess iodine can lead to thyroid dysfunction resulting in either hyperthyroidism as well as hypothyroidism (65, 75), thyroiditis, and goiter development (76). In some mammals, iodide can cause toxicity resulting in mortality of young animals, prolonged parturition, and other signs (75, 77). In birds, excessive iodine can cause reduced egg production by directly inhibiting ovulation (78, 79). Additionally, at least in fish, the 'insensitivity' to iodide was tested in short term high exposure, vs. chronic exposure. In the data presented here, iodine is shown to correlate with consumption, length of time on supplements, and disease state (reproductive disease and abnormal thyroid tissue findings). Some of the levels identified in this paper suggest that iodine may be stored in the body outside of the thyroid gland, allowing for later release, as has been documented in other species (80, 81). Iodine may vary in non-thyroid storage sites across species. It accumulates in bile (80) as well as ova (82) and in some of the animals reported here, follicular iodine was interpreted as high (~9,000–10,000 ng/mL compared to same day serum of >8,000 ng/mL; unpublished) in animals with reproductive disease (characterized by follicular stasis or retention). Normal comparisons are still necessary. In a recent paper on iodinated contrast in catshark (*Scyliorhinus torazame*) computed tomography scans, iodine was seen to accumulate in the gallbladder peaking at day 6 and ovary showing high values at day 260 post administration (83). This storage capacity may help explain some of the high values seen in the current study. It is unclear in males if there is a different level of accumulation as abnormal animals in this study were predominantly female (females comprised 81.7% of individuals & 87.2% of study samples; see Supplementary Table S1). Iodide, in excess, has been labeled as an endocrine disruptor with the thyroid as the main target (84). Additionally, excess iodine has been linked with hyperthyroidism and arrested ovulation which fits with several of the cases here (85). Clearly this is an area of much needed research for this particular disease process (6).

Serum iodine in normal thyroid SR showed a lot of variability with the wild group having higher inorganic iodine relative to the lagoon- and aquarium-housed SR conspecifics. This is likely because of access to iodine rich prey and plant material. In this study, there were not many true goiters to derive any ranges in order to offer diagnostic values for identifying risk of goiter. In fact, the lagoon-housed SR, which were in similar habitats to wild SR (natural sea water environment) had moderately lower iodine values and also showed no evidence of goiter formation evidenced by ultrasonography. These animals do not have access to the diversity of prey species as they are managed in an enclosed lagoon and are fed a prepared diet of shrimp, squid and gel that has a minor amount of iodine present. It is possible that the clearance rate of iodine in the lagoon population is high, but access to biologically available water iodide offers a physiologically appropriate level to prevent goiters.

This current data supports the need to provide supplementation to prevent classic colloidal goiters in elasmobranchs. It also highlights the need to reevaluate the current levels and frequency of recommended supplementation as the physiologic levels of some key elements are elevated over what seems required. While species specific data would be ideal for iodine and trace mineral panels, it seems unlikely that the proposed ranges vary significantly from species to species. Additionally, given the association with both thyroid pathology and reproductive disease in many species further investigation is truly warranted.

Iodine may serve as an indicator for thyroid health, but only for elevated thyroid hormones ('hyperthyroidism'). Iodine levels in managed animals over 400 ng/mL (the upper limit of what wild animals showed) indicate an abnormal status. We recommend levels above 200 ng/mL prompt a recheck and comparison to thyroid ultrasound, often resulting in a reduction of supplement dose and/or increased interval in between dosing. Perhaps mature females require different levels of supplement. The data here suggests that hypothyroidism cannot be conclusively connected to low thyroid levels or low iodine, without corresponding clinical information (overt swelling or ultrasound). Further attention should be considered for long term effects in aquarium populations.

4.3 What is the role of cobalt in elasmobranchs?

Serum cobalt was markedly elevated in aquarium-housed animals compared to wild and lagoon-housed SR counterparts; and higher when total iodine was greater than 400 ng/mL. Comparable studies note values of 1.3–2.6 ng/mL in wild sand tiger sharks (*Carcharias taurus*) (86) and 24.9–180.7 ng/mL in aquarium smooth dogfish (*Mustelus canis*) (87). In the current dataset values ranged from 4.2–2,818.9 ng/mL with the highest belonging to aquarium animals.

Cobalt is known to be stored in the thyroid (88, 89) and in excess has been reported as both causing hypothyroidism (with histologic changes in the thyroid) and having adverse reproductive effects (testicular atrophy and alteration of ovarian function) (90, 91). Cobalt serves as a goitrogen with excessive intake in humans, inhibiting normal iodine uptake by the thyroid, which in turn creates excess iodine, inhibiting thyroid activity (37, 92). Cobalt functions as a systemic radical when unbound by albumin, by generating reactive oxygen species involved with lipid peroxidation (93). In the elasmobranch that does not have albumin, there is potentially increased exposure to the 'radical' form (45, 93). We found a range of thyroid disease scores associated with the <300 and > 300 ng/mL cobalt values, including normal thyroid with high serum cobalt. Mild, moderate, and severe thyroid evaluations were almost two times more frequent when cobalt was >300 ng/mL. Chickens will alter deposition of iodine in yolk in response to feeding of cobalt supplementation (46), supporting cobalt's potential role in reproductive disease.

Cobalt is primarily used in the folate cycle in vitamin B12, with excess excreted in mammals. Orally, it has low toxicity, with 100-fold margin of safety from minimum requirements for feeding domestic species (47). Cobalt can bind iodine in systems of high iodine saturation (94, 95). Pharmacological use of cobalt impacts race horses, due to its chemical interaction with iodine, inhibiting the thyroid (96). Excess cobalt intake is documented to alter thyroid metabolism, and impact goiter development despite iodine sufficient diets in humans (97).

Cobalt was correlated with total iodine and TT3, and moderately so, with inorganic iodine, TT4 and FT4 (Figure 4), though not statistically significant. Elevated cobalt levels, as with iodine, appear

to negatively impact the health of elasmobranchs. Theoretically, abnormally elevated levels of either or both iodine and/or cobalt appear to result in thyroid dysfunction. This in turn would result in a slow progression of ovarian dysfunction culminating in reproductive disease. With a higher incidence of both iodine and cobalt in animals with reproductive disease and thyroid pathology, further investigation should be explored.

4.4 Ultrasound is a good method to assess thyroid disease

Ultrasound is a powerful tool to evaluate an organ like the thyroid where it can provide antemortem data on thyroid size and appearance. Subtle lesions can be seen as well as an enlarging gland prior to seeing outward signs of a ventral swelling. Here, ultrasound was used to tease out differences of thyroid disease, as traditional goiter was seen in only a few cases, while other thyroid pathology was seen in many cases. This allowed for some broad categorization to help understand some of the dynamics of thyroid hormone, iodine and cobalt. An in-depth study on ultrasound size, echogenic character and descriptions of lesions would be ideal but not feasible in this study. Still, it is clear that ultrasonographic changes to the thyroid correlated with disease.

The degree of disease was only generally categorized. Further research and characterization may be worthwhile. Hormone and iodine levels were correlated with subjective evaluation of disease. Causality is difficult, but (as evidenced in the range of values observed in the aquarium-housed animals with normal thyroid) it is suspected that high levels of iodine preceded thyroid pathology, and high values for an extended period of time would likely be a factor. However, given the location and appearance of the thyroid, successful ultrasonography can be challenging. Additionally, a high resolution transducer is recommended as lesions (cysts and subtle nodules) can easily be missed if the correct technique and transducer are not used.

What is unknown, is what degree of percent damage must occur to the thyroid tissue before functionality is altered. This is true in other species where it has been stated that "there is no simple correlation between morphologic lesions and resultant clinical manifestations. A multinodular goiter, for example, in one instance may be associated with normal thyroid function, in another with hyperfunction, and yet another with hypofunction" (98). Overall, ultrasound proved to be either a good adjunct to characterization of severity of disease or an indicator of disease.

4.5 Relationships of disease, thyroid hormone, iodine and cobalt

In the normal shark or ray, thyroid hormone values are low (TT3 < 3 nmol/L, TT4 < 5 nmol/L, and FT4 < 5 pmol/L; Figure 3). If animals were over supplemented or over consume (as indicated by elevated iodine and cobalt levels), all three thyroid parameters will be elevated. Paradoxically, in the most severe disease cases, TT3 dropped while TT4 and FT4 stayed elevated, which speculatively implies loss of functionality.

When looking at all the data together, high values in TT3, TT4, and FT4 positively correlated with degree of morphologic disease (either in size or thyroid lesions) and iodine with a proportional increase in cobalt until the disease became severe and then TT3 and FT4 dropped. The inorganic iodine and TT3 levels, when high, could 'predict' or specifically, be able to distinguish the moderate and moderate–severe disease categories. In the normal animals, uniformly, the iodines were low <300 with low TT4 and a TT3 of 1–3 nmol/L. An important factor is that the amounts of iodine and cobalt in the supplement decreased (by internal request), over several years. Concomitant to that is a general decrease in serum iodine and cobalt in the aquarium population. Serum cobalt was elevated when serum iodine was elevated, and over a short period of time, cobalt was proportionately higher than iodines when the supplement was initially lowered in iodine. Cobalt may take longer to reduce in the body than the iodine in this circumstance. Iodine and cobalt were also highest with females with reproductive disease, it is presumed this is due to iodine and cobalt accumulation in the ova (46, 80, 82). Low cobalt levels were found in animals with traditional goiters and in natural sea water habitats.

Goiters are a well known symptom of thyroid disease in elasmobranchs. Here it is shown that thyroid disease can present not only in enlargement of the gland, but also with lesions similar to that described in humans (8, 9). Thyroid disease was closely associated with reproductive disease in the aquarium study population. High iodine and cobalt levels were also associated with reproductive disease. Anecdotally, in the SR in this study, elevated reproductive steroid hormones concomitantly dropped when iodine levels also decreased (unpublished data). Additionally, it is worth noting that not all elasmobranchs get goiters and there are potentially species-specific susceptibilities (37).

Some changes are reversible. In the cases of classical goiters (e.g., eagle rays, *Aetobatus* spp.,), iodine supplementation indeed reversed the enlargement of the thyroid. In others, mineralizations and large cysts were not resolved over time, likely indicating permanent tissue alteration. Ultrasound would provide an excellent data set if collected over time by a uniform sonographer with high resolution linear transducers.

Limitations of this data set include a limited number of animals within species and disease categories and an inability to monitor and qualify consumption of supplementation directly in all cases. Additionally, there was a lack of a robust series of abnormal biological controls in terms of classic goiter to establish some low ranges of iodine. A future direction can include validation of TT4 CLIA especially at the test's lower detection limits. Additionally, further research can be considered into the interplay of iodine, cobalt and thyroid hormone in elasmobranchs.

5 Conclusion

1 Current available assays for thyroid hormone in elasmobranchs are not appropriate to diagnose hypothyroidism, but may be helpful for hyperthyroidism. CLIA testing for TT4 did not correlate with previous RIA values.
2 Thyroid ultrasound was an excellent method to evaluate the size of the thyroid and identify lesions within the tissue using linear transducers.
3 Thyroid disease in elasmobranchs extends beyond classic goiter development, but needs better characterization.

4 Iodine is a promising test for indicating a problem with the thyroid gland.
5 Iodine accumulates over time in elasmobranchs with overconsumption; interaction with high dietary cobalt may influence accumulation.
6 Animals with reproductive disease also had concurrent high levels of iodine and they are overrepresented in this dataset.
7 Iodine serum levels should be assessed routinely in elasmobranchs.

Author's note

There is a historical partnership between Disney and Mazuri PMI Nutrition International (whose supplement is referred to herein) for multiple patented feed products, none of which are involved in this publication.

Data availability statement

The original contributions presented in the study are included in the article/Supplementary material, further inquiries can be directed to the corresponding author.

Ethics statement

This animal study was approved by the University of Southern Mississippi Institutional Animal Care and Use Committee (18010502). Work completed by Disney's Animals Science and Environment authors was approved by Disney's Animal Care and Welfare Committee (DACWC; IR1707 and IR1807). The study was conducted in accordance with the local legislation and institutional requirements.

Author contributions

CW: Conceptualization, Data curation, Formal analysis, Methodology, Software, Validation, Visualization, Writing – original draft, Writing – review & editing. KS: Conceptualization, Data curation, Formal analysis, Investigation, Methodology, Resources, Writing – original draft, Writing – review & editing. EB: Data curation, Investigation, Writing – review & editing. CB: Data curation, Investigation, Resources, Writing – review & editing, Writing – original draft. MS: Funding acquisition, Resources, Writing – review & editing. JH: Resources, Writing – review & editing. NM: Conceptualization, Data curation, Funding acquisition, Investigation, Project administration, Resources, Writing – original draft, Writing – review & editing.

Funding

The author(s) declare that financial support was received for the research, authorship, and/or publication of this article. The authors declare that this study received funding from The Walt Disney Company. Most funding was provided internally from Disney's Animals, Science and Environment. Partial funding: Disney's Imperiled Species Conservation Program Grant, 2018, paid for the Bimini group's boat fees and some of the baseline blood processing fees, but the funder was not involved in the study design, collection, analysis, interpretation of data, the writing of this article, or the decision to submit it for publication.

Acknowledgments

The authors thank the Animal Husbandry and Animal Health teams at The Seas with Nemo and Friends at Epcot and Castaway Cay, Bahamas (Disney's Animals, Science and Environment) for all of their hard work in the feeding, care, management, handling, and welfare of the animals; as well as their skilled sample collection with special thanks to Karen Echeverria, Scott Williams, and Dr. Eduardo Valdes. We also thank the staff at the Bimini Biology Field Station Foundation for free range sample collection efforts. This study was supported in part by the Bahamas Department of Marine Resources, the National Institute of General Medical Sciences (NIGMS) Grant Number P20GM104932, and COBRE, CORE-NPN, Chemistry Research Core. Thanks to Brian Petroff, John Buchweitz, Justin Zyskowski, and Sarah Rebolloso from the Michigan State University Veterinary Diagnostic Laboratory. The authors want to acknowledge Mazuri PMI Nutrition International for being great partners in working with us to test and improve feed supplementation for better animal health.

Conflict of interest

CW, KS, CB, and NM were employed by The Walt Disney Company.

The remaining authors declare that the research was conducted in the absence of any commercial or financial relationships that could be construed as a potential conflict of interest.

Generative AI statement

The authors declare that no Gen AI was used in the creation of this manuscript.

Publisher's note

All claims expressed in this article are solely those of the authors and do not necessarily represent those of their affiliated organizations, or those of the publisher, the editors and the reviewers. Any product that may be evaluated in this article, or claim that may be made by its manufacturer, is not guaranteed or endorsed by the publisher.

Supplementary material

The Supplementary material for this article can be found online at: https://www.frontiersin.org/articles/10.3389/fvets.2025.1504527/full#supplementary-material

References

1. Sage M. The evolution of thyroidal function in fishes. *Am Zool*. (1973) 13:899–905. doi: 10.1093/icb/13.3.899

2. Dodd JM, Dodd MHI, Duggan RT. Control of reproduction in elasmobranch fishes. In: Rankin JC, Pitcher TJ, Duggan RT, editors. *Control processes in fish physiology*. London and Canberra: Croom Helm (1983). p. 221–49.

3. Anderson WG. Endocrine Systems in Elasmobranchs. In: Shadwick RE, Farrell AP, Brauner CJ, editors. *Physiology of elasmobranch fishes: Internal processes*. London: Elsevier Inc., (2015). p. 457–530.

4. Power DM, Llewellyn L, Faustino M, Nowell MA, Björnsson BT, Einarsdóttir IE, et al. Thyroid hormones in growth and development of fish. *Comp Biochem Physiol Part C Toxicol Pharmacol*. (2001) 130:447–59. doi: 10.1016/S1532-0456(01)00271-X

5. Deal CK, Volkoff H. The role of the thyroid Axis in fish. *Front Endocrinol*. (2020) 11:596585. doi: 10.3389/fendo.2020.596585

6. Mylniczenko ND, Sumigama S, Wyffels JT, Wheaton CJ, Guttridge TL, DiRocco S, et al. Ultrasonographic and hormonal characterization of reproductive health and disease in wild, semiwild, and aquarium-housed southern stingrays (*Hypanus americanus*). *Am J Vet Res*. (2019) 80:931–42. doi: 10.2460/ajvr.80.10.931

7. Duarte-Guterman P, Navarro-Martín L, Trudeau VL. Mechanisms of crosstalk between endocrine systems: regulation of sex steroid hormone synthesis and action by thyroid hormones. *Gen Comp Endocrinol*. (2014) 203:69–85. doi: 10.1016/j.ygcen.2014.03.015

8. Crow GL, Luer WH, Harshbarger JC. Histological assessment of goiters in elasmobranch fishes. *J Aquat Anim Health*. (2001) 13:1–7. doi: 10.1577/1548-8667(2001)013<0001:HAOGIE>2.0.CO;2

9. Ostrander GK, Cheng KC, Wolf JC, Wolfe MJ. Shark cartilage, Cancer and the growing threat of pseudoscience. *Cancer Res*. (2004) 64:8485–91. doi: 10.1158/0008-5472.CAN-04-2260

10. Garner MM. A retrospective study of disease in elasmobranchs. *Vet Pathol*. (2013) 50:377–89. doi: 10.1177/0300985813482147

11. Allain P, Berre S, Krari N, Laine-Cessac P, Le Bouil A, Barbot N, et al. Use of plasma iodine assay for diagnosing thyroid disorders. *J Clin Pathol*. (1993) 46:453–5. doi: 10.1136/jcp.46.5.453

12. Schöne F, Zimmermann C, Quanz G, Richter G, Leiterer M. A high dietary iodine increases thyroid iodine stores and iodine concentration in blood serum but has little effect on muscle iodine content in pigs. *Meat Sci*. (2006) 72:365–72. doi: 10.1016/j.meatsci.2005.08.017

13. Yu S, Wang D, Cheng X, Zhang Q, Wang M. Establishing reference intervals for urine and serum iodine levels: a nationwide multicenter study of a euthyroid Chinese population. *Clin Chim Acta*. (2020) 502:34–40. doi: 10.1016/j.cca.2019.11.038

14. Gorbman A, Lissitzky S, Michel R, Roche J. Thyroidal metabolism of iodine in the shark *Scyliorhinus (Scyllium) canicula*. *Endocrinology*. (1952) 51:311–21. doi: 10.1210/endo-51-4-311

15. Gorbman A. Some aspects of the comparative biochemistry of iodine utilization and the evolution of thyroidal function. *Physiol Rev*. (1955) 35:336–46. doi: 10.1152/physrev.1955.35.2.336

16. Allain P, Mauras Y, Dougé C, Jaunault L, Delaporte T, Beaugrand C. Determination of iodine and bromine in plasma and urine by inductively coupled plasma mass spectrometry. *Analyst*. (1990) 115:813–5. doi: 10.1039/AN9901500813

17. Lopez-Rodriguez MF, Cymbaluk NF, Epp T, Laarveld B, Thrasher M, Card CE. A field study of serum, colostrum, Milk iodine, and thyroid hormone concentrations in postpartum draft mares and foals. *J Equine Vet*. (2020) 90:103018. doi: 10.1016/j.jevs.2020.103018

18. Jin X, Jiang P, Liu L, Jia Q, Liu P, Meng F, et al. The application of serum iodine in assessing individual iodine status. *Clin Endocrinol*. (2017) 87:807–14. doi: 10.1111/cen.13421

19. Taurog A, Chaikoff I. On the determination of plasma iodine. *J Biol Chem*. (1946) 163:313–22. doi: 10.1016/S0021-9258(17)41373-1

20. Tudoreanu L, Vişoiu G, Crivineanu V. Reference ranges of minerals, thyroid hormones and TSH in canine blood serum. *Bull Univ Agric Sci Vet Med Cluj-Napoca Vet Med*. (2015) 72:183–4. doi: 10.15835/buasvmcn-vm:10480

21. Nachreiner RF, Refsal KR, Petroff B, Brudvig J. *Endocrinology reference ranges*. Lansing, MI: Michigan State University Veterinary Diagnostic Laboratory (2024). Available from: https://cvm.msu.edu/assets/documents/VDL/Endocrinology-Reference-Ranges.pdf

22. Mylniczenko ND, Wyffels J, Penfold LM. Progress in Understanding Reproductive Disease is Southern Stingrays (*Dasyatis americana*). Atlanta, GA: American Association of Zoo Veterinarians (2016).

23. Williams SM, Sullivan KE, Livingston S, Valdes EV, Mylniczenko ND. Short term impact of a single dose of iodine supplementation on serum iodine in black blotched stingrays (*Taeniura meyeni*). In: Brooks M, Freel T, Koutsos E, editors. *Proceedings of the Thirteenth Conference on Zoo and Wildlife Nutrition, Zoo and Wildlife Nutrition Foundation and AZA Nutrition Advisory Group*. St. Louis, MO. (2019).

24. Meadows MH. Examining spatial and trophic ecology of Bahamian stingrays, *Styracura schmardae* and *Hypanus americanus*, using stable isotope analysis [Doctoral dissertation]. [United Kingdom]: University of Exeter; (2018).

25. Tagawa M, Hirano T. Changes in tissue and blood concentrations of thyroid hormones in developing chum salmon. *Gen Comp Endocrinol*. (1989) 76:437–43. doi: 10.1016/0016-6480(89)90140-8

26. Tagawa M, Hirano T. Presence of thyroxine in eggs and changes in its content during early development of chum salmon, (*Oncorhynchus keta*). *Gen Comp Endocrinol*. (1987) 68:129–35. doi: 10.1016/0016-6480(87)90068-2

27. Leatherland JF, Lin L, Down NE, Donaldson EM. Thyroid hormone content of eggs and early developmental stages of five *Oncorhynchus* species. *Can J Fish Aquat Sci*. (1989) 46:2140–5. doi: 10.1139/f89-264

28. Sweeting RM, Eales JG. HPLC analysis of in vitro hepatic deiodination products of thyroid hormones in the rainbow trout, (*Oncorhynchus mykiss*). *Gen Comp Endocrinol*. (1992) 85:367–75. doi: 10.1016/0016-6480(92)90081-T

29. Gika H, Lämmerhofer M, Papadoyannis I, Lindner W. Direct separation and quantitative analysis of thyroxine and triiodothyronine enantiomers in pharmaceuticals by high-performance liquid chromatography. *J Chromatogr B*. (2004) 800:193–201. doi: 10.1016/j.jchromb.2003.07.005

30. Wasser SK, Azkarate JC, Booth RK, Hayward L, Hunt K, Ayres K, et al. Non-invasive measurement of thyroid hormone in feces of a diverse array of avian and mammalian species. *Gen Comp Endocrinol*. (2010) 168:1–7. doi: 10.1016/j.ygcen.2010.04.004

31. Wheaton CJ, Mylniczenko ND, Rimoldi JM, Gadepalli RSVS, Hart R, O'Hara BR, et al. Challenges, pitfalls and surprises: development and validation of a monoclonal antibody for enzyme immunoassay of the steroid 1α-hydroxycorticosterone in elasmobranch species. *Gen Comp Endocrinol*. (2018) 265:83–9. doi: 10.1016/j.ygcen.2018.01.028

32. Wahlen R, Evans L, Turner J, Hearn R. The use of collision/reaction cell ICP-MS for the determination of elements in blood and serum samples. (2005) 20:84–9.

33. Mylniczenko ND, Culpepper EE, Clauss T. Diagnostic imaging of elasmobranchs: updates and case examples. In: *The elasmobranch husbandry manual II*. Columbus, Ohio: Ohio Biological Survey, Inc. (2017). p. 303–24.

34. Volkoff H. The thyroid gland of elasmobranch fishes: Structure, function and relations to reproduction and development [Ph. D. Thesis]. Clemson University; (1996).

35. Richman DM, Frates MC. Ultrasound of the Normal thyroid with technical pearls and pitfalls. *Radiol Clin North Am*. (2020) 58:1033–9. doi: 10.1016/j.rcl.2020.06.006

36. Lee MK, Na DG, Joo L, Lee JY, Ha EJ, Kim JH, et al. Standardized imaging and reporting for thyroid ultrasound: Korean Society of Thyroid Radiology Consensus Statement and Recommendation. *Korean J Radiol*. (2023) 24:22–30. doi: 10.3348/kjr.2022.0894

37. Crow GL. Goiter in elasmobranchs. In: Smith M, Warmolts D, Thoney D, Hueter R, editors. *The elasmobranch husbandry manual: Captive care of sharks, rays and their relatives*. Columbus, Ohio: Ohio Biological Survey, Inc. (2004). p. 441–6.

38. R Core Team. R: A language and environment for statistical computing. Vienna, Austria: R Foundation for Statistical Computing (2023).

39. Wood M. Statistical inference using bootstrap confidence intervals. *Significance*. (2004) 1:180–2. doi: 10.1111/j.1740-9713.2004.00067.x

40. Wei T, Simko V. *"R package 'corrplot': visualization of a correlation matrix." Version 0.92*. (2021). Available at: https://github.com/taiyun/corrplot

41. Harrell Jr FE. *Harrell Miscellaneous [R package Hmisc version 5.1-1]. Comprehensive R Archive Network (CRAN)*. (2023). Available at: https://CRAN.R-project.org/package=Hmisc

42. Friendly M. Corrgrams: exploratory displays for correlation matrices. *Am Stat*. (2002) 56:316–24. doi: 10.1198/000313002533

43. Fox J, Hong J. Effect displays in *R* for multinomial and proportional-odds logit models: extensions to the effects package. *J Stat Softw*. (2009) 32:1–24. doi: 10.18637/jss.v032.i01

44. Fox J, Weisberg S. Visualizing fit and lack of fit in complex regression models with predictor effect plots and partial residuals. *J Stat Softw*. (2018) 87:1–27. doi: 10.18637/jss.v087.i09

45. Ćwiertnia A, Kozłowski M, Cymbaluk-Płoska A. The role of Iron and cobalt in gynecological diseases. *Cells*. (2022) 12:117. doi: 10.3390/cells12010117

46. Aghdashi MN, Nobakht A, Mehmannavaz Y. Laying hen performance and yolk iodine, cobalt and iron content increased by dietary supplementation of potassium iodide. *Vitamin B12* and *Ferrous Sulfate*. (2021). PREPRINT (Version 1). Available at Research Square [https://doi.org/10.21203/rs.3.rs-485188/v1].

47. Suttle N. Copper In: Mineral nutrition of livestock. *5th* ed. GB: CABI (2022). 259–300.

48. Bojunga J. Ultrasound of thyroid nodules. *Ultraschall Med-Eur J Ultrasound*. (2018) 39:488–511. doi: 10.1055/a-0659-2350

49. Crow GL, Atkinson MJ, Ron B, Atkinson S, Skillman ADK, Wong GTF. Relationship of water chemistry to serum thyroid hormones in captive sharks with Goitres. *Aquat Geochem*. (1998) 4:469–80. doi: 10.1023/A:1009600818580

50. Sherrill J, Whitaker BR, Wong GTF. Effects of ozonation on the speciation of dissolved iodine in artificial seawater. *J Zoo Wildl Med*. (2004) 35:347–55. doi: 10.1638/03-025

51. Morris AL, Hamlin HJ, Francis-Floyd R, Sheppard BJ, Guillette LJ. Nitrate-induced goiter in captive Whitespotted bamboo sharks *Chiloscyllium plagiosum*. *J Aquat Anim Health*. (2011) 23:92–9. doi: 10.1080/08997659.2011.574079

52. Morris AL, Stremme DW, Sheppard BJ, Walsh MT, Farina LL, Francis-Floyd R. The onset of goiter in several species of sharks following the addition of ozone to a touch pool. *J Zoo Wildl Med*. (2012) 43:621–4. doi: 10.1638/2010-0160R2.1

53. Parkinson L, Noblitt SD, Campbell T, Sladky K. Comparison of two iodine quantification methods in an artificial seawater system housing white-spotted bamboo sharks (*Chiloscyllium plagiosum*). *J Zoo Wildl Med*. (2018) 49:952–8. doi: 10.1638/2017-0005.1

54. Stoskopf MK. Fish medicine. Philadelphia, PA: W.B. Saunders Co. (1993) p. 882.

55. Leatherland JF. Reflections on the thyroidology of fishes: from molecules to humankind. *Guelph Ichthyol Rev*. (1994) 2:1–67.

56. Brown S, Eales J. Measurement of L-thyroxine and 3, 5, 3′-triiodo-L-thyronine levels in fish plasma by radioimmunoassay. *Can J Zool*. (1977) 55:293–9. doi: 10.1139/z77-039

57. Crow GL, Ron B, Atkinson S, Rasmussen LEL. Serum T4 and serum T3 concentrations in immature captive whitetip reef sharks. *Triaenodon obesus J Exp Zool*. (1999) 284:500–4. doi: 10.1002/(SICI)1097-010X(19991001)284:5<500::AID-JEZ5>3.0.CO;2-J

58. Volkoff H, Wourms JP, Amesbury E, Snelson FF. Structure of the thyroid gland, serum thyroid hormones, and the reproductive cycle of the Atlantic stingray. *Dasyatis sabina J Exp Zool*. (1999) 284:505–16. doi: 10.1002/(SICI)1097-010X(19991001)284:5<505::AID-JEZ6>3.0.CO;2-1

59. Gash TA. Seasonal thyroid activity in the bonnethead shark, *Sphyrna tiburo* [Doctoral dissertation/PhD diss]. Texas A& M University; (2000).

60. McComb DM, Gelsleichter J, Manire CA, Brinn R, Brown CL. Comparative thyroid hormone concentration in maternal serum and yolk of the bonnethead shark (*Sphyrna tiburo*) from two sites along the coast of Florida. *Gen Comp Endocrinol*. (2005) 144:167–73. doi: 10.1016/j.ygcen.2005.05.005

61. Rangel BDS, Moreira RG, Niella YV, Sulikowski JA, Hammerschlag N. Metabolic and nutritional condition of juvenile tiger sharks exposed to regional differences in coastal urbanization. *Sci Total Environ*. (2021) 780:146548. doi: 10.1016/j.scitotenv.2021.146548

62. Leary SC, Ballantyne JS, Leatherland JF. Evaluation of thyroid hormone economy in elasmobranch fishes, with measurements of hepatic 5′-monodeiodinase activity in wild dogfish. *J Exp Zool*. (1999) 284:492–9. doi: 10.1002/(SICI)1097-010X(19991001)284:5<492::AID-JEZ4>3.0.CO;2-A

63. Martin B. Steroid-protein interactions in nonmammalian vertebrates. *Gen Comp Endocrinol*. (1975) 25:42–51. doi: 10.1016/0016-6480(75)90037-4

64. Selby C. Interference in immunoassay. *Ann Clin Biochem Int J Lab Med*. (1999) 36:704–21. doi: 10.1177/000456329903600603

65. Leung AM, Braverman LE. Consequences of excess iodine. *Nat Rev Endocrinol*. (2014) 10:136–42. doi: 10.1038/nrendo.2013.251

66. Sprague M, Chau TC, Givens DI. Iodine content of wild and farmed seafood and its estimated contribution to UK dietary iodine intake. *Nutrients*. (2021) 14:195. doi: 10.3390/nu14010195

67. Roseland JM, Spungen JH, Patterson KY, Ershow AG, Gahche JJ, Pehrsson PR. *USDA, FDA, and ODS-NIH Database for the Iodine Content of Common Foods [Internet]*. (2022). Available from: https://www.ars.usda.gov/ARSUSERFILES/80400535/DATA/IODINE/IODINE%20DATABASE_RELEASE_2_DOCUMENTATION.PDF

68. Stoskopf M. Shark diagnostics and therapeutics: A short review. *J. Aquac. Aquat. Sci.* (1990) 5:33–43.

69. Williams SM, Ardente AJ, Mylniczenko ND, Guttridge TL, Sullivan KM, Livingston S, et al. Impact of removing dietary supplementation on serum nutrient concentrations in a managed population of southern stingray (Dasyatis americana). In: *Proceedings of the Zoo and Wildlife Nutrition Foundation/ AZA Nutrition Advisory Group Twelfth Conference on Zoo and Wildlife Nutrition, September 24-27, Fresno, TX*. (2017).

70. Williams SM, Sullivan KE, Livingston S, Valdes EV, Mylniczenko ND. "Short term impact of a single dose of iodine supplementation on serum iodine in black blotched stingrays (*Taeniura meyeni*)." In: *Proceedings of the Thirteenth Conference on Zoo and Wildlife Nutrition, Zoo and Wildlife Nutrition Foundation and AZA Nutrition Advisory Group*. Saint Louis, MO; (2019).

71. Pulassery S, Abraham B, Ajikumar N, Munnilath A, Yoosaf K. Rapid iodine value estimation using a handheld Raman spectrometer for on-site, reagent-free authentication of edible oils. *ACS Omega*. (2022) 7:9164–71. doi: 10.1021/acsomega.1c05123

72. Riggs DS. Quantitative aspects of iodine metabolism in man. *Pharmacol Rev*. (1954) 6:132–1.

73. Zicker S, Schoenherr B. Focus on nutrition: the role of iodine in nutrition and metabolism. *Compend Contin Educ Vet*. (2012) 70:E1–2. doi: 10.1111/j.1753-4887.2012.00541.x

74. Eales JG, Cyr DG, Cook RF. Effect of excess iodide on thyroid function of rainbow trout, *Salmo gairdneri*. *Fish Physiol Biochem*. (1986) 1:171–7. doi: 10.1007/BF02311133

75. Bürgi H. Iodine excess. *Best Pract Res Clin Endocrinol Metab*. (2010) 24:107–15. doi: 10.1016/j.beem.2009.08.010

76. Pennington JA. A review of iodine toxicity reports. *J Am Diet Assoc*. (1990) 90:1571–81. doi: 10.1016/S0002-8223(21)01843-5

77. Arrington LR, Taylor RN, Ammerman CB, Shirley RL. Effects of excess dietary iodine upon rabbits, hamsters. *Rats and Swine J Nutr*. (1965) 87:394–8. doi: 10.1093/jn/87.4.394

78. Preedy VR, Burrow GN, Watson RR. Comprehensive handbook of iodine: Nutritional, biochemical, pathological, and therapeutic aspects. Amsterdam Boston: Elsevier/Academic Press (2009).

79. Lewis PD. Responses of domestic fowl to excess iodine: a review. *Br J Nutr*. (2004) 91:29–39. doi: 10.1079/BJN20031017

80. Leloup J, Fontaine M. Iodine metabolism in lower vertebrates. *Ann N Y Acad Sci*. (1960) 86:316–53. doi: 10.1111/j.1749-6632.1960.tb42815.x

81. Schöne F, Rajendram R. Iodine in farm animals. In: *Comprehensive Handbook of Iodine [Internet]*. Elsevier (2009) 151–70. Available from: https://linkinghub.elsevier.com/retrieve/pii/B9780123741356000169

82. Mathews DM, Johnson NP, Sim RG, O'Sullivan S, Peart JM, Hofman PL. Iodine and fertility: do we know enough? *Hum Reprod*. (2021) 36:265–74. doi: 10.1093/humrep/deaa312

83. Ito T, Furuya M, Tanaka T, Yoshii Y, Murata M, Sasai K. Long-term effects of iopamidol as a contrast medium for computed tomography in cloudy catsharks *Scyliorhinus torazame*. *J Aquat Anim Health*. (2024) 36:239–49. doi: 10.1002/aah.10219

84. Karbownik-Lewińska M, Stępniak J, Iwan P, Lewiński A. Iodine as a potential endocrine disruptor—a role of oxidative stress. *Endocrine*. (2022) 78:219–40. doi: 10.1007/s12020-022-03107-7

85. Mahapatra D, Chandra AK. Biphasic action of iodine in excess at different doses on ovary in adult rats. *J Trace Elem Med Biol*. (2017) 39:210–20. doi: 10.1016/j.jtemb.2016.10.006

86. Hoopes LA, Clauss T, Wetherbee BM, Fox DA. Baseline health and nutritional parameters of wild sand tigers sampled in Delaware Bay. *J Aquat Anim Health*. (2022) 34:101–15. doi: 10.1002/aah.10156

87. Persky ME, Williams JJ, Burks RE, Bowman MR, Ramer JC, Proudfoot JS. Hematologic, plasma biochemistry, and select nutrient values in captive smooth dogfish (*Mustelus canis*). *J Zoo Wildl Med*. (2012) 43:842–51. doi: 10.1638/2012-0002R1.1

88. Brewer K, Maylin GA, Fenger CK, Tobin T. Cobalt use and regulation in horseracing: a review. *CEP*. (2016) 12:1–10. doi: 10.3920/CEP140008

89. Lantin AC, Mallants A, Vermeulen J, Speybroeck N, Hoet P, Lison D. Absence of adverse effect on thyroid function and red blood cells in a population of workers exposed to cobalt compounds. *Toxicol Lett*. (2011) 201:42–6. doi: 10.1016/j.toxlet.2010.12.003

90. Finley BL, Monnot AD, Paustenbach DJ, Gaffney SH. Derivation of a chronic oral reference dose for cobalt. *Regul Toxicol Pharmacol*. (2012) 64:491–503. doi: 10.1016/j.yrtph.2012.08.022

91. Paksy K, Olajos F, Tóth BE, Náray M, Tátrai E, Huszár L. Uptake and distribution of Cobakt in rat ovaries and pituitary: acute effects of cobalt on Preovulatory luteinizing hormone, follicle stimulating hormone, prolactin and progesterone levels, and on ovulation in rats. *Cent Eur J Occup Environ Med*. (1999) 5:313–23.

92. Miller ER, Ammerman CB. Iodine bioavailability. In: *Bioavailability of nutrients for animals*. San Diego CA: Academic Press (1995). 157–67.

93. Leyssens L, Vinck B, Van Der Straeten C, Wuyts F, Maes L. Cobalt toxicity in humans—a review of the potential sources and systemic health effects. *Toxicology*. (2017) 387:43–56. doi: 10.1016/j.tox.2017.05.015

94. Favaudon V, Momenteau M, Lhoste JM. An unusual cobalt complex. Reaction of cobalt (II) porphyrin with iodine in apolar solvents. *Inorg Chem*. (1979) 18:2355–7. doi: 10.1021/ic50199a005

95. Butova VV, Bulanova EA, Polyakov VA, Guda AA, Aboraia AM, Shapovalov VV, et al. The effect of cobalt content in Zn/co-ZIF-8 on iodine capping properties. *Inorg Chim Acta*. (2019) 492:18–22. doi: 10.1016/j.ica.2019.04.011

96. Kinobe RT. Towards the elimination of excessive cobalt supplementation in racing horses: a pharmacological review. *Res Vet Sci*. (2016) 104:106–12. doi: 10.1016/j.rvsc.2015.12.007

97. Elizabeth K, Mohammed M, Devakumar V, Fameesh A. Goiter in pre-pubertal children despite urinary iodine sufficiency. *J Pediatr Assoc India*. (2015) 4:198–201. doi: 10.4103/2667-3592.300847

98. Robbins SL. Thyroid gland In: RS Cotran, V Kumar and SL Robbins, editors. Robbins pathologic basis of disease. Philadelphia, PA, USA: W. B. Saunders (1994). 1121–33.

frontiers | Frontiers in Veterinary Science

TYPE Case Report
PUBLISHED 10 March 2025
DOI 10.3389/fvets.2024.1463428

Check for updates

OPEN ACCESS

EDITED BY
Eric Emile Germain Clua,
USR3278 Centre de recherche insulaire et observatoire de l'environnement (CRIOBE), France

REVIEWED BY
Michael James Murray,
Monterey Bay Aquarium, United States
Ayoze Castro Alonso,
University of Las Palmas de Gran Canaria, Spain

*CORRESPONDENCE
Natalie Mylniczenko
✉ natalie.mylniczenko@disney.com

†These authors have contributed equally to this work

RECEIVED 11 July 2024
ACCEPTED 30 November 2024
PUBLISHED 10 March 2025

CITATION
Greene W, Pereira N, Doescher B, Rojo-Solis C, David H, Faustino R, Reese D, De Voe R, Latson E and Mylniczenko N (2025) Case report: Endolymphatic system disease in elasmobranchs: clinical presentation, diagnosis, and treatment strategies. *Front. Vet. Sci.* 11:1463428. doi: 10.3389/fvets.2024.1463428

COPYRIGHT
© 2025 Greene, Pereira, Doescher, Rojo-Solis, David, Faustino, Reese, De Voe, Latson and Mylniczenko. This is an open-access article distributed under the terms of the Creative Commons Attribution License (CC BY). The use, distribution or reproduction in other forums is permitted, provided the original author(s) and the copyright owner(s) are credited and that the original publication in this journal is cited, in accordance with accepted academic practice. No use, distribution or reproduction is permitted which does not comply with these terms.

Case report: Endolymphatic system disease in elasmobranchs: clinical presentation, diagnosis, and treatment strategies

Whitney Greene[1†], Nuno Pereira[2], Bethany Doescher[3], Carlos Rojo-Solis[4], Hugo David[2], Ricardo Faustino[5], David Reese[6], Ryan De Voe[7], Ed Latson[8,9] and Natalie Mylniczenko[7*†]

[1]Mote Marine Laboratory and Aquarium, Sarasota, FL, United States, [2]Oceanário de Lisboa, Esplanada D. Carlos I, Lisbon, Portugal, [3]Sea Life Park Hawaii, Waimanalo, HI, United States, [4]Oceanogràfic, Ciudad de las Artes y las Ciencias, Valencia, Spain, [5]Research Unit in Medical Imaging and Radiotherapy, Cross I&D Lisbon Research Center, Escola Superior de Saúde da Cruz Vermelha Portuguesa, Lisbon, Portugal, [6]VetCT Consultants in Telemedicine PTY LTD., Applecross, WA, Australia, [7]Disney Animals, Science and Environment, Disney's Animal Kingdom® and the Seas with Nemo and Friends®, Lake Buena Vista, FL, United States, [8]Aquarium of Niagara, Niagara Falls, NY, United States, [9]Ripley's Marine Science Center, Cheektowaga, NY, United States

The inner ear is an often overlooked system in elasmobranchs with few documented reports of disease or other abnormalities in the literature. Similar to terrestrial vertebrates, it is located in the cranium, and there are multiple components to the ear of elasmobranchs including a pair of membranous labyrinths each with three semicircular canals and four chambers or end organs (the saccule, the lagena, the utricle and the macula neglecta) making up the endolymphatic system (ELS). There is species variability among the inner ear anatomy of elasmobranchs, and this may play a role in disease development, progression, and treatment outcomes. Also similar to terrestrial vertebrates, this system plays a key role in hearing, acceleration, and orientation. When affected, clinical signs may include localized areas of swelling or stoma development along the dorsal midline of the head at the endolymphatic pores, atypical swimming behaviors consistent with vestibular disease (spiraling/spinning or barrel rolling, or tilting to one side), and anorexia. Less frequently, the eyes may also be affected and present with exophthalmia, hyphema, and/or panophthalmitis. Herein are case series from five institutions representing a variety of elasmobranch species affected with ELS disease with discussion of anatomy, clinical presentation, diagnostics, etiology, treatment, and outcomes. Endolymphatic disease may be clinically underdiagnosed in elasmobranchs and mistaken for other diseases such as superficial subcutaneous or subdermal abscesses, focal dermatitis, or neuropathies presumed to not be associated with the inner ear system. In addition, disease may be occult for a long period of time prior to overt manifestation of signs or chronic with waxing and waning clinical signs, likely because of anatomy and resultant treatment challenges. Awareness and additional research may help to promote timely identification, improve diagnostic and treatment options, and help to optimize individual animal welfare.

KEYWORDS

shark, endolymphatic pore, labyrinthitis, inner ear, otic disease, neurologic disease, neuropathy, stingray

Introduction

The inner ear is an often overlooked system in elasmobranch medicine, and there are few documented reports of disease in the literature (1–4). Clinical signs are highly varied and may include abnormal swimming patterns such as barrel rolling, spiraling, spinning, tilting to one side, nodules/abscesses in the dorsal surface of the head, anorexia, and associated ophthalmic disease such as hyphema, conjunctivitis, exophthalmia, and panophthalmitis (1, 4).

The ear of elasmobranchs is located within the caudal chondrocranium (5, 6). There are bilateral membranous labyrinths each containing three semicircular canals and four sensory maculae (7–14). Elasmobranchs only possess inner ear labyrinths and have no other accessory organs of hearing (6). There are differences between elasmobranch species with inner ear variation being characterized by three primary axes (15, 16) that are influenced by diet and habitat. Piscivorous elasmobranchs have larger inner ears compared to non-piscivorous species, and reef-associated species have larger inner ears compared to oceanic species (17). Despite a similar inner ear blueprint that is consistent among most fishes, there is considerable variation between species in the size and shape of various structures (17) with the relevant difference between terrestrials and elasmobranchs being an enlarged macula neglecta (8, 12, 18).

The only external indicator of the position of the ears is the presence of small, paired endolymphatic pores (Figure 1) found in the skin on the dorsal chondrocranium. They may or may not be easily

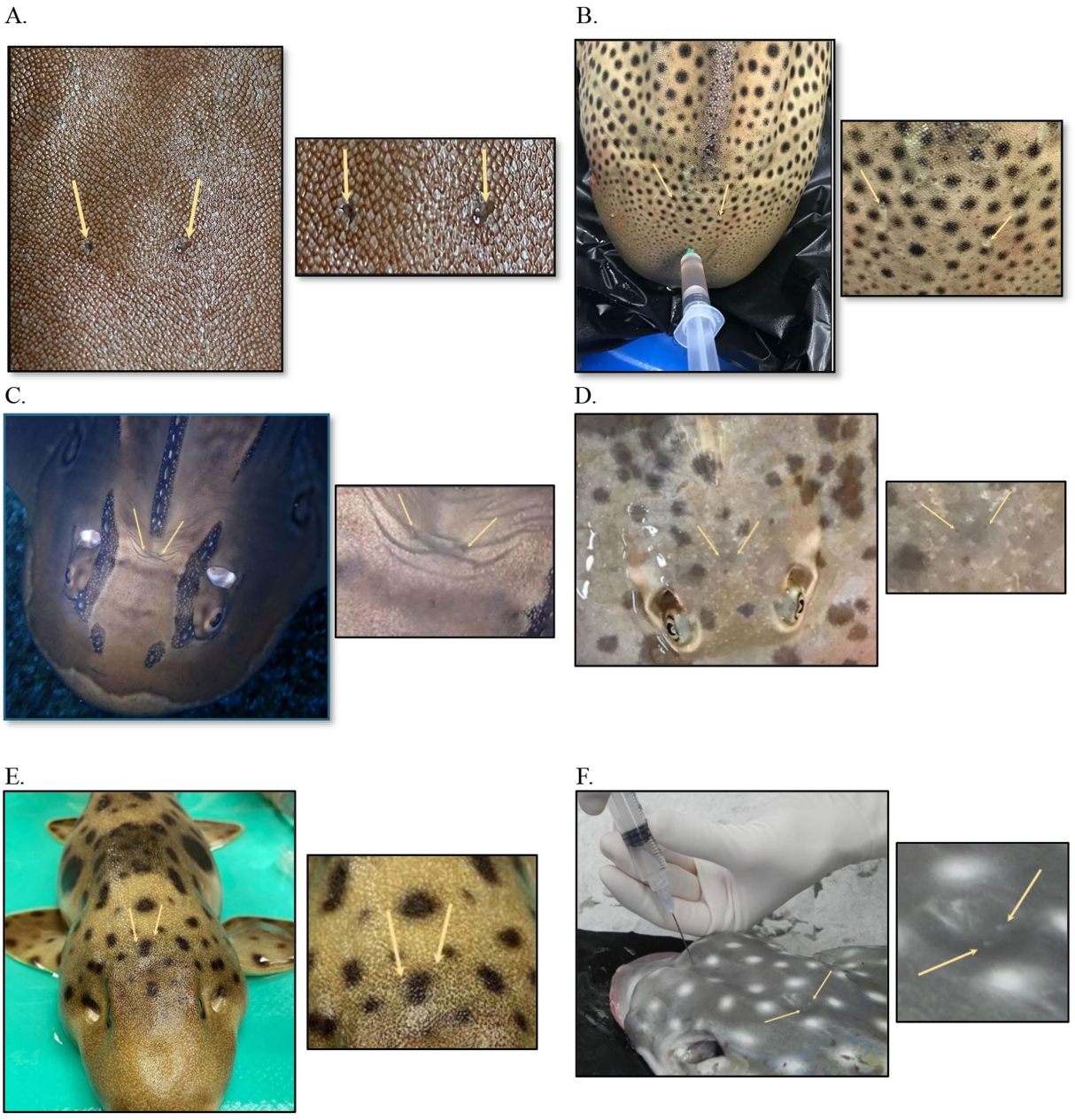

FIGURE 1
Endolymphatic pores in normal elasmobranchs. **(A)** Bamboo shark (*Chiloscyllium punctatum*), close up. **(B)** Zebra shark (*Stegostoma tigrinum*) post-mortem cerebrospinal fluid collection. **(C)** Bowmouth guitarfish (*Rhina ancylostoma*). **(D)** Chilean ray (*Urotrygon chilensis*). **(E)** Coral catshark (*Atelomycterus marmoratus*). **(F)** Spotted eagle ray (*Aetobatus narinari*) cerebrospinal fluid collection, post-mortem.

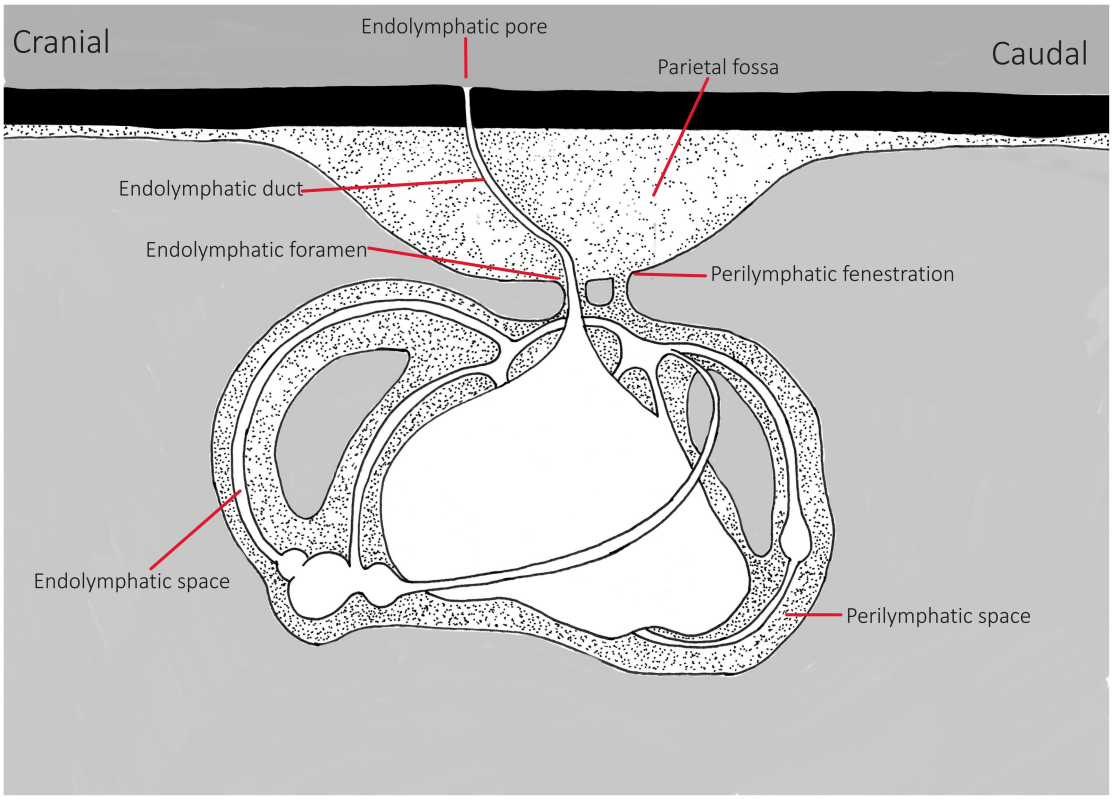

FIGURE 2
Line drawing of basic inner ear of elasmobranchs, representing general anatomy. This is a representation, differences may include variations in size/depth of the parietal fossa, in the endolymphatic duct's direction and width/volume and shape of the perilymph bathing the labyrinth within the chondrocranium and the size of the end organs. Adapted from Chang and Okihiro (5).

visible in healthy animals (5, 13, 19). The endolymphatic pores lie adjacent to one another close to the medial line, just anterior to the supratemporal canal of the lateral line (14), and they connect the inner ear to the outside environment (20) (Figure 2). Each pore leads to the inner ear via paired endolymphatic ducts (or sacs) through the parietal fossa into the endolymphatic foramen within the chondrocranium. The ducts then lead to the otic organs and are lined with small, paired muscles but overall are thin and fragile (5, 11). The fossa can be variably sized with some being spacious, such as the Triakidae (16, 21).

Within the dorsal chondrocranium, there are two perilymphatic foramina (larger ovoid holes, posteromedial to the endolymphatic ducts) that are covered by a membrane (11, 22). These lead into bilateral perilymphatic filled spaces that house the labyrinth in the otic capsule (Figure 2) (5, 11, 13, 16, 21, 23). For a clinically relevant description, Corwin (16) suggests generalized classification of the ears into two categories: "A small ventrally located sacculus, a small ventrally located posterior canal duct, a small macula neglecta, and a small lateral perilymphatic fluid space or falling into the second category, with a large triangular sacculus, a large lateral fluid space, and a large, dorsally positioned posterior canal duct containing a well-developed macula neglecta." These distinctions will have bearing on diagnosis and consideration for treatment strategies.

The endolymphatic ducts initially track rostrally and then retroflex in most species, extending ventrally and caudally in the chondrocranium (14, 23). The ducts are thin tubes that connect to the saccule. The endolymphatic ducts in some species may expand into a large sac into the fossa (11). The function of the ducts is unknown but believed to help with fluid exchange between the ear and the environment and may also function in wave displacement or for pressure equalization (14). Each vestibular chamber has an otolithic mass composed of small mineral crystals called otoconia, compacted by an organic matrix (22–24, 73). These otolithic masses are different from the solid and dense otoliths found in teleosts (13, 24, 25, 73). In some elasmobranchs, the otoconia consist of small particles of exogenous environmental sand (11, 25). There is more detailed literature on the anatomy and function of the endolymphatic system (ELS) and hearing in elasmobranchs; for brevity in this document, the readers are encouraged to further their review with these sources (5–7, 10–14, 17, 18, 20, 22–28).

In an effort to supplement the scarce literature describing clinical disease, the following series will describe the clinical signs, diagnosis, treatments, and outcomes of 23 cases of ELS disease in elasmobranchs (Table 1). These cases will be parsed into six separate case series based on the institution that oversaw the treatment and care of the individual animals. For this entire series, cases are defined by their involvement of the endolymphatic pores and surrounding structures or by direct evidence of involvement of other endolymphatic structures by imaging or pathology. Due to the complex nature of the disease and chronicity of many of these cases, salient points from their histories are listed in an effort to consolidate and discuss all of them. This disease process is likely underdiagnosed; it is the authors' goal to discuss the etiology, clinical signs, diagnostic, and treatment options to help with case identification and management.

TABLE 1 Summary table of all endolymphatic system disease cases in twenty three elasmobranchs.

Case series #	Number	Species	Gender	Age	Superficial disease only	Complex disease (neurologic)	Recurrence of clinical signs	Occurrence	Culture	Died	Euthanasia	ELD Pathology (Gross exam or imaging)	Resolution	Comments
1	1	*Rhina ancylostomus*	Male	3	N	Y	N	0	*Enterococcus faecalis*	Y	Y	Y	N	*Enterococcus faecalis* cultured from blood and aspirate samples
	2	*Rhina ancylostomus*	Male	6	N	Y	Y	1	*Enterococcus faecalis*	Y	N	Y	N	Superficial on first presentation
	3	*Urobatis jamaicensis*	Male	8	N	Y	Y	1	*Mycobacterium chelonae*	Y	N	Y	N	Superficial on first presentation; *Mycobacterium chelonae* serially cultured
	4	*Urogymnus asperrimus*	Female	6	N	Y	Y	1	Negative	N	N	Y (imaging)	Y	Superficial on first presentation
	5	*Chiloscyllium plagiosum*	Female	9	Y	N	N	0	*Enterococcus faecalis*	N	N	Y (imaging)	Y	*Enterococcus faecalis* cultured from blood and aspirate samples
2	6	*Heterodontus portusjacksoni*	Female	~4	N	Y	N	0	*Fusarium solani*	Y	N	Y	N	Died quickly
	7	*Heterodontus portusjacksoni*	Female	~6	N	Y	N	0	*Fusarium solani*	Y	N	Y	N	
	8	*Heterodontus portusjacksoni*	Female	~6	N	Y	Y	1	*Fusarium solani*	Y	N	Y	N	Superficial on first presentation
	9	*Heterodontus portusjacksoni*	Male	~6	N	Y	N	0	*Fusarium solani*	Y	N	Y	N	
	10	*Heterodontus portusjacksoni*	Male	2	N	Y	N	0	*Fusarium solani, Citrobacter braaki, Stenotrophomonas maltophilia*	Y	N	Y	N	*Fusarium solani* (abscess and brain); *Citrobacter braaki* (abscess); *Stenotrophomonas maltophilia* (brain)
	11	*Heterodontus portusjacksoni*	Male	3	N	Y	N	0	*Fusarium solani*	Y	N	Y (imaging)	N	
3	12	*Mobula hypostoma*	Male	8	N	Y	Y	1	N/A	Y	Y	Y	N	

(Continued)

10.3389/fvets.2024.1463428

TABLE 1 (Continued)

Case series #	Number	Species	Gender	Age	Superficial disease only	Complex disease (neurologic)	Recurrence of clinical signs	Occurrence	Culture	Died	Euthanasia	ELD Pathology (Gross exam or imaging)	Resolution	Comments
4	13	*Carcharias taurus*	Male	25	N	Y	Y	1	Negative	Y	N	Y	N	
	14	*Hypanus americanus*	Female	15	Y	N	N	0	N/A	N	N	N	Y	
5	15	*Carcharhinus plumbeus*	Female	7	Y	N	N	0	*Enterococcus faecalis*	Y	N	N	N	Meningitis and mild perivascular lymphoplasmacytic encephalitis
	16	*Carcharhinus plumbeus*	Female	7	Y	N	Y	1	*Enterococcus faecalis*	Y	Y	N	N	
	17	*Chiloscyllium plagiosum*	Female	4	N	Y	Y	1	*Enterococcus faecalis*	Y	Y	N	N	Signs resolved but recurred after transport to new facility
6	18	*Triaenodon obesus*	Female	3	N	Y	Y	1	*Enterococcus faecalis*	Y	N	N	Y	Resolved before death
	19	*Triaenodon obesus*	Female	4	N	Y	Y	7	*Enterococcus faecalis*	Y	Y	N	Y	Recurred seven times in three years; Resolved before death
	20	*Triaenodon obesus*	Male	2	Y	N	N	0	*Enterococcus faecalis*	Y	N	Y	N	Initially no neurologic signs, asymptomatic 5 yrs., then symptomatic. Cancer.
	21	*Triaenodon obesus*	Female	2	Y	N	Y	2	*Enterococcus faecalis; Staphylococcus epidermidis*-methicillin resistant	Y	N	N	Y	Resolved before death
	22	*Triaenodon obesus*	Female	1	Y	N	Y	5	*Enterococcus faecalis*	Y	N	N	Y	Resolved before death
	23	*Triaenodon obesus*	Female	<1	Y	N	Y	10	*Enterococcus faecalis*	N	N	N	N	Continues to recur

10.3389/fvets.2024.1463428

Case series 1

Case 1: Bowmouth guitarfish

A 3-year-old male bowmouth guitarfish (*Rhina ancylostoma*) presented acutely for abnormal swimming consisting of barrel rolling and tilting to his left side. The differentials included scuticociliosis, central nervous system (CNS) disease (meningitis/encephalitis), and ELS disease. Physical examination revealed swollen endolymphatic pores (Figure 3) with purulent debris expelled on palpation. Initial workup consisted: of debridement, culture, cytology, blood work,

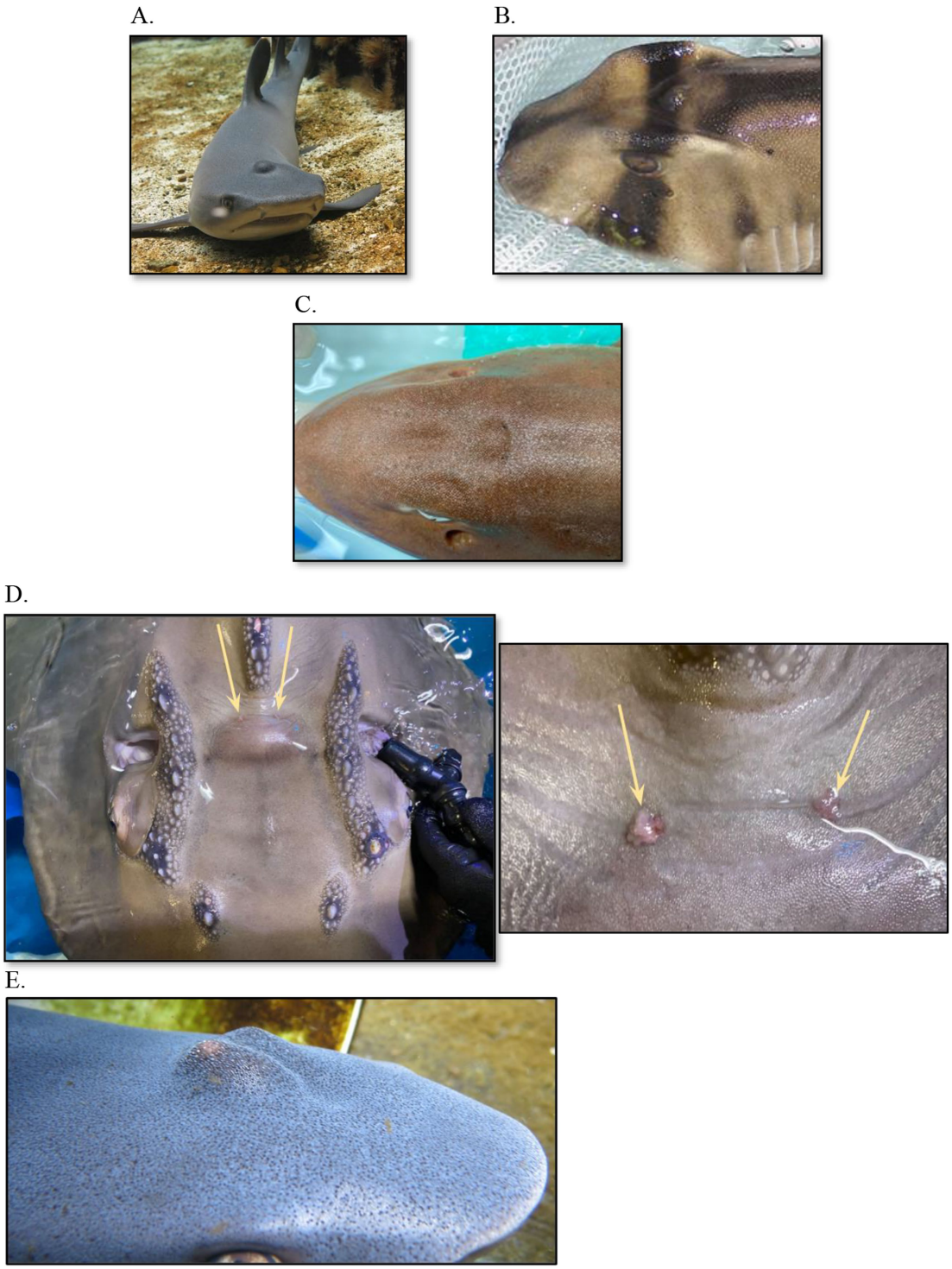

FIGURE 3
Swelling along the dorsal midline associated with endolymphatic system disease in various elasmobranch species. **(A)** White tip reef shark (*Triaenodon obesus*); **(B)** Port Jackson shark (*Heterodontus portusjacksoni*); **(C)** Bamboo shark (*Chiloscyllium punctatum*); **(D)** Bowmouth guitarfish (*Rhina ancylostoma*), zoomed out and up close; **(E)** White tip reef shark (*Triaenodon obesus*).

cerebrospinal fluid (CSF) collection, and wound treatment. Serial blood work was performed throughout treatment and was overall unremarkable although *Enterococcus faecalis* was cultured from blood and pore samples. Empirical treatment was started with metronidazole (500 mg IV and PO SID; Pfizer, New York, NY, USA), doxycycline (2.5 mg/kg PO SID; Pfizer, New York, NY, USA), fluid support (250 mL elasmobranch ringers IV SID), oxytetracycline (4.1 mg/kg IM SID; Pfizer, New York, NY, USA), ketoprofen (6 mg/kg IV SID; Ketofen®, Zoetis, Parsippany-Troy Hills, NJ, USA), and meclizine (0.5 mg/kg PO SID; Trigen Laboratories, 2,631 Causeway Center Dr., Tampa, FL, USA). The guitarfish initially improved clinically (increased appetite and decrease in clinical signs) on this treatment but then began to subsequently decline. Secondary wounds developed along the ventral surface and fins, and additional neurologic signs presented (increased spinning frequency and severity). Metronidazole drug levels were found to be high at 96 µg/mL (29, 30) on day 6 of treatment coincident with these increased neurologic signs (Table 2). Metronidazole was discontinued, misoprostol and phenytoin powder (LS Polyox puffer 5 g per gram; Wedgewood Pharmacy, Swedesboro, NJ, USA) was initiated topically, and the guitarfish was transferred to a larger holding area with clinical improvement once metronidazole was stopped.

Due to progression of the skin wounds, the patient was transferred to a large isolated animal holding area where he declined further. The guitarfish became completely anorectic and began displaying increasing periods of resting behavior and continued disorientation. The wounds continued to progress, and blood work revealed increasing and progressive inflammation and anemia. Parasites and CNS disease were ruled out through diagnostics, with ELS disease identified as the primary differential. Treatments were increased to include daily assist feeding (~1,150 mL gruel SID), ampicillin (18 mg/kg IV SID; Pfizer, New York, NY, United States), polymyxin B (15,000 IU/kg (1,250,000 IU) IV SID; Xellia Pharmaceuticals, Copenhagen, Denmark), fluid support (elasmobranch ringers 250 mL IV SID), prednisone (0.25–0.5 mg/kg PO SID; Jubilant Cadista Pharmaceuticals Inc., 207 Kiley Dr., Salisbury, MD, USA), tramadol (3.6 mg/kg PO SID; ULTRAM®, Cipher Pharmaceuticals, 5,750 Explorer Dr., Mississauga, ON L4W 5 K9, Canada), gabapentin (3.7 mg/kg PO SID; Pfizer, New York, NY, USA), meclizine (0.5 mg/kg PO SID), ketoprofen (5 mg/kg PO), intralipid (0.5–1 mL/kg IV SID; INTRALIPID® 20%; Baxter International, Deerfield, IL, United States), pentoxifylline (25 mg/kg PO SID; Pentoxil Upsher-Smith Laboratories, Maple Grove, MN, United States), erythropoietin (150 IU/kg IM; EPOGEN® Amgen, Thousand Oaks, CA 91320, USA), and misoprostol was continued topically. Treatments were performed daily, but the wounds, including significant tail involvement, continued to progress. The animal did not improve, and the vestibular signs persisted. Due to quality of life concerns and poor prognosis, the guitarfish was humanely euthanized.

On necropsy, the most significant finding was the accumulation of tan purulent material and reddening around the endolymphatic pores that followed the contour of the skull and was associated with the inner ear structures. Additional sectioning of the skull showed the accumulation of thick tan material within the labyrinth canals, more severe on the left when compared to the right side. The tail showed signs of chondritis, presumed from trauma during the clinical course. Histopathology confirmed the clinical diagnosis of a bacterial infection within both inner ears (vestibular labyrinthitis). Gram-positive coccobacilli were present in moderate numbers and consistent with the postmortem culture results (pure culture of *Enterococcus faecalis*). A similar milder inflammatory process was evident in the perilymphatic spaces (left more severe than right), consistent with the gross appearance of exudate superficially and cultured the same organism. Both of these findings were the likely cause for the initial clinical signs (circling and disorientation). Serum levels of drugs were assessed to identify if dosages and intervals resulted in levels considered therapeutic in other animals (Table 2). Despite achieving levels in antibiotics that were sensitive

TABLE 2 Drug level comparison between different species.

Drug	Species	Drug level/C_{max}	Units	Dose (mg/kg)	Source
Carprofen	Bowmouth Guitarfish 2	0.7; 0.6; 0.303	µg/mL	5	Case series 1
	Rainbow trout	2.52	µg/mL	2.5	(62)
	Canine (domestic)	5.43–35.30	µg/mL	0.7–4.0	(63)
	Quail	6.53	µg/mL	10	(64)
Meclizine	Yellow Ray	1,500; 2000; 2,900	µg/mL	1.5	Case series 1
	Bowmouth Guitarfish 2	140	µg/mL	0.5	Case series 1
Metronidazole	Bowmouth Guitarfish 1	61; 40; 65	µg/mL	6	Case series 1
	Bowmouth Guitarfish 2	170	µg/mL	30	Case series 1
	Canine (domestic)	8.84 ± 5.4	µg/mL	5 (IV); 20 (PO)	(65)
	Geese	60.27	µg/mL	50	(66)
	Horses	22+/−8 (PO); 9+/−2	µg/mL	20	(67)
Ketoprofen	Bowmouth Guitarfish 1	0; 0; 0; 0	mcg/ml	4; 5; 6	Case series 1
	Canine (domestic)	2.02 ± 0.41 (PO); 0.54	µg/mL	1 (PO); 10 (TDK)	(68)
	Nile Tilapia	18.15 (IM); 24.07 (IV)	µg/mL	3 (IM & IV)	(69)
Tramadol	Bowmouth Guitarfish 1	170	µg/mL	4.8	Case series 1
	Canine (domestic)	2.52 ± 0.43	µg/mL	4 (IM)	(70)
	Muscovy Ducks	0.78	µg/mL	30	(71)

to the organism, clinical signs were not abated, suggesting penetration to the target tissues may not have been sufficient.

Case 2: Porcupine ray

A 6-year-old female porcupine ray (*Urogymnus asperrimus*) presented after a noted swelling on the midline on the dorsum just caudal to the eyes along with backwards swimming. Fine needle aspiration (FNA) yielded purulent material, and cytology revealed marked heterophilic and histiocytic inflammation with mild eosinophilic and lymphocytic components and reactive fibroplasia, but the animal was otherwise clinically and behaviorally normal and in good body condition. The animal was anesthetized for the examination, and initial treatment consisted of debridement with subsequent wound care and treatments including manuka honey-impregnated gauze (MEDIHONEY Calcium Alginate Dressing; Allegro Enterprises, Bryanston, Johannesburg, South Africa) and amikacin pluronic gel (Amikacin: Polox-A-Gel; Wedgewood Pharmacy, Swedesboro, NJ, United States), along with carprofen (4 mg/kg PO SID; RIMADYL®, Zoetis, Parsippany-Troy Hills, NJ, United States), cefpodoxime (5.5 mg/kg PO SID; Simplicef®, Zoetis, Parsippany-Troy Hills, NJ, United States), amoxicillin–clavulanic acid (19 mg/kg PO BID; Clavamox®, Zoetis, Parsippany-Troy Hills, NJ, United States), and ceftazidime (20 mg/kg IM q72h; Pfizer, New York, NY, United States). *Enterococcus faecalis* was consistently cultured from the abscess throughout the course of treatment. A sand box was introduced to the enclosure to help prevent any wounds from rubbing and resting along the ventral surface.

The swelling improved and the animal continued to remain clinically normal, but the swelling recurred several months later, worse than the initial presentation. On physical examination, the swelling was more pronounced and the original fistulated area was easily re-opened. A more extensive wound exploration indicated association with infection of the ELS, diagnosed by cytology and culture of purulent material aspirated from the area. Debridement and wound flushing proceeded along with the placement of an indwelling catheter through an extant fistula created by disease (Figure 4A). In brief, a red rubber catheter was inserted into the deepest region of the wound (presumably in the perilymphatic spaces) and sutured into place using flexible tubing from an equine subpalpebral lavage (SPL) system (MILA International, Dubai, United Arab Emirates) (Figure 4A). Due to the nature of the skin, a hobby drill was required to make a hole in the skin to thread the tubing and suture an extension set onto the catheter using a Chinese finger trap knot. This pattern allowed a tube to be firmly secured to the skin by a single point, and the physical forces are redistributed along a series of crosses and knots applied around the tube. In addition, the catheter was capped with a one-way valve injection cap (MicroClave® Male Adapter Plug, Manufacturer Item #:10014487; Zoetis, Loveland, CO, United States), and a foam piece was affixed to the end to allow floatation; otherwise, movement in the water resulted in abrasions on the skin with the distal end of the catheter. Radiographs were taken with iohexal (240 mg/mL; GE Healthcare Inc., Marlborough, MA, USA) contrast infused into the catheter to see the extent of the lesion (Figure 5).

Following successful placement, the ray was treated in the water through voluntary training with daily enrofloxacin (Zoetis, Parsippany-Troy Hills, NJ, United States) flushes (mixed with saline at 20 mg/kg) via the catheter for a total flush volume of 60 mL, but this caused erythema and local irritation so enrofloxacin was discontinued but flushes continued with regular saline, which resolved the reaction. The animal was treated with continued parenteral antibiotics and analgesia over time during handlings: amikacin (2.5–5 mg/kg; AMIGLYDE-V®, Zoetis, Parsippany-Troy Hills, NJ, USA), meloxicam (0.1 mg/kg IM; Boehringer Ingelheim, Ingelheim am Rhein, Germany), ketoprofen (2–4 mg/kg IM), danofloxacin (7 mg/kg IM), and florfenicol (40 mg/kg IM; AdvaCare Pharma, 1,623 Central Ave #210, Cheyenne, WY, USA). The ray did well with compliance and treatments with the catheter, and the swelling continued to decrease over time. Parenteral treatments completed but flushes continued for over 2 months at which point the animal was moved back to her exhibit and has had no recurrence of clinical signs to date, several years later. Focal therapy in this case had the most profound and rapid return to normal function.

Case 3: Yellow ray

An 8-year-old male yellow ray *(Urobatis jamaicensis)* presented for an acute development of localized swelling along the dorsal midline of the head associated with the endolymphatic pores (31). The animal was otherwise clinically normal, in good body condition, and serial blood work was generally unremarkable. Physical examination revealed a large abscess (confirmed with cytology) with a deep draining tract entering the labyrinth.

Repeated cultures were positive for *Mycobacterium chelonae*. Multiple anesthesia events occurred for debridement and varying wound treatments which included: infusing ciprofloxacin ophthalmic solution followed by insertion of vancomycin pluronic gel (Wedgewood Pharmacy, Swedesboro, NJ, USA); using a small fragment of trimethoprim sulfadimethoxine tablet (approximately 5% of a 960 mg tablet) and placing in the subcutaneous cavity and holding it in place with a small strip of honey-impregnated gauze; packing the tract with ciprofloxacin and clindamycin POP (plaster of Paris) beads, capped with gelfoam and sutured in place with 3–0 PDS into almost complete apposition (Figure 4B); and a mixture of silver collosate and collagen powder (Collasate Silver gel, The Hymed Group, 1817 Apple Tree Lane, Bethlehem, PA, USA). The animal was treated with ceftazidime (20 mg/kg IM q48h), ketoprofen (4–5 mg/kg IM q48h), meclizine (1.5 mg/kg PO SID long term), ciprofloxacin (26 mg/kg PO SID; Pfizer, New York, NY, USA), and danofloxacin (10 mg/kg IM q96hr). The external lesion appeared to be healing well over the course of the treatment period.

Multiple cone beam computed tomography (CBCT) scans with and without contrast were taken over the course of the case. To obtain images with contrast, 2 mL/kg of IV of iohexal was administered via the ventral tail vein followed with 3 mL of elasmobranch ringers IV. The case was resolved after a month of treatment but recurred with a dorsal cranium swelling 1 month later. Abnormal swimming with spinning developed and persisted for the remaining course of treatment. Treatment with meclizine (0.6 mg/kg PO SID) improved the abnormal swimming throughout this period, but the animal's final examination was 1 year after initial presentation for overall low appetite and continued abnormal swimming. At this examination, due to persistent presence of organism and continued clinical signs, systemic mycobacteriosis was presumed. More intensive treatments were initiated (assist feeding, amikacin (2.5–5 mg/kg IM), azithromycin (10 mg/kg PO SID; Pfizer, New York, NY, United States), and ketoprofen (4–5 mg/kg IM)), and quality of life was discussed. The ray was found dead 3 days later, and necropsy confirmed systemic

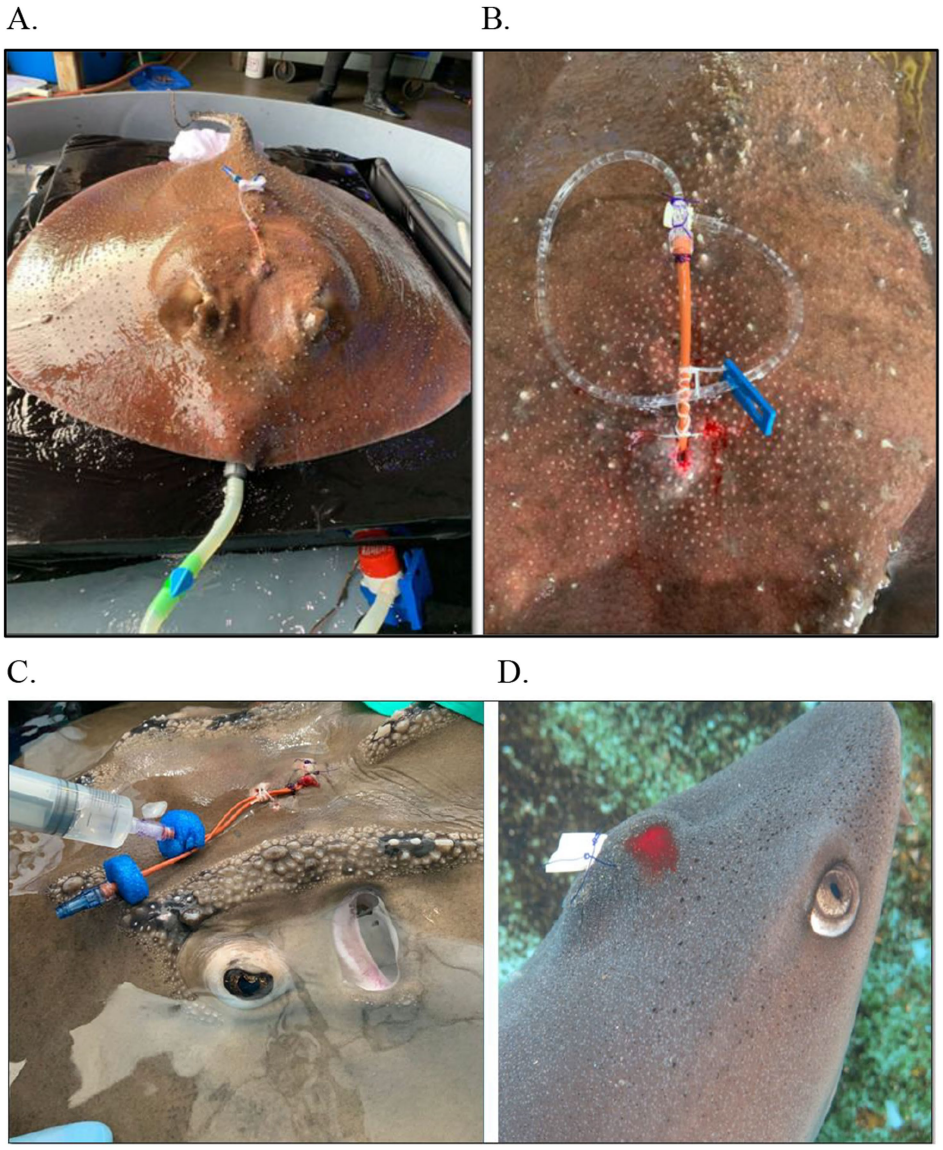

FIGURE 4
Various drains and debridement as part of a multimodal treatment plan for endolymphatic disease in elasmobranch species. **(A)** Porcupine Ray (*Urogymnus asperrimus*); **(B)** Bowmouth guitarfish (*Rhina ancylostoma*) with flushing; **(C)** White tip reef shark (*Triaenodon obesus*) tagging post aspiration.

mycobacteriosis with continued infection in the labyrinth, showing no improvement from treatments; this is likely because focal treatments were limited to the superficial structures of the ELS.

Case 4: Bamboo shark

A 9-year-old female brownbanded bamboo shark (*Chiloscyllium plagiosum*) presented with a midline, dorsal head swelling associated with the endolymphatic pores. On initial examination, the area was aspirated and flushed using a 22 g catheter until the fluid ran clean, CBCT was performed, and the animal was treated with ketoprofen 5 mg/kg IM and danofloxacin 10 mg/kg IM, once. Cytology of the lesion revealed necrosis and chronic-active inflammation with reactive fibroplasia. Cultures were negative, and serial blood work was unremarkable. A gram-stained slide from deep samples revealed occasional gram-negative mixed bacteria, including small coccobacilli and diplococci. CBCT survey and an IV iohexol contrast series (as in Case 3) were performed, and there were no abnormal findings noted in the endolymphatic system.

The animal was monitored over the course of 6 months. CBCT with contrast was repeated, and no significant findings were noted. The animal was considered fully resolved with no recrudescence at publication.

Case 5: Bowmouth guitarfish

A 6-year-old male bowmouth guitarfish presented for intermittent mild spinning (reported as occasional somersaults). On examination, the animal was found to be in good body condition, and the right endolymphatic pore was erythematous, but with no swelling or discharge while the left pore was normal; no other abnormalities were observed. Additional diagnostics and treatments were not pursued

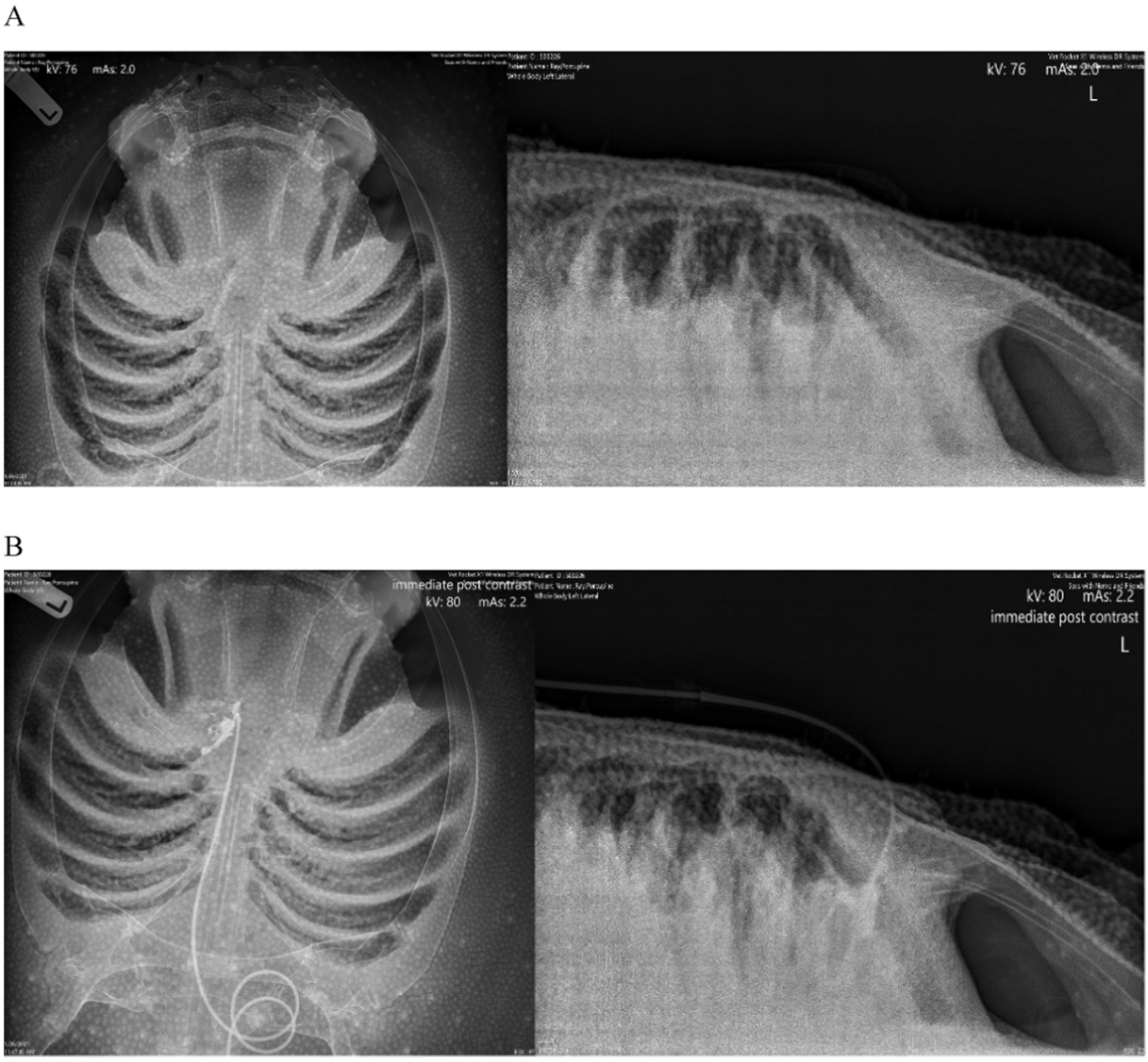

FIGURE 5
Pre and post contrast radiographic images of a porcupine ray (*Urogymnus asperrimus*) with endolymphatic system disease. **(A)** Survey view, ventrodorsal (VD) view and lateral. **(B)** Post iodinated-contrast infused into the affected area, VD view and lateral.

due to the intermittent and improving nature of the abnormal swimming. Six months later, the animal was reported to have a decrease in appetite and marked swelling and erythema of the endolymphatic pore region was noted (Figure 6). Following initial reporting, video and direct observations showed the animal to have an episode where it went onto its back as well as abnormal swimming with notable evidence of vestibular dysfunction. On initial examination, the animal was found to be under conditioned. Blood work showed a leukocytosis compared to in house normal ranges. CSF showed no abnormalities.

Given the previous cases, both systemic and focal treatments were pursued. There were three major treatments throughout the course of disease. For the first, the animal was sedated, and the area of the pores was aseptically prepared. Given the tall dome of the bowmouth, three holes were drilled through the skin (in already thinned areas from presumed pressure necrosis) (Figure 6) to allow flushing and draining: one dorsally and two more ventrally. One liter of Elasmobranch Balanced Salt Solution Salt Solution (Thermo Fisher Scientific, 168 Third Avenue, Waltham, MA United States), 1,000 mL; NaCl, 8 g; urea, 21 g) (32) was flushed through the affected area and then infused with animax ointment (triamcinolone, neomycin, nystatin, and thiostrepton; Animax® Ointment, Dechra Pharmaceuticals, 24 Cheshire Avenue, Northwich, United Kingdom). The animal was assist fed gruel (1% body weight) with 30 mg/kg metronidazole tablets and 6 mg/kg carprofen.

The second procedure occurred the following day with more time to plan a strategy and involved surgical placement of a catheter into the abscess region. In brief, a red rubber catheter, attached to an extension set, was connected with a two nylon finger trap and capped with a one-way syringe adaptor. Two floating foam pieces were attached to maintain the caudal end of the catheter floating to prevent skin abrasion and trauma. The cranial tip of the catheter was inserted through the abscess, directed rostrally into the dorsocaudal hole (made previously at first treatment) and guided through the tissue into

FIGURE 6
Surgery and catheterization for treatment of endolymphatic disease in a Bowmouth guitarfish (*Rhina ancylostoma*). **(A)** Clinical presentation; **(B)** Flushing the parietal fossa during first exam (Procedure #1); **(C)** Catheterization into parietal fossa during procedure #2; **(D)** Surgical approach to fossa and catheterization into perilymphatic fenestration during procedure #3; **(E)** Closure of surgical site and securing catheter; **(F)** View of catheterization at necropsy with a metal probe inserted into the endolymphatic pore, up close and yellow arrows indicate the endolymphatic pore.

the cranial medioventral hole (made using a curved 14 g needle to bore through the skin) and thread with a soft rubber tube from a subpalpebral lavage kit. The catheter was affixed to the caudal area of the abscess (between the pores) with a finger trap and a second securing suture with the same material to the left of the dorsal ridge and a finger trap. The catheter was cut to fit immediately within the

abscess but not outside of the cranial hole and drilled holes into the catheter that was within the abscess to provide adequate flushing opportunity. The region was then flushed with elasmobranch ringers infused with 100 mg of ampicillin.

With no improvement 1 week later, the third procedure was performed with two indwelling catheters placed within the inner ears via a surgical approach into the parietal fossa and the area was flushed and antibiotics and steroids were infused. CBCT image reconstruction of the area from case 1 facilitated anatomical understanding. The pores were left intact, an incision was made caudal to the area, and the perilymphatic openings (fenestrations) were visualized as slightly medial to the pores and in-line with the spiracles (Figure 6); the endolymphatic ducts and openings were not seen, and this may be due to the significant inflammation present or anatomical variation. This surgical approach allowed visualization of the sac/fossa area which helped identify the opening to the inner ear and also allow further exploration. An 8 Fr red rubber catheter was placed by approaching from the contralateral side and sliding in from the medial aspect and then curving down and more caudally to get into the inner ear (~7 cm deep) (Figure 6D). This was repeated on the other side. Samples were collected from each side for culture and cytology. Both sides were flushed with 250 mL EBSS, producing copious purulent material from the left side with less material from the right. Flushing continued until the fluid ran clear (~150 mL) at which point the catheters were secured and 5 mL of Solu-Cortef followed by 5 mL ampicillin approximately 15 min later were infused bilaterally. Both catheters were secured in place with 2.0 MonoWeb in the soft tissue on the ventral surface of the sac using a finger trap pattern. Three simple interrupted sutures were placed to oppose the incision, one simple interrupted across the incision, and then a finger trap to keep both catheters together (Figure 6E). An extant stoma was used to thread a 5 Fr silicone tubing from the SPL kit and then finger trap both catheters that were bunched together. Each side was sealed with a one-way syringe valve cap, and small pieces of foam float material were added to the tips to avoid rubbing on the patient's body (Figure 6E). Flushes were done daily under light sedation.

In addition to the surgical treatments and subsequent flushes/infusions, the following treatments were utilized throughout the course of disease: carprofen 5 mg/kg PO SID, meclizine 0.5 mg/kg PO SID, metronidazole 16 mg/kg PO SID changed to enrofloxacin 10 mg/kg PO SID and ceftazidime 20 mg/kg IV q48hr, intralipid 20% 2 mL/kg IV followed by EBSS 10 mL/kg IV, and misoprostol powder topically to wounds. Drug levels were taken at multiple time points throughout the course of treatment for carprofen, metronidazole, and meclizine which helped guide the course and dosing of treatments.

There were signs of disease progression throughout the course of treatment including increasing frequency and severity of vestibular episodes with some of these episodes associated with tachypnea (respiratory rate > 100 bpm), anemia post-surgery, anorexia, and signs of toxicity on complete blood cell count (CBC) later in the course. However, there was immediate improvement after the third surgery, thus supporting the need for local and aggressive focal treatments.

Cytologic findings were consistent with chronic-active inflammation with chronic hemorrhage, necrosis, and formation of granulation tissue. Some signs of toxicity (foaminess and increased frequency of basophils) on a CBC later in the progression and *Enterococcus faecalis* was cultured from multiple sites including blood and the endolymphatic samples. Vestibular signs improved following the third procedure, but the animal continued to remain anorexic. Despite treatments, the animal was found dead 14 days following initiation of therapy.

The most significant finding at necropsy was the presence of multiple areas of acute necrosis of the gill that were widely scattered throughout the arches as well as moderate infarcts in the liver. This was believed to be the result of sepsis secondary to the ongoing debilitation and the extensive infection within the ELS. Sectioning of the skull and examination of each of the structures of the inner ears and labyrinth systems confirmed the origin of the disease as all these structures were extensively congested and reddened throughout although infection was not overtly evident (Figure 7A). The main conclusion was that this animal had chronic disease of the ELS that likely compromised him in more subtle ways than appreciated.

Case series 2

Six cases of endolymphatic infections in adult Port Jackson sharks (*Heterodontus portusjacksoni*) were observed over a 22-year period and treated. An original cluster of four cases (1) (three females and one male, all wild born) presented as regional swelling around the endolymphatic pores that were fungal abscesses which also were associated with disease in the EL ducts associated with labyrinthitis and in some animals a non-purulent diffuse meningitis. Ocular lesions such as scleritis, corneal edema, corneal rupture, iritis, and/or exophthalmia were present in three of the four sharks. Histology of the head nodules showed a granulomatous reaction with thin and visible fungal hyphae and heavy cellular infiltration. There were similar fungal hyphae inside the endolymphatic duct cartilage walls. Treatments included enrofloxacin (15 mg/kg PO q48hr for 2 weeks) which was ineffective, but prolonged treatments with ceftazidime (30 mg/kg IM q72hr for 2 months) seemed partially effective in some sharks. Flunixin meglumine (2 mg/kg IM q48-72 hr., three injections total; Finadine®; Merck Animal Health, 126 East Lincoln Avenue, Rahway, NJ, USA) was used as an adjunct with some improvement. Itraconazole (20 mg/kg PO q48hr; Sporanox®, Janssen Pharmaceutica, 1,125 Trenton-Harbourton Road. Titusville, NJ, USA) administered for 2 months was ineffective in all cases. *Fusarium solani* was isolated from all cultures.

Subsequent cases occurred in two males born in the aquarium, 20 years after the first series (2). The first case, a 2-year-old male, presented with a 2-week period of anorexia, and an intermittent circular and spiral swimming pattern to the left side. A dorsal subcutaneous head nodule was visible. Treatment was initiated with terbinafine (20 mg/kg PO SID; Lamisil, Novartis Pharmaceuticals UK, The WestWorks, 195 Wood Ln, London W12 7FQ, United Kingdom) and 10 days later raised to 40 mg/kg and ceftazidime (30 mg/kg IM q72hr). Three weeks later, clinical signs continued with exophthalmia of the left eye manifesting with congested sclera, left gill slit muscle paralysis, and fistulation of the head nodule. Treatments were initiated with meloxicam (5 mg/kg IM q48hr) and focal aspiration of material in the nodule. Clinical signs did not improve, and the animal was humanely euthanized. A

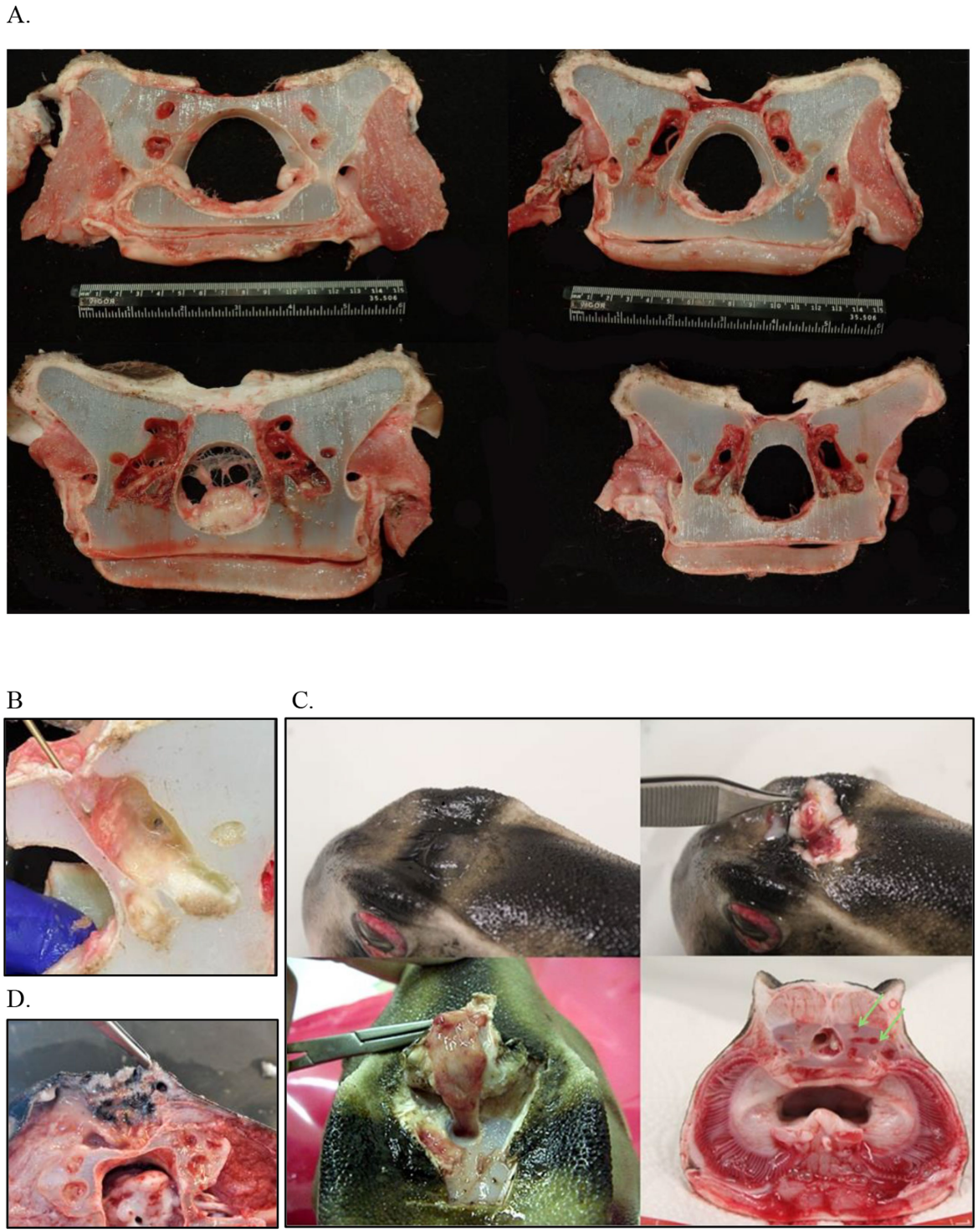

FIGURE 7
Postmortem examples of endolymphatic disease in elasmobranchs. **(A)** Cranial to caudal cross sections of the inner ear at necropsy in a bowmouth guitarfish (*Rhina ancylostoma*); **(B)** The opening that was catheterized in a bowmouth guitarfish (*Rhina ancylostoma*) #2 from Case Series 1 with the probe is showing the direction of the fenestration into the otic capsule. **(C)** Necropsy of a Port Jackson shark (*Heterodontus portusjacksoni*) with unilateral labyrinthitis. The infected labyrinth (green arrows) shows severe congestion of the semicircular canals. **(D)** Adenocarcinoma in a whitetip reef shark (*Triaenodon obesus*) at necropsy.

postmortem CT scan and magnetic resonance imaging (MRI) were performed (Figure 8).

The CT scan confirmed left-sided exophthalmia with an intact endocranium. MRI allowed greater visualization and contrast of soft tissue structure of eye and the ear showing periocular edema, loss of endolymph in the left labyrinth, and the presence of a fistula connecting the infected parietal fossa with the left eye (Figure 8). MRI was more informative about the inner ear and eye lesions than

the CT images, and MRI three-dimensional (3D) constructive interference in steady state (3D-CISS) sequences were more informative than T1 and T2 images.

Histology showed conjunctivitis, labyrinthitis, and meningitis with at least one cranial nerve root affected. There was also mycotic contamination of the labyrinth cartilage. Two bacteria were isolated: *Citrobacter braakii* was cultured from the abscess during the treatment and *Stenotrophomonas maltophilia* from the brain at the necropsy. *Fusarium solani* (complex) was cultured from both areas.

The final case was a 3-year-old male born in the aquarium, who presented with two discrete episodes of circular swimming. With the first episode, examination and ultrasound images of the parietal fossa were normal. The animal was treated for 6 months with ceftazidime (30 mg/kg IM q72hr), vitamin C (30 mg/kg PO SID; Ascor®, McGuff Pharmaceuticals Inc., 4,040 W Carriage Drive, Santa Ana, CA, United States), and a combined antifungal therapy of terbinafine (40 mg/kg PO SID) and itraconazole (10 mg/kg PO SID) and assist feeds. Response to treatment was intermittent with no recurrence of the pore swelling. With the second episode, 6 months later, spiral swimming episodes were observed along with swollen endolymphatic pores. The antifungal doses were increased (terbinafine 50 mg/kg and itraconazole 20 mg/kg) but despite 8 months of treatment, the spiral swimming continued to progress, and the shark was humanely euthanized. Blood work was not informative in this case, and *Fusarium solani* was not cultured from this individual. The animal did not have a necropsy because it was reserved for future imaging studies.

Case series 3

An 8-year-old male lesser devil ray (*Mobula hypostoma*) presented with a change in swimming pattern involving large circles to the right. Blood work showed no changes over baseline for this individual, physical examination, and coelomic and cranial ultrasounds revealed no significant findings; thus, no treatment was initiated as the patient was otherwise eating well and was stable. Three months later, the behavior escalated and the animal began swimming in tighter circles. Empirical treatment was started for a presumed infection and/or inflammation of the ELS with ceftazidime (30 mg/kg IM q72hr) for two doses and methylprednisolone (1 mg/kg) for one dose. With no improvement, amikacin (2.5 mg/kg q72hr) was introduced, which resulted in an improvement of the swimming pattern. The animal returned to normal for 2 weeks followed by recurrence of clinical signs. New blood work showed a significant rise in the granulocytes

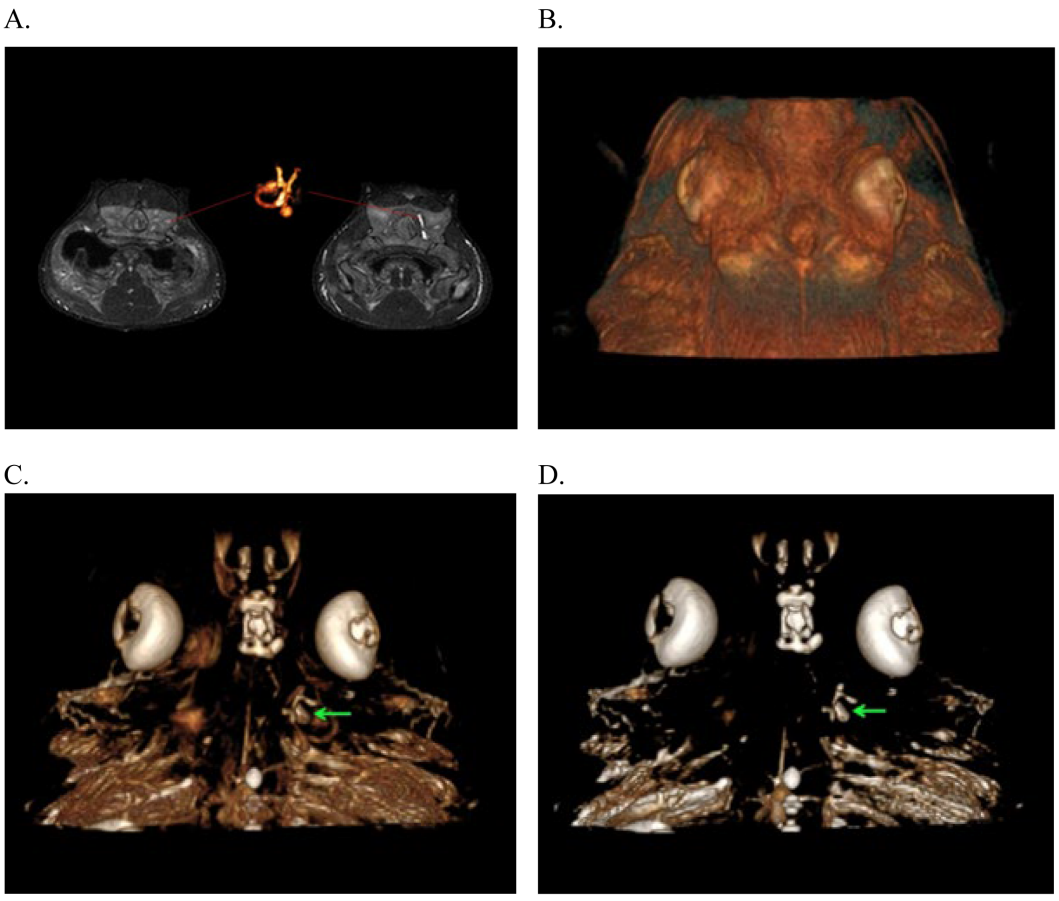

FIGURE 8
Magnetic Resonance Imaging from the 3D-CISS sequence of the endolymphatic system in Port Jackson sharks (*Heterodontus portusjacksoni*). These images illustrate the absence of signal in the infected left membranous labyrinth. **(A)** Images highlighting the MR signal of the unaffected right membranous labyrinth and its corresponding 3D reconstruction. **(B–D)** 3D reconstruction of the head with successive transparency applied for virtual dissection of tissues to highlight the presence of the membranous labyrinth in the unaffected right inner ear, filled with lymph (green arrows).

prompting a change in treatment to enrofloxacin (5 mg/kg PO q48hr), ketoprofen (4 mg/kg IM q48hr), and betahistine dihydrochloride (8 mg/kg q12hr; Betahistine, NHS England London, Wellington House, London). In the following week, there was no improvement with persistent and severe vestibular signs, prompting humane euthanasia. Histopathology confirmed the presence of a granuloma in the right side of the ELS. Bacterial cultures of the ELS, cerebrospinal fluid, and kidney were all negative.

Case series 4

A 25-year-old male sand tiger shark (*Carcharias taurus*) presented for acute onset of swimming in circles to the right except during feeding sessions. Enrofloxacin (15 mg/kg PO q48hr) was administered for 14 days, and the animal improved after this treatment. Recrudescence occurred a year later showing similar clinical signs with the addition of intermittent anorexia, open mouth breathing with no buccal pumping and flared out branchial slits, and a swollen area around the head's dorsal midline associated with the endolymphatic pores. Oral enrofloxacin (15 mg/kg PO q48hr) was resumed with the addition of vitamin B complex tablets (3 tablets (each containing 250 mg thiamine, 250 mg pyridoxine, and 500ug cyanocobalamin) PO q48hr; Hidroxil, Almirall, LLC, 101 Lindenwood Dr. #400, Malvern, PA, USA). After a month of treatment, the clinical signs did not improve, and the animal continued to be anorectic. Treatment was then changed to ceftazidime (30 mg/kg IM q72hr), vitamin C (12 mg/kg IM q72hr), and vitamin B12 (2000 µg IM q72hr; Phoenix, Clipper Distributing Company, LLC, 302 S 59th St, St Joseph, MO, USA), methylprednisolone (1 mg/kg IM once; Pfizer, New York, NY, USA), and methenolone enanthate (200 mg IM once; Samex Overseas, Gujarat, India) to stimulate appetite. A FNA from the swelling showed a dense brown material with cytology showing high numbers of red blood cells and some scant white blood cells (WBCs) (mostly heterophils) but no obvious infectious agent was noticed. A CBC identified heterophilic inflammation. When appetite improved, oral treatments were resumed with enrofloxacin, meloxicam (0.2 mg/kg PO q48hr), and terbinafine (10 mg/kg PO SID) based on the suspicion of a fungal etiology affecting the ELS (based on Case Series #2). Despite initial improvement in appetite, the swimming pattern did not change significantly. A second procedure was performed to repeat a FNA, create a stoma, and flush the affected area. Sample cultures did not yield any growth. Oral treatment continued for 3 weeks with partial resolution of the clinical condition. Manageable vestibular signs continued for 14 months after initial presentation until an escalation of clinical signs occurred. Treatments were switched to gabapentin (25 mg/kg PO), and diazepam (0.25 mg/kg PO; Valium®, Roche Laboratories Inc., 9,115 Hague Rd. Indianapolis, IN, USA) was added for appetite stimulation twice per week. The animal did well on this treatment course, and the gabapentin was decreased progressively to 18 mg/kg and diazepam to 0.05 mg/kg. Swimming improved, and the animal had decreased open mouth breathing episodes but approximately 6 months later presented again with tight circle swimming, anorexia, and edema around the pelvic fins and the base of the claspers. Diazepam and gabapentin doses were increased, and vitamin B complex tablets were resumed again (Hidroxil 3 tablets PO q48hr). The animal's condition improved slightly for approximately 6 months. Over the last week prior to death, clinical signs progressed again, and the animal showed accelerated swimming, active open mouth breathing, anorexia, and small white round skin lesions around the entire body and was found dead prior to the next examination. On necropsy, the region of the endolymphatic pores was swollen, and the parietal fossa and the EL ducts were filled with thickened, brown fluid. In addition, the brain had an asymmetric appearance with a subjective increase in size of the left side as well as branchial necrosis.

A second case presented of a 15-year-old female southern stingray (*Hypanus americanus*) with recurrent episodes of swelling with a fistula on the dorsal area of the head between the eyes, associated with the ELS, and presenting clinical signs were anorexia and lethargy. Initial treatment included with ceftazidime (30 mg/kg IM q72hr) and vitamin B 12 (5 µg/mL IM) and later changed to enrofloxacin (15 mg/kg PO q48hr) and vitamin C (20 mg/kg PO q48hr) for 14 days. The patient improved with the latter treatments. Serial blood work was done, where WBC count (20,000 cells/µl) and creatine kinase (1,185 IU/mL) increased transiently throughout the clinical presentation, but other clinical pathology findings were within normal limits. The swelling on the head was considered fully resolved 13 months post-initial presentation and continues to be quiescent at time of publication. Since resolution occurred, no further diagnostics were pursued.

Case series 5

A 7-year-old female sandbar shark (*Carcharhinus plumbeus*) developed a swelling along the dorsal chondrocranium centered between the eyes accompanied by poor appetite and abnormal swimming with the mouth slightly open. The swelling continued to enlarge and became erythematous over time. The animal was anesthetized, and purulent material was aspirated from the area for cytology and culture. A 5 mm stoma was made through the skin to allow drainage following flushing with two 60 mL syringes of saline. A heavy growth of *Enterococcus faecalis* was cultured, and the biopsy revealed a lymphocytic and histiocytic dermatitis with fibroplasia and neovascularization. The animal was found dead 17 days after initial treatment. Necropsy showed inflammation around the top of the chondrocranium, while most of the other examined tissues appeared normal. The histopathology report for the brain and spinal cord identified meningitis and mild perivascular lymphoplasmacytic encephalitis. The dorsal skin and vertebra showed regionally extensive cellulitis.

A second 7-year-old female sandbar shark (*Carcharhinus plumbeus*) from the same system was observed with a slight swelling in the same area along the dorsal chondrocranium. The animal was eating well and otherwise clinically normal. Amoxicillin (400 mg PO SID; Zoetis Inc., 10 Sylvan Way Parsippany, NJ USA) was initiated. The swelling resolved, and she remained clinically normal for 3 months. The second sandbar shark was transported to another facility and was initially doing well. The amoxicillin was administered 400 mg with each feeding for just under 3 months. A swelling over the chondrocranium recurred and continued to enlarge. Culture results from the recurrence of the lesion were positive for *Enterococcus faecalis*. The swelling continued to enlarge, and she developed difficulty swimming so she was euthanized about 6 weeks later. Histologic diagnosis of the head lesion was severe inflammation with proliferative, reactive fibroplasia. The brain showed severe histiocytic, neutrophilic, and heterophilic meningoencephalitis.

A third case involved a 4-year-old female white spotted bamboo shark (*Chiloscyllium plagiosum*) that presented anorexic, with an

abnormal swimming posture, and a swelling along the dorsal chondrocranium. Treatment was initiated with enrofloxacin (22.7 mg PO) and assist feeding with Hill's A/D Critical Care soft food (Hill's Pet Nutrition, Inc., 6,002 N 51st St, Tampa, FL USA). The same procedure and treatments were repeated 5 days later, and an aspirated sample of the area was submitted for culture. A gram stain and cytology showed gram+ cocci, and the antibiotic was changed to amoxicillin–clavulanic acid (125 mg PO SID).

The culture isolated a heavy growth of *Enterococcus faecalis,* and a second culture was repeated 3 weeks later which showed repeated results. Blood culture was negative for aerobic and anaerobic organisms. After 2 months of daily treatment, the shark began eating on her own and was clinically normal. She remained clinically normal for 6 months when signs recurred, and she progressively deteriorated over a week and was euthanized. On gross necropsy, there was inflammation and fluid causing swelling along the dorsal chondrocranium.

Case series 6

Six cases of ELS disease were identified and treated in whitetip reef sharks (*Triaenodon obesus*). All cases presented over a 5-year period in juvenile to sub-adult sharks (1–4 years of age) including five females and one male. The most common presenting signs were focal swelling of the region surrounding the endolymphatic pores, anorexia, and vestibular signs including abnormal swimming patterns, barrel rolling, head tilting, and resting on the bottom in lateral or dorsal recumbency. One case presented with a "scoliosis-like" abnormal body posture, erratic swimming with head tilt, and anorexia and often would be observed laying in lateral or dorsal recumbency when at rest.

Recurrence of clinical signs was observed in 5/6 sharks at intervals of months to years between events. Serial cultures were obtained at initial presentation and during episodes of recurrence in four of the six sharks. *Enterococcus faecalis* was cultured from all the abscesses with pure growth of *E. faecalis* reported in 9/11 samples. One case also cultured positive for *Staphylococcus epidermidis*-methicillin resistance. The high frequency of recurrence was likely due to recrudescence or persistence of deeper infection.

Based on the culture sensitivities, amoxicillin (80–100 mg/kg PO SID; US Antibiotics, 201 Industrial Dr., Bristol, TN, USA) was started. Other treatments included enrofloxacin (10 mg/kg PO SID), ciprofloxacin (19 mg/kg PO SID), danofloxacin (10 mg/kg IM q5days), carprofen (3.3 mg/kg PO SID q5days), meloxicam (0.2 mg/kg IM or PO q24-48 hr), metoclopramide (0.5 mg/kg IM or PO q24-48 hr), and/or vitamin C (100 mg/kg PO SID). Ceftiofur (6.6 mg/kg q7days; EXCEDE®, Zoetis, Parsippany-Troy Hills, NJ, United States) was used in two of the initial cases, but it proved ineffective with no change in clinical signs. Antibiotic treatment was switched from injectable to oral administration when the sharks began to eat. With instances of recurrence, oral amoxicillin was used concurrently with danofloxacin injections. Antibiotic treatment typically continued for 2–4 weeks past the cessation of clinical signs (resolution of pore swelling). NSAIDs were used in half of the cases, and their use was positively correlated with the return of normal food consumption. Two of the cases received 1–5 oral or injectable doses on either meloxicam or carprofen on consecutive days. The third case received meloxicam every other day for 34 days. Two sharks with recurrent lesions were maintained on long-term vitamin C therapy at half of their initial treatment dose. Additional treatments were used in certain cases depending on the clinical signs and condition of the animal. Cold laser treatment was used (EVO MLS, multiwave locked system, VET Therapy Laser machine-Class IV laser) at 6.44 Joule and 2.05 J/cm^2 for 9 s applied to the affected area. Clinical improvement was observed with lancing of the abscess accompanied with flushing and debridement. In one shark, the abscess was opened with a 2.5 cm incision and flushed with saline and amikacin. A Penrose drain was sutured in place to prevent immediate closure of the wound. The drain was removed 4 days later, and the wound closed by second intention. No significant difference was noted between simple lancing and flushing *vs* short-term drain placement in any of the cases.

In 4/6 cases, the sharks developed sub-optimal body condition over time, in spite of maintaining normal dietary intake and being otherwise asymptomatic for months to years. Five of the six affected sharks died, but mortality was not immediately associated with ELS disease in four of the cases. In these four cases, there was no evidence of active disease for months to years prior to death, so the ELS region was not examined during necropsy.

In the fifth case, the animal had a mild swelling associated with the endolymphatic pores for more than 5 years but had no other clinical signs. In addition, there was no change noted in the swelling following a course of antibiotics administered for a different problem. At 8 years of age, he presented with recurrent bouts of intermittent anorexia. Nine months later, it was observed that the swelling on the head was significantly larger than previously and had developed a cobblestone appearance. Localized soft swellings were identified via palpation and ultrasound; purulent material was observed seeping from these sites. Culture revealed a pure growth of *Enterococcus faecalis*. After 1 month of waxing and waning appetite, metoclopramide (0.5 mg/kg q48hr) was added to the meloxicam (0.2 mg/kg q48hr) and amoxicillin (90 mg/kg PO SID) treatment protocol for this shark. This addition appeared to help stabilize the animal's appetite in the weeks prior to death. On necropsy, transection through the swelling on the head revealed a nodular mass that was a mottled gray and white color dorsally (1 cm) and medium yellow color ventrally (1 cm) (Figure 7D). The mass extended from the skin down to the chondrocranium where it caused areas of thinning of the cartilage. There was multi-focal abscessation present bilaterally along the periphery of the mass. On histopathology, the mass was identified as an adenocarcinoma that had metastasized to the heart. This shark was also reported to have regionally extensive, marked lymphocytic meningitis. It is hypothesized that the chronic inflammation in this area may have promoted the development of this neoplasm as has been described in other species (33, 34).

The sixth case continues to show cyclical disease and is treated routinely at the time of publication.

Discussion

Endolymphatic system disease involves the endolymphatic pores, parietal fossa, endolymphatic ducts, and the inner ear of elasmobranchs. It has variable clinical presentations, with the two most common being a swelling on the dorsal chondrocranium and abnormal swimming patterns. Swimming characteristics include spiraling or rolling and repeated directional circling that frequently corresponded with location of disease. These clinical signs are shared with a variety of diseases including central nervous system inflammation or infection [meningitis or encephalitis (e.g.,

scuticociliates)], skeletal abnormalities [wing ray (ceratotrichia trauma), vertebral malformations or misalignments, and pelvic fin conformational abnormalities], eye lesions, biotoxins, and, in some cases, stereotypy. Disease often waxes and wanes with chronicity often ranging from months to years. It is underrepresented as a differential in neuropathic disease and is difficult to diagnose and treat.

Cases in this series were divided into generalized categories: (1) superficial disease (involving the pores, fossa, ducts, and possible dorsal chondrocranium) and (2) complex disease (involving the deeper structures—perilymphatic and endolymphatic spaces and labyrinth). The latter category always involved neurologic signs. Usually, complex disease was accompanied with superficial signs. Some cases did involve ocular structures and components of the central nervous system which are highlighted separately.

Table 1 presents a summary and breakdown of all cases discussed herein. The anatomically affected areas were varied with (8/23) manifesting superficially as a swelling along the dorsal chondrocranium with no apparent inner ear involvement. 15/23 animals presented with some form of neurologic signs. Many of these individuals had swelling along the dorsal chondrocranium as well but have been classified as 'complex' due to the presence of neurologic clinical signs at presentation. While providing a framework for staging this disease process is ideal, it was not possible with this data set due to the great variability among the cases. The authors attempted to start this process by the categories of 'simple' versus 'complex'. However, true staging of this disease process would be ideal and warrants future consideration and investigation.

21/23 animals had cultures performed as part of the diagnostic workup (Table 1). Of the 21 cultures, one revealed no growth, 12 isolated *Enterococcus faecalis*, six identified *Fusarium solani*, one isolated *Mycobacterium chelonae*, and two had mixed organisms. 19/23 of the affected animals died with 5/19 euthanized and the others dying naturally. 14/23 animals had the endolymphatic system examined on necropsy. 13/23 animals had recurrence of disease with 4/13 recurring multiple times. Only 4/23 animals are currently alive and resolved from all endolymphatic-associated clinical signs.

Blood work was generally not helpful with diagnosis in these cases, and any alterations were secondary to consequences of the disease (trauma to muscle, anorexia/loss of body condition, and secondary infections). Some general trends included increased total white blood cell counts above normal, increased granulocytes in affected animals, signs of toxicity (35) among white blood cells, anemia, and increases in muscle enzymes later in disease progression. In elasmobranchs, low numbers of neutrophils in addition to more frequent fine eosinophilic granulocytes (heterophil equivalent), coarse eosinophilic granulocytes (eosinophil equivalent), and basophils are observed (36). Left-shifted neutrophil and heterophil populations have been observed in the blood of various elasmobranch species, while abnormal granulation tends to be less prominent in elasmobranchs than in other non-mammalian vertebrate taxa (35). Though blood work was generally not helpful clinically, it is recommended as a minimally invasive diagnostic and may help with long-term management and tracking of trends over time.

It can be challenging to obtain diagnostically significant samples due to unique anatomy (small endolymphatic pores and difficult to reach areas of the labyrinth), an aquatic environment, and equipment or clinical limitations. Anatomically, the pores and duct openings are different among species and hard to access. It is critical to understand species differences to facilitate successful sample collection. Aspiration of material from superficial structures is straightforward, but deeper sampling required catheterization or with advanced disease resultant fistulas provided access to deeper affected tissues. Cerebrospinal fluid (CSF) evaluation was used to rule out meningitis or encephalitis in Case Series 1 (Figure 9). Cultures (aerobic, anaerobic, mycobacterial, fungal, and PCR for scuticociliates) and cytology from aspirated material proved to be useful in guiding treatment.

In one series, all necropsied cases of Port Jackson sharks (5 of the 6 cases) found *Fusarium solani*. *F. solani* infections in elasmobranchs have been described mainly with skin, lateral line, skeletal muscle, and cartilage (37–40, 72). They are environmental saprophytic fungi and are important causes of human and animal infections due to the production of mycotoxins and are often associated with temperature related stress (7). Previous literature refers to chondritis lesions in other elasmobranch species, although in those cases it was found in juvenile animals (39, 41–43, 72). *Enterococcus faecalis* was cultured from the blood and/or endolymphatic system samples in 12/23 of the current cases. Delaune and Anderson (44) reported culturing *Enterococcus faecalis* from a spotted eagle ray (*Aetobatus narinari*) that presented due to swelling located on the dorsal head originating from an abscess in the brain. The animal was treated and made a full recovery while never exhibiting abnormal neurologic signs (44). Enterobacteriaceae have been found as intestinal inhabitants of terrestrial and marine vertebrate species and may be normal flora but have also been considered opportunistic pathogens (45, 46). *Mycobacterium chelonae* was also cultured in the yellow stingray case, and this organism has been found as the causative agent of disease in other species, including guitarfish (47). Chang and Okihiro (5) found that the most common cause for meningoencephalitis was bacterial or protozoal with the most commonly isolated agent being *Carnobacterium maltaromaticum*. A study looking at blood cultures from healthy captive and free ranging stingrays found that a single positive blood culture without other corroborating diagnostics (e.g., gross lesions or histologic confirmation) is not sufficient to confirm septicemia in elasmobranchs (48). Repeatability of tests, consistency of results from different sources in the body, and white cells engulfing morphologically appropriate organisms over time may increase the validity that certain organisms are normal microflora *vs* pathogenic.

Imaging can be difficult in elasmobranchs depending on the targeted anatomical area. Ultrasound would be ideal but of limited either by dense dermal denticles in several species or due to the anatomical location, size of the ducts, and depth of the labyrinth encased within cartilage, all of which are not physically possible to scan. Ultrasound could be useful, where skin texture allows, for clinical evaluation of swelling on the dorsal chondrocranium but the area below is not penetrable by ultrasound waves. Radiographs have some value but can be technically difficult to obtain, and the images acquired may not allow a detailed enough view of the severity of disease (Figure 5). The best modality is computed tomography (CT) or magnetic resonance imaging (MRI). MRI offers superior contrast for the examination of soft tissues when compared to CT. MRI images can significantly enhance characterization of lesions within the inner ear and eyes. Notably, the images (Figure 10) obtained through the 3D-CISS sequence exhibited heightened efficacy in lesion discrimination compared to T1-weighted and T2-weighted images. Fluid attenuated inversion recovery (FLAIR) is an additional sequence that nulls/reduces signal of fluids with low protein and cellularity, such as cerebrospinal fluid (CSF) and endolymph. When the composition

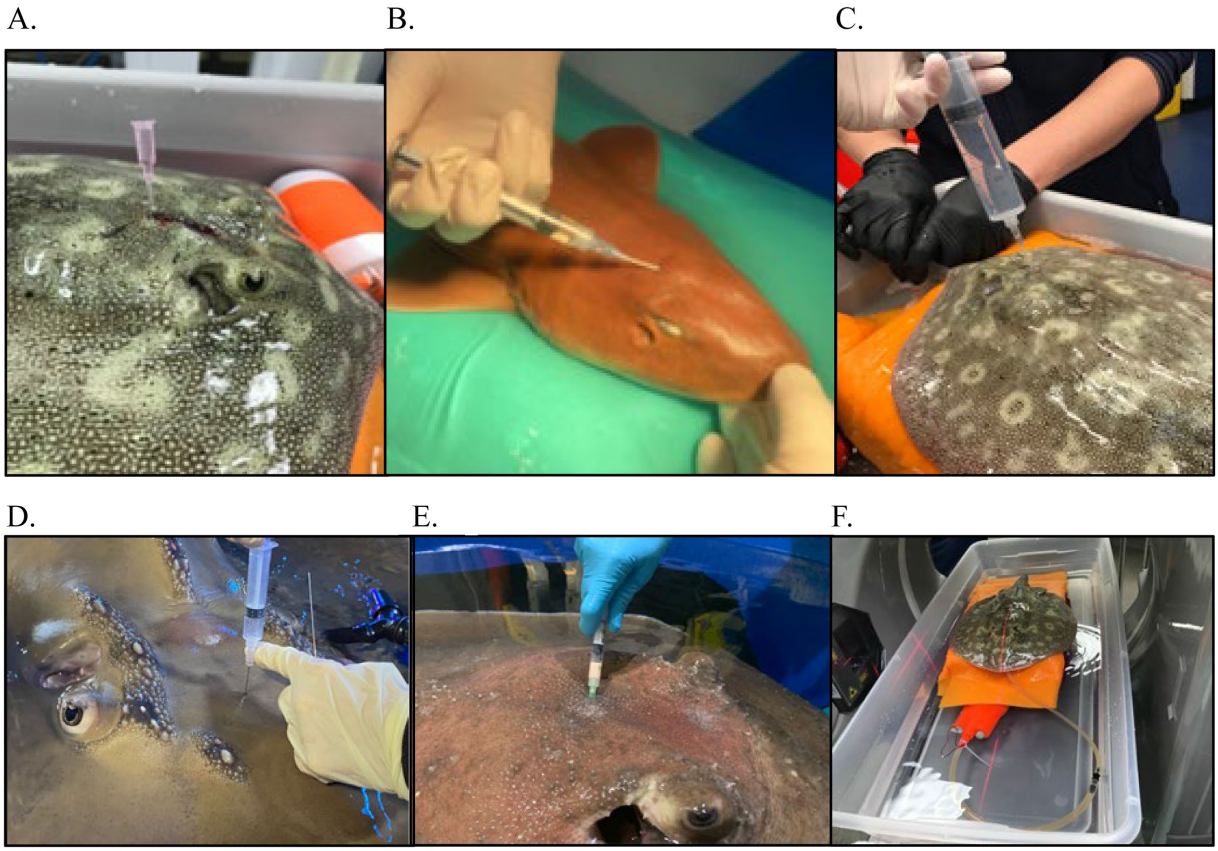

FIGURE 9
Examples of various diagnostics for endolymphatic disease in elasmobranchs. **(A)** Marking of affected area for sample collection and treatment administration in a yellow ray (*Urobatis jamaicensis*); **(B)** Flushing of affected region as part of debridement in a white-spotted bamboo shark (*Chiloscyllium plagiosum*); **(C)** Flushing the affected region as part of debridement in a yellow ray (*Urobatis jamaicensis*); **(D)** Abscess aspiration in a porcupine ray (*Urogymnus asperrimus*); **(E)** Cerebrospinal fluid (CSF) collection in a bowmouth guitarfish (*Rhina ancylostoma*); **(F)** Cone-beam computed tomography of an anesthetized yellow ray (*Urobatis jamaicensis*), ventilated while raised out of water to maximize image quality.

of the endolymph is altered, FLAIR sequences can declare this by an abnormally persistent high signal. Though superior for images, MRI is technically more challenging to accomplish. CT is more readily accessible, faster, and excellent for imaging the musculoskeletal system, including the otic capsule. CT's value in diagnoses is demonstrated in the yellow ray in Case Series 1 and how it helped guide the trajectory for sampling or catheterization.

Treatment approaches among the cases were highly varied, and though many of the treatment modalities did not appear to cause harm, it is challenging to decipher what may have directly resulted in positive outcomes. Several strategies resulted in remission, but recrudescence of clinical signs occurred in more than half of the cases. This is likely because disease did not truly resolve but became quiescent with waxing and waning clinical signs. Complete resolution occurred with simple and superficial disease. Complicated disease with deep infection was difficult to treat and was associated with chronicity. Direct treatments in the region, while difficult, showed clinically relevant changes in microbial loads, inflammation, and clinical signs. Catheterization into the pore and then the ducts was not feasible in these cases, even in the largest elasmobranchs, due to the size of the pores and the inability to see the orientation of the ducts, a 'natural path' was not identifiable or palpable. A surgical approach to catheterize into the otic capsule and the perilymphatic or endolymphatic spaces may be necessary to effectively reach the area for either a sample or direct flushing and treatments. As there were not enough cases to determine whether there were long-term negative consequences, there should be a consideration for damage to the fenestral membrane and other otic structures. Given the degree of disease seen and the variability of anatomy, it is unclear if catheterization is going into perilymphatic space or directly into the labyrinth. However, deep exploration has identified purulent material in these areas with significant tissue inflammation and trauma that has already occurred. In at least Case 5, series 1, the fenestral membrane was not appreciated in either foramen and the ducts were also not seen. It was unclear if the latter was anatomical variation or if disease resulted in enough tissue damage as to destroy extant ductal tissue. Negative outcomes in these cases were associated with chronicity and secondary consequences of persistent inflammation, anorexia, and neurologic signs. Euthanasia was elected in five cases, either due to worsening or an inability to improve the welfare of the patient. When death occurred naturally, it was not always anticipated.

Catheterization of the perilymphatic space was successfully performed in the second bowmouth guitarfish in Case Series 1 (Figure 6). Despite being an invasive surgical procedure, it resulted in resolution of the neurologic signs as soon as the animal recovered. It was determined that the endolymphatic ducts could not be catheterized via an approach through the pores, in this species. The anatomy is very intricate, and the curve was too extreme for an

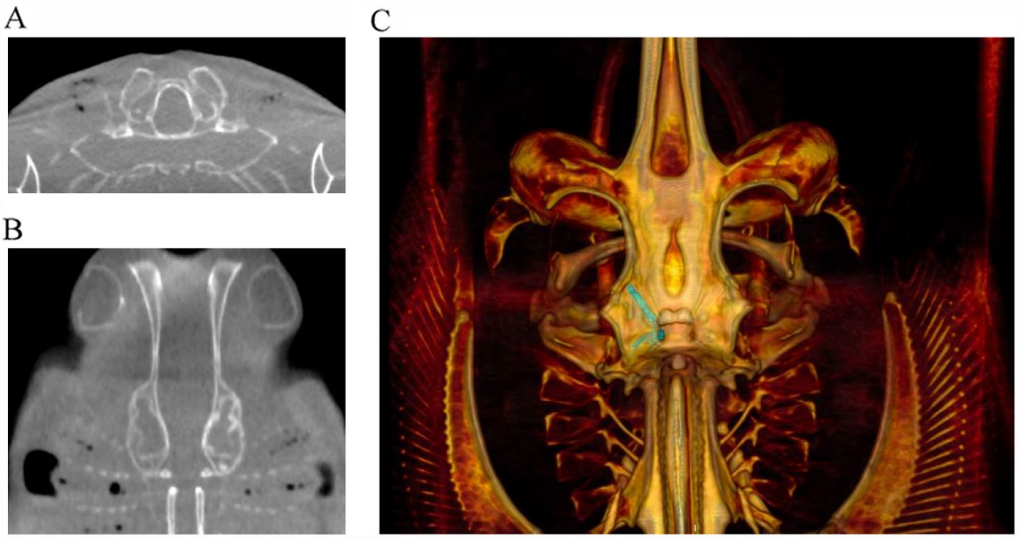

FIGURE 10
Examples of cone beam CT (CBCT) images of right-sided otitis media in a bowmouth guitarfish (*Rhina ancylostoma*). **(A)** Transverse plane and **(B)** dorsal plane image demonstrating the expansile appearance and thinning of the mineral margins of the otic capsule. **(C)** Volume rendered image of the same individual viewed from dorsal with the endolymphatic duct segmented in green.

approach through the pores that would ultimately damage the endolymphatic ducts. Rather, the approach needs to be made via surgically created access to the chondrocranium, avoiding the endolymphatic pores (Figure 6). This procedure was successful in the resolution of neurologic signs of the animal, but the animal likely already septic and refractory to treatments and ultimately died. If this procedure had been implemented sooner, the outcome may have been different. Certainly, focused and direct treatments are recommended and warrant further exploration.

Several supportive care and ancillary treatments had positive effects, while others had equivocal effects. Meclizine was used with improvement of spinning behaviors in multiple cases, and one case had evidence-based data showing its clinical effects (31). Assist feeding was required in several cases due to chronicity of disease resulting in hyporexia and anorexia; this maintained those patients throughout the course of disease. The addition of a sandpit or sandbox to the holding area was helpful at minimizing wounds and other abrasions that could have resulted from the animal resting on the bottom. Antibiotic-impregnated beads were used in several cases with varying levels of success. Sterilized plaster of Paris (POP), hydroxyapatite, and Matrix III have all been studied and are bioabsorbable beads. POP is inexpensive, and there are various studies looking at the elution properties of various antibiotics from POP beads (49, 50). There were often challenges with application of drains due to the nature of elasmobranch skin but elements of the subpalpebral lavage system were the most useful in Case Series 1 and facilitated focal treatment and regular flushing (Figure 4). Some treatments such as laser therapy and betahistine have only been rarely described in veterinary literature and in the case of betahistine, only in dogs and cats (51–53); it is unclear in those cases how effective these treatments were.

The ability to provide focal topical treatment (most notably flushing) in the affected area made a significant difference in several cases. In cases with superficial infections, resolution occurred with minimal treatments and shorter courses. For the more severe cases in Case Series 1, the bowmouth guitarfish and porcupine ray had catheters placed to allow focal treatment. The previous cases showed sufficient evidence of refractory disease with treatments that theoretically should have been effective. The authors appreciated a significant impact from this focal approach with the clinical course and improvement of disease. Though more invasive, the effect was greater than systemic treatments. In contrast, presumed therapeutic levels of metronidazole did not abate *E. faecalis* infection that was sensitive to the antibiotic or improve disease. It was posited that antibiotics did not reach the tissues parenterally. Early treatment is likely to have a better outcome.

A thought experiment for further treatment included consideration for ablation of the inner ear tissue mechanically via the fenestration via laser, hydrothermal, or possible chemical ablation (54–56). In addition, some postmortem investigations were conducted to assess the feasibility of a traditional modified 'bulla osteotomy' and total ear canal ablation. Depending on the species, this may require significant traversing of thick cartilage to get to a very small and narrow space. This would likely require advanced imaging, such as fluoroscopy, for guidance into the correct areas. The spiracles in rays may provide a site of entry.

Lack of pharmacokinetic and pharmacodynamic data is a deficit in elasmobranch clinical medicine. In lieu of that, evaluating drug levels was very helpful in Case Series 1 to help guide treatments and dosing. For instance, some medications had no or low levels at the intended dosing and interval, such as ketoprofen, thus suggesting this plan was ineffective. Meclizine dosed at 1.5 mg/kg PO SID produced levels at 2900 ng/mL which was considered presumably higher than desired (57). While not overtly causing problems, in an abundance of caution, this prompted a change in the dosing regimen. In one of the cases using metronidazole, additional neurologic signs manifested, and serum levels had accumulated to higher than expected values and once removed, signs improved. Carprofen was used in Case Series 1 and showed levels that are therapeutic in other species (Table 2). There is a lot of variability in the pharmacokinetics of drugs, especially between different species.

A combination of multiple diagnostics including serial blood work, culture, cytology, ultrasound where feasible, advanced imaging, and

CSF collection all helped with diagnosing the disease and managing treatment. Postmortem examinations were crucial to characterizing disease and for elucidating anatomy for future cases. In reviewing available literature (4, 40, 58), information on endolymphatic disease is minimal with only one case highlighting otitis interna in a white tip reef shark (58), although other cases are alluded to. Since ELS disease is likely underdiagnosed antemortem, it is also highly likely it is missed postmortem as the inner ear is not typically included in a standard necropsy tissue collection set. The importance of always examining the inner ears during elasmobranch necropsies cannot be under emphasized in neurologic cases, especially as described in this study. One reference suggested that the occurrence of disease is more frequent in small sharks (58), but the present case series expands that notion with increased variety of species and size of patient. That reference also adds an additional differential of trauma (usually pore and sac) resulting in secondary infections, which was not identified in this case series. In addition, bilateral disease is referenced, which was not always easy to determine or reported in the cases presented here.

Etiology of this condition is unknown but is most likely multifactorial. The primary pathway for pathogens to enter the ELS would likely be through the endolymphatic pores into the endolymphatic ducts. For most elasmobranchs, the presence of pathogens in the water poses the primary threat for colonization or contamination of the ELS via these pores. Among all the cases, bacterial presence was common, and second most frequent were fungi. It is possible in those cases they were primary pathogens, but secondary presence is possible as a complication of chronicity. In Case Series 2 (Port Jackson sharks), the primary pathogen was considered to be *Fusarium solani*. Poor culture recovery of microorganisms can also be a factor in lack of diagnosis as aquatic organisms require certain media and temperatures, as well as sample handling parameters that promote good recovery of organisms.

One etiologic consideration is an abnormal composition or absence of otoconia in the labyrinth of animals under managed care. An absence of otoconia may affect hearing less than vestibular functions such as posture, balance, and perception of gravitational forces. In elasmobranchs, hearing relies on two mechanisms: a non-otolithic one that perceives sound through the parietal fossa and the macula neglecta (which lacks otoconia), while the other mechanism detects sound through the otoconia or otoconial mass present in the sacculus (6, 16). Vestibular functions are associated with otoconial mass-associated organs—the utricle, saccule, and lagena (6, 16). Further research is necessary to understand the development of exogenous otoconia in the inner ear elasmobranchs with exogenous otoconia under human care and if this is a factor in developing ELS disease. In addition, another consideration could be through the normal formation of exogenous otoconia, such as sand particles, which traverse the ELS into the deep labyrinth (25, 59). In several elasmobranchs, it is assumed that there is a mixture of exogenous and endogenous otoconia, except for Port Jackson sharks, which only have exogenous otoconia, potentially rendering them even more susceptible to ELS disease. This may be one of the reasons why such pronounced fungal infections were found only in Port Jackson sharks in these clinical cases. This potential process may impact the management of this species under human care as Port Jackson sharks born in human care facilities may entirely lack otoconia due to lack of tank substrate or inappropriate material. It is unclear if this is a factor in other species. Further research is necessary to clarify any potential problems in the inner ear development of elasmobranchs with exclusively exogenous otoconia born in human care systems and whether this is a factor in developing ELS disease.

There are many challenges associated with ELS disease, and one of the major ones is prevention or early detection due to the delayed presentation of clinical signs, chronicity, and complex nature of the disease. Thus, the authors advocate for routine preventative medicine examinations to include careful examination of the endolymphatic pores. In addition, aquarium staff should conduct focused observations of the EL pores as well as recognize clinical signs for prompt evaluation. Consideration for advanced imaging (especially with recurrence), while difficult, will help with diagnosis and extent of disease and provide data for species-specific anatomy. With recrudescent disease, a thorough evaluation is necessary to identify if more diagnostics or intensive treatments are warranted. If there are neurologic clinical signs, this indicates inner ear involvement which should prompt a higher level of diagnostic screening.

The majority of cases in this manuscript presented with swelling on the head or spinning behavior. The histories frequently showed chronicity, waxing and waning signs, and recrudescence of clinical signs were common. There were secondary complications including epithelial and ocular lesions (conjunctival edema, hyperemia, corneal edema, iritis, and exophthalmia), inflammation of the endolymphatic ducts, damage to the inner ear, and opportunistic infections from damage to skin, fins, and tails in animals that do not routinely rest or come in contact with environmental elements. In one Port Jackson shark, unilateral paralysis of the gill slits was observed, which was attributed to cranial nerve root injury identified histologically. The severity of disease can be variable and is related to the unique anatomy of the ELS, which will vary based on species. It is unclear why the ELS may be more prone to microbial infection, but a possible explanation may be the increased chance of pathogen exposure at these areas and the role of biofilms and microbiome. Recent literature suggests that the microbiome of wild *vs* managed care animals is markedly different (60, 61). Given the high proportion of *Enterobacter* identified, this should be a consideration. Causative factors and mitigation strategies are theoretical and beyond the scope of this document.

Understanding this unique anatomy is crucial for diagnosis and then developing and carrying out treatment plans. If disease was superficial, there was often a good outcome when it was identified early and treatment was initiated. If the infection was deeper or more extensive involving the inner labyrinth, then intense focal therapy was likely indicated. However, gaining access to these locations is not simple due to the convoluted and intricate nature of the anatomy. Advanced imaging was helpful for many of these cases for monitoring progression and gauging prognosis.

Conclusion

Endolymphatic disease encompasses a wide array of pathologies that are capable of affecting elasmobranchs. Understanding the anatomy of the elasmobranch ELS and the differences between the species will help to better understand the etiologies and clinical signs of disease. Chronic or recurrent disease can be occult and very challenging to treat. The unique and intricate anatomy can make treatments challenging and penetration to target tissues questionable. Focused treatments seem essential to avoid recurrences of disease. It is recommended to routinely check the endolymphatic pores during routine examinations of elasmobranchs. Advanced imaging can help with guiding treatment plans and gauging prognosis. Most importantly, always include the inner ear tissues in elasmobranch

necropsies. Endolymphatic disease appears to be an underdiagnosed condition among elasmobranch species, and more awareness and knowledge on the specific anatomy, physiology, and pathology may prompt timely diagnosis and treatment.

Data availability statement

The datasets presented in this article are not readily available in accordance with privacy protection guidelines. Requests to access the datasets should be directed to the corresponding author.

Ethics statement

Ethical approval was not required for this study involving animals in accordance with the local legislation and institutional requirements because all cases were clinical cases with veterinary care. This study is a review and compilation of multiple clinical cases and the associated diagnostics and treatments. No animals were used for the purpose of research and animal welfare, ethics, and humane care were used for all cases. Written informed consent was obtained from the participant/patient(s) for the publication of this case report.

Author contributions

WG: Data curation, Formal analysis, Writing – original draft, Writing – review & editing. NP: Data curation, Writing – original draft, Writing – review & editing. BD: Data curation, Writing – original draft, Writing – review & editing. CR-S: Data curation, Writing – original draft, Writing – review & editing. HD: Data curation, Writing – original draft, Writing – review & editing. RF: Data curation, Writing – original draft, Writing – review & editing. DR: Data curation, Writing – original draft, Writing – review & editing. RD-V: Data curation, Writing – original draft, Writing – review & editing. EL: Data curation, Writing – original draft, Writing – review & editing. NM: Conceptualization, Data curation, Project administration, Supervision, Writing – original draft, Writing – review & editing.

Funding

The author(s) declare that no financial support was received for the research, authorship, and/or publication of this article.

Acknowledgments

The authors would like to thank the following individuals from Disney's The Seas with Nemo and Friends®: Dr. Dan Fredholm and Dr. Kyle Donnelly for case management and collaboration, Charlene Burns and Karen Echeverria for unwavering case support and photo documentation, Scott Martin for his continued care and technical expertise, Amy Jo for her interest and presentation on the porcupine ray and the aquarium staff for their continued compassion, dedication, and skills in the care of these cases, Ken Conley, Harley Newton, and Carlos Rodriguez for postmortem evaluation, photography, and support to learn anatomy. The authors also thank the Sea Life Park Hawaii Aquarium staff for their dedication to the animals in their care and to Dr. Annie Clift and Elizabeth Mahi for assistance with medical treatments and postmortem evaluation and photography. The authors thank the Oceanos team of aquarists and vet personnel at the Oceanogràfic for their dedication to care for animals housed in the facility and the Oceanário de Lisboa staff who took care of the Port Jackson sharks and the lesser devil ray during these laborious clinical cases. The authors also thank the pathologists, Prof. Conceição Peleteiro, who participated in the postmortem work of the first cases, and Prof. Pedro Faísca, who is our current pathologist and finally thank the Clínica S24 - Centro de Diagnóstico team for the imaging logistical support. The authors additionally thank Dr. Carl Speilvogel of Aquarium of Niagara for his clinical support and case management and specially thank Dr. Ri Chang, Monterey Bay Aquarium, for anatomical guidance.

Conflict of interest

RD-V and NM were employed by The Walt Disney Company. NP was employed by Sea Life Park Hawaii.

The remaining authors declare that the research was conducted in the absence of any commercial or financial relationships that could be construed as a potential conflict of interest.

Publisher's note

All claims expressed in this article are solely those of the authors and do not necessarily represent those of their affiliated organizations, or those of the publisher, the editors and the reviewers. Any product that may be evaluated in this article, or claim that may be made by its manufacturer, is not guaranteed or endorsed by the publisher.

References

1. Pereira N, Nunes GD, Baylina N, Peleteiro MC, Rosado L. Fusarium solani infection in the eye, brain, otic capsule and endolymphatic tubes in captive port Jackson sharks (*Heterodontus portusjacksoni*). In: Proceedings of the 33rd annual conference of the International Association for Aquatic Animal Medicine; (2002). p. 54-6.

2. Pereira N, Faustino R, Faísca P, Veríssimo C, David H, Baylina N. Twenty years later: a new case of endolymphatic tube infection, internal otitis and meningitis caused by Fusarium Solani in a port Jackson shark (*Heterodontus Portusjacksoni*). In: Proceedings of the International Association for Aquatic Animal Medicine (IAAAM) meeting and conference (2018).

3. Rich AF, Zendri F, Thornton S, Verin R. Meningoencephalitis with chondrocranial subcutaneous abscessation and septicaemia in a captive lemon shark (*Negaprion brevirostris*). *J Fish Dis*. (2021) 44:113–7. doi: 10.1111/jfd.13276

4. Steele LM, Okihiro MS, Berlemont R, Dillon JG, Young KA, Hesami S, et al. *Carnobacterium maltaromaticum* associated with meningoencephalitis and otitis in stranded common thresher sharks (*Alopias vulpinus*). *Vet Pathol*. (2022) 59:850–9. doi: 10.1177/03009858221102600

5. Chang RK, Okihiro MS. A practical guide to necropsy of the elasmobranch chondrocranium and causes of mortality in wild and aquarium-housed California elasmobranchs. *Front Vet Sci*. (2024) 11:1410332. doi: 10.3389/fvets.2024.1410332

6. Meredith TL, Kajiura SM, Hueter RE, Gardiner JM, Collin SP, Hart NS, et al. Advances in the sensory biology of elasmobranchs In: JC Carrier, CA Simpfendorfer, MR Heithaus and KE Yopak, editors. Biology of sharks and their relatives. *3rd* ed. Boca Raton: CRC Press (2022). 143–76.

7. Carrier JC, Simpfendorfer CA, Heithaus MR, Yopak KA. Biology of sharks and their relatives. *3rd* ed. London: CRC Press (2022).

8. Chapuis L, Collin SP. The auditory system of cartilaginous fishes. *Rev Fish Biol Fish*. (2022) 32:521–54. doi: 10.1007/s11160-022-09698-8

9. Corwin JT. Audition in elasmobranchs In: WN Tavolga, AN Popper and RR Fay, editors. Hearing and sound communication in fishes. New York: Springer-Verlag (1981). 81–102.

10. Heuter RE, Mann DA, Maruska KP, Sisneros JA, Demski LS. Sensory biology of elasmobranchs In: JC Carrier, JA Musick and MR Heithaus, editors. Biology of sharks and their relatives. Boca Raton: CRC Press (2004)

11. Maisey JG. Remarks on the inner ear of elasmobranchs and its interpretation from skeletal labyrinth morphology. *J Morphol*. (2001) 250:236–64. doi: 10.1002/jmor.1068

12. Myrberg AA Jr. The acoustical biology of elasmobranchs. *Environ Biol Fish*. (2001) 60:31–46. doi: 10.1023/A:1007647021634

13. Popper AN, Fay R. Structure and function of the elasmobranch auditory system. *Am Zool*. (1977) 17:443–52. doi: 10.1093/icb/17.2.443

14. Tester AL, Kendall JI, Milisen WB. Morphology of the ear of the shark genus Carcharhinus, with particular reference to the macula neglecta. *Pac Sci*. (1972) 26:264–74.

15. Corwin JT. The relation of inner ear structure to the feeding behavior in sharks and rays. *Scan Electron Microsc*. (1978) 2:1105–12.

16. Corwin JT. Functional anatomy of the auditory system in sharks and rays. *J Exp Zool Suppl*. (1989) 252:62–74. doi: 10.1002/jez.1402520408

17. Sauer DJ, Radford CA, Mull CG, Gennari SM, Huveneers C, Ketten DR, et al. Quantitative assessment of inner ear variation in elasmobranchs. *Sci Rep*. (2023) 13:11939. doi: 10.1038/s41598-023-39151-0

18. Corwin JT. Morphology of the macula neglecta in the shark genus Carcharhinus. *J Morphol*. (1977) 152:341–61. doi: 10.1002/jmor.1051520306

19. Staggl MA, Abed-Navandi D, Kriwet J. Cranial morphology of the orectolobiform shark, *Chiloscyllium punctatum* Müller & Henle, 1838. *Vert Zool*. (2022) 72:311–70. doi: 10.3897/vz.72.e84732

20. Barber V, Emerson C. Scanning electron-microscopic observations on the inner-ear of the skate, *Raja ocellata*. *Cell Tissue Res*. (1980) 205:199–215. doi: 10.1007/BF00234680

21. Waller GNH, Baranes A. Chondrocranium morphology of northern Red Sea triakid sharks and relationships to feeding habits. *J Fish Biol*. (1991) 38:715–30. doi: 10.1111/j.1095-8649.1991.tb03160.x

22. Maisey JG, Lane JA. Labyrinth morphology and the evolution of low-frequency phonoreception in elasmobranchs. *C R Palevol*. (2010) 9:289–309. doi: 10.1016/j.crpv.2010.07.021

23. Evangelista C, Mills M, Sieback UE, Collin SP. A comparison of the external morphology of the membranous inner ear in elasmobranchs. *J Morphol*. (2010) 271:483–95. doi: 10.1002/jmor.10812

24. Mickle MF, Higgs DM. Towards a new understanding of elasmobranch hearing. *Mar Biol*. (2022) 169:12. doi: 10.1007/s00227-021-03996-8

25. Mills M, Rasch R, Siebeck UE, Collin SP. Exogenous material in the inner ear of the adult port Jackson shark, *Heterodontus portusjacksoni* (Elasmbranchii). *Anat Rec*. (2011) 294:373–8. doi: 10.1002/ar.21338

26. Hanson M, Westerberg H, Oblad M. The role of magnetic statoconia in dogfish (*Squalus acanthias*). *J Exp Biol*. (1990) 151:205–18. doi: 10.1242/jeb.151.1.205

27. Lychakov DV. Evolution of the otolith membrane: structural organization. *Zh Evol Biokhim Fiziol*. (1988) 24:541–7.

28. Lychakov DV, Boyadzhieva-Mikhailova A, Christov I, Evdokimov II. Otolithic apparatus in Black Sea elasmobranchs. *Fish Res*. (2000) 46:27–38. doi: 10.1016/S0165-7836(00)00130-2

29. Kaye CM, Sankey MG, Thomas LA. A rapid and specific semi-micro method involving high-pressure liquid chromatography for the assay of metronidazole in plasma, saliva, serum, urine and whole blood. *Br J Clin Pharmacol*. (1980) 9:528–9. doi: 10.1111/j.1365-2125.1980.tb05856.x

30. Ralph ED, Clarke JT, Libke RD, Luthy RP, Kirby WM. Pharmacokinetics of metronidazole as determined by bioassay. *Antimicrob Agents Chemother*. (1974) 6:691–6. doi: 10.1128/AAC.6.6.691

31. Puishys L, Mylniczenko N, De Voe R, Fredrickson A, Salles D, Harmon T, et al. Abnormal swimming is associated with inner ear damage and improves with meclizine treatment and increased habitat complexity: a case study in *Urobatis jamaicensis*. *J Zoo Aquarium Res*. (2024) 12:36–41. doi: 10.19227/jzar.v12i1.702

32. Mylniczenko N, Clauss T. Pharmacology of elasmobranchs: updates and techniques In: M Smith, D Warmolts, D Thoney, R Hueter, M Murray and J Ezurra, editors. The elasmobranch husbandry manual II: Recent advances in the Care of Sharks, rays and their relatives. Columbus: Ohio Biological Survey (2017). 277–88.

33. Korniluk A, Koper O, Kemona H, Dymicka-Piekarska V. From inflammation to cancer. *Ir J Med Sci*. (2017) 186:57–62. doi: 10.1007/s11845-016-1464-0

34. Nakano-Narusawa Y, Yokohira M, Yamakawa K, Ye J, Tanimoto M, Wu L, et al. Relationship between lung carcinogenesis and chronic inflammation in rodents. *Cancers*. (2021) 13:2910. doi: 10.3390/cancers13122910

35. Stacy NI, Hollinger C, Arnold JE, Cray C, Pendl H, Nelson PJ, et al. Left shift and toxic change in heterophils and neutrophils of non-mammalian vertebrates: a comparative review, image atlas, and practical considerations. *Vet Clin Pathol*. (2022) 51:18–44. doi: 10.1111/vcp.13117

36. Arnold J. Hematology of the sandbar shark, *Carcharhinus plumbeus*: standardization of complete blood count techniques for elasmobranchs. *Vet Clin Pathol*. (2005) 34:115–23. doi: 10.1111/j.1939-165X.2005.tb00023.x

37. Cañizares-Cooz D, García-Párraga D, Plá-González E, Rojo-Solis C, Encinas T, Morón-Elorza P. Fungal diseases in elasmobranchs and their possible treatment with a special mention to azole antifungal agents. *Animals*. (2024) 14:43. doi: 10.3390/ani14010043

38. Dove ADM, Clauss TM, Marancik P, Camus AC. Emerging diseases of elasmobranchs in aquaria In: M Smith, D Warmolts, D Thoney, R Hueter, M Murray and J Ezurra, editors. The elasmobranch husbandry manual II: Recent advances in the Care of Sharks, rays and their relatives. Columbus: Ohio Biological Survey (2017). 263–77.

39. Fernando N, Hui SW, Tsang CC, Leung SY, Ngan AHY, Leung RWW, et al. Fatal Fusarium solani species complex infections in elasmobranchs: the first case report for black spotted stingray (*Taeniura melanopsila*) and a literature review. *Mycoses*. (2015) 58:422–31. doi: 10.1111/myc.12342

40. Stidworthy MF, Thornton SM, James R. A review of pathologic findings in elasmobranchs: a retrospective case series In: M Smith, D Warmolts, D Thoney, R Hueter, M Murray and J Ezurra, editors. The elasmobranch husbandry manual II: Recent advances in the Care of Sharks, rays and their relatives. Columbus: Ohio Biological Survey (2017). 277–88.

41. Crow GL, Brock JA. Cranial morphology of the orectolobiform shark, *Chiloscyllium punctatum* Müller & Henle, 1838. *Vertebr Zool*. (2019) 72:311–70.

42. Muhvich AG, Reimschuessel R, Lipsky MM, Bennett RO. *Fusarium solani* isolated from newborn bonnethead sharks, *Sphyrna tiburo* (L.). *J Fish Dis*. (1989) 12:57–62. doi: 10.1111/j.1365-2761.1989.tb01291.x

43. Smith AG, Muhvich AG, Muhvich KH, Wood C. Fatal *Fusarium solani* infections in baby sharks. *J Med Vet Mycol*. (1989) 27:83–91. doi: 10.1080/02681218980000121

44. Delaune AJ, Anderson CE. Diagnosis and treatment of an enterococcus fecalis abscess in the cranial vault of a spotted eagle ray (*Aetobatus Narinari*). *J Zoo Wildl Med*. (2020) 51:249–52. doi: 10.1638/2019-0155

45. Juste-Poinapen NMS, Yang L, Ferreira M, Poinapen J, Rico C. Community profiling of the intestinal microbial community of juvenile hammerhead sharks (*Sphyrna lewini*) from the Rewa Delta, Fiji. *Sci Rep*. (2019) 9:1–11. doi: 10.1038/s41598-019-43522-x

46. Perry CT, Pratte ZA, Clavere-Graciette A, Ritchie KB, Hueter RE, Stevens JD, et al. Elasmobranch microbiomes: emerging patterns and implications for host health and ecology. *Anim Microb*. (2021) 3:61. doi: 10.1186/s42523-021-00121-4

47. Tuxbury KA, Young SA, Bradway DS, Marola JL, Salfinger M, Garner MM. Acute disseminated mycobacteriosis in captive Atlantic guitarfish (*Rhinobatos lentiginosus*). *J Vet Diagn Invest*. (2017) 29:935–8. doi: 10.1177/1040638717721731

48. Mylniczenko ND, Harris B, Wilborn RE, Young FA. Blood culture results from healthy captive and free-ranging elasmobranchs. *J Aquat Anim Health*. (2007) 19:159–67. doi: 10.1577/H06-039.1

49. Adams K, Couch L, Cierny G, Calhoun J, Mader JT. In vitro and in vivo evaluation of antibiotic diffusion from antibiotic-impregnated polymethylmethacrylate beads. *Clin Orthop Relat Res*. (1992) 278:244–52. doi: 10.1097/00003086-199205000-00037

50. Ethell MT, Bennett RA, Brown MP, Merritt K, Davidson JS, Tran T. In vitro elution of gentamicin, amikacin, and ceftiofur from polymethylmethacrylate and hydroxyapatite cement. *Vet Surg*. (2000) 29:375–82. doi: 10.1053/jvet.2000.7535

51. Brum AM, Pascon JPE, Champion T, Tinucci-Costa M. Betahistine dihydrochloride in canine peripheral vestibular syndrome-case report. *Cienc Anim Bras*. (2010) 11:239–44. doi: 10.5216/cab.v11i1.1753

52. Dadone L, Harrison T. Chapter 30: Zoological applications of laser therapy In: RJ Riegel and JC Godbold, editors. Laser therapy in veterinary medicine: Photobiomodulation. Hoboken: John Wiley & Sons (2017)

53. Tighilet B, Trottier S, Lacour M. Dose-and duration-dependent effects of betahistine dihydrochloride treatment on histamine turnover in the cat. *Eur J Pharmacol*. (2005) 523:54–63. doi: 10.1016/j.ejphar.2005.09.017

54. Harrison RV, Mount RJ, Hirakawa H. Total ablation of cochlear haircells by perilymphatic perfusion with water. *Hear Res*. (1997) 110:229–33. doi: 10.1016/S0378-5955(97)00085-3

55. Majdani O, Wittkopf J, Dietrich MS, Labadie RF. Penetration of CO2 laser into the otic capsule using a hand-held, flexible-fiber delivery system. *Lasers Surg Med*. (2009) 41:509–13. doi: 10.1002/lsm.20800

56. McCaughey RG, Wong BJ, Tafoya J, Sun Y, Jain R. Laser ablation of otic capsule tissue. *Proc SPIE Int Soc Opt Eng*. (2008) 6854:270–6. doi: 10.1117/12.766919

57. Wang Z, Lee B, Pearce D, Qian S, Wang Y, Zhang Q, et al. Meclizine metabolism and pharmacokinetics: formulation on its absorption. *J Clin Pharmacol*. (2012) 52:1343–9. doi: 10.1177/0091270011414575

58. Steadman R, Garner MM. Elasmobranchs In: KA Terio, D McAloose and J St Leger, editors. Pathology of wildlife and zoo animals. London, United Kingdom: Academic Press (2018). 975–1008.

59. Mulligan KP, Gauldie RW. The biological significance of the variation in crystalline morph and habit of otoconia in elasmobranchs. *Copeia*. (1989) 1989:856–71. doi: 10.2307/1445969

60. Clavere-Graciette AG, McWhirt ME, Hoopes LA, Bassos-Hull K, Wilkinson KA, Stewart FJ, et al. Microbiome differences between wild and aquarium whitespotted eagle rays (*Aetobatus narinari*). *Anim Microbiome*. (2022) 4:34. doi: 10.1186/s42523-022-00187-8

61. Muñoz-Baquero M, Lorenzo-Rebenaque L, García-Vázquez FA, García-Párraga D, Martínez-Priego L, De Marco-Romero G, et al. Unveiling microbiome signature in inner body fluids: comparison between wild and aquarium small-spotted catshark (*Scyliorhinus canicula*). *Front Mar Sci*. (2023) 10:1190030. doi: 10.3389/fmars.2023.1151119

62. Uney K, Corum DD, Terzi E, Corum O. Pharmacokinetics and bioavailability of Carprofen in rainbow trout (*Oncorhynchus mykiss*) Broodstock. *Pharmaceutics*. (2021) 13:990. doi: 10.3390/pharmaceutics13070990

63. McKellar QA, Pearson T, Bogan JA, Gaibraith EA, Lees P, Ludwig B, et al. Pharmacokinetics, tolerance and serum thromboxane inhibition of carprofen in the dog. *J Small Anim Pract*. (1990) 31:443–8. doi: 10.1111/j.1748-5827.1990.tb00510.x

64. Turk E, Tekeli IO, Corum O, Durna Corum D, Kirgiz FC, Cetin G, et al. Pharmacokinetics of meloxicam, carprofen, and tolfenamic acid after intramuscular and oral administration in Japanese quails (*Coturnix coturnix japonica*). *J Vet Pharmacol Ther*. (2021) 44:388–96. doi: 10.1111/jvp.12972

65. Sekis I, Ramstead K, Rishniw M, Schwark WS, McDonough SP, Goldstein RE, et al. Single-dose pharmacokinetics and genotoxicity of metronidazole in cats. *J Feline Med Surg*. (2009) 11:60–8. doi: 10.1016/j.jfms.2008.06.011

66. Fadel C, Łebkowska-Wieruszewska B, Bourdo K, Poapolathep A, Hassoun G. Metronidazole pharmacokinetics in geese (*Anser anser* domesticus) after intravenous and oral administrations. *J Vet Pharmacol Ther*. (2023) 47:208–14. doi: 10.1111/jvp.13421

67. Steinman A, Gips M, Lavy E, Sinay I, Soback S. Pharmacokinetics of metronidazole in horses after intravenous, rectal and oral administration. *J Vet Pharmacol Ther*. (2000) 23:353–7. doi: 10.1046/j.1365-2885.2000.00294.x

68. Ravuri HG, Satake N, Balmanno A, Skinner J, Kempster S, Mills PC. Pharmacokinetic evaluation of a novel transdermal ketoprofen formulation in healthy dogs. *Pharmaceutics*. (2022) 14:646. doi: 10.3390/pharmaceutics14030646

69. Greene W, Mylniczenko ND, Storms T, Burns CM, Lewbart GA, Byrd L, et al. Pharmacokinetics of ketoprofen in Nile tilapia (*Oreochromis niloticus*) and rainbow trout (*Oncorhynchus mykiss*). *Front Vet Sci*. (2020) 7:585324. doi: 10.3389/fvets.2020.585324

70. Giorgi M, Del Carlo S, Łebkowska-Wieruszewska B, Kowalski CJ, Saccomanni G. Pharmacokinetics of tramadol and metabolites after injective administrations in dogs. *Pol J Vet Sci*. (2010) 13:639–44. doi: 10.2478/v10181-010-0027-y

71. Bailey RS, Sheldon JD, Allender MC, Papich MG, Chinnadurai SK. Pharmacokinetics of orally administered tramadol in Muscovy ducks (*Cairina moschata domestica*). *J Vet Pharmacol Ther*. (2019) 42:380–4. doi: 10.1111/jvp.12743

72. Kaiser S. *Fusarium solani* fungal infection of the lateral line canal system in captive scalloped hammerhead sharks (*Sphyrna lewini*) in Hawaii. *J Wildl Dis*. (1995) 31:562–5. doi: 10.7589/0090-3558-31.4.562

73. Ladich F, Schulz-Mirbach T. Diversity in fish auditory systems: one of the riddles of sensory biology. *Front Ecol Evol*. (2016) 4:28. doi: 10.3389/fevo.2016.00028

Frontiers in Veterinary Science

Transforms how we investigate and improve animal health

The third most-cited veterinary science journal, bridging animal and human health with a comparative approach to medical challenges. It explores innovative biotechnology and therapy for improved health outcomes.

Discover the latest Research Topics

See more →

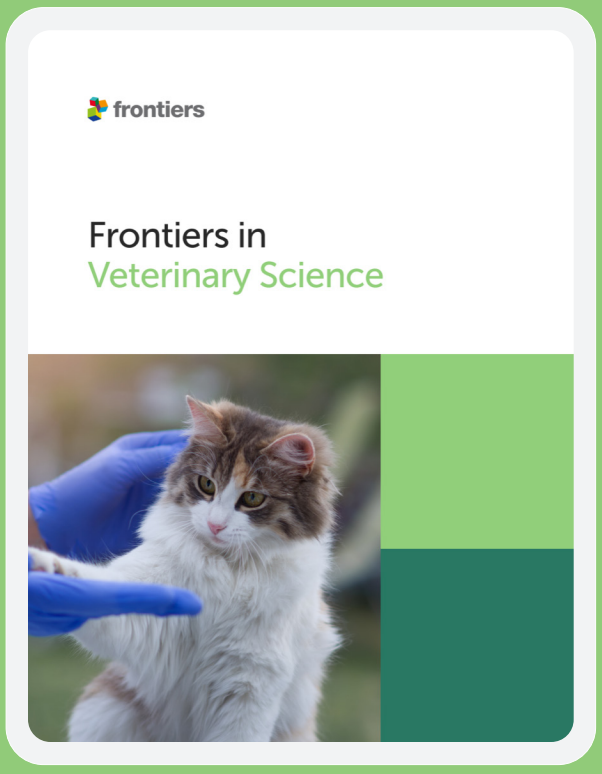

Frontiers

Avenue du Tribunal-Fédéral 34
1005 Lausanne, Switzerland
frontiersin.org

Contact us

+41 (0)21 510 17 00
frontiersin.org/about/contact